Les exciton-polarisations dans les microcavités planaires

Dimitri Solnyshkov

▶ **To cite this version:**

Dimitri Solnyshkov. Les exciton-polarisations dans les microcavités planaires. Agrégats Moléculaires et Atomiques [physics.atm-clus]. Université Blaise Pascal - Clermont-Ferrand II, 2007. Français. NNT : 2007CLF21801 . tel-00718657

HAL Id: tel-00718657
https://theses.hal.science/tel-00718657

Submitted on 17 Jul 2012

HAL is a multi-disciplinary open access archive for the deposit and dissemination of scientific research documents, whether they are published or not. The documents may come from teaching and research institutions in France or abroad, or from public or private research centers.

L'archive ouverte pluridisciplinaire **HAL**, est destinée au dépôt et à la diffusion de documents scientifiques de niveau recherche, publiés ou non, émanant des établissements d'enseignement et de recherche français ou étrangers, des laboratoires publics ou privés.

N° d'Ordre : D.U. 1801

UNIVERSITE BLAISE PASCAL

U.F.R. Sciences et Technologies

ECOLE DOCTORALE DES SCIENCES FONDAMENTALES

THESE

présentée pour obtenir le grade de

DOCTEUR D'UNIVERSITE

Spécialité : Physique des Matériaux

par **SOLNYSHKOV Dmitry**

Master de Physique

EXCITON-POLARITONS IN PLANAR MICROCAVITIES

Soutenue publiquement le 06/12/2007, devant la commission d'examen.

Jury : AMAND Thierry (rapporteur)

CARUSOTTO Iacopo (rapporteur)

CIUTI Cristiano (rapporteur)

GIPPIUS Nikolay (président)

LEYMARIE Joel (examinateur)

MALPUECH Guillaume (directeur de thèse)

CONTENTS

Acknowledgements

During the years of my thesis research I have collaborated with a number of outstanding scientists, and I appreciate strongly their impact on my scientific career. The knowledge they shared with me allowed me to grow up as a scientist.

First of all I would like to thank my supervisor Guillaume Malpuech. We have been working in a close team for a long time, and not only in science. I have learned a lot from him, and we have implemented a lot of bright ideas together.

I appreciate very much the work I have done with Mikhail Glazov. It is impossible to overestimate his knowledge and his excellent way of explaining complicated problems.

We have published a lot of papers with Alexey Kavokin and Ivan Shelykh. Their creativity was always impressive and almost always fruitful.

Not long before the end of my PhD studies I have started to work with Nikolay Gippius, and our collaboration has already given an important outcome. Many times his critical advices have saved me a long time of efforts, that could have been wasted otherwise.

In the early years of my scientific career I have been working in Ioffe Institute. I would like to express my gratitude to the scientists with whom I collaborated: Tatiana Shubina, Sergey Ivanov, Reginald Kyutt, and Alexey Toropov. Thanks to them I have obtained experience in different areas of physics: crystal growth, optics and X-rays.

Last but not least, I would like to thank my wife, Oxana Solnyshkova, without whom all this would not have been possible. It is a miracle and incredible luck to have a wife who can listen to scientific stories each evening and never complain.

Introduction

Strong coupling of light and matter in semiconductor nanostructures gives rise to many new interesting effects, the most direct being the creation of a composite particle called exciton-polariton. This half-light, half-matter particle carrying the properties of both its origins, can demonstrate extremely rich physics, including various nonlinear spin effects, the famous Bose-Einstein condensation (BEC), predicted long ago but observed only very recently, and maybe even the superfluidity.

The coupling of light and matter itself has been studied for several decades (starting from the seminal paper by J.J. Hopfield, 1958), and quite extensively, but all the effects that may come out of it have not been discovered yet neither theoretically nor experimentally. The properties of exciton-polaritons are so unusual that it has been foretold that the BEC, observed for atoms at the temperatures of the order of nanokelvins, can be produced even at room temperature for exciton-polaritons. For some time, since the proposal of BEC-based polariton lasers by A. Imamoglu *et al* (1996) and the proposal of room-temperature polariton lasers by G. Malpuech *et al* (2002), this was rather a dream, although very tempting, but in 2006 the Grenoble group of Le Si Dang has observed the BEC of polaritons in a CdTe cavity at 40 K (J. Kasprzak *et al*, 2006). Similar experiments of S. Christopoulos *et al* (2006) have demonstrated polariton lasing in a GaN cavity at room temperature. Next year, R. Balili *et al* (2007) have reported the BEC of polaritons in a GaAs cavity at 4K. These temperatures are determined by the exciton stability and by the strength of light-matter coupling in corresponding materials. Now, with these results, the topic of exciton-polaritons in microcavities becomes very hot. It is necessary to explain some existing results, and to propose the ways to obtain and use new effects.

In the first chapter of this thesis we introduce the theoretical models we will use throughout the text. We also give an introduction on linear properties of microcavities in the framework of the transfer matrix formalism. The full theoretical description of the non-linear effects which are of the topical interest nowadays can be done only using the quantum kinetic theory and density matrix formalism. Since the complete density matrix of the quantum system we are dealing with would be too complicated for any kind of calculations (analytic or numeric), we use two distinct limits: the Boltzmann equation and the Gross-Pitaevskii equation. The first one corresponds to the limit when any coherence is lost immediately as a result of interactions, and only diagonal elements of the density matrix are kept. The second is

the opposite: only coherent processes are taken into account, and no loss of coherence can be described.

Which parameters determine the possibility of the BEC of polaritons? How the existing structures should be improved? Which structures are best suitable for manufacturing an effective room-temperature polariton laser? These practical questions we answer in chapter 2, using the Boltzmann equations to simulate polariton relaxation in different GaN-based microcavities. We plot the kinetic phase diagrams of GaN microcavities, showing the regions in which they can operate as polariton lasers.

The polaritonic nonlinear effects have already been studied for a long time. The optical (or polariton) parametric oscillator configuration with three macroscopically occupied states has proven to be very interesting, demonstrating rich polarization dynamics. It was in this configuration that the bosonic nature of polaritons has been proven clearly for the first time by P.G. Savvidis *et al* (2000). In chapter 3 we present the model based on spin-dependent Boltzmann equations, and demonstrate its power by simulating three different experiments involving polarization effects. We reproduce such effects as polarization rotation due to the TE-TM splitting, the self-induced Larmor precession, and the polarization inversion. The model proves to be extremely useful, allowing description of all polarization experiments, even the dynamic ones.

Once the polariton condensates have been obtained, it becomes even more important to study their properties. Chapter 4 is devoted to spatial propagation of polaritons and polarization effects. We first demonstrate a simple analytical model that can be used to describe polariton propagation in the linear case, and then compare it with the behavior of polariton condensate, describing it with the Gross-Pitaevskii equation. We also consider a resonantly-pumped macroscopically occupied polariton mode, analyze its stability and calculate the dispersions of the excitations taking into account the polarization degree of freedom, which leads to completely new effects with potentially rich applications such as the multistability of polariton system. We demonstrate that even in a system with pump and decay linear dispersion of excitations leading to superfluidity of polaritons can be observed at particular conditions.

One intriguing question that has not yet been answered is the following. The BEC of weakly interacting particles had been usually associated with superfluidity, because the Bogoliubov dispersion of the weakly-interacting Bose gas satisfies the Landau criterion of superfluidity. However, none of the groups reporting the BEC of polaritons have observed linear dispersion and superfluidity. In the last chapter we propose the explanation to be that

the Bose-glass phase is formed in the reported experiments due to the disorder. We study the transition between the Bose glass and superfluid phases of polaritons and find the thresholds for polariton superfluidity in cavities of two different types: CdTe (less disordered, but smaller light-matter interaction) and GaN (more disordered, but stronger light-matter interaction). In both cases the thresholds turn out to be accessible, though close to the border of the strong coupling regime.

Chapter 1. Mathematical tools and the exciton-polaritons

In this chapter we give an introduction on exciton-polaritons in planar microcavities. We then introduce the general mathematical tools that will be used afterwards for the description of exciton-polaritons in various conditions. The most general description of the evolution of a quantum system is given by its density matrix. However, for such a complex system as exciton-polaritons in a microcavity, the equation for the density matrix for most of the problems would be impossible to treat analytically or numerically. Therefore, simplifying assumptions have to be taken. We work in two opposite limits: completely incoherent, but allowing to describe relaxation (Boltzmann equations) and completely coherent, but not allowing to include relaxation processes (Gross-Pitaevskii equation).

Contents

1.1. Microcavity exciton-polaritons

The exciton-polariton or simply polariton, as we will call it throughout the thesis, is a composite quasiparticle consisting of a photon and an exciton (which is a composite particle itself). A cavity polariton is formed in a quantum microcavity, which consists of an active layer (e.g.

quantum well) sandwiched between mirrors. The mirrors are usually distributed Bragg reflectors (DBR), consisting of a series of $\lambda/4$ layers with high and low refractive indices. The polariton is only formed when the microcavity operates in the strong coupling regime (when the interaction between photon and exciton is larger than any dephasing). The strong coupling was first observed by Claude Weisbuch *et al* (1992). Polaritons are good bosons; their bosonic nature has been clearly demonstrated experimentally for the first time by P.G. Savvidis *et al* (2000).The most unusual property of a polariton is its dispersion, which is strongly non-parabolic. The particular shape of the dispersion depends on many parameters, including the detuning (the difference between the photon and exciton energy levels). The effective mass of a polariton in the vicinity of the ground state of dispersion is very light, close to that of a cavity photon ($m_{pol} \cong 5\times10^{-5} m_e$, where m_e is the free electron mass). This particular property is very important for Bose condensation, since it makes the theoretical threshold density for exciton-polaritons condensation about 10^5 times lower than that of excitons. This allows to expect Bose condensation of polaritons at much higher temperatures than it could be possible for excitons. Indeed, the Bose condensation of polaritons has been observed very recently in CdTe by J. Kasprzak *et al* (2006), in GaN by S. Christopoulos *et al* (2007), and in GaAs by R. Balili *et al* (2007). These works are published in the most well-known scientific journals (Nature, Physical Review Letters, Science), which demonstrates that the topic is currently very hot.

1.1.1. Two-oscillator description of strong coupling

The classical polariton dispersion can be obtained from a simple two-oscillator model by diagonalization of a Hamiltonian. We will show an example with only a single excitonic state here:

$$H(\mathbf{k}) = \begin{pmatrix} E_X(\mathbf{k}) & \hbar\Omega \\ \hbar\Omega & E_C(\mathbf{k}) \end{pmatrix} \tag{1.1}$$

Here $E_X(\mathbf{k})$ is the exciton dispersion with an effective mass of the order of m_e and $E_C(\mathbf{k})$ is the photon dispersion with an effective mass of the order of $10^{-5} m_e$.

The eigenvalues of this matrix are given by

$$\det(\mathbf{M} - \lambda\mathbf{I}) = 0 \Leftrightarrow (E_X - \lambda)(E_C - \lambda) - \hbar^2\Omega^2 = 0 \tag{1.2}$$

The solutions of this equation are :

$$\begin{aligned} E_U(k) &= \frac{E_C(k) + E_X(k)}{2} + \frac{1}{2}\sqrt{\left(E_C(k) - E_X(k)\right)^2 + 4\hbar^2\Omega^2} \\ E_L(k) &= \frac{E_C(k) + E_X(k)}{2} - \frac{1}{2}\sqrt{\left(E_C(k) - E_X(k)\right)^2 + 4\hbar^2\Omega^2} \end{aligned} \tag{1.3}$$

where E_U and E_L are the energies of the upper and lower polariton branches, respectively.

To find one of the eigenvectors, we look for the solutions of

$$\begin{pmatrix} E_X(\mathbf{k}) & \hbar\Omega \\ \hbar\Omega & E_C(\mathbf{k}) \end{pmatrix} \begin{pmatrix} X_U(k) \\ C_U(k) \end{pmatrix} = E_U(k) \begin{pmatrix} X_U(k) \\ C_U(k) \end{pmatrix} \tag{1.4}$$

with the normalization condition $X_U^2 + C_U^2 = 1$. The solution is :

$$\begin{aligned} C_U &= \frac{E_U - E_X}{\sqrt{\hbar^2\Omega^2 + (E_U - E_X)^2}} \\ X_U &= \frac{\hbar^2\Omega^2}{\sqrt{\hbar^2\Omega^2 + (E_U - E_X)^2}} \end{aligned} \tag{1.5}$$

The same procedure for the second eigenvector gives :

$$X_L = C_U, C_L = -X_U \tag{1.6}$$

where $X_{L(U)}$ and $C_{L(U)}$ are the Hopfield coefficients for the upper (lower) polariton branch.

An example of dispersion for a microcavity with GaN quantum wells obtained using Eq. (1.3) is shown in figure 1.1. The parameters for this calculation are given in section 2.1.2. The non-parabolicity of the lower polariton branch is clearly visible.

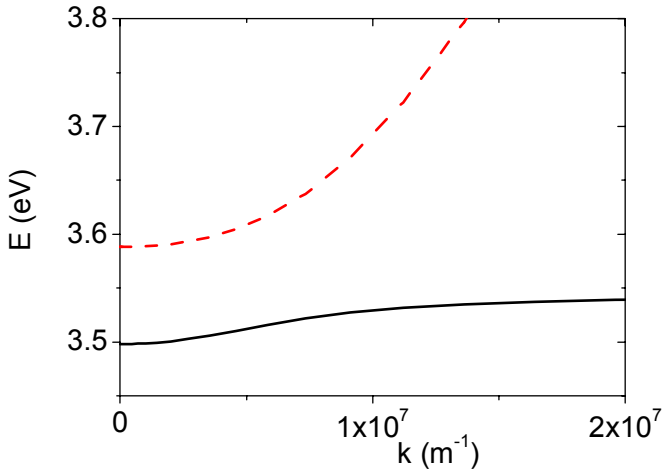

Figure 1.1. Dispersion of a GaN microcavity with QWs. The typical non-parabolicity is clearly visible. Rabi splitting is 90 meV.

In a more complicated case the energies of the excitonic and photonic modes can include imaginary parts, which allows to account for dissipative processes. In case of spatial dispersion of excitonic resonances, one has to write an implicit dispersion equation, like discussed by J. Lagois (1977). In our case, we do not need to use this approximation.

1.1.2. Transfer matrix method applied to DBR

Another powerful method which allows to calculate the optical properties of a Bragg mirror or of a microcavity as a whole is the transfer matrix method. The idea of the method is to represent the effect of each layer on the electromagnetic wave passing through this layer by a matrix, and the wave itself by a vector, its components being the components of the electromagnetic field (E_τ and H_τ). It is convenient to use the tangential component basis E_τ, H_τ for s-polarization and H_τ, E_τ for p-polarization. We follow the method described by A. Kavokin and G. Malpuech (2003).

One can write the transfer matrix across a layer of a thickness *a* with refractive index *n*:

$$T = \begin{bmatrix} \cos ka & in^{-1}\sin ka \\ in\sin ka & \cos ka \end{bmatrix} \tag{1.7}$$

where *k* is the wavevector of light in corresponding material. The transfer matrix of several layers is a product of their transfer matrices. For an infinite Bragg mirror one can write the dispersion equation involving a transfer matrix of a period of the mirror:

$$\cos Q(a+b) = (T_{11} + T_{22})/2 \tag{1.8}$$

where Q is the effective wave-vector of light in the mirror and *a*, *b* are the respective thicknesses of the two layers. Real Q solutions form allowed bands and complex Q solutions form photonic gaps or stop-bands.

At the central frequency of the stop-band the transfer matrix of the mirror period becomes:

$$T = \begin{bmatrix} -n_a/n_b & 0 \\ 0 & -n_b/n_a \end{bmatrix} \tag{1.9}$$

The reflection coefficient is obtained from the condition

$$T\begin{bmatrix} 1+r \\ n_0(1-r) \end{bmatrix} = -\frac{n_a}{n_b}\begin{bmatrix} 1+r \\ n_0(1-r) \end{bmatrix} \tag{1.10}$$

where n_0 is the refraction coefficient of the medium (vacuum).

In the vicinity of the stop-band center $\bar{\omega} = 2\pi c/\bar{\lambda}$ one can linearize the matrix T as a function of $\omega - \bar{\omega}$ and obtain the following expression for the reflection coefficient:

$$r = \exp\left(i\frac{n_a n_b \bar{\lambda}}{2n_0(n_b - n_a)c}(\omega - \bar{\omega}) \right) \tag{1.11}$$

The coefficient

$$L_{DBR} = \frac{n_a n_b \bar{\lambda}}{2(n_b - n_a)} \tag{1.12}$$

is called the effective length of a Bragg mirror.

In the case of oblique incidence the transfer matrices are modified and become different for s- and p-polarizations. S-polarization is also called TE (transverse electric) and corresponds to electric field of light wave oscillating in the plane, whereas p-polarization (TM or transverse magnetic) corresponds to magnetic field being in the plane. The expression for the reflection coefficient can be obtained in the following form:

$$r_{s,p} = \bar{r}_{s,p} \exp\left(i \frac{n_c}{c} L_{DBR}^{s,p} \cos\varphi_0 \left(\omega - \bar{\omega}_{s,p} \right) \right) \tag{1.13}$$

where for s-polarization

$$\bar{r}_s = \left(1 - 4 \frac{n_f}{n_0} \frac{\cos\varphi_f}{\cos\varphi_0} \left(\frac{n_a \cos\varphi_a}{n_b \cos\varphi_b} \right)^{2N} \right)^{1/2} \tag{1.14}$$

$$\bar{\omega}_s = \frac{\pi c}{2(a+b)} \frac{n_a \cos\varphi_a + n_b \cos\varphi_b}{n_a n_b \cos\varphi_a \cos\varphi_b} \tag{1.15}$$

$$L_{DBR}^s = \frac{2 n_a^2 n_b^2 (a+b) \cos^2\varphi_a \cos^2\varphi_b}{n_0^2 \left(n_b^2 - n_a^2 \right) \cos^2\varphi_0} \tag{1.16}$$

where N is the number of periods in a finite mirror, φ_0 is the incidence angle, $\varphi_{a,b}$ are the propagation angles in the layers with refractive indices $n_{a,b}$, and φ_f is the propagation angle in the material behind the mirror which has a refractive index n_f. They are linked by the Snell-Descartes law:

$$n_0 \sin\varphi_0 = n_a \sin\varphi_a = n_b \sin\varphi_b = n_f \sin\varphi_f \tag{1.17}$$

In p-polarization :

$$\bar{r}_p = \left(1 - 4 \frac{n_f}{n_0} \frac{\cos\varphi_0}{\cos\varphi_f} \left(\frac{n_a \cos\varphi_b}{n_b \cos\varphi_a} \right)^{2N} \right)^{1/2} \tag{1.18}$$

$$\bar{\omega}_p = \frac{\pi c}{2} \frac{n_a \cos\varphi_b + n_b \cos\varphi_a}{n_a n_b \left(a \cos^2\varphi_a + b \cos^2\varphi_b \right)} \tag{1.19}$$

$$L_{DBR}^p = \frac{2 n_a^2 n_b^2 \left(a \cos^2\varphi_a + b \cos^2\varphi_b \right)}{n_0^2 \left(n_b^2 \cos^2\varphi_a - n_a^2 \cos^2\varphi_b \right)} \tag{1.20}$$

The optical TE-TM splitting, which is the difference between the eigenmodes of a cavity in two different polarizations, originates from the difference in the above effective DBR lengths and reflectivities. The exact expression for this splitting will be given below.

1.1.3. Light-matter interaction in a quantum well

We will describe the optical properties of a quantum well following the non-local dielectric response theory developed in the end of 1980s by L.C. Andreani, F. Tassone, F. Bassani (1991) and E.L. Ivchenko (1991) as it is given in the textbook of A. Kavokin and G. Malpuech (2003). This theory is based on the assumption that the exciton-induced dielectric polarization can be written in the form:

$$4\pi P_{exc}(z) = \int_{-\infty}^{\infty} \chi(z,z') E(z') dz' \tag{1.21}$$

where

$$\chi(z,z') = \tilde{\chi}(\omega)\Phi(z)\Phi(z') \tag{1.22}$$

with

$$\chi(\omega) = \frac{Q}{\omega_0 - \omega - i\gamma}, Q = \varepsilon_B \omega_{LT} \pi a_B^3 \tag{1.23}$$

Here $\Phi(z)$ is the exciton wave-function taken with equal electron and hole coordinates (z), ω is the frequency of the incident light, γ is the homogeneous broadening of the exciton resonance caused by the acoustic phonons, for example, and ω_{LT} and a_B are two intrinsic excitonic parameters called longitudinal-transverse (LT) splitting and Bohr radius. The Bohr radius in GaAs is 150 A, whereas in wide-bandgap semiconductors it can be as low as 30 A.

The exciton LT splitting ω_{LT} is a measure of the exciton-light coupling strength in bulk semiconductors. The reason is the following (considering cubic crystals for simplicity): at k=0, there is no distinction between longitudinal and transverse excitons. Hence, optically active states must be threefold degenerate at k=0. If the interaction with radiation is neglected, longitudinal and transverse excitons are found to be split by the long-range part of the exchange interaction. Hence the interaction with the radiation field must compensate for this splitting, by shifting the energy of the transverse exciton at k=0 by an amount exactly equal to ω_{LT}. The quantitative relation between the LT splitting and oscillator strength reads:

$$\omega_{LT} = \frac{2\pi}{\varepsilon_\infty} \frac{\hbar e^2}{m_0 \omega_0} \frac{f}{V} \tag{1.24}$$

where ω_0 is the energy of the exciton resonance and f is the oscillator strength.

For the ground exciton state in GaAs $\hbar\omega_{LT} = 0.08\,\text{meV}$, while in wide-bandgap materials (GaN, ZnO) it is an order of magnitude larger.

Using the above expression (1.21) for polarization, one can solve the Maxwell's equation and find the reflection and transmission coefficients of the QW. We will not detail this procedure. Finally, one obtains in the case of normal incidence of light,

$$r(\omega)=\frac{i\Gamma_0}{\tilde{\omega}_0-\omega-i(\Gamma_0+\gamma)} \tag{1.25}$$

$$t(\omega)=1+r(\omega) \tag{1.26}$$

where

$$\Gamma_0=\frac{Qk_0}{2\sqrt{\varepsilon_B}}\left(\int\Phi(z)\cos kz\,dz\right)^2 \tag{1.27}$$

is an important characteristic called exciton radiative broadening and

$$\tilde{\omega}_0=\omega_0+\frac{Qk_0}{2\sqrt{\varepsilon_B}}\iint dzdz'\Phi(z)\Phi(z)\sin k|z-z'| \tag{1.28}$$

The radiative broadening Γ_0 is connected with the exciton radiative lifetime τ by the relation

$$\tau=\frac{1}{2\Gamma_0} \tag{1.29}$$

This radiative lifetime is about 10 ps in typical GaAs-based QWs.

At oblique incidence these results are modified, because the Maxwell's equations become more complicated. We will present the resulting expressions for the reflection and transmission coefficients in order to have a complete description of quantum well interaction with electromagnetic field:

$$r_s(\omega)=\frac{i\tilde{\Gamma}_0}{\tilde{\omega}_0-\omega-i(\tilde{\Gamma}_0+\gamma)} \tag{1.30}$$

$$t_s(\omega)=1+r_s(\omega) \tag{1.31}$$

where $\tilde{\Gamma}_0=\Gamma_0/\cos\varphi$, and for the p-polarization case :

$$r_p(\omega)=p_0(\omega)-p_1(\omega),\ t_p(\omega)=1+p_0+p_1 \tag{1.32}$$

where

$$p_0=\frac{i\tilde{\Gamma}_x\cos\varphi}{\omega_0-\omega-i(\tilde{\Gamma}_x\cos\varphi+\gamma)} \tag{1.33}$$

$$p_1=\frac{i\tilde{\Gamma}_x\left(\cos^{-1}\varphi-\cos\varphi\right)}{\omega_0+\Delta\omega-\omega-i\left(\tilde{\Gamma}_z\left(\cos^{-1}\varphi-\cos\varphi\right)+\gamma\right)} \tag{1.34}$$

with

$$\tilde{\Gamma}_x=\Gamma_0\cos\varphi \tag{1.35}$$

$$\tilde{\Gamma}_z=\Gamma_0\frac{\sin^2\varphi}{\cos\varphi} \tag{1.36}$$

$$\Delta\omega \approx \omega_{LT}\pi a_B^3 \int \Phi^2(z)\,dz \tag{1.37}$$

The parameters $\tilde{\Gamma}_{x,z}$ are proportional to the oscillator strength of excitons polarized parallel and normal to the interface, correspondingly, and $\Delta\omega$ is the splitting between these states. The normal component is zero for heavy hole excitons, as it follows from the interband selection rules.

In a similar way one can analyse the optical response of several quantum wells.

1.1.4. Microcavity with a QW

Let us consider a symmetric microcavity with a single QW in the center. The transfer matrix approach consists in representing each layer (or set of layer) by its transfer matrix. This can be done for a QW since its reflection and transmission coefficients have been determined in the previous section. The transfer matrix of the QW is, therefore:

$$T_{QW} = \frac{1}{t}\begin{bmatrix} t^2 - r^2 & r \\ -r & 1 \end{bmatrix} \tag{1.38}$$

The transfer matrix across the cavity with the QW inside is a product :

$$T_c = \begin{bmatrix} e^{ikL_c/2} & 0 \\ 0 & e^{-ikL_c/2} \end{bmatrix} \frac{1}{t}\begin{bmatrix} t^2 - r^2 & r \\ -r & 1 \end{bmatrix} \begin{bmatrix} e^{ikL_c/2} & 0 \\ 0 & e^{-ikL_c/2} \end{bmatrix} \tag{1.39}$$

To find the eigenfrequencies of the exciton-polariton modes of a microcavity one should search for non-trivial solution of Maxwell's equations under the requirement of no light incident from outside the cavity. This yields

$$T_c \begin{bmatrix} r_B \\ 1 \end{bmatrix} = A \begin{bmatrix} 1 \\ r_B \end{bmatrix} \tag{1.40}$$

where r_B is the angular-dependent reflection coefficient of the Bragg mirrors for the light incident from inside the cavity and A is a constant.

Excluding A from the system (1.40) one can write the explicit dispersion equation:

$$\frac{-\frac{r}{t}r_B + \frac{1}{t}e^{-ikL_c}}{\frac{r}{t} + \frac{t^2 - r^2}{t}e^{ikL_c}r_B} = r_B \tag{1.41}$$

This dispersion equation can be represented in the following form:

$$\left(r_B(2r+1)e^{ikL_c} - 1\right)\left(r_B e^{ikL_c} + 1\right) = 0 \tag{1.42}$$

For the even modes and normal incidence using linearized expression for the Bragg mirror reflectivity

$$r_B \approx \overline{r}\left(1 + iL_{DBR}\frac{n_c}{c}(\omega - \omega_c)\right) \tag{1.43}$$

one can obtain the dispersion equation in its final shape

$$\left(\omega_0 - \omega - i\gamma\right)\left(\omega_c - \omega - i\gamma_c\right) = V^2 \tag{1.44}$$

where

$$\gamma_c = \frac{1-\overline{r}}{\overline{r}\,\frac{n_c}{c}\left(L_{DBR}+L_c\right)},\ V^2 = \frac{1+\overline{r}}{\overline{r}}\frac{\Gamma_0 c}{n_c\left(L_{DBR}+L_c\right)} \tag{1.45}$$

The solutions of the dispersion equation are :

$$\omega_{1,2} = \frac{\omega_0+\omega_c}{2} - \frac{i}{2}\left(\gamma+\gamma_c\right) \pm \sqrt{\left(\frac{\omega_0-\omega_c}{2}\right)^2 + V^2 - \left(\frac{\gamma-\gamma_c}{2}\right)^2 + \frac{i}{2}\left(\omega_0-\omega_c\right)\left(\gamma_c-\gamma\right)} \tag{1.46}$$

the parameter V is the strength of coupling between the cavity photon mode and the exciton resonance. If $\omega_0 = \omega_c$ the splitting of the two solutions is given by $\sqrt{4V^2 - \left(\gamma-\gamma_c\right)^2}$. If

$$V > \left|\frac{\gamma-\gamma_c}{2}\right|, \tag{1.47}$$

the system is in the strong coupling regime, characterized by two distinct exciton-polariton branches manifested as resonances in the reflection and transmission spectra. The splitting between them is referred to as vacuum-field Rabi splitting. In the opposite case the system is in the weak coupling regime, when the exciton and photon modes cross. The exciton decay rate is increased at the resonance point of the two branches.

In the general case of oblique incident light to obtain the s- and p-polarization dispersion branches one should solve equation (1.41) with angular-dependent reflection and transmission coefficients of the QW (1.30) and (1.32), and with the angular-dependent reflection coefficients for the Bragg mirrors (1.14) and (1.18).

1.1.5. Optical TE-TM splitting

An approximate analytical expression for the TE-TM splitting in a microcavity with a QW has been given in the paper of Panzarini *et al* (1999). The splitting of an empty cavity is given by

$$\Omega_{LT} \approx \frac{L_c L_{DBR}}{\left(L_c + L_{DBR}\right)^2}\frac{2\cos\varphi_{eff}\sin^2\varphi_{eff}}{1-2\sin^2\varphi_{eff}}\Delta \tag{1.48}$$

where $\varphi_{eff} \approx \arcsin\frac{\sin\varphi_0}{n_c}$, $L_{DBR} \equiv \frac{n_a n_b \pi c}{\left(n_b - n_a\right)\omega_B}$, φ_0 is the incidence angle in vacuum, L_c is the cavity width, $n_{a,b}$ are the refractive indices of the layers composing the DBRs, n_c is the refractive index of the cavity, ω_B is the central frequency of the optical stop-band of the DBRs, and $\Delta = \omega_B - \omega_c$ is the difference between the cavity-mode eigenfrequency at normal incidence ω_c and ω_B. Eq. (1.48) predicts a quadratic dependence of the splitting of the eigen-energies of bare photon

modes of the cavity on the incidence angle. This splitting gives rise to an effective magnetic field in the coherent part of the spin-dependent Boltzmann equations (1.74) and to rotation of the pseudospin vector around the corresponding axis.

1.2. Boltzmann equation

The kinetic Boltzmann equation has been derived by Ludwig Boltzmann in 1872, it is one of the basic equations of physical kinetics. The Boltzmann equation describes the time evolution of the distribution function. An equilibrium distribution satisfies the Boltzmann equation automatically, and any non-equilibrium distribution has a tendency to evolve into an equilibrium distribution, which is why one can say that the Boltzmann equiation describes the *relaxation* dynamics of classical particles.

In the first subsection we will show the derivation of a Boltzmann equation for classical particles (i.e. ideal gas). In the next subsection it will be demonstrated how a Boltzmann-type equation can be derived from a quantum Hamiltonian of interacting bosons without spin.

1.2.1. Boltzmann equation for classical particles

Let us consider a distribution function $f(t,\mathbf{r},\Gamma)$ where t is the time parameter, $\mathbf{r}$ is the set of space coordinates and Γ are the generalized coordinates describing the particle parameters that are not changing between scatterings (like particle momenta for a monoatomic gas). We follow the procedure from E.M. Lifshitz and L.P. Pitaevskii (1980) here.

Without interactions the distribution function obeys the Liouville theorem, which states that:

$$\frac{df}{dt}=0 \tag{1.49}$$

In the absence of external field one can take into account the conservation of the coordinates Γ and write:

$$\frac{df}{dt}=\frac{\partial f}{\partial t}+\mathbf{v}\nabla f \tag{1.50}$$

where $\mathbf{v}$ is the particle velocity. Taking into account the interactions, this equation changes into

$$\frac{df}{dt}=\mathrm{St}\,f \tag{1.51}$$

where $\mathrm{St}\,f$ is the collision integral. Then, (1.50) can be rewritten as:

$$\frac{\partial f}{\partial t}=-\mathbf{v}\nabla f+\mathrm{St}\,f \tag{1.52}$$

Of course, the collision integral should be somehow defined for this equation to make sense. Let us write the total number of collisions leading to transitions $\Gamma,\Gamma_1 \to \Gamma',\Gamma_1'$ in a volume dV per unit of time:

$$dV\, d\Gamma \int \omega\left(\Gamma',\Gamma_1';\Gamma,\Gamma_1\right) ff_1 d\Gamma_1 d\Gamma' d\Gamma_1' \tag{1.53}$$

where ω is the transition probability. Then let us write the transitions into $d\Gamma$ from outside: $\Gamma',\Gamma_1' \to \Gamma,\Gamma_1$. The total number of collisions leading to these transitions will be

$$dV\, d\Gamma \int \omega\left(\Gamma,\Gamma_1;\Gamma',\Gamma_1'\right) f'f_1' d\Gamma_1 d\Gamma' d\Gamma_1' \tag{1.54}$$

The difference of (1.53) and (1.54) is the change of the number of particles in $dVd\Gamma$ due to collisions per unit of time:

$$\mathrm{St}\, f = \int \left(\omega' f'f_1' - \omega ff_1\right) d\Gamma_1 d\Gamma' d\Gamma_1' \tag{1.55}$$

The second term in (1.55) can be rewritten using the condition of microscopic reversibility of transitions (this was first done by E.C.G. Stuckelberg, 1952), after which the collision integral obtains its final form:

$$St\, f = \int \omega' \left(f'f_1' - ff_1\right) d\Gamma_1 d\Gamma' d\Gamma_1' \tag{1.56}$$

and we can write the classical kinetic Boltzmann equation:

$$\frac{\partial f}{\partial t} + \mathbf{v}\nabla f = \int \omega' \left(f'f_1' - ff_1\right) d\Gamma_1 d\Gamma' d\Gamma_1' \tag{1.57}$$

It is assumed here that the interactions of the particles are immediate. Therefore, this equation can be used to describe the evolution of a system on a time scale longer than the characteristic time of a single interaction. Any kinetic equation for a distribution function that has the shape (1.52) or (1.57) is usually called Boltzmann equation.

1.2.2. Semi-classical Boltzmann equations for bosons and fermions

A derivation of the semi-classical Boltzmann equation from the microscopic Hamiltonian is given in Appendix I. Uhlenbeck and Gropper (1932) first proposed to include the quantum character of particles involved, taking into account their fermionic or bosonic nature. The semi-classical Boltzmann equation for bosons reads:

$$\frac{dn_{\mathbf{k}}}{dt} = P_{\mathbf{k}} - \Gamma_{\mathbf{k}} n_{\mathbf{k}} - n_{\mathbf{k}} \sum_{\mathbf{k}'} W_{\mathbf{k}\to\mathbf{k}'} \left(1 + n_{\mathbf{k}'}\right) + \left(1 + n_{\mathbf{k}}\right) \sum_{\mathbf{k}'} W_{\mathbf{k}'\to\mathbf{k}} n_{\mathbf{k}'} \tag{1.58}$$

and for fermions it is modified the following way :

$$\frac{dn_{\mathbf{k}}}{dt} = P_{\mathbf{k}} - \Gamma_{\mathbf{k}} n_{\mathbf{k}} - n_{\mathbf{k}} \sum_{\mathbf{k}'} W_{\mathbf{k}\to\mathbf{k}'} \left(1 - n_{\mathbf{k}'}\right) + \left(1 - n_{\mathbf{k}}\right) \sum_{\mathbf{k}'} W_{\mathbf{k}'\to\mathbf{k}} n_{\mathbf{k}'} \tag{1.59}$$

The coefficients $(1+n_{\mathbf{k}})$ and $(1-n_{\mathbf{k}})$ describe stimulation of transitions for bosons and suppression of transitions for fermions due to increase of the occupancies of corresponding states $n_{\mathbf{k}}$.

1.3. Spin-dependent Boltzmann equations

We will start the derivation of spin-dependent semi-classical Boltzmann equations for bosons with spin 1 from the Liouville equation for the complete density matrix of the system. This has been first done by M.M. Glazov *et al* (2005). The equations we finally find are valid for any bosons interacting with the reservoir, but their form in the pseudospin representation is best suited for the description of exciton-polaritons, to which they will be applied in chapter 3.

In the interaction representation the Liouville equation reads (same as Eq. (1.1) of Appendix I):

$$i\hbar\frac{d\rho}{dt}=\left[\hat{H}(t),\rho\right] \tag{1.60}$$

where H is the time-dependent Hamiltonian of the system, in our particular case taking into account the weak interaction of bosons with each other and their interaction with reservoir:

$$\begin{aligned} H=&\sum_{\mathbf{k},\sigma}\Omega_{\mathbf{k}}a^{+}_{\mathbf{k}\sigma}a_{\mathbf{k}\sigma}+\hbar\sum_{\mathbf{k},\sigma}\omega_{\mathbf{k}}b^{+}_{\mathbf{k}}b_{\mathbf{k}}+\hbar\sum_{\mathbf{k},\sigma}\Omega_{LT,\mathbf{k}}a^{+}_{\mathbf{k}\sigma}a_{\mathbf{k}-\sigma}+\\ &+\sum_{\mathbf{k},\mathbf{q},\sigma}U_{\mathbf{k},\mathbf{q}}a^{+}_{\mathbf{k},\sigma}a_{\mathbf{k}-\mathbf{q},\sigma}\left(b_{\mathbf{q}}+b^{+}_{-\mathbf{q}}\right)+\frac{1}{4}\sum_{\mathbf{k},\mathbf{q},\sigma}\left[V^{(1)}_{\mathbf{k},\mathbf{k}',q}a^{+}_{\mathbf{k},\sigma}a^{+}_{\mathbf{k}',\sigma}a_{\mathbf{k}-\mathbf{q},\sigma}a_{\mathbf{k}'+\mathbf{q},\sigma}+2V^{(2)}_{\mathbf{k},\mathbf{k}',\mathbf{q}}a^{+}_{\mathbf{k},\sigma}a^{+}_{\mathbf{k}',-\sigma}a_{\mathbf{k}-\mathbf{q},\sigma}a_{\mathbf{k}'+\mathbf{q},-\sigma}\right]+h.c.\end{aligned} \tag{1.61}$$

Here $a_{\mathbf{k}\sigma}\left(a^{+}_{\mathbf{k}\sigma}\right)$ are the annihilation (creation) operators for the bosons with wave-vector **k** having the spin projection $\sigma=\pm1$ on the chosen axis, $b_{\mathbf{k}}$ and $b^{+}_{\mathbf{k}}$ are the operators for phonons (by which the interaction with reservoir is described), $\Omega_{\mathbf{k}}$ and $\omega_{\mathbf{k}}$ are the boson and phonon bare energies, respectively. The matrix element $U_{\mathbf{k},\mathbf{q}}$ describes the interaction of bosons and phonons, and the matrix elements $V^{(1)}_{\mathbf{k},\mathbf{k}',\mathbf{q}}$ and $V^{(2)}_{\mathbf{k},\mathbf{k}',\mathbf{q}}$ describe the scattering of bosons in triplet and singlet configurations. In the case of polaritons, this scattering is anisotropic, and $V^{(1)}\neq V^{(2)}$. The term with Ω_{LT} describes the effect of a magnetic field (LT-splitting in the case of polaritons).

We separate the Hamiltonian into two parts, as a sum of "shift" (coherent) and "scattering" (incoherent) terms. Here the "shift" term describes interaction of exciton-polaritons without wavevector transfer (**q'**=0) but having possibly different spins:

$$\begin{aligned} H_{shift}=&\sum_{\mathbf{k},\sigma=\uparrow,\downarrow}\left(\hbar\Omega_{LT,\mathbf{k}}a^{+}_{\sigma,\mathbf{k}}a_{-\sigma,\mathbf{k}}+V^{(1)}_{\mathbf{k},\mathbf{k},0}\left(a^{+}_{\sigma,\mathbf{k}}a_{\sigma,\mathbf{k}}\right)^2+V^{(2)}_{\mathbf{k},\mathbf{k},0}a^{+}_{\sigma,\mathbf{k}}a^{+}_{-\sigma,\mathbf{k}}a_{\sigma,\mathbf{k}}a_{-\sigma,\mathbf{k}}\right)+\\ &+\sum_{\mathbf{k},\mathbf{k}'\neq\mathbf{k},\sigma=\uparrow,\downarrow}\left(V^{(1)}_{\mathbf{k},\mathbf{k}',0}a^{+}_{\sigma,\mathbf{k}}a^{+}_{\sigma,\mathbf{k}'}a_{\sigma,\mathbf{k}}a_{\sigma,\mathbf{k}'}+V^{(2)}_{\mathbf{k},\mathbf{k}',0}a^{+}_{\sigma,\mathbf{k}}a^{+}_{-\sigma,\mathbf{k}'}a_{\sigma,\mathbf{k}}a_{-\sigma,\mathbf{k}'}\right)\end{aligned} \tag{1.62}$$

The "scattering" term describes scattering between states with wave vector transfer (q≠0) :

$$H_{scatt}=\frac{1}{4}\sum_{\mathbf{k},\mathbf{k}',\mathbf{q}\neq 0,\sigma=\uparrow,\downarrow} e^{\frac{it}{\hbar}\left(E(\mathbf{k})+E(\mathbf{k}')-E(\mathbf{k}+\mathbf{q})-E(\mathbf{k}'-\mathbf{q})\right)}\left\{V^{(1)}_{\mathbf{k},\mathbf{k}',\mathbf{q}}a^{+}_{\sigma,\mathbf{k}'+\mathbf{q}}a^{+}_{\sigma,\mathbf{k}'-\mathbf{q}}a_{\sigma,\mathbf{k}}a_{\sigma,\mathbf{k}'}+\right.$$
$$\left.+2V^{(2)}_{\mathbf{k},\mathbf{k}',\mathbf{q}}a^{+}_{\sigma,\mathbf{k}+\mathbf{q}}a^{+}_{-\sigma,\mathbf{k}'-\mathbf{q}}a_{\sigma,\mathbf{k}}a_{-\sigma,\mathbf{k}'}\right\}+\frac{1}{2}\sum_{\mathbf{k},\mathbf{q}\neq 0,\sigma=\uparrow,\downarrow}U_{\mathbf{k},\mathbf{q}}\left(b_{\mathbf{q}}+b^{+}_{-\mathbf{q}}\right)a^{+}_{\sigma,\mathbf{k}+\mathbf{q}}a_{\sigma,\mathbf{k}}\left(e^{\frac{it}{\hbar}\left(E(\mathbf{k})+\omega(\mathbf{k})-E(\mathbf{k}+\mathbf{q})\right)}+e^{\frac{it}{\hbar}\left(E(\mathbf{k})-\omega(-\mathbf{k})-E(\mathbf{k}-\mathbf{q})\right)}\right)+h.c. \tag{1.63}$$

We write the Liouville equation for the total density matrix of the system ρ:

$$i\hbar\frac{d\rho}{dt}=\left[H(t),\rho\right]=\left[H_{shift}(t)+H_{scatt}(t),\rho\right] \tag{1.64}$$

Eq. (1.64) can be treated within the Born-Markov approximation. The Markov approximation is, in general, not true for the coherent processes described by the Hamiltonian H_{shift}, but is a reasonable approximation for the scattering processes involving the momentum transfer. We apply the Markov approximation to the scattering part of Eq. (1.64) which therefore rewrites:

$$\frac{d\rho}{dt}=\frac{1}{i\hbar}\left[H_{shift}(t),\rho\right]-\frac{1}{\hbar^2}\int_{-\infty}^{t}\left[H_{scatt}(t),\left[H_{scatt}(\tau),\rho(\tau)\right]\right]d\tau \tag{1.65}$$

The density matrix can be factorized into the product of phonon density matrix and boson density matrices corresponding to the different states in the reciprocal space by using the Born approximation:

$$\rho=\rho_{ph}\otimes\prod_{\mathbf{k}}\rho_{\mathbf{k}} \tag{1.66}$$

The polarization effects in a simple bosonic system are conveniently described by using the pseudospin formalism if the bosons can be treated as a two-level system described by a 2x2 density matrix $\rho_{\mathbf{k}}$, which is completely analogous to the spin density matrix of electrons. It is convenient to decompose the density matrix as:

$$\boldsymbol{\rho}_{\mathbf{k}}=\frac{N_k}{2}\mathbf{I}+\mathbf{S}_{\mathbf{k}}\cdot\boldsymbol{\sigma} \tag{1.67}$$

where $\mathbf{I}$ is the identity matrix, $\boldsymbol{\sigma}$ is the Pauli-matrix vector, $\mathbf{S}_{\mathbf{k}}$ is the pseudospin of a bosonic state characterized by the wave vector $\mathbf{k}$. It corresponds to the Poincaré vector of partially polarized light (see Fig. 1.2). The common convention is to use the basis of circularly polarized states, i.e. to associate states having definite S_z with the states with the spin projection on an axis equal to ±1. These states emit circularly polarized light. Their linear combinations correspond to eigenstates of S_x and S_y yielding linearly polarized emission. The pseudospin parallel to x-axis corresponds to x-polarized light, the pseudospin antiparallel to x-axis corresponds to y-polarized light, the pseudospin oriented along y-axis describes diagonal linear polarizations.

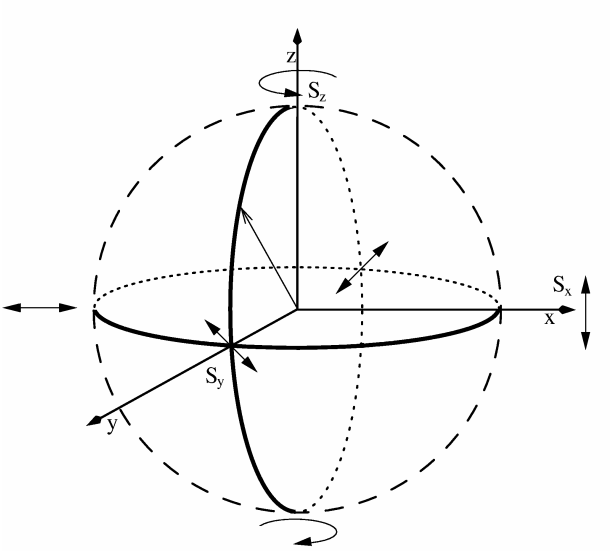

Figure 1.2. A Poincaré sphere with a pseudospin. The equator of the sphere corresponds to different linear polarisations, while the poles correspond to two circular polarisations.

If the density matrix is decomposed in the way described above, the diagonal elements of the density matrix $\rho_{\mathbf{k}}$ give the populations of the spin-up and spin-down states: $N_{\mathbf{k},\uparrow} = \mathrm{Tr}\left(a^{+}_{\mathbf{k}\uparrow} a_{\mathbf{k}\uparrow} \rho_{\mathbf{k}}\right)$, $N_{\mathbf{k},\downarrow} = \mathrm{Tr}\left(a^{+}_{\mathbf{k}\downarrow} a_{\mathbf{k}\downarrow} \rho_{\mathbf{k}}\right)$, and the off-diagonal components are linked with the in-plane projection of the pseudospin $S_{\perp,\mathbf{k}} = S_{x,\mathbf{k}}\mathbf{e}_x + S_{y,\mathbf{k}}\mathbf{e}_y$ in the following way: $S_{x,\mathbf{k}} - iS_{y,\mathbf{k}} = \mathrm{Tr}\left(a^{+}_{\mathbf{k}\uparrow} a_{\mathbf{k}\downarrow} \rho_k\right)$. Here $\mathbf{e}_x$ and $\mathbf{e}_y$ are the unit vectors in the cavity plane. The difference with the results from section 1.1.2 is that we did not trace out the pseudospins, thus keeping information on the polarization.

Finally, a Lindblad-type equation for the polariton density matrix can be obtained, which allows the derivation of the spin-dependent Boltzmann equations for the boson occupation numbers and in-plane projections of their pseudospins. These equations will be written explicitly in the following subsections.

1.3.1. Interactions with acoustic phonons

The dynamics with acoustic phonons is given by the following expression:

$$\left(\frac{dN_{\mathbf{k}\uparrow,\downarrow}}{dt}\right)\Bigg|_{phon} = \sum_{\mathbf{k}'}\Big[\left(W_{\mathbf{k}'\mathbf{k}} - W_{\mathbf{k}\mathbf{k}'}\right)\left(N_{\mathbf{k}\uparrow,\downarrow}N_{\mathbf{k}'\uparrow,\downarrow} + \left(\mathbf{S}_{\mathbf{k}}.\mathbf{S}_{\mathbf{k}'}\right)\right) + \left(W_{\mathbf{k}'\mathbf{k}}N_{\mathbf{k}'\uparrow,\downarrow} - W_{\mathbf{k}\mathbf{k}'}N_{\mathbf{k}\uparrow,\downarrow}\right)\Big] \quad (1.68)$$

$$\left(\frac{d\mathbf{S}_{\perp,\mathbf{k}}}{dt}\right)\Bigg|_{phon} = \sum_{\mathbf{k}'}\left[\frac{1}{2}\left(W_{\mathbf{k}'\mathbf{k}} - W_{\mathbf{k}\mathbf{k}'}\right)\left(\left(N_{\mathbf{k}\uparrow} + N_{\mathbf{k}\downarrow}\right)\mathbf{S}_{\perp,\mathbf{k}'} + \left(N_{\mathbf{k}'\uparrow} + N_{\mathbf{k}'\downarrow}\right)\mathbf{S}_{\perp,\mathbf{k}}\right) + \left(W_{\mathbf{k}'\mathbf{k}}\mathbf{S}_{\perp,\mathbf{k}'} - W_{\mathbf{k}\mathbf{k}'}\mathbf{S}_{\perp,\mathbf{k}}\right)\right] \quad (1.69)$$

where the scattering rates W are

$$W_{\mathbf{k}\mathbf{k}'} = \begin{cases} \dfrac{2\pi}{\hbar}\left|V_{\mathbf{k},\mathbf{k}'\text{-}\mathbf{k}}\right|^2 n_{ph,\mathbf{k}'\text{-}\mathbf{k}}\,\delta\left(\Omega_{\mathbf{k}'} - \Omega_{\mathbf{k}} - \omega_{\mathbf{k}'\text{-}\mathbf{k}}\right), |\mathbf{k}'| > |\mathbf{k}| \\ \dfrac{2\pi}{\hbar}\left|V_{\mathbf{k},\mathbf{k}'\text{-}\mathbf{k}}\right|^2 \left(n_{ph,\mathbf{k}'\text{-}\mathbf{k}} + 1\right)\delta\left(\Omega_{\mathbf{k}'} - \Omega_{\mathbf{k}} - \omega_{\mathbf{k}'\text{-}\mathbf{k}}\right), |\mathbf{k}'| < |\mathbf{k}| \end{cases} \quad (1.70)$$

The Dirac delta functions in (1.70) account for the energy conservation during any scattering act. Mathematically they appear from integration of the time-dependent exponents in (1.65). In numerical calculations, the delta functions should be replaced by resonant functions having finite amplitudes proportional to the inverse energy broadenings of corresponding states.

1.3.2. Interaction with bosons

The part describing the interactions between the bosons reads

$$\begin{aligned} \frac{dN_{\mathbf{k}\uparrow}}{dt} = \sum_{\mathbf{k}',\mathbf{k}''}\Big\{ & W^{(1)}_{\mathbf{k},\mathbf{k}',\mathbf{k}''}\Big[(N_{\mathbf{k}\uparrow} + N_{\mathbf{k}'\uparrow} + 1)N_{\mathbf{k}+\mathbf{k}''\uparrow}N_{\mathbf{k}'-\mathbf{k}''\uparrow} - (N_{\mathbf{k}+\mathbf{k}''\uparrow} + N_{\mathbf{k}'-\mathbf{k}''\uparrow} + 1)N_{\mathbf{k}\uparrow}N_{\mathbf{k}'\uparrow}\Big] + \\ & + W^{(2)}_{\mathbf{k},\mathbf{k}',\mathbf{k}''}\Big[(N_{\mathbf{k}\uparrow} + N_{\mathbf{k}'\downarrow} + 1)(N_{\mathbf{k}+\mathbf{k}''\uparrow}N_{\mathbf{k}'-\mathbf{k}''\downarrow} + N_{\mathbf{k}+\mathbf{k}''\downarrow}N_{\mathbf{k}'-\mathbf{k}''\uparrow} + 2\left(\mathbf{S}_{\perp,\mathbf{k}+\mathbf{k}''}\cdot\mathbf{S}_{\perp,\mathbf{k}'-\mathbf{k}''}\right)) - \\ & (N_{\mathbf{k}\uparrow}N_{\mathbf{k}'\downarrow} + \left(\mathbf{S}_{\perp,\mathbf{k}}\cdot\mathbf{S}_{\perp,\mathbf{k}'}\right))(N_{\mathbf{k}+\mathbf{k}''\uparrow} + N_{\mathbf{k}'-\mathbf{k}''\downarrow} + N_{\mathbf{k}+\mathbf{k}''\downarrow} + N_{\mathbf{k}'-\mathbf{k}''\uparrow} + 2)\Big] + \\ & + 2W^{(12)}_{\mathbf{k},\mathbf{k}',\mathbf{k}''}\Big[N_{\mathbf{k}''\uparrow}(\mathbf{S}_{\perp,\mathbf{k}'}\cdot\mathbf{S}_{\perp,\mathbf{k}'-\mathbf{k}''}) + N_{\mathbf{k}'-\mathbf{k}''\uparrow}(\mathbf{S}_{\perp,\mathbf{k}'}\cdot\mathbf{S}_{\perp,\mathbf{k}+\mathbf{k}''}) - N_{\mathbf{k}\uparrow}\mathbf{S}_{\perp,\mathbf{k}'}\cdot(\mathbf{S}_{\perp,\mathbf{k}'-\mathbf{k}''} + \mathbf{S}_{\perp,\mathbf{k}+\mathbf{k}''})\Big] + \\ & + W^{(12)}_{\mathbf{k},\mathbf{k}',\mathbf{k}''}[(\mathbf{S}_{\perp,\mathbf{k}}\cdot\mathbf{S}_{\perp,\mathbf{k}+\mathbf{k}''})(N_{\mathbf{k}'-\mathbf{k}''\uparrow} + N_{\mathbf{k}'-\mathbf{k}''\downarrow} - N_{\mathbf{k}'\uparrow} - N_{\mathbf{k}'\downarrow}) + (\mathbf{S}_{\perp,\mathbf{k}}\cdot\mathbf{S}_{\perp,\mathbf{k}'-\mathbf{k}''})(N_{\mathbf{k}+\mathbf{k}''\uparrow} + N_{\mathbf{k}+\mathbf{k}''\downarrow} - N_{\mathbf{k}'\uparrow} - N_{\mathbf{k}'\downarrow})]\Big\} \end{aligned} \quad (1.71)$$

Let us look into the physical meaning of different terms in (1.71). First term with $W^{(1)}_{\mathbf{k},\mathbf{k}',\mathbf{k}''}$ describes scattering of bosons with the same spin taking into account bosonic stimulation. Second term with $W^{(2)}_{\mathbf{k},\mathbf{k}',\mathbf{k}''}$ describes scattering of bosons with opposite spins with all possible combinations. The scalar product of the in-plane pseudospin components $\left(\mathbf{S}_{\perp,\mathbf{k}}\cdot\mathbf{S}_{\perp,\mathbf{k}'}\right)$ accounts for the polarization sensitivity of scattering. Third and fourth terms with $W^{(12)}_{\mathbf{k},\mathbf{k}',\mathbf{k}''}$ describe polarization-dependent effects when two bosons with the same spin are interacting at the same time with two bosons having opposite spins. The equations for $N_{\downarrow}$ are obtained by replacing $\uparrow$ by $\downarrow$ and vice versa.

$$
\begin{aligned}
&\frac{d\mathbf{S}_{\perp,\mathbf{k}}}{dt} = \\
&= \sum_{\mathbf{k}',\mathbf{k}''} \Bigg\{ \frac{W^{(1)}_{\mathbf{k},\mathbf{k}',\mathbf{k}''}}{2} \mathbf{S}_{\perp,\mathbf{k}} \left[N_{\mathbf{k}+\mathbf{k}''\uparrow} N_{\mathbf{k}'-\mathbf{k}''\uparrow} + N_{\mathbf{k}+\mathbf{k}''\downarrow} N_{\mathbf{k}'-\mathbf{k}''\downarrow} - N_{\mathbf{k}'\uparrow} (N_{\mathbf{k}+\mathbf{k}''\uparrow} + N_{\mathbf{k}'-\mathbf{k}''\uparrow} + 1) - N_{\mathbf{k}'\downarrow} (N_{\mathbf{k}+\mathbf{k}''\downarrow} + N_{\mathbf{k}'-\mathbf{k}''\downarrow} + 1) \right] + \\
&+ W^{(1)}_{\mathbf{k},\mathbf{k}',\mathbf{k}''} \left(\mathbf{S}_{\perp,\mathbf{k}+\mathbf{k}''} (\mathbf{S}_{\perp,\mathbf{k}'} \cdot \mathbf{S}_{\perp,\mathbf{k}'-\mathbf{k}''}) + \mathbf{S}_{\perp,\mathbf{k}'-\mathbf{k}''} (\mathbf{S}_{\perp,\mathbf{k}'} \cdot \mathbf{S}_{\perp,\mathbf{k}+\mathbf{k}''}) - \mathbf{S}_{\perp,\mathbf{k}'} (\mathbf{S}_{\perp,\mathbf{k}+\mathbf{k}''} \cdot \mathbf{S}_{\perp,\mathbf{k}'-\mathbf{k}''}) \right) + \\
&+ \frac{W^{(2)}_{\mathbf{k},\mathbf{k}',\mathbf{k}''}}{2} \Big[2(\mathbf{S}_{\perp,\mathbf{k}} + \mathbf{S}_{\perp,\mathbf{k}'}) \left(N_{\mathbf{k}+\mathbf{k}''\uparrow} N_{\mathbf{k}'-\mathbf{k}''\downarrow} + N_{\mathbf{k}+\mathbf{k}''\downarrow} N_{\mathbf{k}'-\mathbf{k}''\uparrow} + 2(\mathbf{S}_{\perp,\mathbf{k}+\mathbf{k}''} \cdot \mathbf{S}_{\perp,\mathbf{k}'-\mathbf{k}''}) \right) - \\
&(\mathbf{S}_{\perp,\mathbf{k}} (N_{\mathbf{k}'\uparrow} + N_{\mathbf{k}'\downarrow}) + \mathbf{S}_{\perp,1} (N_{\mathbf{k}\uparrow} + N_{\mathbf{k}\downarrow})) (N_{\mathbf{k}+\mathbf{k}''\uparrow} + N_{\mathbf{k}'-\mathbf{k}''\uparrow} + N_{\mathbf{k}+\mathbf{k}''\downarrow} + N_{\mathbf{k}'-\mathbf{k}''\downarrow} + 2) \Big] - \\
&- 2W^{(12)}_{\mathbf{k},\mathbf{k}',\mathbf{k}''} \bar{S}_{\perp,\mathbf{k}} \left(\left(\mathbf{S}_{\perp,\mathbf{k}'} \cdot \mathbf{S}_{\perp,\mathbf{k}+\mathbf{k}''} \right) + \left(\mathbf{S}_{\perp,\mathbf{k}'} \cdot \mathbf{S}_{\perp,\mathbf{k}'-\mathbf{k}''} \right) \right) + \\
&+ \frac{W^{(12)}_{\mathbf{k},\mathbf{k}',\mathbf{q}}}{2} \mathbf{S}_{\perp,\mathbf{k}'-\mathbf{k}''} \left[2((N_{\mathbf{k}'\uparrow} + 1) N_{\mathbf{k}+\mathbf{k}''\uparrow} + (N_{\mathbf{k}'\downarrow} + 1) N_{\mathbf{k}+\mathbf{k}''\downarrow}) + (N_{\mathbf{k}+\mathbf{k}''\uparrow} + N_{\mathbf{k}+\mathbf{k}''\downarrow} - N_{\mathbf{k}'\uparrow} - N_{\mathbf{k}'\downarrow}) (N_{\mathbf{k}\uparrow} + N_{\mathbf{k}\downarrow}) \right] + \\
&+ \frac{W^{(12)}_{\mathbf{k},\mathbf{k}',\mathbf{k}''}}{2} \mathbf{S}_{\perp,\mathbf{k}+\mathbf{k}''} \left[2((N_{\mathbf{k}'\uparrow} + 1) N_{\mathbf{k}'-\mathbf{k}''\uparrow} + (N_{\mathbf{k}'\downarrow} + 1) N_{\mathbf{k}'-\mathbf{k}''\downarrow}) + (N_{\mathbf{k}'-\mathbf{k}''\uparrow} + N_{\mathbf{k}'-\mathbf{k}''\downarrow} - N_{\mathbf{k}'\uparrow} - N_{\mathbf{k}'\downarrow}) (N_{\mathbf{k}\uparrow} + N_{\mathbf{k}\downarrow}) \right] \Bigg\}
\end{aligned}
\tag{1.72}
$$

The equation for the in-plane pseudospin contains a set of terms similar to that of (1.71). The terms with $W^{(1)}_{\mathbf{k},\mathbf{k}',\mathbf{k}''}$ describe in-plane pseudospin evolution due to the interaction of bosons with the same spin. One can note, for example, that the increase of linear polarization can take place due to stimulated scattering from the two initial states as described by the term $\frac{W^{(1)}_{\mathbf{k},\mathbf{k}';\mathbf{k}''}}{2} \mathbf{S}_{\perp,\mathbf{k}} N_{\mathbf{k}+\mathbf{k}''} N_{\mathbf{k}'-\mathbf{k}''}$. The polarization degree is kept constant in this case. One can see that the pseudospin of each state is affected by the pseudospins of all other states: the transfer of pseudospin from the state $\mathbf{k}+\mathbf{k}''$ to the state $\mathbf{k}$ depends on the scalar product of the pseudospins of the two other states: $\left(\mathbf{S}_{\mathbf{k}'} \cdot \mathbf{S}_{\mathbf{k}'-\mathbf{k}''} \right)$.

Next group of terms with $W^{(2)}_{\mathbf{k},\mathbf{k}',\mathbf{k}''}$ describe scattering of bosons with opposite spins with all possible combinations. Since linearly-polarized state corresponds to equal occupation numbers $N_\uparrow, N_\downarrow$, scattering with opposite spins leads to direct transfer of in-plane pseudospin, which is why this group includes a term $\mathbf{S}_{\perp,\mathbf{k}} \left(\mathbf{S}_{\perp,\mathbf{k}+\mathbf{k}''} \cdot \mathbf{S}_{\perp,\mathbf{k}'-\mathbf{k}''} \right)$, which was not there in the previous group.

The last group of terms with $W^{(12)}_{\mathbf{k},\mathbf{k}',\mathbf{k}''}$ describe polarization-dependent effects when two bosons with the same spin are interacting at the same time with two bosons having opposite spins. It is interesting to note that the terms $\frac{W^{(12)}_{\mathbf{k},\mathbf{k}';\mathbf{k}''}}{2} \mathbf{S}_{\perp,\mathbf{k}'-\mathbf{k}''} \left(2\left(\left(N_{\mathbf{k}'\uparrow} + 1 \right) N_{\mathbf{k}+\mathbf{k}'\uparrow} + \left(N_{\mathbf{k}'\downarrow} + 1 \right) N_{\mathbf{k}+\mathbf{k}''\downarrow} \right) \right)$ that couple the pseudospin of the initial state with the pseudospin of the final state, in the spontaneous regime when $N_{\mathbf{k}'}$ can be neglected, one can obtain the linear polarization inversion depending on the sign of $W^{(12)}_{\mathbf{k},\mathbf{k}',\mathbf{k}''}$, which is negative in the case of exciton-polaritons.

The scattering rates are defined as follows

$$W^{(1)}_{\mathbf{k},\mathbf{k}',\mathbf{k}''} = \frac{2\pi}{\hbar}\left|V^{(1)}_{\mathbf{k},\mathbf{k}',\mathbf{q}}\right|^2 \delta\left(\Omega_{\mathbf{k}} + \Omega_{\mathbf{k}'} - \Omega_{\mathbf{k}+\mathbf{k}''} - \Omega_{\mathbf{k}'-\mathbf{k}''}\right)$$
$$W^{(2)}_{\mathbf{k},\mathbf{k}',\mathbf{k}''} = \frac{2\pi}{\hbar}\left|V^{(2)}_{\mathbf{k},\mathbf{k}',\mathbf{k}''}\right|^2 \delta\left(\Omega_{\mathbf{k}} + \Omega_{\mathbf{k}'} - \Omega_{\mathbf{k}+\mathbf{k}''} - \Omega_{\mathbf{k}'-\mathbf{k}''}\right) \qquad (1.73)$$
$$W^{(12)}_{\mathbf{k},\mathbf{k}',\mathbf{k}''} = \frac{2\pi}{\hbar}\mathrm{Re}\left(V^{(1)}_{\mathbf{k},\mathbf{k}',\mathbf{k}''}V^{*(2)}_{\mathbf{k},\mathbf{k}',\mathbf{k}''}\right)\delta\left(\Omega_{\mathbf{k}} + \Omega_{\mathbf{k}'} - \Omega_{\mathbf{k}+\mathbf{k}''} - \Omega_{\mathbf{k}'-\mathbf{k}''}\right)$$

Here as in Eq. (1.70) the delta functions ensure the energy conservation. The signs of the terms $W^{(1)}_{\mathbf{k},\mathbf{k}',\mathbf{k}''}, W^{(2)}_{\mathbf{k},\mathbf{k}',\mathbf{k}''}$ and $W^{(12)}_{\mathbf{k},\mathbf{k}',\mathbf{k}''}$ can differ in different systems. Although $W^{(1)}_{\mathbf{k},\mathbf{k}',\mathbf{k}''}, W^{(2)}_{\mathbf{k},\mathbf{k}',\mathbf{k}''}$ are always positive, $W^{(12)}_{\mathbf{k},\mathbf{k}',\mathbf{k}''}$ can be positive or negative depending on the phase shift between the matrix elements of the singlet and triplet scattering. In particular it is negative if these matrix elements are real and have opposite signs. Realistic values of the matrix elements for exciton-polaritons are discussed in chapter 3. As one can see, the system of equations (1.71), (1.72) is rather heavy for analysis. The corresponding numerical simulations also can hardly be carried out without sufficient simplifications.

1.3.3. Rotation terms

The rotation terms, derived from the "coherent" part of the complete Hamiltonian, read:

$$\left(\frac{dN_{\mathbf{k}\uparrow}}{dt}\right)\Bigg|_{rot} = -\left(\frac{dN_{\mathbf{k}\downarrow}}{dt}\right)\Bigg|_{rot} = \mathbf{e}_z \cdot \left[\mathbf{S}_{\perp,\mathbf{k}} \times \mathbf{\Omega}_{eff,\mathbf{k}}\right] \qquad (1.74)$$

$$\left(\frac{d\mathbf{S}_{\perp,\mathbf{k}}}{dt}\right)\Bigg|_{rot} = \left[\mathbf{S}_{\perp,\mathbf{k}} \times \mathbf{\Omega}_{\mathrm{int},\mathbf{k}}\right] + \frac{\left(N_{\mathbf{k}\uparrow} - N_{\mathbf{k}\downarrow}\right)}{2}\bar{\mathbf{\Omega}}_{eff,\mathbf{k}} \qquad (1.75)$$

where $\mathbf{e}_z$ is a unitary vector in the direction of the structure growth axis, $\mathbf{\Omega}_{eff,\mathbf{k}}$ is a possible effective magnetic field, which may be present in a bosonic system and affect its behavior (e.g. TE-TM splitting for polaritons), $\bar{\mathbf{\Omega}}_{eff,\mathbf{k}}$ is obtained from $\mathbf{\Omega}_{eff,\mathbf{k}}$ by the rotation by 90° about the structure growth axis, and the effective magnetic field $\mathbf{\Omega}_{\mathrm{int},\mathbf{k}}$ is produced by the disbalance of the σ^+ and σ^- bosons. It is given by the following expression deduced from H_{shift}:

$$\hbar\mathbf{\Omega}_{\mathrm{int},\mathbf{k}} = 2\mathbf{e}_z \sum_{\mathbf{k}'}\left(V^{(1)}_{\mathbf{k},\mathbf{k}',0} - V^{(2)}_{\mathbf{k},\mathbf{k}',0}\right)\left(N_{\mathbf{k}'\uparrow} - N_{\mathbf{k}'\downarrow}\right) \qquad (1.76)$$

This is the self-induced Larmor precession which will be described more in detail for polaritons in chapter 3.

All the terms described in the above subsections describe the relaxation of bosons with spin towards an equilibrium distribution. They need to be completed by specific pumping and decay terms to describe the functioning of polariton parametric oscillator (chapter 3).

1.4. Gross-Pitaevskii equation

In this section we introduce the tools for description of a Bose condensate once it is formed. We will work in the approximation of weak interactions and diluteness of the Bose gas. The perturbation technique for this purpose was first developed by Bogoliubov, who worked with uniform Bose gas. Then this solution was generalized for the case of non-uniform dilute gas by Gross and Pitaevskii. We will develop the latter formalism from the very beginning. Since we are studying the condensate, its coherence should not be lost in our description, and therefore the Boltzmann approach developed in earlier sections in not suitable.

The Bose-Einstein condensate is a special state of matter formed by a system of bosons, predicted by A. Einstein (1925). Let us briefly show why do bosons accumulate in a single quantum state under certain conditions. Let us consider N non-interacting bosons at a temperature T in a volume R^d (here d is the dimensionality of the system). The bosons are distributed according to the Bose-Einstein distribution function (k_B=1):

$$f_B\left(\mathbf{k},T,\mu\right)=\frac{1}{\exp\left(\left(E\left(\mathbf{k}\right)-\mu\right)/T\right)-1} \tag{1.77}$$

where k is the particle wave-vector, E(**k**) is the dispersion and μ is the chemical potential (always negative for Bosons, if one counts the energy E(**k**) from zero). The chemical potential can be understood as the energy needed to add one particle to the system. Its value is given by the normalization condition:

$$N(T,\mu)=\sum_{\mathbf{k}} f_B\left(\mathbf{k},T,\mu\right)=\frac{1}{\exp\left(-\mu/T\right)-1}+\sum_{\mathbf{k},k\geq 2\pi/R} f_B\left(\mathbf{k},T,\mu\right) \tag{1.78}$$

where we have separated the ground state from the others for convenience. One can calculate the total particle density by integration over the reciprocal space:

$$n\left(T,\mu\right)=\lim_{R\to\infty}\frac{N\left(T,\mu\right)}{R^d}=n_0+\frac{1}{\left(2\pi\right)^d}\int f_B\left(\mathbf{k},T,\mu\right)d^d\mathbf{k} \tag{1.79}$$

where

$$n_0\left(T,\mu\right)=\lim_{R\to\infty}\frac{1}{R^d}\frac{1}{\exp\left(-\mu/T\right)-1} \tag{1.80}$$

The integral in (1.79) is an increasing function of μ, therefore, if one increases the particle density, the chemical potential also increases. The maximum particle density which can be accommodated in the excited states of the system is therefore

$$n_c\left(T\right)=\lim_{\mu\to 0}\frac{1}{\left(2\pi\right)^d}\int f_B\left(\mathbf{k},T,\mu\right)d^d\mathbf{k} \tag{1.81}$$

This function can be calculated analytically in the case of a parabolic dispersion relation. It is convergent if d>2 and divergent if $d \le 2$. In higher than 2 dimensions n_c gives an expression for critical density above which the extra particles collapse in the ground state only, which is called the Bose-Einstein condensate.

For the 2D case we consider, the Bose-Einstein condensation strictly speaking does not take place. However, a transition to a superfluid state called Kosterlitz-Thouless phase transition may take place. In a finite 2D system quasi-condensation of bosons is also possible, because in this case the integral (1.81) takes finite value, since the integration is done on the reciprocal space excluding the diverging region around the ground state.

1.4.1. Equation for the field operator

Because of the long-rage correlations between the elements of the one-body density matrix in a system with macroscopically occupied state (Bose condensate) the field operator $\hat{\mathbf{\Psi}}(\mathbf{r})$ can be written in a basis of single-particle wave functions φ_i even for interacting and non-uniform systems:

$$\hat{\mathbf{\Psi}}(\mathbf{r}) = \sum_i \varphi_i \hat{a}_i, \tag{1.82}$$

where $\hat{a}_i \left(\hat{a}_i^\dagger\right)$ are the annihilation (creation) operators of a particle in the state φ_i. The 'condensate' term can be separated from the other components:

$$\hat{\mathbf{\Psi}}(\mathbf{r}) = \varphi_0(\mathbf{r})\hat{a}_0 + \sum_{i\neq 0} \varphi_i(\mathbf{r})\hat{a}_i \tag{1.83}$$

Here one introduces the Bogoliubov approximation, which consists of replacing the annihilation and creation operators with c-number $\sqrt{N_0}$ (this is the macroscopic occupation of the condensate). This is equivalent to ignoring the noncommutativity of these operators and is a good approximation when $N_0 \gg 1$. This is also equivalent to treating the macroscopic component of the field operator as a classical field. Thus the equation (1.83) can be rewritten as

$$\hat{\mathbf{\Psi}}(\mathbf{r}) = \mathbf{\Psi}_0(\mathbf{r}) + \delta\hat{\mathbf{\Psi}}(\mathbf{r}) \tag{1.84}$$

At very low temperatures and if the gas is dilute, the non-condensate component can be neglected, because the depletion due to these factors is small. In this case the system behaves like a classical object. The function $\mathbf{\Psi}_0(\mathbf{r})$ is called the wave function of the condensate and plays the role of an order parameter.

The diluteness condition means that the scattering length a which can be related with the matrix element of interparticle interaction in the Born approximation should be much smaller than the distance between particles:

$$a \sim n^{-1/3}, \tag{1.85}$$

where n is the particle concentration $n = N_0 / V$ (V is the normalization volume).

To write the Gross-Pitaevskii equation for the classical field $\boldsymbol{\Psi}_0(\mathbf{r})$ describing the nonuniform Bose gas at zero temperature, let us start from the field operator in the Heisenberg representation, which fulfils the exact equation

$$\begin{aligned} &i\hbar\frac{\partial}{\partial t}\hat{\Psi}(\mathbf{r},t) = \left[\hat{\Psi}(\mathbf{r},t), \hat{H}\right] = \\ &\left[-\frac{\hbar^2\nabla^2}{2m} + V_{ext}(\mathbf{r},t) + \int \hat{\Psi}^{\dagger}(\mathbf{r}',t) V(\mathbf{r}'-\mathbf{r}) \hat{\Psi}(\mathbf{r}',t)\, d\mathbf{r}'\right]\hat{\Psi}(\mathbf{r},t) \end{aligned} \tag{1.86}$$

For an effective soft interaction potential $V(\mathbf{r})$ one can replace the operator $\hat{\boldsymbol{\Psi}}(\mathbf{r})$ by the classical field $\boldsymbol{\Psi}_0(\mathbf{r})$. Assuming the function $\boldsymbol{\Psi}_0(\mathbf{r})$ varies slowly on the scale of distance between particles, one can substitute **r** for **r**' and obtain finally the Gross-Pitaevskii equation:

$$i\hbar\frac{\partial}{\partial t}\Psi_0(\mathbf{r},t) = \left(-\frac{\hbar^2\nabla^2}{2m} + U(\mathbf{r},t) + \alpha\left|\Psi_0(\mathbf{r},t)\right|^2\right)\Psi_0(\mathbf{r},t) \tag{1.87}$$

Here $\alpha = \int V(\mathbf{r})\, d\mathbf{r}$ is the interaction coupling constant, which can be expressed in terms of the *s*-wave scattering length a: $\alpha = 4\pi\hbar^2 a / m$. The value of the interaction constant for exciton-polaritons will be discussed in further chapters.

The equation (1.87) is also called the nonlinear Schroedinger equation, because without the nonlinear term proportional to α it reduces to the ordinary Schroedinger equation.

1.4.2. Dispersion of excitations of a condensate

Let us find the dispersion of weak excitations of the classical field described by (1.86). We shall consider small deviations from the constant average value $\sqrt{N}$:

$$\Xi(\mathbf{r},t) = \sqrt{n} + Ae^{i(\mathbf{kr}-\omega t)} + B^* e^{-i(\mathbf{kr}-wt)} \tag{1.88}$$

where A and B are small complex amplitudes. Substituting this into (1.87), linearizing by A and B and separating terms with different complex exponents, one obtains a system of equations ($p = \hbar k$):

$$\begin{aligned} \hbar\omega A &= \frac{p^2}{2m}A + \alpha n(A+B) \\ -\hbar\omega B &= \frac{p^2}{2m}B + \alpha n(A+B) \end{aligned} \tag{1.89}$$

If one solves this system for ω, one obtains the famous Bogoliubov dispersion law:

$$(\hbar\omega)^2 = \left(\frac{p^2}{2m}\right)^2 + \frac{p^2}{m}\alpha n \tag{1.90}$$

The dispersion described by this law is linear for small p and approaches the free particle dispersion for large p. The change between the two takes place when energy becomes equal to αn. From this dispersion one can obtain the speed of excitations, or the speed of sound in a dilute Bose gas with interactions:

$$c = \sqrt{\frac{\alpha n}{m}} \tag{1.91}$$

This linearization approach can be used very efficiently to find the dispersions and to analyze stability in many complicated cases, as will be shown afterwards.

1.4.3. Superfluidity of a condensate

One of the most important properties of a condensate described by the Gross-Pitaevskii equation is that the condensate is superfluid. Its superfluidity follows directly from the Landau criterion, which tells whether the creation of excitations is energetically favourable in a liquid propagating through a capillary.

Let us consider a uniform fluid at zero temperature flowing along a capillary at a constant velocity $\vec{v}$. The only dissipative process assumed is the creation of elementary excitations due to the scattering by the walls of the capillary. The basic idea of the derivation is to calculate energy and momentum in the reference frame moving with the fluid and in the static one, making the link between the two frames by a Galilean transformation. If a single excitation with momentum $\hbar\vec{k}$ appears, the total energy in the moving frame is $E = E_0 + \varepsilon(\vec{k})$, where E_0 is the energy of the ground state and $\varepsilon(\vec{k})$ is the dispersion of the fluid excitations. In the static frame however, the energy and momentum of the fluid read:

$$E' = E_0 + \varepsilon(\vec{k}) + \hbar\vec{k}.\vec{v} + \frac{1}{2}Mv^2 \tag{1.92}$$

$$\vec{P}' = \vec{p} - M\vec{v} \tag{1.93}$$

where M is the total mass of the fluid.

Equation (1.92) shows that the energy of the elementary excitation in the static system is $\varepsilon(\vec{k}) + \hbar\vec{k}.\vec{v}$. Dissipation is possible, only if the creation of elementary excitations is profitable energetically which means:

$$\varepsilon(\vec{k}) + \hbar\vec{k}.\vec{v} < 0 \tag{1.94}$$

Dissipation can therefore take place only if $v > \frac{\varepsilon(\vec{k})}{\hbar k}$. The flow stays superfluid if velocity is smaller than:

$$v_c = \min\left(\frac{\varepsilon(\vec{k})}{\hbar k}\right) \tag{1.95}$$

Formula (1.95) is the Landau criterion of superfluidity. In case of a parabolic dispersion v_c is zero and there is no superfluid motion. On the opposite, in case of Bogoliubov dispersion v_c is nothing but the speed of sound which means that the fluid can move without dissipation with any velocity smaller than the speed of sound.

The link between Bose-Einstein condensation and superfluidity is even more profound. If $\hat{\Psi}(\mathbf{r},t)$ is a solution of the equation for the field operator in the Heisenberg representation (1.86), then

$$\Psi'(\mathbf{r},t) = \Psi(\mathbf{r}-\mathbf{v}t,t)\exp\left(\frac{i}{\hbar}\left(m\mathbf{v}\cdot\mathbf{r}-\frac{1}{2}mv^2t\right)\right) \tag{1.96}$$

where $\mathbf{v}$ is a constant vector, is also a solution of the same equation. This gives us the Galilean transformation of the field operator. In the coordinate system where the sample is at rest, the condensate wave function of a uniform fluid is given by $\Psi_0 = \sqrt{n_0}e^{-i\mu t/\hbar}$, where n_0 is a constant. In the frame where the fluid moves with velocity $\mathbf{v}$, the order parameter instead takes the form $\Psi_0 = \sqrt{n_0}e^{iS}$, where

$$S = \frac{1}{\hbar}\left(m\mathbf{v}\cdot\mathbf{r}-\left(\frac{1}{2}mv^2+\mu\right)t\right) \tag{1.97}$$

is the new phase, while the amplitude n_0 has not changed. Equation (1.97) shows that the velocity is proportional to the gradient of the phase:

$$\mathbf{v}_s = \frac{\hbar}{m}\nabla S \tag{1.98}$$

and can be identified as the superfluid velocity. This equation establishes the irrotationality of the superfluid motion, the phase of the order parameter playing the role of a velocity potential. The equation (1.98) is a genuine consequence of Bose-Einstein condensation, i.e. of the existence of the classical field Ψ_0 associated with the macroscopic component of the field operator.

1.4.4. BEC in non-equilibrium situation

The particular situation of BEC at non-equilibrium has been treated in a number of papers. For example, the various timescales of the condensate formation have been considered by H.T.C. Stoof (1991). D.G. Barci, E.S. Fraga, and R.O. Ramos (2000) have developed non-equilibrium field theory description of BEC also addressing the question of condensate formation. Among older papers on the kinetics of condensation of interacting bosons one can cite E. Levich and V. Yakhot

(1977). The authors have as well addressed the different timescales of condensation by means of the kinetic equation they have developed.

In the works cited above the authors were assuming bosons having infinite lifetime; their main interest was the evolution of the particle distribution (condensate fraction) with time. Another important non-equilibrium situation can be linked with finite lifetime of the particles. Here one can apply the ideas from the laser theory, because photons in a laser have a finite lifetime by definition. This is why the researchers have started to explore the field of "atom lasers". One of the first works on this topic has been done by A.N. Oraevskii (1997), K. Helmerson *et al* (1999) and by T. Lahaye *et al* (2004). For polaritons the influence of the finite lifetime is an important, but open question. A recent work of M. Wouters and I. Carusotto (2007) presents a phenomenological model of nonequilibrium condensate of polaritons allowing to calculate its dispersion of excitations. By the nature of this model its results are very close to the previous results of C. Ciuti and I. Carusotto (2005) for the Goldstone mode obtained in the case of quasi-resonant pumping in scalar approximation, and to the results presented in chapter 4. Main conclusion of this paper is that in case of non-equilibrium situation the dispersion of the excitations contains a diffusive part.

1.5. Conclusions

We have introduced the basic tools necessary for the description of microcavity exciton-polaritons. Transfer matrix method allows to use the electromagnetic approach to find the dispersion of polaritons in different polarizations. The Boltzmann equations allow to describe polariton relaxation, taking into account their polarization properties. The Gross-Pitaevskii equation can be applied once a condensate of polaritons is formed and its properties need to be studied. In some situations, more complicated schemes are necessary, that we do not use here. For example, one can describe the transition from completely coherent to completely incoherent case with increasing dephasing, using quantum equations with high-order correlators. This is a work in progress, that one can read about in I.A. Shelykh *et al* (2005) and in other articles to be published (see e.g. I.A. Shelykh *et al*, 2007).

Chapter 2. Polariton laser based on GaN

In this chapter we introduce the concept of polariton laser. We present a kinetic model of polariton relaxation which allows simulation of polariton lasers. We compare bulk and quantum well polariton lasers based on GaN and demonstrate that they can operate at room temperature. We plot the kinetic phase diagrams of GaN cavities showing the range of parameters at which the cavities can operate as polariton lasers.

Contents

2.1. Polariton laser

The polariton laser itself is a device, a concept of which has been first proposed by A. Imamoglu *et al* (1996). This device is completely based on the properties of Bose-Einstein condensate, this is why it was during some time called 'boser'. The idea is that the coherent emission should be provided not by stimulated transitions associated with population inversion, but rather by natural properties of a Bose condensate of polaritons, which should form in a microcavity in a thermodynamic equilibrium once the density exceeds certain value. The particular property of this laser is that the population inversion is not required: the system starts to emit coherent light once the population of the ground state exceeds 1. This is what raised interest in polariton lasers: an opportunity to investigate fundamental physics of Bose condensation at the same time as creating new device with unusual properties.

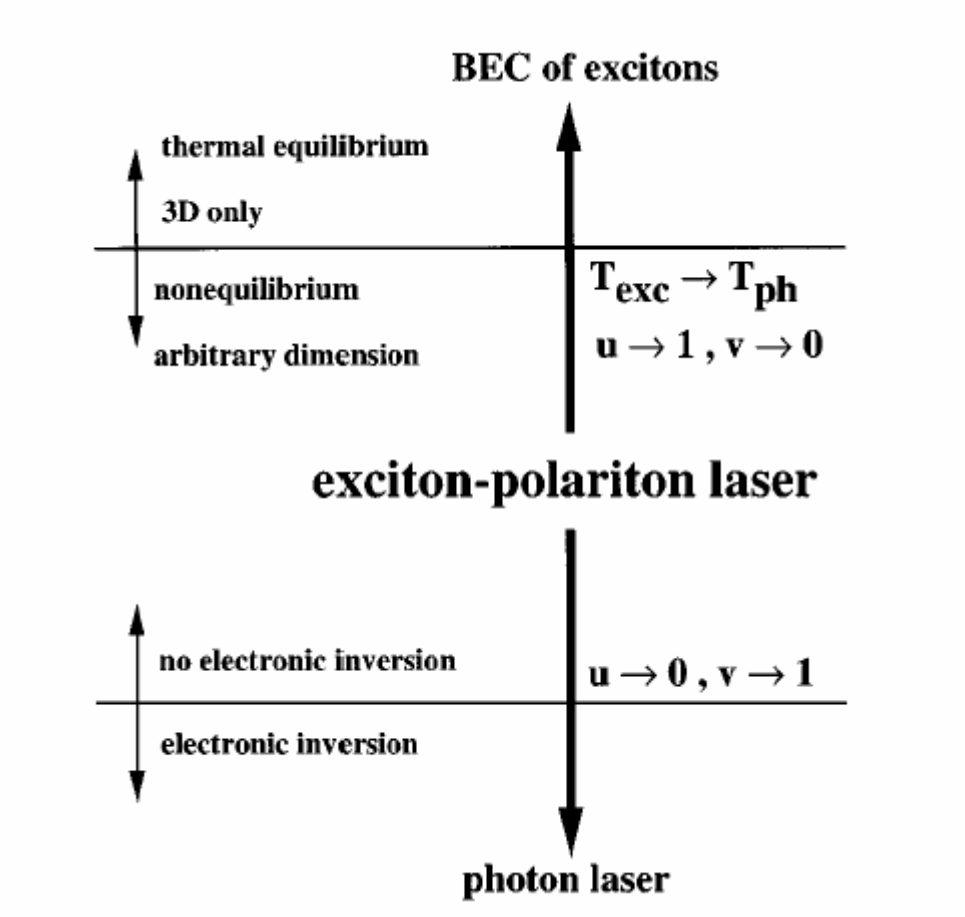

Figure 2.1. Diagram comparing the exciton-polariton laser to the concepts of exciton BEC and photon laser. The u and v coefficients are excitonic and photonic fractions (Hopfield coefficients), correspondingly (figure from A. Imamoglu *et al*, 1996).

To operate as a polariton laser, the microcavity should be in the strong coupling regime. It means that the Rabi splitting (the light-matter interaction constant), which manifests itself as the splitting between the two polariton branches, should be larger than the broadening induced by all possible sources, in particular, temperature. Therefore, only semiconductors with large exciton oscillator strength can be considered as materials for the active region of a room-temperature polariton laser. Such semiconductors include GaN and ZnO. Their utilisation for the fabrication of RT polariton lasers has first been proposed by G. Malpuech *et al* (2002) and M. Zamfirescu *et al* (2002). Even in bulk GaN cavities the exciton oscillator strength is strong enough to observe Rabi splitting at room temperature (A. Kavokin and B. Gil, 1998).

The main problem preventing the creation of a polariton laser was the bottleneck, which has first been given this name and theoretically described by Tassone *et al* (1997). The bottleneck is a region of the polariton dispersion, where the relaxation of polaritons slows down. In this region, where one passes from the excitonic effective mass of the polariton to the photonic one, the acoustic phonons become less efficient, because they can not exchange large quantities of energy and small wave vectors at the same time. This term was first attributed to 3D polaritons, due to the shape of the dispersion, and the same effect as 2D polariton as 2D polaritons with respect to acoustic phonon emission. Different ways to overcome this problem have been proposed. For the CdTe cavity the solution has proven to be positive detuning, which reduces the bottleneck by changing the polariton dispersion. For GaN the question of the bottleneck will be the main subject of the current chapter.

The polariton laser does not always operate at thermal equilibrium. The population of polaritons can be more or less thermalized depending on the system properties and excitation conditions. In this chapter we consider polariton laser as a device and speak of it as such, whereas in chapters 4 and 5 we will pay attention to the properties of polariton condensates and macroscopically occupied modes in different conditions.

2.2. Polaritons in GaN

In this section we consider polaritons in bulk GaN cavities and in cavities with GaN quantum wells. We describe the specifics of GaN, present the most recent experimental data and calculate the polariton dispersions that will be used for the kinetic simulation of polariton relaxation.

GaN is a wide-bandgap semiconductor (Eg~3.4 eV, direct bandgap) which is mostly grown in hexagonal (wurtzite) structure. Only at high pressures (37-65 GPa) does it crystallize into the rocksalt phase. A metastable zinc-blende GaN can exist at any pressure. Main commercial application of GaN is for fabrication of blue light emitting diodes (LEDs), which has started only in the 90s. Before this material was believed to be useless for optoelectronics mainly because of its low quality. The blue and green LED market is almost completely occupied only by InGaN materials. Another field of application is vertical cavity surface emitting lasers (VCSELs) based on nitride materials. An optically pumped nitride VCSEL with InGaN quantum wells and GaN/AlGaN DBRs operating at room temperature has been demonstrated by T. Someya *et al* (1999). A VCSEL is something very close to the polariton laser by its structure, and the main difference is that the former operates in the weak coupling regime, and the latter – in the strong coupling regime. The main advantage of the polariton laser should be its low threshold, allowing to fabricate devices with lower power consumption.

One of the main drawbacks of GaN is its crystalline quality. The main problem is obtaining large high-quality crystals which could be used as substrates for epitaxial growth. This is a direct consequence of thermodynamical properties of GaN, in particular, the melting conditions are so extreme, that the application of the common growth methods from stoichiometric liquids is technically impossible (I. Grzegoryu and S. Porowski, under ed. B. Gil, 2002). Since high-quality GaN substrates for homoepitaxy were not available, the development of GaN-optoelectronics was based on MOCVD of GaN structures on sapphire substrates, though highly mismatched. In these structures the dislocation densities are as high as 10^8-10^{10} cm^{-2}, but efficient luminescence is nevertheless possible, because GaN and its alloys are more tolerant to the structural defects than the conventional III-V systems due to lower diffusion length of carriers and lower mobility of defects. The most typical defects for GaN are threading dislocations. Another typical defect is an inversion domain, which is characterized, as follows from its name, by the inverse order of Ga and N atomic layers. The inversion domains have been shown to be the origin of the 3.42 eV PL band in GaN epitaxial layers and nanocolumns (T.V. Shubina *et al,* 2003).

The choice of the substrate is an important factor for GaN growth. While best results were obtained on sapphire substrate with an ELO process (epitaxial lateral overgrowth), other substrates can be used. SiC provides a better thermal management and a back side electrode, thus simplifying the process. The crystalline quality and surface preparation are, however, not as good as those of sapphire. In addition, the availability and price of SiC substrates are still

limitations. GaN substrates offer first of all a high quality homoepitaxy, but also a reasonable thermal conductivity and an excellent back side contact. The choice of the substrate can strongly affect the properties of GaN polariton laser as we will see below (e.g. figure 2.2).

2.2.1. Bulk GaN

The excitonic structure of GaN is quite complex. There are 3 excitonic bands (A,B,C) which differ in exciton energy, oscillator strength and effective mass (S. Bechtedt, ed. by B.Gil, 2002). The energy of excitonic levels depends on the structure strain, which in bulk samples is determined mostly by the type of the substrate and the growth procedure (see figure 2.2). This may even lead to the exchange of the relative positions of A and B excitonic levels. The same can be said about the exciton oscillator strength (emission intensity) of these lines.

For a given set of excitonic levels, one can calculate the polariton dispersion using the standard multiple-oscillator approach. However, the result is complicated by several factors. The oscillator strength is different for different projections of the electric field on the c-axis of the structure, and the mass is also anisotropic. For B and C bands there is a mixing between singlet and triplet states, which creates two optically active branches for each band (P.P. Paskov *et al*, 2001). Therefore, the final exciton-polariton dispersion includes 6 branches. The true dispersion is usually not resolved experimentally in realistic structures, because the splittings between some branches are tiny relative to broadening in GaN. For the first time the strong coupling between excitonic resonances and light in bulk GaN at room temperature was observed by F. Semond *et al* (2005), and then on another sample by R. Butté *et al* (2006). It is the latter that we simulate theoretically in this chapter because of its better quality.

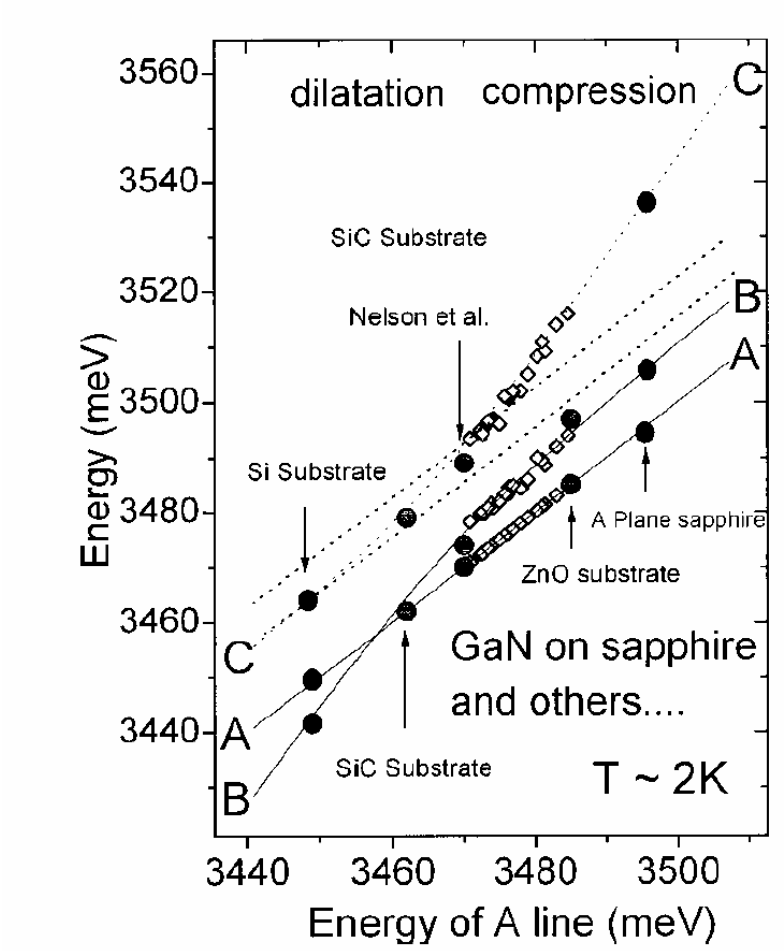

Fig. 2.2. Evolution of the transition energies in GaN epilayer grown with strain along the [0001] direction on various substrates: sapphire with GaN buffer layer, SiC, Si, ZnO. Black circles on the right-hand side correspond to growth on A-plane sapphire. The literature locates the continuum of A exciton between the two bold dashed lines (figure from A. Alemu *et al*, 1998)

An example of polariton dispersion in a bulk GaN microcavity is shown on figure 2.3. This figure has been calculated using the diagonalization method described above (see Eq. (1.2)) and the values given in P.P. Paskov *et al* (2004), but for a cavity (not for a bulk sample without resonator). To obtain the dispersions in TE and TM polarizations we had to use the polarization-dependent optical parameters of Bragg mirrors and the expressions for the light-matter coupling constant, which have been extensively introduced in chapter 1. The parameters correspond to free-standing GaN, which means that some buffer strain relaxation techniques should be used in case of growth on an ordinary substrate. Fig. 2.3 shows two sets of dispersions corresponding to TE and TM polarizations of incident light.

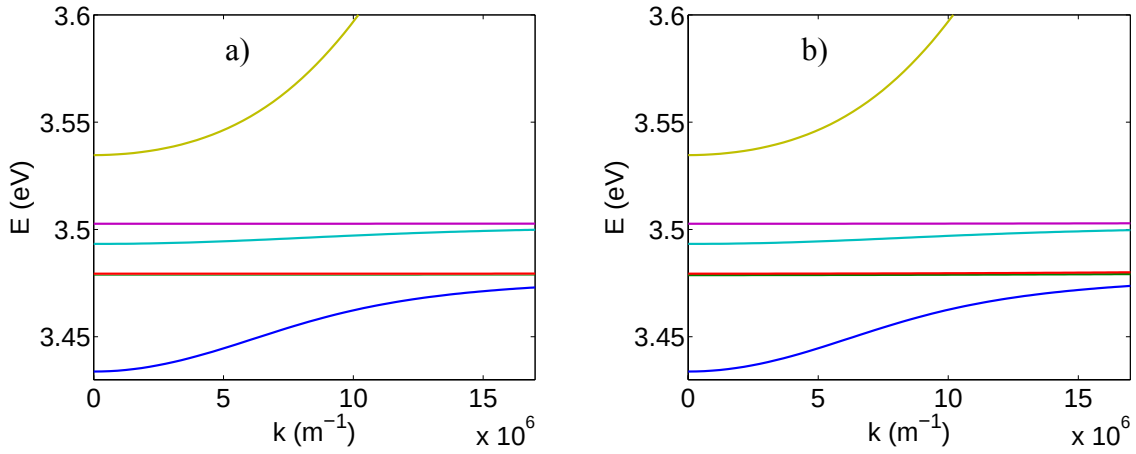

Figure 2.3. Polariton dispersion in a bulk GaN cavity in TE (a) and TM (b) polarizations. The intermediate branches are usually mixed together by inhomogeneous broadening.

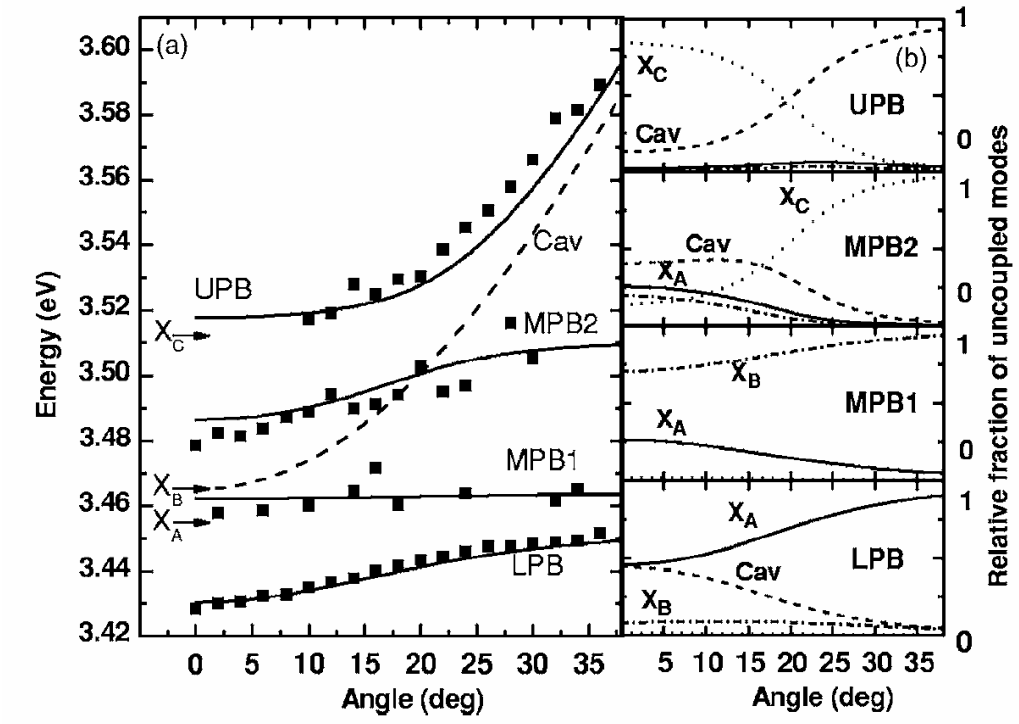

Figure 2.4. Experimentally resolved a) dispersions of exciton-polaritons in bulk GaN microcavity at room temperature together with theoretical fit b) relative fractions of each of the uncoupled modes (figure from R. Butte *et al*, 2006).

In our polariton relaxation simulations described below we have considered a real sample – bulk GaN $3\lambda/2$ microcavity with 35-period lattice-matched $Al_{0.85}In_{0.15}N/Al_{0.2}Ga_{0.8}N$ bottom DBR and 10-period SiO_2/Si_3N_4 top DBR (grown and studied by R. Butte *et al,* 2006). In this sample 4 polariton branches are resolved experimentally (Fig. 2.4) with splittings of the order of 30-40 meV.

In GaN cavities there is always large inhomogeneous broadening due to excitonic and photonic disorder. In the state-of-the-art cavity described above the exciton inhomogeneous broadening is supposed to be around 5 meV. However, usually much larger values have been reported (e.g. 19 meV in I.R. Sellers *et al*, 2005, where the strong coupling at room temperature was observed for the first time), reaching sometimes 30 meV. Such broadening mixes all the intermediate polariton branches, which are not strongly split. This is why, to simplify the picture, only two relevant branches of the dispersion have been included in our kinetic simulations. One is the lower polariton branch with 2D density of states (always determined by the dimensionality of photon). The other is an excitonic branch with 3D density of states (see figure 2.5), which can be considered as a reservoir.

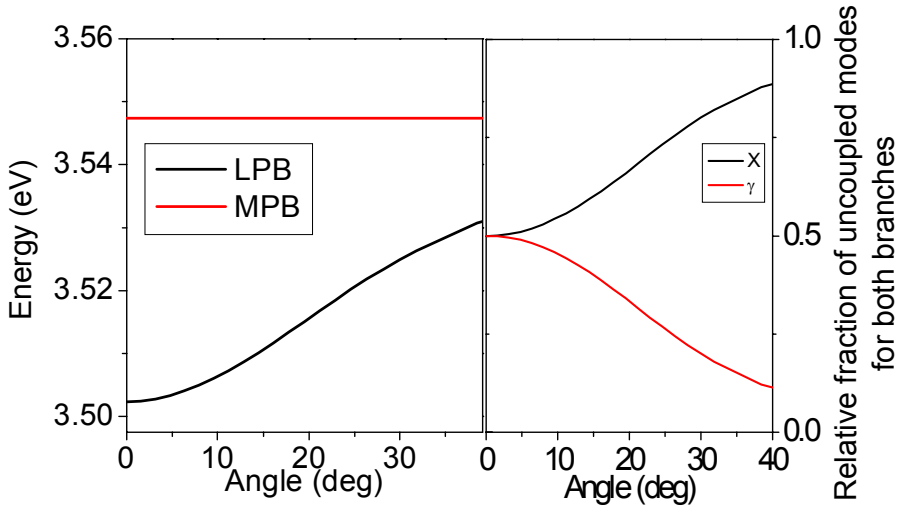

Figure 2.5. The simplified polariton dispersion used in the bulk cavity simulation

2.2.2. GaN Quantum Wells

The GaN quantum wells of the state of the art quality exhibit excitonic inhomogeneous broadening of the order of 25 meV (as reported by G. Christmann *et al*,

2006). Different excitonic levels are usually not resolved. The exact value of the broadening depends on many parameters. Its main origin are the fluctuations of the quantum well thickness. Also, due to the piezoelectric effect an electric field appears in the quantum well strained by the barriers. Therefore, the inhomogeneous broadening depends on the thickness of the barriers and on their composition, as has been shown by F. Natali *et al* (2005), figure 2.6. Since the broadening can strongly vary, it is important to investigate the threshold dependence on this parameter.

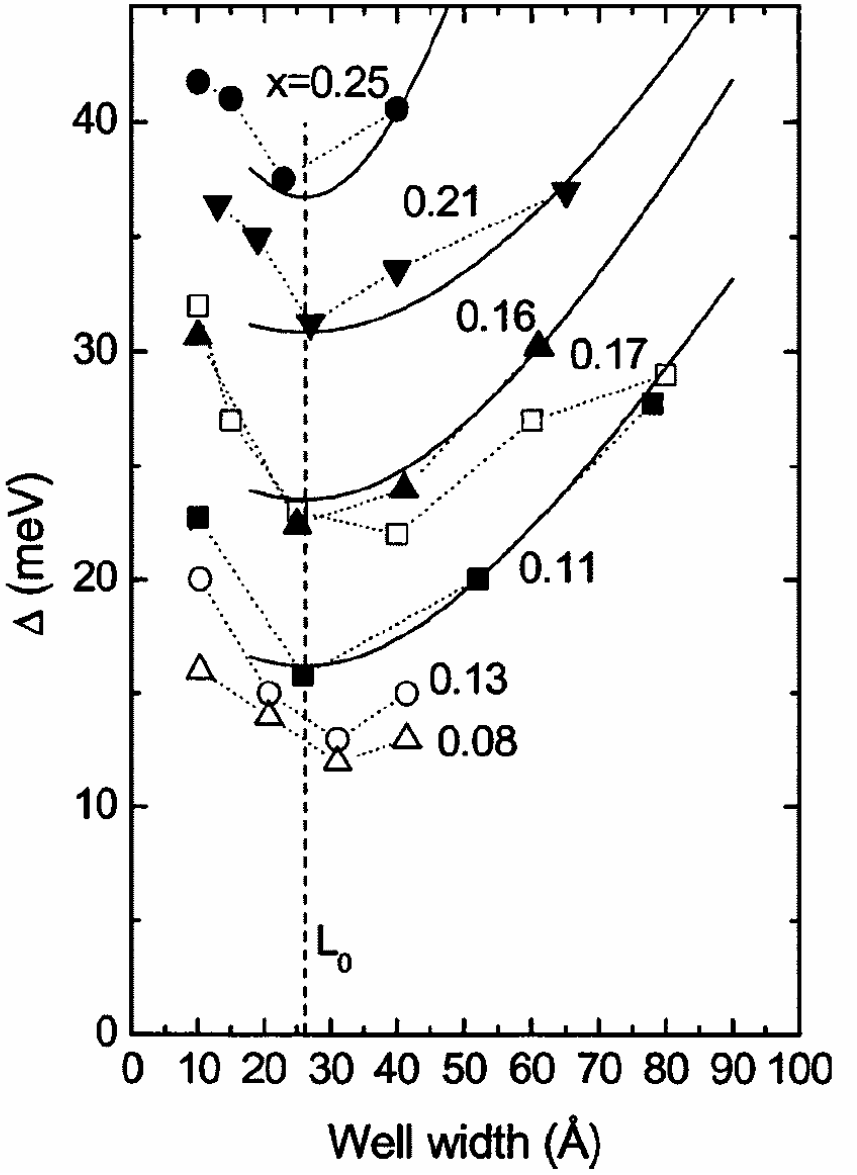

Figure 2.6. QW emission linewidth dependence on the well width for different $Al_xGa_{1-x}N$ barrier compositions *x*. Solid and open symbols are experimental results, curves are calculated using an approximated formula (figure from F. Natali *et al*, 2005).

We have performed kinetic simulations for a QW cavity with Rabi splitting and thickness being the same as in the case of bulk cavity. Taking the state-of-the-art GaN QW cavity described in G. Christmann *et al* (2006) we estimate that it is necessary to have 18 QWs to provide identical parameters. For QW cavities, only one pair of polariton branches is usually resolved, so we take into account one lower and one upper polariton branch. The upper and lower polariton branches for the cavity we have simulated are shown in figure 1.1 as an example of QW polariton dispersion. Here we took the following parameter values: $E_C(0) = E_X(0) = 3.543\,\text{eV}$, $m_e = 0.2m_0$, $m_h = 1.1m_0$, $m_X = m_e + m_h$, $2\Omega = 90\,\text{meV}$, $n_{eff} = 2.55$, $L_c = 211\,\text{nm}$, $m_C = \dfrac{hn_{eff}}{cL_c}$.

2.2.3. GaN cavities

The progress with the growth of GaN cavities has been difficult. Although high-reflectivity distributed Bragg reflectors (DBRs) with R>99% have been reported quite long ago (see the review by R. Butte, 2005), the cavities with these reflectors have shown small quality factors $Q = \lambda/\Delta\lambda$. Recent findings by G. Christmann *et al* (2006) show that this is due to fluctuations of quality (i.e. disorder) of the cavities, and that on a small scale a quality factor as high as 2800 can be measured.

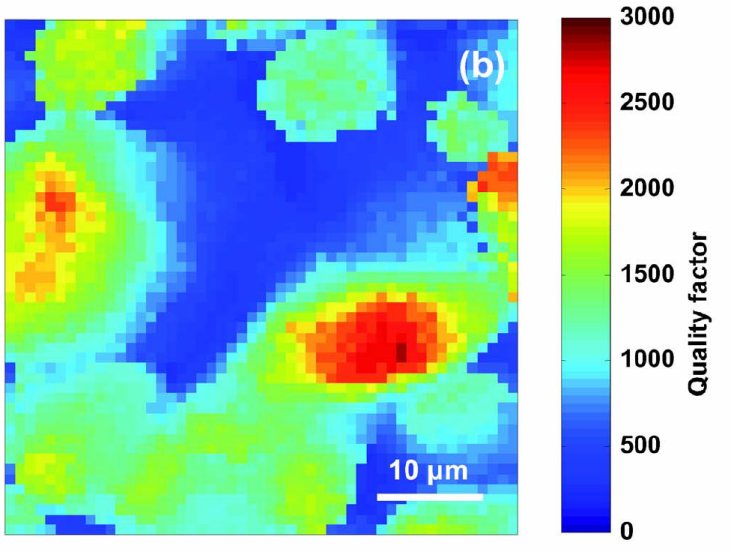

Figure 2.7. Spatial distribution of cavity quality factor (figure from G. Christmann *et al*, 2006).

Since the quality factor (or the cavity lifetime) is crucially important for Bose condensation of polaritons, in the following we consider a small region of cavity with a high value of a quality factor of the order of 2000. It is in this region that the condensate of polaritons forms. We have also investigated the threshold dependence on the cavity quality factor.

2.3. Kinetic simulation of polariton relaxation

We have studied the polariton relaxation in the case of a pulsed non-resonant optical pumping in the semi-classical Boltzmann approximation (see chapter 1), which allows accounting for bosonic stimulation. Electron-hole pairs are created by means of a short optical pulse with high energy. Usually this energy is chosen to be inside a transparency window of the Bragg mirror. We assume that because of the interaction with LO phonons, the carriers rapidly relax to form a cloud of correlated electron-hole pairs or excitons. We therefore assume, as an initial polariton distribution function, a Botzmann distribution, which has an effective temperature of LO phonons (90 meV for GaN, first observed by R. Dingle *et al*, 1971). This is clearly an overestimation of the initial effective temperature, but it is anyway necessary to make some approximation as a starting point. We then solve a system of Boltzmann equations, which reads:

$$\frac{dn_{\mathbf{k}}}{dt} = P_{\mathbf{k}} - \Gamma_{\mathbf{k}} n_{\mathbf{k}} - n_{\mathbf{k}} \sum_{\mathbf{k}'} W_{\mathbf{k}\to\mathbf{k}'} \left(n_{\mathbf{k}'} + 1\right) + \left(n_{\mathbf{k}} + 1\right) \sum_{\mathbf{k}'} W_{\mathbf{k}'\to\mathbf{k}} n_{\mathbf{k}'} \qquad (2.1)$$

where n_k is the occupation number of a state with wave-vector **k**, P_k and $\Gamma_k n_k$ terms describe pumping and decay of particles, and $W_{k\to k'}$ are the scattering rates between the states with corresponding wave-vectors. These rates are calculated using the Fermi Golden rule considering exciton-phonon, exciton-exciton and exciton-electron interactions.

We have assumed cylindrical symmetry of the reciprocal space for 2D branches and spherical symmetry for the excitonic 3D branch in the case of bulk microcavity. We take into account only the bright excitonic states. This means an underestimation of the reservoir density of states by a factor of 2 at most. Since the reservoir states are not strongly populated, the discrepancy of the exciton density due to this approximation should not be strong. Taking into account the dark states is difficult from the numeric point of view, because it would mean solving spin-dependent Boltzmann equations which are especially heavy. The reservoir of excitons is described explicitly by the 3D branch in the bulk model and by the upper part of the 2D branch in the QW model. The discretization of the reciprocal space requires particular

attention. The main requirement is that the distribution function should not vary too abruptly from one cell to another. Therefore the spacing of the cells should be small in the regions where the dispersion (and hence the distribution function) changes strongly. The ground state requires particular attention, because the condensation is linked with a discontinuity of the distribution function. If one accounts for the finite system size R, it gives the natural limit for the spacing between the state at k=0 and the next one. The inhomogeneous broadening of the polariton line is taken into account when scattering rates are calculated (as described in A. Kavokin and G. Malpuech, 2003). It essentially relaxes the energy conservation constraints on the scattering processes.

This simulator of polariton relaxation is best described in the textbook of A. Kavokin and G. Malpuech (2003). The results obtained with its help have been published in a number of papers, including G. Malpuech *et al* (2002) for a GaN cavity; G. Malpuech, A. Kavokin, A. Di Carlo, and J.J. Baumberg (2002) for GaAs cavity, and in the textbook cited above for CdTe cavity. It is interesting to compare this approach with a slightly different approach of D. Porras *et al* (2002). In this paper the authors separate the reservoir from the lower polariton branch (as we do in the case of bulk GaN), and consider the reservoir as having Boltzmann distribution. This approximation should significantly decrease computational costs of the model. As compared with this paper, our model includes also exciton-electron interaction and inhomogeneous broadening, both being important in the case of GaN (see results below). Our model may be in general more precise in the pulsed excitation case, when the evolution of the reservoir can be complicated.

2.3.1. Exciton-phonon interaction

Exciton-phonon interaction in nitrides is well described in a chapter by X.B. Zhiang and B. Gil in "Low-dimensional nitride semiconductors" edited by B. Gil (2002). The main mechanisms of interaction of excitons with phonons in GaN are: Froehlich interaction (LO phonons), deformation potential and piezoelectric field (acoustic phonons).

The matrix element of the interaction of excitons with acoustic phonons by means of the deformation potential can be written as

$$M_{ac}(\mathbf{q}) = \sqrt{\frac{\hbar q}{2\rho c_s V}} G(\mathbf{q}) \tag{2.2}$$

where $\rho = 6150\,\mathrm{kg/m^3}$ is the density and $c_s = 7960\,\mathrm{m/s}$ is the speed of sound in the medium (we take the speed of sound in the direction [001], because in GaN it is different in different directions; however, the difference would not affect strongly the results). Here G is

the product of deformation coefficients of the conduction and valence bands with overlap integrals between exciton and photon mode. In 2D one has to separate the overlap integrals in the plane and in the growth direction. The expression for G reads:

$$G\left(q_{\square},q_z\right)=D_eI_e^{\perp}\left(q_z\right)I_e^{\square}\left(q_{\square}\right)+D_hI_h^{\perp}\left(q_z\right)I_h^{\square}\left(q_{\square}\right) \tag{2.3}$$

The expressions for the overlap integrals in 2D read:

$$\begin{aligned} I_{e(h)}^{\square}\left(\mathbf{q}_{\square}\right)&=\left(\sqrt{\frac{2}{\pi}}\frac{1}{a_b^{2D}}\right)^2\int d^2r\,e^{-\left(2|r|/a_b^{2D}\right)}\exp\left(im_{e(h)}\mathbf{q}_{\square}\mathbf{r}/\left(m_e+m_h\right)\right)\\ &=\left(1+\left(\frac{m_{e(h)}q_{\square}a_b^{2D}}{2M_x}\right)^2\right)^{-3/2}\end{aligned} \tag{2.4}$$

For an infinite quantum well, we approximate the z-dependence of the overlap integral as follows:

$$\begin{aligned} I_{e(h)}^{\perp}\left(q_z\right)&=\int dz\left|f_{e(h)}\left(z\right)\right|^2e^{iq_zz}\\ &=\frac{4ie^{-\frac{1}{2}iq_z\pi}\left(e^{iq_z\pi}-1\right)}{q_z\left(4-q_z{}^2\right)\pi}\end{aligned} \tag{2.5}$$

The second expression sets the limits for the effective interaction between excitons and phonons depending on the phonon wave vector in the growth direction.

In 3D the overlap integral reads:

$$I_{e(h)}\left(\mathbf{q}\right)=\left(1+\left(\frac{m_{e(h)}a_B\mathbf{q}}{2M}\right)^2\right)^{-2} \tag{2.6}$$

The piezoelectric interaction matrix element in wurtzite structures writes, according to E. Cohen and M.D. Sturge (1982):

$$\begin{aligned} M_{TA(LA)}\left(q\right)=e\sqrt{\frac{\hbar q}{2\rho c_{s.TA(LA)}V}}&[e_{15}\sin^2\theta\left(U_z\sin\theta+U_y\cos\theta\right)\\ &+e_{13}U_y\sin\theta\cos\theta+e_{33}U_z\cos^2\theta]\end{aligned} \tag{2.7}$$

where $c_{s.TA(LA)}$ are the transverse and the longitudinal sound velocities, respectively. $U_{x,y,z}$ is the displacement of atoms in the unit cell, θ is the angle between $\mathbf{q}$ and z axis, and e_{15},e_{33},e_{13} are the nonzero components of the piezoelectric tensor in wurtzite structures. The angular factors in the Eqn. (2.7) can be spherically averaged to give effective piezoelectric constants for TA and LA phonons, respectively:

$$\left\langle e_{TA}^2 \right\rangle = \frac{1}{7}e_{33}^2 + \frac{4}{35}e_{33}\left(e_{31}+2e_{15}\right) + \frac{8}{105}\left(e_{31}+2e_{15}\right)^2$$
$$\left\langle e_{LA}^2 \right\rangle = \frac{2}{35}\left(e_{33}-e_{31}-e_{15}\right)^2 + \frac{16}{105}e_{15}\left(e_{33}-e_{31}-e_{15}\right) + \frac{16}{35}e_{15}^2 \tag{2.8}$$

Using the Fermi Golden Rule one can write the scattering rate for an exciton or an exciton-polariton with excitonic fraction x_k to go from a state $\mathbf{k}$ to a state $\mathbf{k}'$ by interaction with an acoustic phonon in the 2D case (here 0, 1 correspond to phonon absorption and emission):

$$W_{\mathbf{k}\to\mathbf{k}'}^{ac.ph} = \frac{2\pi}{\hbar}\frac{L}{2\pi}x_k x_{k'}\int_{q_z}\frac{\hbar q}{2\rho SL}\left(\frac{\left|G\left(\mathbf{k}-\mathbf{k}'\right)\right|^2}{c_s} + \frac{e^2\left\langle e_{TA}^2\right\rangle}{c_{s.TA}} + \frac{e^2\left\langle e_{LA}^2\right\rangle}{c_{s.LA}}\right)\left(0,1+N_{\mathbf{k}-\mathbf{k}'+\mathbf{q}_z}^{ac.ph}\right)\times$$
$$\times\frac{\hbar\gamma_{k'}/\pi}{\left(E\left(k'\right)-E\left(k\right)\mp\hbar\omega_{\mathbf{k}-\mathbf{k}'+\mathbf{q}_z}\right)^2+\left(\hbar\gamma_{k'}\right)^2}dq_z \tag{2.9}$$

and in the 3D case :

$$W_{\mathbf{k}\to\mathbf{k}'}^{ac.ph} = \frac{2\pi}{\hbar}\frac{V}{8\pi^3}x_k x_{k'}\int_{\mathbf{q}}\frac{\hbar q}{2\rho V}\left(\frac{\left|G\left(\mathbf{k}-\mathbf{k}'\right)\right|^2}{c_s} + \frac{e^2\left\langle e_{TA}^2\right\rangle}{c_{s.TA}} + \frac{e^2\left\langle e_{LA}^2\right\rangle}{c_{s.LA}}\right)\left(0,1+N_q^{ac.ph}\right)\times$$
$$\times\frac{\hbar\gamma_{k'}/\pi}{\left(E\left(k'\right)-E\left(k\right)\mp\hbar\omega_q\right)^2+\left(\hbar\gamma_{k'}\right)^2}d\mathbf{q} \tag{2.10}$$

The integration in 3D case is more complicated because it is performed for a 3D vector $\mathbf{q}$.

The interaction with LO phonons is mainly mediated by the Froehlich mechanism (H. Froehlich, 1937). The matrix element of interaction reads:

$$M_{LO}\left(\mathbf{q}\right) = \frac{-e}{q}\sqrt{\frac{\hbar\omega_{LO}}{2V}\left(\frac{1}{\varepsilon_0\varepsilon_\infty}-\frac{1}{\varepsilon_0\varepsilon_s}\right)} = \frac{M_0^{LO}}{q\sqrt{V}} \tag{2.11}$$

where $\hbar\omega_{LO}$ is the optical phonon energy (90 meV in GaN), ε_∞ is the optical dielectric constant, ε_s is the static dielectric constant, V is the normalization volume. In 2D one considers quantized optical phonons having $q_z^m = m\pi/L$, where L is the QW width. The overlap between exciton and phonon wave-function quickly vanishes when *m* increases. Therefore it is sufficient to consider only the first confined phonon state. Considering a flat dispersion for LO phonons, one can write the 2D scattering rate:

$$W_{\mathbf{k}\to\mathbf{k}'}^{LO.ph} = \frac{2}{\pi^2\hbar}\frac{L}{S}x_k x_{k'}\left|M_0^{LO}\right|^2\left(0{,}1+\frac{1}{\exp\left(-\hbar\omega_{LO}/k_BT\right)-1}\right)\times$$
$$\times\frac{\hbar\gamma_{k'}}{\left(E(k')-E(k)\mp\hbar\omega_{LO}\right)^2+\left(\hbar\gamma_{k'}\right)^2} \tag{2.12}$$

There is no integration because we account for a single value of quantized wave vector in *z* direction, and the in-plane component of the phonon wave vector is negligible compared with this value.

In 3D the integration for LO phonons is the same as for the acoustic phonons (Eq. (2.10)), except that the energy of the phonon does not depend on its wave vector (flat dispersion).

2.3.2. Exciton-exciton interaction

The exciton-exciton interaction has been considered in Born approximation. We have taken the constant of paraexciton interaction (triplet configuration), which is different in 3D and 2D. The 2D value is (F. Tassone and Y. Yamamoto, 1999):

$$M_{ex} \approx 6\frac{E_b a_B^2}{S} \tag{2.13}$$

and the 3D value is (A.I. Bobrysheva *et al*, 1972):

$$M_{ex} \approx \frac{13\pi}{3}\frac{E_b a_B^3}{V} \tag{2.14}$$

These approximations remain valid for wavevectors smaller than the inverse Bohr radius. They are based on the fact that the exchange term dominates other interaction terms.

The binding energy and the exciton Bohr radius are, of course, different in both cases. The difference in these matrix elements is one of the main sources of the threshold difference in bulk and QW cavities, because the exciton-exciton interaction becomes dominant once the states become strongly occupied.

The polariton-polariton scattering rate reads:

$$W_{\mathbf{k}\to\mathbf{k}'}^{pol} = \frac{2\pi}{\hbar}\sum_{\mathbf{q}}\left|M_{ex}\right|^2 x_k x_{k'} x_q x_{\mathbf{q}+\mathbf{k}'-\mathbf{k}} N_{\mathbf{q}}^{pol}\left(1+N_{\mathbf{q}+\mathbf{k}'-\mathbf{k}}^{pol}\right)\times$$
$$\times\frac{\hbar\gamma_{k'}/\pi}{\left(E(k')-E(k)+E(\mathbf{q}+\mathbf{k}'-\mathbf{k})-E(q)\right)^2+\left(\hbar\gamma_{k'}\right)^2} \tag{2.15}$$

Passing to the thermodynamic limit in the plane, this rate can be expressed as (2D):

$$W^{pol}_{\mathbf{k}\to\mathbf{k}'} = \frac{S}{2\pi^2\hbar}\int d^2\mathbf{q}\left|M_{ex}\right|^2 x_k x_{k'} x_q x_{\mathbf{q}+\mathbf{k}'-\mathbf{k}} N^{pol}_{\mathbf{q}}\left(1+N^{pol}_{\mathbf{q}+\mathbf{k}'-\mathbf{k}}\right)\times \\ \times\frac{\hbar\gamma_{k'}}{\left(E(k')-E(k)+E(\mathbf{q}+\mathbf{k}'-\mathbf{k})-E(q)\right)^2+\left(\hbar\gamma_{k'}\right)^2} \tag{2.16}$$

and in 3D :

$$W^{pol}_{\mathbf{k}\to\mathbf{k}'} = \frac{V}{4\pi^3\hbar}\int d^3\mathbf{q}\left|M_{ex}\right|^2 x_k x_{k'} x_q x_{\mathbf{q}+\mathbf{k}'-\mathbf{k}} N^{pol}_{\mathbf{q}}\left(1+N^{pol}_{\mathbf{q}+\mathbf{k}'-\mathbf{k}}\right)\times \\ \times\frac{\hbar\gamma_{k'}}{\left(E(k')-E(k)+E(\mathbf{q}+\mathbf{k}'-\mathbf{k})-E(q)\right)^2+\left(\hbar\gamma_{k'}\right)^2} \tag{2.17}$$

As one can see, the *a priori* unknown distribution of polaritons is needed to calculate scattering rates. This means that in any simulation these scattering rates should be updated dynamically throughout the simulation time, which can be extremely time consuming.

Polariton-polariton scattering has been shown to be extremely efficient when a microcavity is excited resonantly, and it leads to many interesting effects discussed in all further chapters (we will be considering only cavities with QWs in these chapters, therefore, using Eq. (2.13) as the estimate for the exciton-exciton interaction in triplet configuration). It also plays a fundamental role in the case of non-resonant excitation.

2.3.3. Exciton-electron interaction

The exciton-electron scattering rate can be written using the Fermi Golden Rule:

$$W^{el}_{\mathbf{k}\to\mathbf{k}'} = \frac{2\pi}{\hbar}\sum_{\mathbf{q}}\left|M^{el}_{\mathbf{q},\mathbf{k},\mathbf{k}'}\right|^2 x_k x_{k'} N^{el}_{\mathbf{q}}\left(1-N^{el}_{\mathbf{q}+\mathbf{k}'-\mathbf{k}}\right)\times \\ \times\frac{\hbar\gamma_{k'}/\pi}{\left(E(k')-E(k)+\frac{\hbar^2}{2m_e}\left(q^2-\left|\mathbf{q}+\mathbf{k}'-\mathbf{k}\right|^2\right)\right)^2+\left(\hbar\gamma_{k'}\right)^2} \tag{2.18}$$

where $N^{el}_{\mathbf{q}}$ is the electron distribution function and m_e the electron mass. The electrons are considered to be always at thermal equilibrium, and their distribution is given by the Fermi-Dirac function with a chemical potential

$$\mu_e = k_B T \ln\left(\exp\left(\frac{\hbar^2 n_e}{2\pi k_B T m_e}\right)-1\right) \tag{2.19}$$

where n_e is the electron concentration. $M^{el}_{\mathbf{q}}$ is the matrix element of interaction between an electron and an exciton. For the 3D case, we use the matrix element in Born approximation which was calculated by H. Haug and S. Koch (1977). For the 2D case, a more rigorous calculation has been developed in A. Kavokin, G. Malpuech (2003). The matrix

element is composed by a direct contribution and an exchange contribution. In 2D case the integrals for both can be done analytically, which gives the following result:

$$M_{dir}^{el} = \frac{2\pi e^2}{S\varepsilon|\mathbf{k}-\mathbf{k}'|}\left[\left(1+\xi_h^2\right)^{-3/2} - \left(1+\xi_e^2\right)^{-3/2}\right]$$
$$M_{exc}^{el} = \frac{8\pi e^2}{S\varepsilon}\frac{\left[\left(1+\xi_c^2\right)^{-3/2} - \left(1+4\xi_h^2\right)^{-3/2}\right]}{\left[a_B^{-2} + |\mathbf{q}-\beta_e\mathbf{k}'|^2\right]^{1/2}} \qquad (2.20)$$

where $\xi_{e,h} = \frac{1}{2}\beta_{e,h}|\mathbf{k}'-\mathbf{k}|a_B^{2D}$, $\xi_c = |\beta_e\mathbf{k}'+\mathbf{k}'-\mathbf{k}-\mathbf{q}|a_B^{2D}$, $\beta = m_e/m_{exc}$.

The scattering rate in the integral representation in 2D is written as :

$$W_{\mathbf{k}\to\mathbf{k}'}^{el} = \frac{S}{2\pi^2\hbar}\int_{\mathbf{q}} d^2\mathbf{q}\left|M_{\mathbf{q},\mathbf{k},\mathbf{k}'}^{el}\right|^2 x_k x_{k'} N_{\mathbf{q}}^{el}\left(1-N_{\mathbf{q}+\mathbf{k}'-\mathbf{k}}^{el}\right)\times$$
$$\times\frac{\hbar\gamma_{k'}}{\left(E(k')-E(k)+\frac{\hbar^2}{2m_e}\left(q^2-|\mathbf{q}+\mathbf{k}'-\mathbf{k}|^2\right)\right)^2+\left(\hbar\gamma_{k'}\right)^2} \qquad (2.21)$$

and in 3D as :

$$W_{\mathbf{k}\to\mathbf{k}'}^{el} = \frac{V}{4\pi^3\hbar}\int_{\mathbf{q}} d^3\mathbf{q}\left|M_{\mathbf{q},\mathbf{k},\mathbf{k}'}^{el}\right|^2 x_k x_{k'} N_{\mathbf{q}}^{el}\left(1-N_{\mathbf{q}+\mathbf{k}'-\mathbf{k}}^{el}\right)\times$$
$$\times\frac{\hbar\gamma_{k'}}{\left(E(k')-E(k)+\frac{\hbar^2}{2m_e}\left(q^2-|\mathbf{q}+\mathbf{k}'-\mathbf{k}|^2\right)\right)^2+\left(\hbar\gamma_{k'}\right)^2} \qquad (2.22)$$

The exciton-electron interaction has been predicted by G. Malpuech *et al* (2002) to facilitate the relaxation of polaritons towards the ground state. The exact value of free electron density due to residual n-doping in GaN is unknown, this was one of the adjustable parameters of the model. Results shown in the following section correspond to the density of $5\text{x}10^{11}$ cm^{-2}. This value is quite close to the values reported experimentally. For example, in the chapter of T. Paskova and B. Monemar on GaN growth in "Low-dimensional nitride semiconductors" edited by B. Gil (2002) the authors give the free carrier concentration of (6-7)$\text{x}10^{16}$ cm^{-3} as one of the best parameters ever achieved for GaN, which corresponds to surface density of $1.2\text{x}10^{12}$ cm^{-2} in our case (cavity thickness is 210 nm), two times the value we use. This residual doping does not have a significant impact on light-matter coupling.

The issues of polarization are neglected in the simulation, because its main goal is to show the possibility to overcome the relaxation problems linked with bottleneck effect (see below).

2.4. Simulation results

We present detailed results for a bulk cavity here, because for a cavity with QWs (although with parameters different from ours) the calculations have been performed and published by G. Malpuech *et al* (2002). However, the kinetic phase diagrams are presented for the first time for both types of cavities here. In further sections, a comparison of bulk and QW GaN polariton laser properties (threshold dependencies on temperature *etc*) will be shown.

2.4.1. Polariton relaxation in a bulk cavity

One of the evident outcomes of a kinetic relaxation simulation is a distribution function. We start by presenting initial and final polaritons distribution functions below and above threshold. Note that since we perform simulation in a pulse excitation case, the "final" distribution function is not a static one, but rather a function corresponding to a moment of time, when the occupation of the ground state is maximal. All these results were calculated at 300 K with cavity lifetime 0.5 ps and inhomogeneous broadening 15 meV. Figure 2.8 shows polariton distribution below threshold. At around 10^7 m^{-1} one can clearly see a bottleneck, which, however, is not strongly populated. Above threshold the distribution changes drastically – see figure 2.9. The occupation numbers of the ground state and the nearby states become very high, and the bosonic stimulation becomes dominant. There is no signature of a bottleneck any more. Once again, the "final" distribution is not a static one, which is why all the polaritons do not condense in the ground state only, but rather occupy also the nearby states.

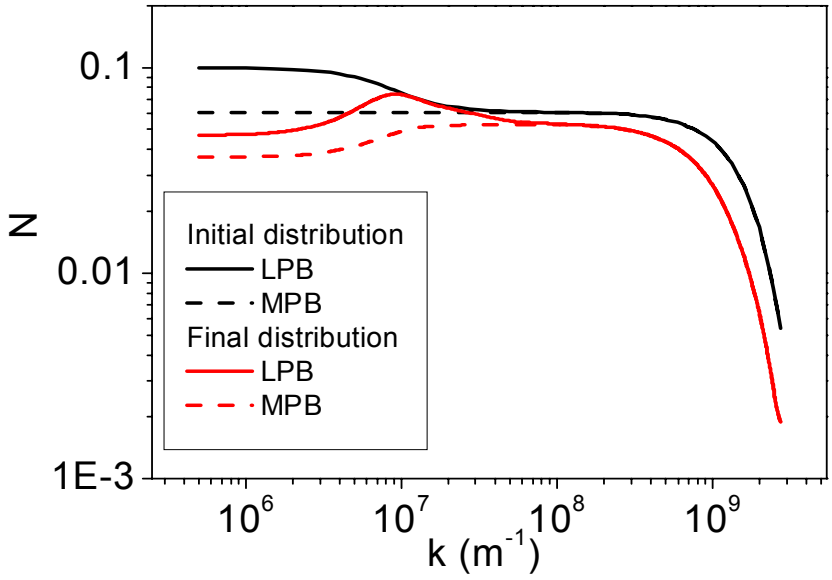

Figure 2.8. Polariton distribution below threshold, t_i=0 ps, t_f=8 ps, n_i=2x10^{13} cm^{-2}.

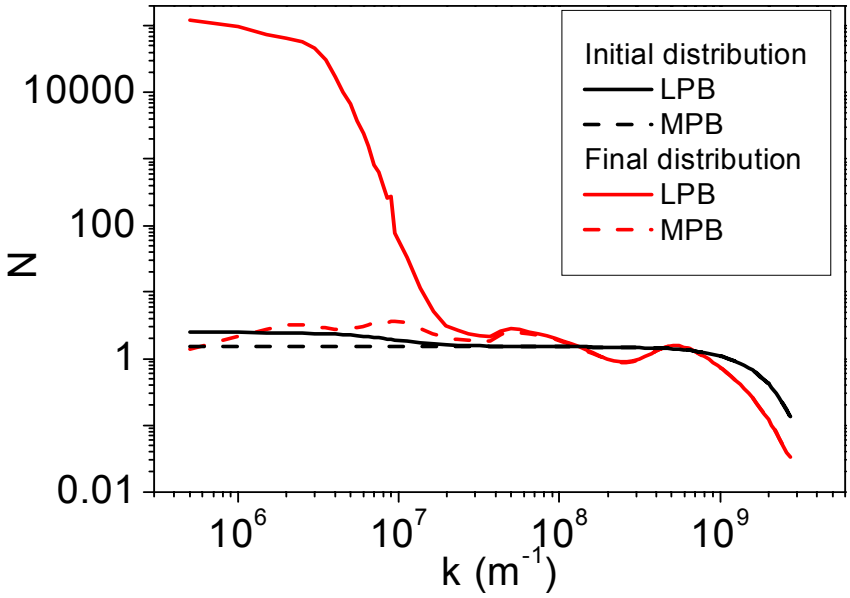

Figure 2.9. Polariton distribution above threshold, t_i=0 ps, t_f=8 ps, n_i=3.5x10^{13} cm^{-2}.

With the polariton distribution function calculated over the time, one can find an experimentally measurable quantity – the angular-dependent time-integrated emission intensity (figure 2.10). Here one does not in general see a bottleneck below threshold, the angular dependence is very broad and flat. The bottleneck becomes visible only in a very narrow range of pumping intensity. Above threshold, the emission is concentrated in a cone of several degrees. This narrowing is a manifestation of the Bose-Einstein condensation.

The angular-dependent time-integrated emission intensity can be directly compared with the experimental one (figure 2.11) published by S. Christopoulos *et al* (2007). Under the same experimental conditions, the agreement is very good. Flat distribution below threshold and narrow distribution above threshold are well reproduced. Note that flat angular distribution of time-integrated intensity of emission does not mean the absence of the bottleneck, because the intensity of emission contains also the photonic fraction of the states, which decreases the luminescence efficiency of the states with high wave vectors. To be equally emitting, these states need to be higher populated, thus the flat emission intensity is a manifestation of a bottleneck.

One can also calculate the 3D image of polariton condensation in momentum space (figure 2.12), like the one presented in J. Kasprzak *et al* (2006) or earlier in K.B. Davis *et al* (1995). This image clearly demonstrates that above threshold the polaritons are strongly redistributed and that the most occupied state is the ground state. Such an image has been the first proof of Bose-Einstein condensation of cold atoms in the 90s.

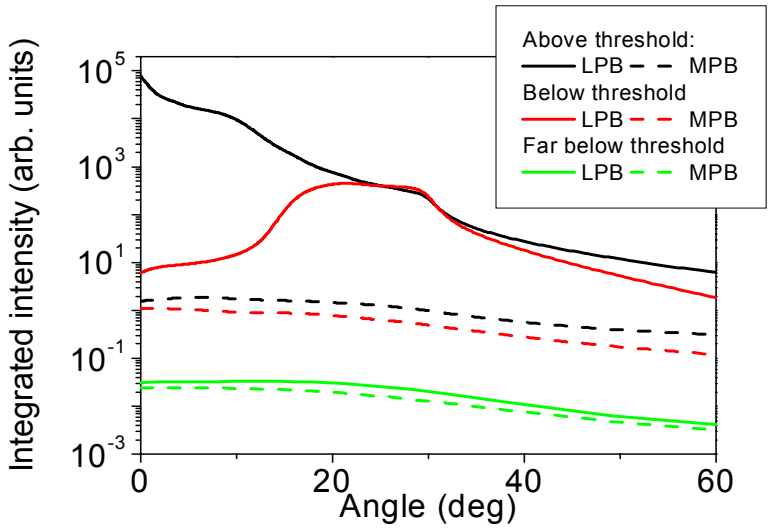

Figure 2.10. Angular distribution of time-integrated emission below and above threshold; $n_{i1}=1x10^{13}cm^{-2}$; $n_{i2}=3x10^{13}cm^{-2}$; $n_{i3}=3.5x10^{13}cm^{-2}$.

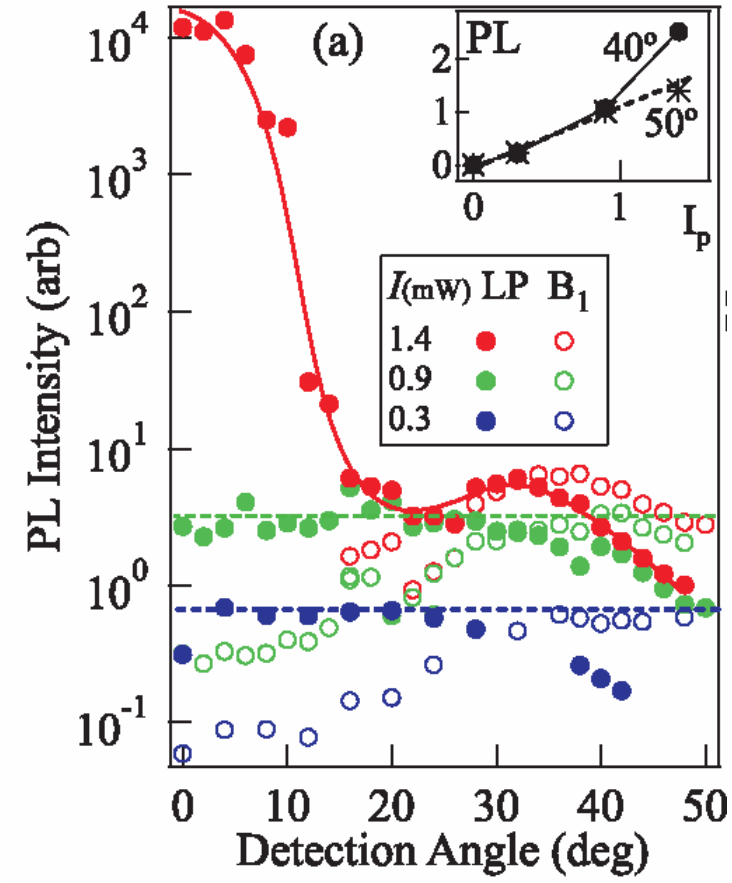

Figure 2.11. Experimental results showing time-integrated PL intensity versus angle (figure from S. Christopoulos *et al*, 2007).

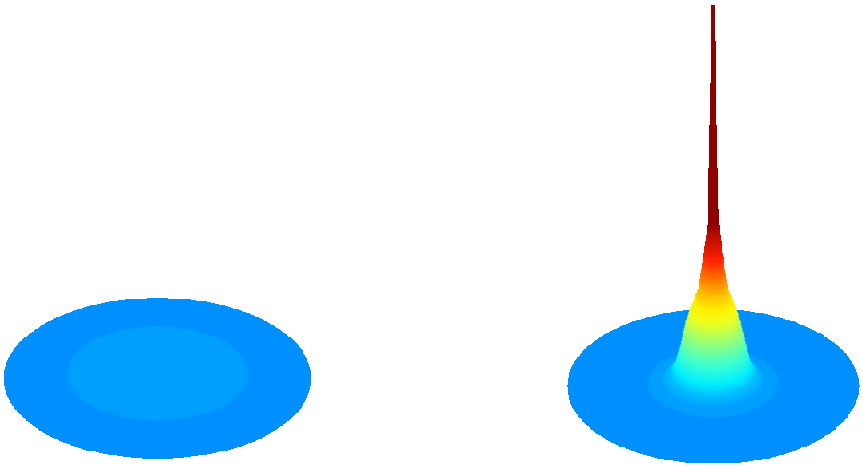

Below threshold (x1000) *Above threshold*

Figure 2.12. 3D reciprocal space images of time-integrated emission

Another comparison can be made with the dependence of the intensity of emission from the ground state on the pumping power (initial density of excitons created by the laser pulse). The theoretical curve is shown on figure 2.13, and the corresponding experimental one – on figure 2.14. This dependence shows a clear threshold with a very high jump of intensity (of the order of 10^3). Such a threshold can only be obtained with a relatively high bottleneck population of polaritons which collapses to the ground state once the bosonic stimulation becomes strong enough. The shape of this curve depends strongly on the electron density, which was a fitting parameter in our calculations, as mentioned before. Higher electron density facilitates polariton relaxation and thus weakens the intensity jump at threshold. With the value chosen, the agreement between theory and experiment is very good.

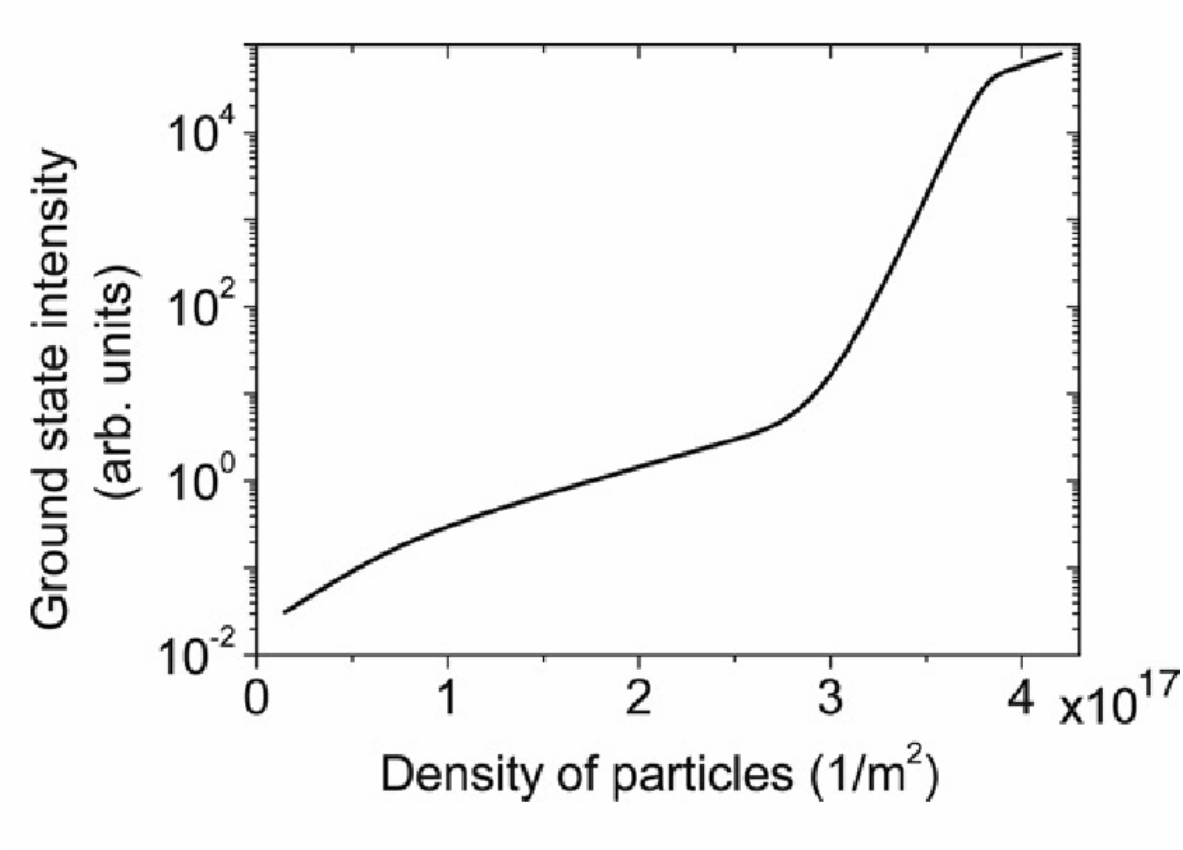

Figure 2.13. Time-integrated intensity of emission from the ground state versus particle density

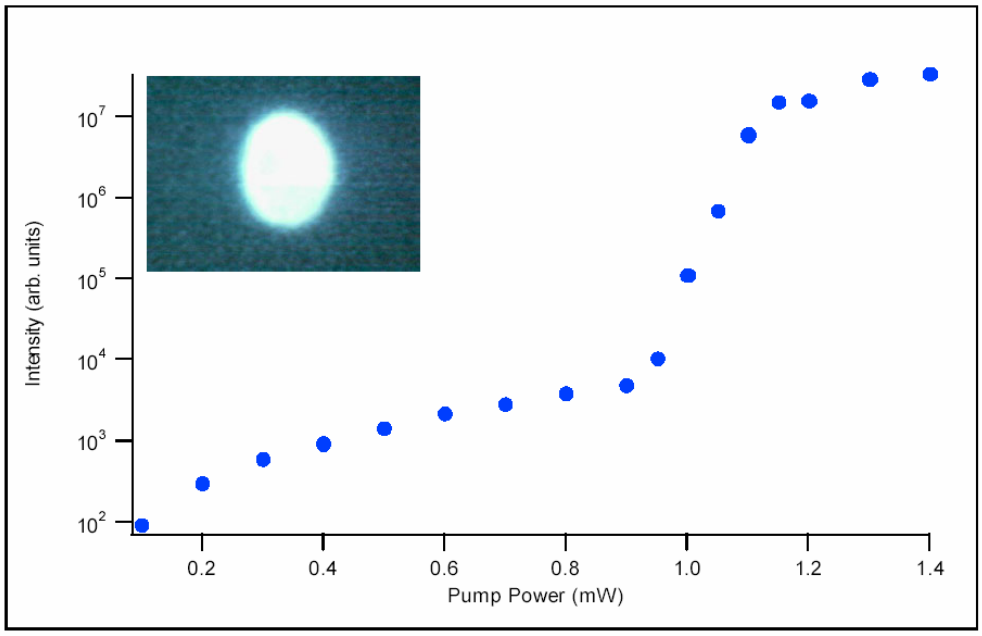

Figure 2.14. Power-dependent emission from a bulk GaN microcavity at T=300 K; inset showing spatial image of emission (from G. Baldassari H. v. H. *et al*, 2007)

2.4.2. Kinetic phase diagrams of bulk and QW cavities

In this section we present the kinetic phase diagrams of both bulk and QW GaN microcavities. We compare the two in order to find a better candidate for the fabrication of the polariton laser.

Figure 2.15 shows the dependence of the time-integrated intensity of emission from the ground state versus the initial polariton density (which is proportional to the pumping power) for bulk and QW cavities at 300 K (cavity lifetime 0.5 ps, inhomogeneous broadening 15 meV). This curve has a typical non-linearity corresponding to the threshold of bosonic stimulation. The threshold densities $3x10^{12}$ cm^{-2} in QW cavity and $9x10^{13}$ cm^{-2} in bulk cavity lie well below the Mott densities $3x10^{13}$ and $5x10^{14}$ cm^{-2} correspondingly, which are determined from the exciton Bohr radius (34 Å for bulk and 20 Å for QWs). We took QW width of 40A. We therefore expect that they arise in the strong coupling regime. The difference in the thresholds is explained mostly by the exciton-exciton interaction matrix element, which depends on the exciton Bohr radius and binding energy. However, the dynamics of relaxation in bulk and QW is also different, and that plays a role as well. The emission intensity jump at threshold is of about 3 orders of magnitude. In a normal laser, this would correspond to a beta factor smaller than 10^{-3}. Such a small beta in a normal bulk semiconductor laser would lead to a lasing threshold, orders of magnitude larger than the one we found for a bulk cavity.

Figure 2.16 shows the polariton lasing threshold versus temperature calculated for QW (a) and bulk (b) cavities for pulsed excitation (black curve) and in the thermodynamic equilibrium (assuming an infinite particle lifetime – shown in red). It therefore represents a comparison between a thermodynamic and a kinetic phase diagram for the polariton phase transition. The kinetic curves show a large threshold at low temperature because of the slow relaxation kinetics in this temperature range. This threshold is almost flat because of disorder-induced broadening (15 meV). At higher temperature, the threshold increases versus the temperature T because of the strong increase of the threshold in the thermodynamic equilibrium. At 300 K only one order of magnitude difference remains between the kinetic and thermodynamic thresholds. The threshold for QW cavities is found to be about 10 times lower than that for bulk cavities in a broad range of temperatures. The difference in thresholds between the QW and bulk cavities is mostly due to the difference in the matrix elements of exciton-exciton interaction, as mentioned above.

The figure 2.17 shows the threshold dependence on the cavity lifetime for two different temperatures: 300 K and 50 K. At 50 K the difference between the kinetic curve and

thermodynamic one is much higher than at 300 K, and so the kinetic curve approaches this limit very slowly with the increase of the lifetime. Again, the threshold is lower for QW cavities. The dependence on lifetime is more pronounced for cavities with QWs because a larger part of excitons is coupled to light within such cavities, whereas in bulk the lifetime of most excitons is not determined by the cavity lifetime.

We have also studied the dependence of the threshold density on the inhomogeneous broadening. The figure 2.18 has been calculated at 1 K and at 300 K, with 0.5 ps lifetime. One can see that the decrease of disorder can lead to strong decrease of the threshold density, especially at low temperatures.

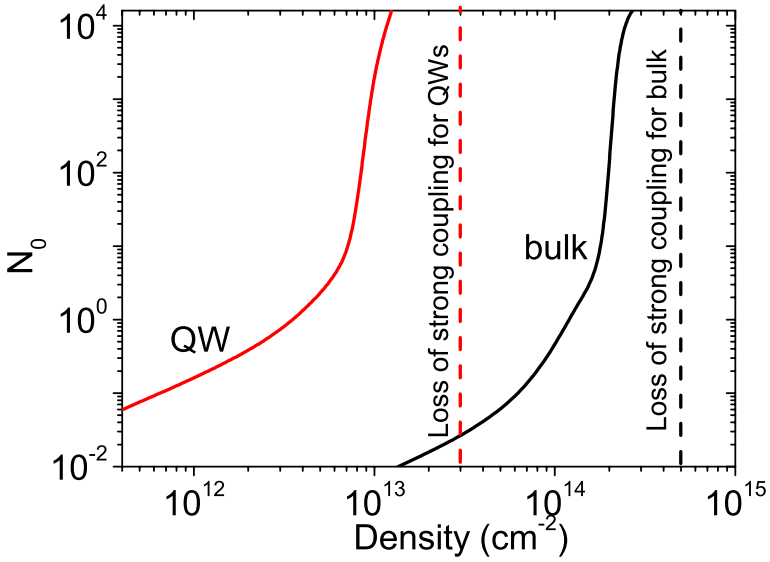

Figure 2.15. Threshold as a function of polariton density for bulk and QW cavities at 300 K

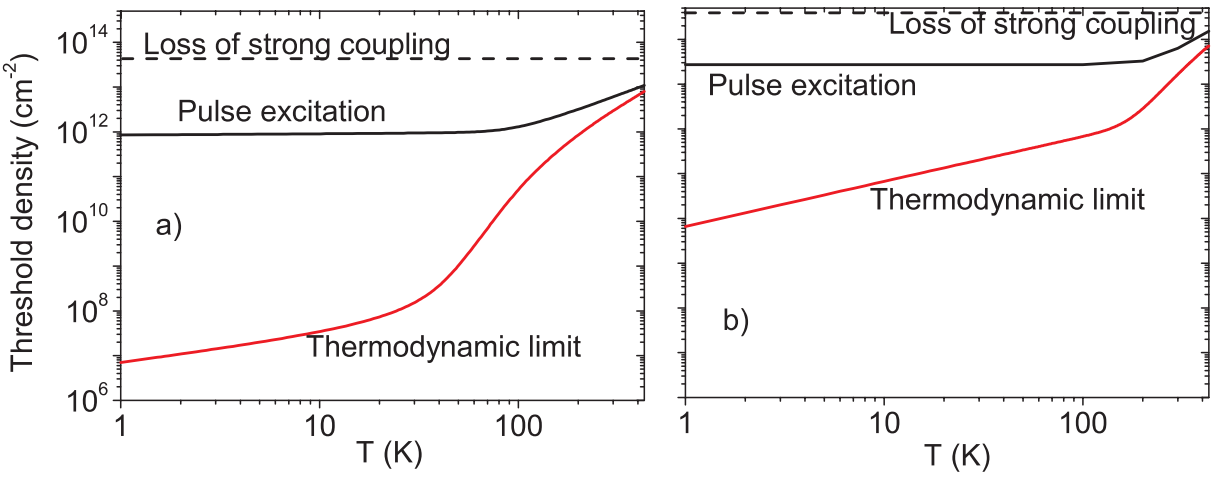

Figure 2.16. Threshold as a function of temperature for a) QW and b) bulk cavities

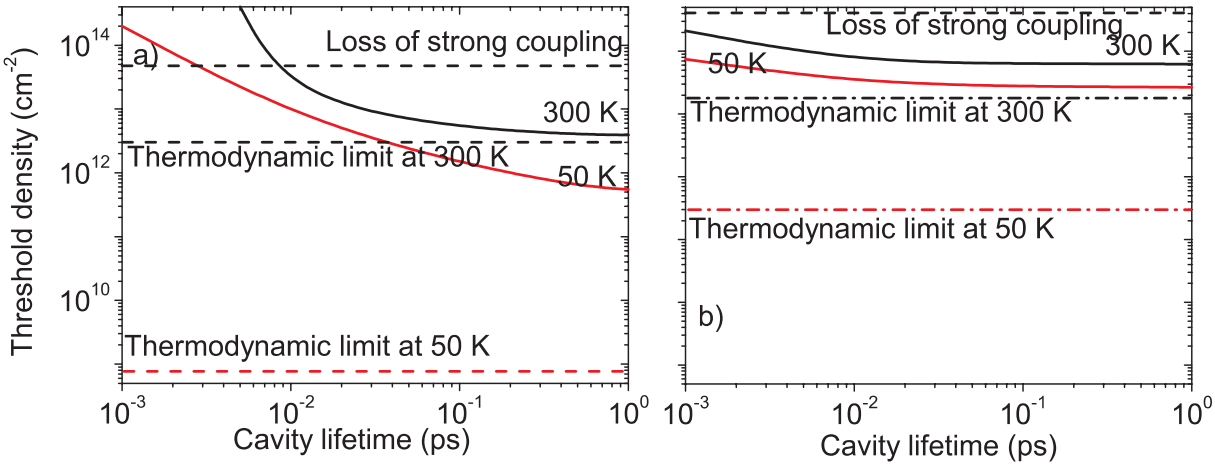

Figure 2.17. Threshold as a function of cavity lifetime for a) QW and b) bulk cavities

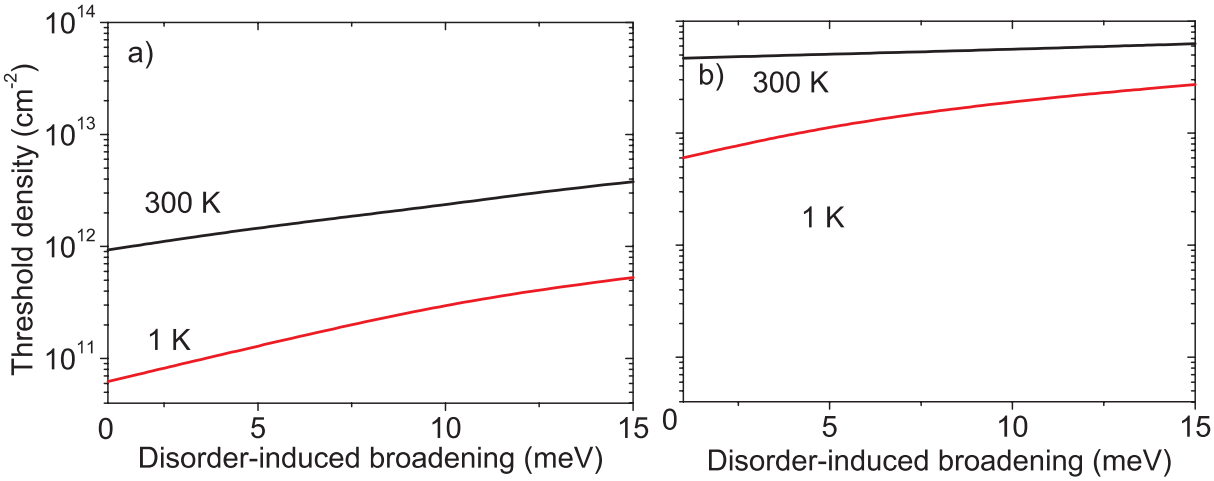

Figure 2.18. Threshold as a function of inhomogeneous broadening for a) QW and b) bulk cavities

2.5. Conclusions

Only a few years ago the polariton laser was a dream far from achievement, but in the last two years polariton Bose condensation and lasing has been observed in three different materials by three groups. The theoretical predictions have proven to be right.

We have shown that presently grown bulk GaN cavities can indeed operate as a polariton laser at room temperature. Our calculations compare very well with existing experimental results. Similar cavities with QWs, which present a technological challenge, would have a lower lasing threshold, but also a lower maximal density. We present a set of kinetic phase diagrams of polariton lasing and found the range of key parameters in which polariton lasers can operate. This analysis shows that GaN structures should operate close to the thermodynamic equilibrium at 300 K.

Chapter 3. Spin-dependent polariton-polariton scattering

This chapter is devoted to various polarization effects which can be observed in polaritonic systems. Such effects are most prominent in the optical parametric oscillator configuration, and we will concentrate on this particular situation. However, another interesting case is the Kerr rotation in a diluted magnetic cavity, which will be described in the last section of this chapter. All these effects are conveniently described with the pseudospin formalism that has been introduced in chapter 1.

Contents

3.1. Spin-dependent Boltzmann equations for polaritons

In this section we will use the spin-dependent Boltzmann equations for bosons introduced in chapter 1, adding several terms describing polariton-specific behaviour, like pseudospin rotation due to TE-TM splitting, self-induced Larmor precession and others.

The general form of the kinetic equations written in terms of the occupation numbers and pseudospins reads:

$$\frac{dN_{\mathbf{k}\uparrow,\downarrow}}{dt} = -\frac{N_{\mathbf{k}\uparrow,\downarrow}}{\tau_k} + \left(\frac{dN_{\mathbf{k}\uparrow,\downarrow}}{dt}\right)\Big|_{rot} + \left(\frac{dN_{\mathbf{k}\uparrow,\downarrow}}{dt}\right)\Big|_{phon} + \left(\frac{dN_{\mathbf{k}\uparrow,\downarrow}}{dt}\right)\Big|_{pol-pol} \tag{3.1}$$

$$\frac{d\mathbf{S}_{\perp,\mathbf{k}}}{dt} = -\frac{\mathbf{S}_{\perp,\mathbf{k}}}{\tau_k} + \left(\frac{d\mathbf{S}_{\perp,\mathbf{k}}}{dt}\right)\Big|_{rot} + \left(\frac{d\mathbf{S}_{\perp,\mathbf{k}}}{dt}\right)\Big|_{phon} + \left(\frac{d\mathbf{S}_{\perp,\mathbf{k}}}{dt}\right)\Big|_{pol-pol} \tag{3.2}$$

where the first term describes the radiative decay of exciton polaritons, the indices *rot*, *phon*, *pol-pol* correspond to the pseudospin rotation in the effective magnetic field, the scattering with acoustic phonons and polariton-polariton scattering respectively.

The interaction terms have been written in chapter 1 for bosons with spin ± 1 interacting with a reservoir by means of phonons (Eqs. (1.68)-(1.72)). In this section we will pay special attention to the different types of pseudospin rotation terms, which are specific for exciton-polaritons.

3.1.1. TE-TM splitting

The TE-TM splitting (already mentioned in chapter 1) is a splitting between two linear polarizations of a photon: TE, when the plane of oscillations of the electric field lies in the plane of the cavity, and TM, when the plane of oscillations of the magnetic field lies in the plane of the cavity. This splitting is also called longitudinal-transverse, or LT. It results from several factors, namely, different reflectivity and penetration length of dielectric mirrors for TE and TM polarizations, different angular dispersions in these polarizations, and energy dependence of the refractive index of the cavity. An extensive theoretical analysis of various cavities with QWs is given in Panzarini *et al* (1999). The formulae from this paper will be used throughout the thesis. Generally, the TE-TM splitting is proportional to the polariton wave vector squared. The exciton state in a QW in a cavity is also split, but this splitting is usually much smaller than the photon TE-TM splitting. In this chapter we use the TE-TM splitting as a fitting parameter.

3.1.2. Self-induced Larmor precession

The self-induced Larmor precession discovered for the polariton parametric amplifiers (see below) by I. Shelykh *et al* (2004) is one of the effects caused by the anisotropy of the polariton-polariton interaction (i.e. dependence of the scattering amplitude on mutual orientation of the pseudospins of two interacting polaritons). Because of this anisotropy, an imbalance between σ^+ and σ^- populations is responsible for the appearance of an effective magnetic field in the *z*-direction. The main idea is that a term $2\mathbf{e}_z\sum_{\mathbf{k}'}\left(V^{(1)}_{\mathbf{k},\mathbf{k}',0}-V^{(2)}_{\mathbf{k},\mathbf{k}',0}\right)\left(N_{\mathbf{k}'\uparrow}-N_{\mathbf{k}'\downarrow}\right)$ can be rewritten as an effect of an action of a magnetic field Ω_{eff} on the polariton in-plane pseudospin $S_\perp$.

3.1.3. Rotation terms

The rotation terms taking into account the TE-TM (LT) splitting and effective magnetic field read, as in chapter 1:

$$\left(\frac{dN_{\mathbf{k}\uparrow}}{dt}\right)\Bigg|_{rot}=-\left(\frac{dN_{\mathbf{k}\downarrow}}{dt}\right)\Bigg|_{rot}=\mathbf{e}_z\cdot\left[\mathbf{S}_{\perp,\mathbf{k}}\times\mathbf{\Omega}_{LT,\mathbf{k}}\right] \tag{3.3}$$

$$\left(\frac{d\mathbf{S}_{\perp,\mathbf{k}}}{dt}\right)\Bigg|_{rot}=\left[\mathbf{S}_{\perp,\mathbf{k}}\times\mathbf{\Omega}_{\mathrm{int},\mathbf{k}}\right]+\frac{\left(N_{\mathbf{k}\uparrow}-N_{\mathbf{k}\downarrow}\right)}{2}\bar{\mathbf{\Omega}}_{LT,\mathbf{k}} \tag{3.4}$$

where $\mathbf{e}_z$ is a unitary vector in the direction of the structure growth axis, $\mathbf{\Omega}_{LT,\mathbf{k}}$ is an effective in- plane magnetic field produced by TE- TM splitting, $\bar{\mathbf{\Omega}}_{LT,\mathbf{k}}$ is obtained from $\mathbf{\Omega}_{LT,\mathbf{k}}$ by the rotation by 90° about the structure growth axis, the effective magnetic field $\mathbf{\Omega}_{\mathrm{int},\mathbf{k}}$ produced by the imbalance of the σ^+ and σ^- polaritons is given by the following expression deduced from the interaction Hamiltonian:

$$\hbar\mathbf{\Omega}_{\mathrm{int},\mathbf{k}}=2\mathbf{e}_z\sum_{\mathbf{k}'}\left(V^{(1)}_{\mathbf{k},\mathbf{k}',0}-V^{(2)}_{\mathbf{k},\mathbf{k}',0}\right)\left(N_{\mathbf{k}'\uparrow}-N_{\mathbf{k}'\downarrow}\right) \tag{3.5}$$

This is exactly the self-induced Larmor precession described above.

3.1.4. Polarization inversion during polariton-polariton scattering

One can show analytically that in the spontaneous scattering regime the pseudospin dynamics during polariton-polariton scattering acts reduces to

$$\frac{d\mathbf{S}_{0\perp}}{dt}=\frac{4\tau_0}{\hbar^2}\mathrm{Re}\left(V^{(1)}V^{(2)*}\right)\left(N_{1\uparrow}+N_{1\downarrow}\right)\mathbf{S}_{1\perp} \tag{3.6}$$

Here the indices 0 and 1 mark two different states (final and initial, respectively). The matrix elements $V^{(1)}$ and $V^{(2)}$ have opposite signs since two polaritons with parallel spins always repel, while two polaritons with opposite spins attract each other and can even form a bound state (bipolariton). As a result, the in-plane components of the pseudospin of polaritons scattered to the signal state are antiparallel to those of the pump, resulting in the signal polarization inversion (rotation by 90 degrees). This result holds both below and above threshold. The effect was explained for the first time by K.V. Kavokin *et al* (2005).

3.1.5. Polariton parametric amplifier

A specific experimental configuration, where the LPB is resonantly excited at a *magic angle*, is called a polariton (or optical) parametric amplifier. This magic angle is characterized by the fact that a pair of polaritons created by the pump in the pump state, which corresponds to this angle, can scatter into the signal and idler states while conserving the energy and momentum at the same time:

$$\begin{gathered} 2k_p = k_i \\ 2E_{LPB}\left(k_p\right) = E_{LPB}\left(0\right) + E_{LPB}\left(k_i\right) \end{gathered} \tag{3.7}$$

These conditions can be satisfied due to the non-parabolicity of the LPB in the strong coupling regime. The magic angle determined by (3.7) is usually close to the inflection point of the LPB dispersion. Due to the effect of bosonic stimulation, scattering intensity into the signal state can be greatly amplified by sending a weak probe pulse into this state. This is what is called parametric amplification. A schematic diagram of a polariton parametric oscillator is presented in figure 3.1.

However, in the experiments described in this chapter the threshold of parametric amplification is passed not by sending a probe to the signal state, but by increasing the intensity of the pump.

Different theoretical pictures of the polariton parametric oscillator have been drawn in literature. A micromodel describing polariton parametric oscillator and amplifier was proposed by C. Ciuti *et al* (2000) and in C. Ciuti *et al* (2001). In their model several important simplifying approximations have been used. The main one was to consider the pumped polariton state as a classical field which is valid only for the *cw* pumping below the stimulation threshold. An extended description of this model and its results can be found in a chapter by C. Ciuti, P. Schwendimann and A. Quattropani of a book edited by J. Baumberg, L. Viña, and S. Quin (2003). Other works (e.g. N.A. Gippius *et al*, 2004) are based on the

Gross-Pitaevskii equation. This allows taking into account all states of reciprocal space, but the spontaneous scattering, decoherence or relaxation associated with phonons are completely neglected. All these works neglect the spin degree of freedom, and so these models are not able to describe the polarisation properties of the emitted light.

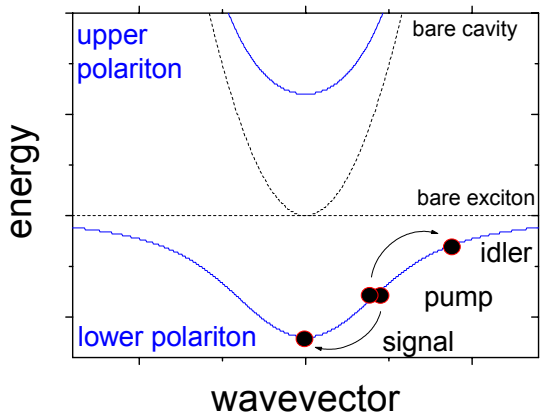

Figure 3.1. Polariton dispersion branches and the three states that form a polariton parametric oscillator

The model that we present here has the advantage of taking into account the polarization specifics of the polariton parametric amplifier and various decoherence processes. It lacks, however, the dispersion renormalization effects, which can affect the polarization as well. This question will be addressed in chapter 4, and it is also a subject of the work in progress.

3.2. Stationary OPO configuration

In this section we consider a *cw* pumped GaAs microcavity in OPO configuration. Extended experimental signal polarization studies have been performed by Krizhanovksii *et al* (2006), and here we present complete theoretical simulation of this data (which is also published in the paper mentioned above). It is the same GaAs cavity with 6 InGaAs QWs on which the bosonic nature of polaritons has been clearly demonstrated for the first time by a pump-probe experiment in the OPO configuration by P.G. Savvidis *et al* (2000). The structure exhibits Rabi splitting $\Omega = 6\,\mathrm{meV}$. Experimental measurements were carried out at 2K by

exciting with a *cw* laser in resonance with renormalized LPB at an angle of 12 degrees, close to the point of inflection of the LPB (Fig. 3.2(a), inset).

Figure 3.2 presents main experimental results. As one can immediately see, the circular polarization degree of the signal ρ_c depends on the pump power for both linear and circular polarization of the pump, with the maximum of polarization corresponding to the onset of stimulated scattering. For linear pumping, ρ_c depends as well on the angle of rotation of the polarization plane of the pump (0 degrees correspond to TE polarization). Detailed experimental maps of the signal polarization for different angles of rotation of the pump above the stimulation threshold are given in Fig. 3.3. Data were obtained for $\phi_{exc} = 45°$ (Fig. 3.3(a)) and $-33°$ (Fig. 3.3(b)), respectively, close to the angles for which $\rho_c = 0$, and at $\phi_{exc} = 0°$ (TE, Fig. 3.3(d)) and $\phi_{exc} = 90°$ (TM, Fig. 3.3(c)), for which the absolute value of ρ_c is maximal. It is found that when $\phi_{exc} = 45°$ and $-33°$, the linear polarization of the signal is rotated by $90 \pm 5°$ relative to the pump. For TE and TM excitation, $\rho_c = 40\% - 60\%$ and the linear polarization is rotated by 60 (120) degrees anticlockwise to the pump.

All this interesting and rich behavior can be described by the spin-dependent Boltzmann equations developed for bosons in chapter 1 and written for polaritons in section 3.1.

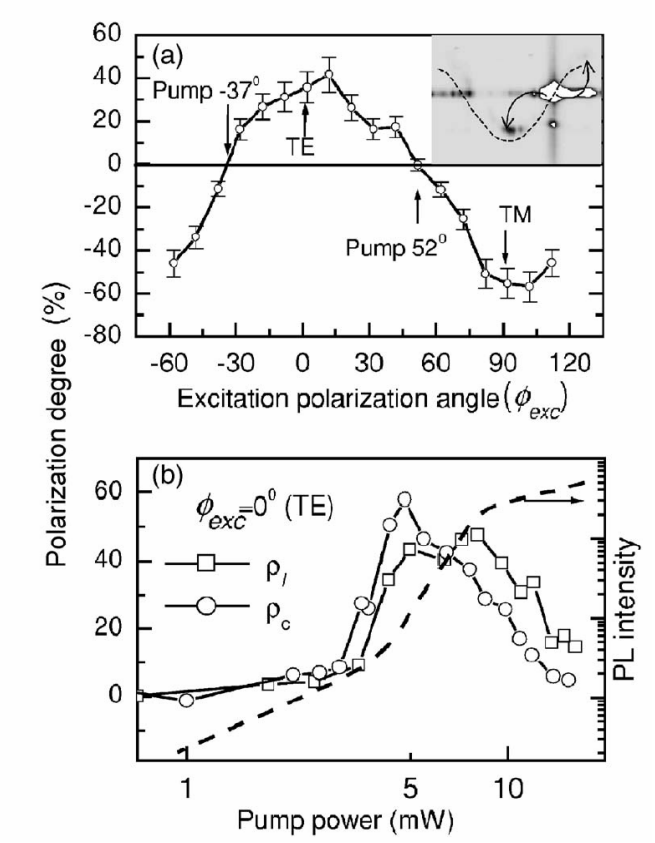

Figure 3.2. Experimental results with signal polarization degree for a stationary OPO configuration (Krizhanovskii *et al*, 2006).

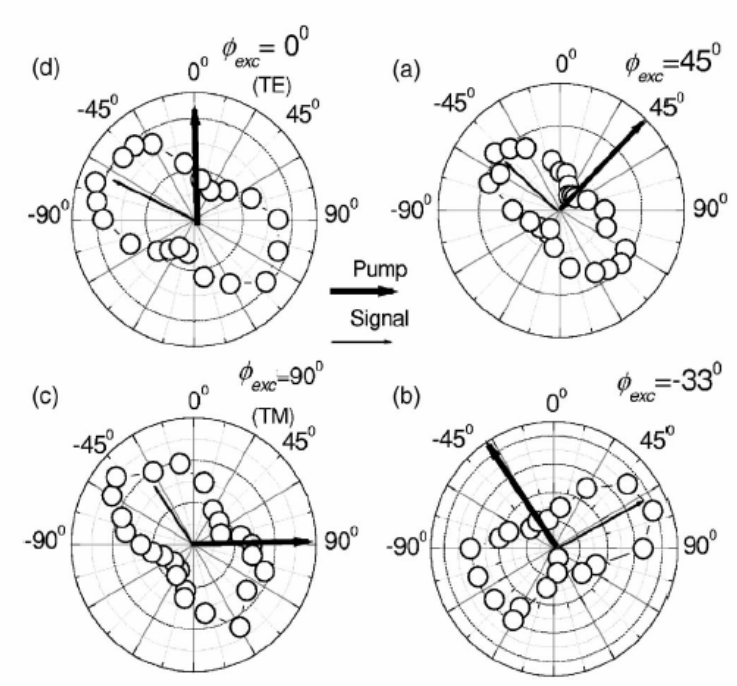

Figure 3.3. Polarization map of the signal for different angles of rotation of the polarization plane of the pump (Krizhanovskii *et al*, 2006).

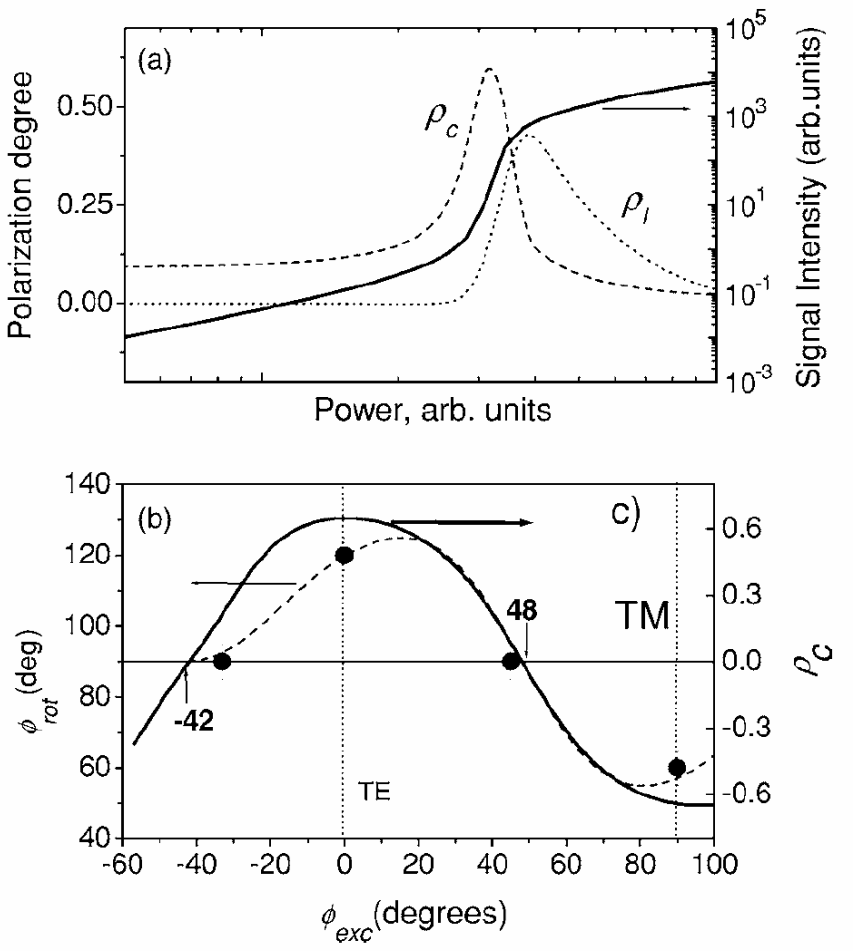

Figure 3.4. Theoretical simulation of the circular polarization degree and rotation of polarization plane of the signal versus pumping power and pump polarization angle: a) signal polarization degree and intensity versus pumping power; b) polarization rotation angle; c) signal circular polarization degree versus the pump polarization angle.

We consider three factors which can change the polariton pseudospin: 1) TE-TM splitting, which acts as an effective magnetic field in the plane of the structure; 2) self-induced Larmor precession (effective magnetic field in the growth direction); 3) polariton-polariton scattering (polarization inversion).

Figure 3.4 presents the results of numerical simulations for a linearly polarized pump at an angle with respect to TE. The parameters have been taken as follows: $V^{(1)} = 6xE_b a_B^2 / S$ where $a_B = 100\,\dot{A}$ is the two dimensional exciton Bohr radius, $E_b = 8\,\text{meV}$ is the exciton binding energy, x is the exciton fraction, and S is the laser spot area ($50\,\mu\text{m}$ diameter), $V^{(2)} = -0.01V^{(1)}$, $\tau = 4\,\text{ps}$. To fit the data we assumed $\Omega_{in-plane} = 0.05\,\text{meV}$ arises from the splitting between polariton states having polarization axes at +48 and -42 degrees

with respect to TE. The solid line in Fig. 3.4(a) shows the power dependence of the signal intensity, ρ_c and ρ_l versus pump power for $\phi_{exc} = 0$. The three curves show a clear threshold and have very similar forms to those observed experimentally in Fig. 3.2(b). ρ_c and ρ_l decay far above threshold, also as observed experimentally. In this regime the rotation of the pseudospin about the *z* axis becomes faster than the polariton lifetime, resulting in a decay of the time-averaged polarization.

The calculated variation of ρ_c versus ϕ_{exc} just above threshold in Fig. 3.4(b) shows that ρ_c is 0 when the pump polarization is parallel to one of the polarization eigenstates $\phi_{exc} = -42°$ or $\phi_{exc} = 48°$. For all other ϕ_{exc} the in-plane effective field rotates the pseudospin of the polaritons, which gains some circular projection, in good agreement with Fig. 3.2(a). The circular polarization changes sign for positive or negative angles with respect to -42 and +48 degrees, and achieves a maximum value when the in-plane magnetic field and the pseudospin are perpendicular to one another (45 degree tilt with respect to -42 and +48 degrees). The appearance of a nonzero circular component in the pump state gives rise to an effective magnetic field in the *z* direction. This field rotates the in-plane polarization in a direction which depends on the sign of ρ_c (the self-induced Larmor precession). The polaritons are then scattered from the pump to the signal. The in-plane polarization is in addition rotated by 90 degrees during this scattering event by the polariton-polariton scattering term.

The dependence of the angle ϕ_{rot} between the planes of polarization of the signal and the pump on ϕ_{exc}, is shown in Fig. 3.4(b). ϕ_{rot} is found to be exactly 90° when ρ_c is 0 and less (larger) than 90 when ρ_c is negative (positive) because of the self-induced Larmor precession. It is seen that the simulations (dashes), with the direction of the in-plane effective field different from that derived by the TE-TM directions, are in excellent agreement with experiment (circles). The most likely source of the in-plane field is the asymmetry of the QW in the z-direction (for the description of its effect see G. Malpuech *et al,* 2006).

3.3. Dynamic OPO study

In this section we present experimental and theoretical results on the polarization dynamics of a GaAs microcavity with a single 8 nm $Ga_{0.95}In_{0.05}As$ QW in the pulsed excitation case. The experiment is described in P. Renucci *et al* (2005) and together with theory in D.D. Solnyshkov *et al* (2007).

The experimental data presented below have been collected on two samples. The sample 1 consists of two Bragg mirrors made of 22(26) $AlAs/Al_{0.1}Ga_{0.9}As$ layers with a single *8 nm* wide $Ga_{0.95}In_{0.05}As$ QW embedded in the middle. The vacuum Rabi splitting is 3.5 *meV* and the photon lifetime in the cavity is $\tau_c \sim 8\ ps$. The sample 2 is similar to the previous one. It consists of two Bragg mirrors made of 17(27) $AlAs/Al_{0.1}Ga_{0.9}As$ layers; a single *8 nm* wide $Ga_{0.95}In_{0.05}As$ quantum well (QW) is embedded in the middle. The vacuum Rabi splitting is 3.7 *meV*, and the photon lifetime in the cavity is $\tau_c \sim 3\ ps$. In both samples, the cavity is wedged, so that the detuning δ between the cavity and exciton modes could be varied by moving the excitation spot on the sample surface. This has allowed to study the detuning dependence of the polariton spin relaxation.

The excitation beam, resonant with the LPB, is incident at an angle of 8° (±1°), so that it generates LPB polaritons in a state with initial in-plane wave vector $k_p \approx 1\times10^4$ cm^{-1}. The cavity photon lifetime is deduced from time resolved emission measurements performed at negative cavity detuning (δ = - 9 meV for sample 1 and δ = - 3 meV for sample 2). In the linear excitation case the polarization of the incident light was parallel to the crystallographic axis [110].

3.3.1. The model

Figure 3.5 shows a schematic diagram of the model of the polariton parametric amplifier that we consider in this section. The LPB dispersion curve has been calculated based on the parameters of the samples used in experiments. Our approach is to treat the polariton parametric amplifier as a spinor three-level system (pump, signal and idler) connected with a dissipative reservoir which consists mainly of bare exciton states, very close in energy to the pump and idler states in the zero detuning case. This coupling provides an additional mechanism of decay for the polariton population and pseudo-spin. Pump, signal and idler are coupled by the polariton- polariton parametric scattering, while the reservoir is taken into account by introduction of an effective spin decay time of the three main states. Polariton-

polariton scattering is treated within the framework of the Born-Markov approximation (for the description of the spinor parametric amplifier beyond markovian approximation see I.A. Shelykh *et al;* 2005; I.A. Shelykh *et al,* 2007).

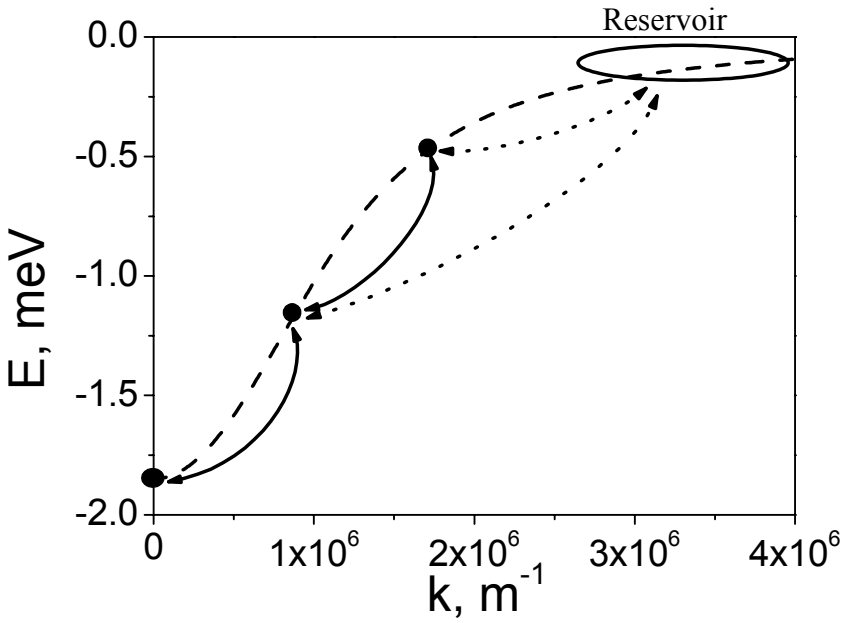

Figure 3.5. Schematic diagram of parametric amplifier with reservoir. The dashed line is the lower polariton dispersion. The black circles on the line are the signal pump and idler state respectively. The solid line arrows are sketching the parametric polariton scattering process. The dotted arrows show the phonon induced transfer between the idler state, the pump state and the excitonic reservoir.

To make the simulations feasible one can either neglect polariton-polariton collisions and consider the scattering with acoustic phonons and free electrons as the only mechanism of the energy relaxation in the system (see e.g. K.V. Kavokin *et al,* 2004), or retain all the scattering mechanisms but restrict the number of states in the reciprocal space to some reasonable minimum. The latter approach is standard in description of the polariton parametric amplifier. Usually only three states are taken into account: the signal, the pump and the idler (this restriction has been first performed by C.Ciuti *et al*, 2000). This is a reasonable approximation in the cavities with strong negative detuning where these three

states have extremely small wave numbers and thus lie at the photonic part of the LPB, so that their scattering with acoustic phonons is prohibited by energy and momentum conservation. On the other hand, for zero and positive detuning the pump and idler states are efficiently coupled with a thermal reservoir of polaritons in the excitonic part of the LPB. As we show, this coupling should be taken into account in order to achieve a satisfactory description of the influence of the detuning on the spin dynamics of parametric amplifiers.

We solve numerically the following system of kinetic equations that we write explicitly for a polariton parametric amplifier coupled with a reservoir:

$$\frac{dN_{s\uparrow}}{dt} = -\frac{N_{s\uparrow}}{\tau_s} + \left(\frac{dN_{s\uparrow}}{dt}\right)\Big|_{po} - N_{s\uparrow}\left(\frac{1}{\tau_s^r} + \frac{1}{2\tau_{s,z}^r}\right) + \frac{N_{s\downarrow}}{2\tau_{s,z}^r} \tag{3.8}$$

$$\frac{dN_{s\downarrow}}{dt} = -\frac{N_{s\downarrow}}{\tau_s} + \left(\frac{dN_{s\downarrow}}{dt}\right)\Big|_{po} - N_{s\downarrow}\left(\frac{1}{\tau_s^r} + \frac{1}{2\tau_{s,z}^r}\right) + \frac{N_{s\uparrow}}{2\tau_{s,z}^r} \tag{3.9}$$

$$\frac{d\mathbf{S}_{s\perp}}{dt} = -\mathbf{S}_{s\perp}\left(\frac{1}{\tau_s} + \frac{1}{\tau_s^r}\right) + \left(\frac{d\mathbf{S}_{s\perp}}{dt}\right)\Big|_{po} + [\mathbf{S}_{s\perp} \times \mathbf{\Omega}_{\text{int}}] - \frac{\mathbf{S}_s^x}{\tau_{s,x}^r} - \frac{\mathbf{S}_s^y}{\tau_{s,y}^r} \tag{3.10}$$

$$\frac{dN_{p\uparrow}}{dt} = -\frac{N_{p\uparrow}}{\tau_p} + \left(\frac{dN_{p\uparrow}}{dt}\right)\Big|_{po} - N_{p\uparrow}\left(\frac{1}{\tau_p^r} + \frac{1}{2\tau_{p,z}^r}\right) + \frac{N_{p\downarrow}}{2\tau_{p,z}^r} \tag{3.11}$$

$$\frac{dN_{p\downarrow}}{dt} = -\frac{N_{p\downarrow}}{\tau_p} + \left(\frac{dN_{p\downarrow}}{dt}\right)\Big|_{po} - N_{p\downarrow}\left(\frac{1}{\tau_p^r} + \frac{1}{2\tau_{p,z}^r}\right) + \frac{N_{p\uparrow}}{2\tau_{p,z}^r} \tag{3.12}$$

$$\frac{d\mathbf{S}_{p\perp}}{dt} = -\mathbf{S}_{p\perp}\left(\frac{1}{\tau_p} + \frac{1}{\tau_p^r}\right) + \left(\frac{d\mathbf{S}_{p\perp}}{dt}\right)\Big|_{po} + [\mathbf{S}_{p\perp} \times \mathbf{\Omega}_{\text{int}}] - \frac{\mathbf{S}_p^x}{\tau_{p,x}^r} - \frac{\mathbf{S}_p^y}{\tau_{p,y}^r} \tag{3.13}$$

$$\frac{dN_{i\uparrow}}{dt} = -\frac{N_{i\uparrow}}{\tau_i} + \left(\frac{dN_{i\uparrow}}{dt}\right)\Big|_{po} - N_{i\uparrow}\left(\frac{1}{\tau_i^r} + \frac{1}{2\tau_{i,z}^r}\right) + \frac{N_{i\uparrow}}{2\tau_{i,z}^r} \tag{3.14}$$

$$\frac{dN_{i\downarrow}}{dt} = -\frac{N_{i\downarrow}}{\tau_i} + \left(\frac{dN_{i\downarrow}}{dt}\right)\Big|_{po} - N_{i\downarrow}\left(\frac{1}{\tau_i^r} + \frac{1}{2\tau_{i,z}^r}\right) + \frac{N_{i\downarrow}}{2\tau_{i,z}^r} \tag{3.15}$$

$$\frac{d\mathbf{S}_{i\perp}}{dt} = -\mathbf{S}_{i\perp}\left(\frac{1}{\tau_i} + \frac{1}{\tau_i^r}\right) + \left(\frac{d\mathbf{S}_{i\perp}}{dt}\right)\Big|_{po} + [\mathbf{S}_{i\perp} \times \mathbf{\Omega}_{\text{int}}] - \frac{\mathbf{S}_i^x}{\tau_{i,x}^r} - \frac{\mathbf{S}_i^y}{\tau_{i,y}^r} \tag{3.16}$$

where the indices s,p, and i correspond to the signal, pump, and idler respectively. The index *po* corresponds to the parametric process (where the summation over **q** and **k'** should be omitted in this case). $\tau_{s,p,i}$ are the radiative lifetimes of signal, pump and idler given by

$$\tau_{s,p,i} = \frac{\tau_0}{\left|C_{L;k_s,k_p,k_i}\right|^2} \tag{3.17}$$

where τ_0 is the photon life time in the cavity and $\left|C_{L;k_s,k_p,k_i}\right|^2$ are the photon fractions of signal, pump and idler respectively. The $\tau^r_{s,p,i}$ are the decay times associated with irreversible escape of particles to the reservoir (these are much longer than the radiative lifetimes), and $\tau^r_{s,p,i;x,y,z}$ are the spin relaxation times induced by the coupling to the reservoir of the x,y,z components of the pseudospin of signal, pump and idler respectively. The coupling of a state with the reservoir depends on its exciton fraction, on temperature (via the occupation of acoustic phonons modes) and on the energy difference between the state and the reservoir. These decay times are therefore given by

$$\tau^r_{s,p,i,x,y,z} = \tau^r_{x,y,z}\left|X_{L;k_s,k_p,k_i}\right|^2 e^{-\left(\frac{E_r - E_{s,p,i}}{k_B T}\right)} \tag{3.18}$$

where $\left|X_{L;k_s,k_p,k_i}\right|^2$ are the exciton fractions in signal pump and idler, $E_{r,s,p,i}$ are the energies of the reservoir, signal, pump, and idler, $\tau^r_{x,y,z}$ are the fitting parameters related to the exciton pseudospin decay time in the reservoir. Note that the signal is always effectively separated from the reservoir because of the large energy difference.

As explained above and illustrated by Fig. 3.5, we have chosen a model accounting for three discrete polariton states, namely the signal state, the pump state, and the idler state. The excitonic reservoir is located in the vicinity of the bare exciton energy and is characterized by spin relaxation times $\tau^r_{x,y,z}$. As the wave vectors corresponding to signal, pump and idler states are relatively small, the TE-TM-splitting of polariton modes is also small there, ranging from 0 at signal to a few μeV at the idler state, which yields the pseudospin rotation period of about 300 ps in the sample we consider. The field $\mathbf{\Omega}_{\text{int}}$ describes the effects of the self-induced Larmor precession and depends on the polariton concentration and on the circular polarization degree of pump. In the reservoir, the TE-TM splitting can be accounted for by introduction of an effective magnetic field randomly oriented in the plane of the structure. In this case, the in-plane linear polarization should decay twice slower than circular one in the reservoir. In the motional narrowing regime, characterized by the fact that the polariton linewidth is narrower than the linewidth of a photon or an exciton alone, we arrive to

$$\tau_{rs}^{circ} = \frac{1}{\left\langle \Omega_{LT,r}^2 \right\rangle \tau_{scatt}}, \quad \tau_{rs}^{lin} = \frac{2}{\left\langle \Omega_{LT,r}^2 \right\rangle \tau_{scatt}} \tag{3.19}$$

where $\hbar \left\langle \Omega_{LT,r}^2 \right\rangle^{1/2}$ is an average value of the LT-splitting in the reservoir, τ_{scatt} is a characteristic scattering time within the reservoir, τ_{rs}^{circ} is the decay time of the circular polarization and τ_{rs}^{lin} is that the decay time of linear polarization. As we shall see in the next section, this picture does not fit well with experimental findings which show a relatively fast relaxation of the circular polarization in the reservoir, and almost no relaxation of the linear polarization. This suggests that in fact the relaxation times in two polarizations differ much stronger than what is predicted by Eq. (3.19). As clearly follows from the experimental data, the polarization parallel to the crystallographic axes [110] and [1-10] is quite well conserved in the reservoir. The most likely explanation of it would be that the reservoir is mainly composed of localized exciton states which are known to be strongly polarized along the main crystallographic axes (S.V. Goupalov, E.L. Ivchenko, A.V. Kavokin, 1998). We shall use this hypothesis in the further analysis. Choosing the X-axis in pseudo-spin space parallel to the [110] and [1-10], we shall assume: $\tau_y^r = \tau_z^r = 11ps << \tau_x^r = 200ps$. These two times are the only adjustable parameters of the model.

To calculate the matrix element of exciton-exciton interaction, we have used once again the formula $V_{k,k',q}^{ex(1)} = 6xE_b \frac{a_b^2}{S}$ where E_b is the exciton binding energy, a_b the 2D Bohr radius and S the laser spot size.

3.3.2. Circular pumping, the effect of detuning

Figure 3.6 shows the experimental data and theoretical simulation for sample 1 at different detunings in the spontaneous scattering regime. At negative detuning the system exhibits a polarization lifetime of about 300 ps as well as fast decay of the emission (30 ps). This fast decay shows that polaritons are not scattered out of the light cone (polariton trap zone) before to escape from the cavity by tunnelling across the mirrors. Three states composing the parametric amplifier have energies deeply inside the polariton trap and are therefore efficiently protected from the influence of the reservoir. The polarisation decay rate for these states approaches the intrinsic one, given by the value of the TE-TM splitting in the pump state.

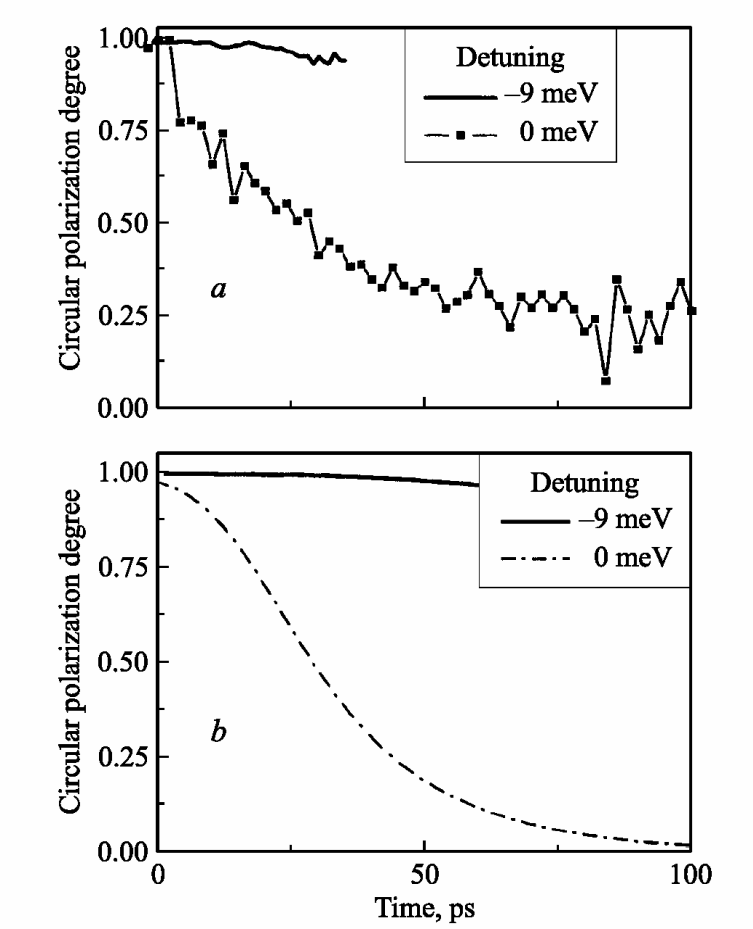

Figure 3.6. Circular polarization degree of the luminescence for different detuning (circular pumping, below threshold): a) experimental and b) theoretical results for sample 1 with $\tau_C \approx 8$ ps.

At zero and positive detuning the situation changes drastically. In this cavity and at these detunings, the energy spacing between the pump and the reservoir becomes smaller than 1.5 meV which is small enough to allow for their efficient coupling by phonon or free carrier scattering. As a result, a much longer decay time of the emission is observed. After a short initial polarization plateau (t<10 ps) which we attribute to surface Rayleigh scattering, the circular polarization drops with a decay time of about 100 ps. At short time delay, the ground state emission is governed by parametric luminescence mechanism. Later (t>30-50 ps), the particles remaining in the system lose their polarization due to interaction with the reservoir. This shows that in the first 10 ps, the ground state emission is governed by the parametric luminescence mechanism. After that, most of the particles remaining in the system have lost their polarization by interacting with the reservoir.

3.3.3. Linear pumping, polarization inversion

Figure 3.7 shows the experimental data and corresponding theoretical simulation for the sample 1 under linear pumping, below and above the stimulation threshold (δ=0). Below threshold, the polarisation of emission is almost constant (-8%) and is opposite to the pump polarisation. Above threshold, the polarisation degree achieves a large negative value of -65% and then, in the long time limit, decreases to the spontaneous scattering value of -8%. These data are very well reproduced theoretically (see figure 3.7(b)). This peculiar non-monotonic behaviour of the linear polarization degree of emission is due to the anisotropy of the polariton-polariton interaction (see section 3.1.4). In the spontaneous regime, Eq. (3.10) which describes the motion of the signal pseudospin can be simplified and reduced to:

$$\frac{d\mathbf{S}_{s,\perp}}{dt} = W^{(12)}_{0,k_p,k_p}\left(N_{\uparrow p} + N_{p\downarrow}\right)\mathbf{S}_{p,\perp} - \frac{\mathbf{S}_{\mathbf{s},\perp}}{\tau_s} \tag{3.20}$$

where k_p is the in-plane wave vector of the pump. An analytical formula can be written for the linear polarisation degree of the signal in this case:

$$\rho_l = \frac{4W^{(12)}_{0,k_p,k_p}}{W^{(1)}_{0,k_p,k_p} + 4W^{(2)}_{0,k_p,k_p}} \tag{3.21}$$

Note that the similar formula has been first proposed by K.V. Kavokin *et al* (2005) from qualitative arguments. In the isotropic case ($2V^{(2)}_{0,k_p,k_p} = V^{(1)}_{0,k_p,k_p}$) the linear polarisation degree of the signal should be +100 %. If $V^{(2)}$ is neglected, the memory of the initial linear polarisation is lost and ρ_l is equal to 0 as one can also see in G. Dasbach *et al* (2005). For our microcavity sample, the relative values of scattering constants have been estimated as in P. Renucci *et al* (2005):

$$2V^{(2)}_{0,k_p,k_p} = -0.08V^{(1)}_{0,k_p,k_p} \tag{3.22}$$

$V^{(1)}_{0,k_p,k_p}$ and $V^{(2)}_{0,k_p,k_p}$ have opposite signs which reflects the different mechanisms of interaction between polaritons having the parallel spins (triplet configuration) and opposite spins (singlet configuration). In triplet configuration the interaction is repulsive because of the Pauli principle. On the other hand, the singlet configuration can lead to formation of an excitonic molecule (bi-exciton or bi-polariton), thus interaction between polaritons having opposite spins is likely to be attractive. Our measurements and analysis show that polariton-polariton scattering is a very efficient channel of relaxation of the linear polarisation in

microcavities. Actually, in the spontaneous regime 92% of initial linear polarisation may be lost in a single polariton-polariton scattering event. On the other hand, in the stimulated regime, 8% of remaining linear polarization constitute a seed which allows to build up a huge population of polarized polaritons and achieve the negative polarisation degree of about 65 %

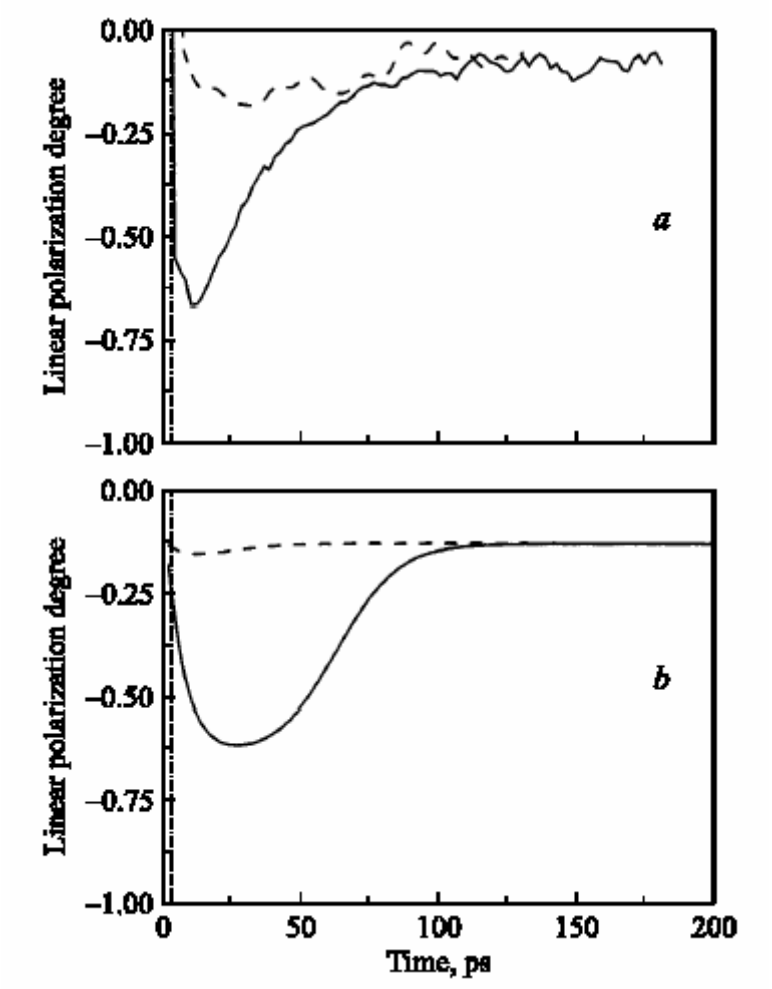

Figure 3.7. Linear polarization degree of the luminescence of the sample 1 for different pumping intensities (linear pumping): a) experiment, b) theory. The dashed line corresponds to 0.25 W/cm^2 (below threshold) and solid line corresponds to 2 W/cm^2 (above threshold). (Note that the initial polarization positive peak in (a) is due to diffusion of the excitation pulse on the sample surface).

3.3.4. Elliptic pumping, self-induced Larmor precession

The self-induced Larmor precession discovered for PPO by I. Shelykh *et al* (2004) and described in section 3.1 is one of the effects caused by the anisotropy of the polariton-polariton interaction (i.e. dependence of the scattering amplitude on mutual orientation of the pseudospins of two interacting polaritons). Because of this anisotropy, an imbalance between σ^+ and σ^- populations is responsible for the appearance of an effective magnetic field in the Z-direction (Eq. (3.6)) which is able to rotate the linear polarisation plane. Figure 3.8 shows time dependences of circular and linear polarization degrees for elliptic pumping at different pumping intensities (below and above threshold) measured on the sample 1. Below the threshold, the circular polarisation degree decays similarly to the circular excitation case. On the other hand, the linear polarization shows a single oscillation which starts from negative values of the polarization degree. We interpret this oscillation as a manifestation of the self-induced Larmor precession effect. Above the stimulation threshold, the circular polarisation degree of the emission is again very similar to the circular excitation case showing a long plateau followed by a fast decay. The oscillation of the linear polarisation degree is still visible, but remarkably it has a longer period than in the spontaneous case both in experiment and theory. This is easy to understand, as the effective magnetic field acting on the polariton pseudospin is density dependent and its intensity decreases as time goes. Thus the oscillation period should rapidly increase versus time in a pulsed experiment. In the stimulated regime, the circular polarisation degree is kept for a long time, but the intensity of emission decays much faster. Thus the overall effective field which rotates the in-plane polarisation is decaying faster in the stimulated regime than in the spontaneous regime. That is why the period of self-induced Larmor precession is much longer if the stimulated scattering dominates.

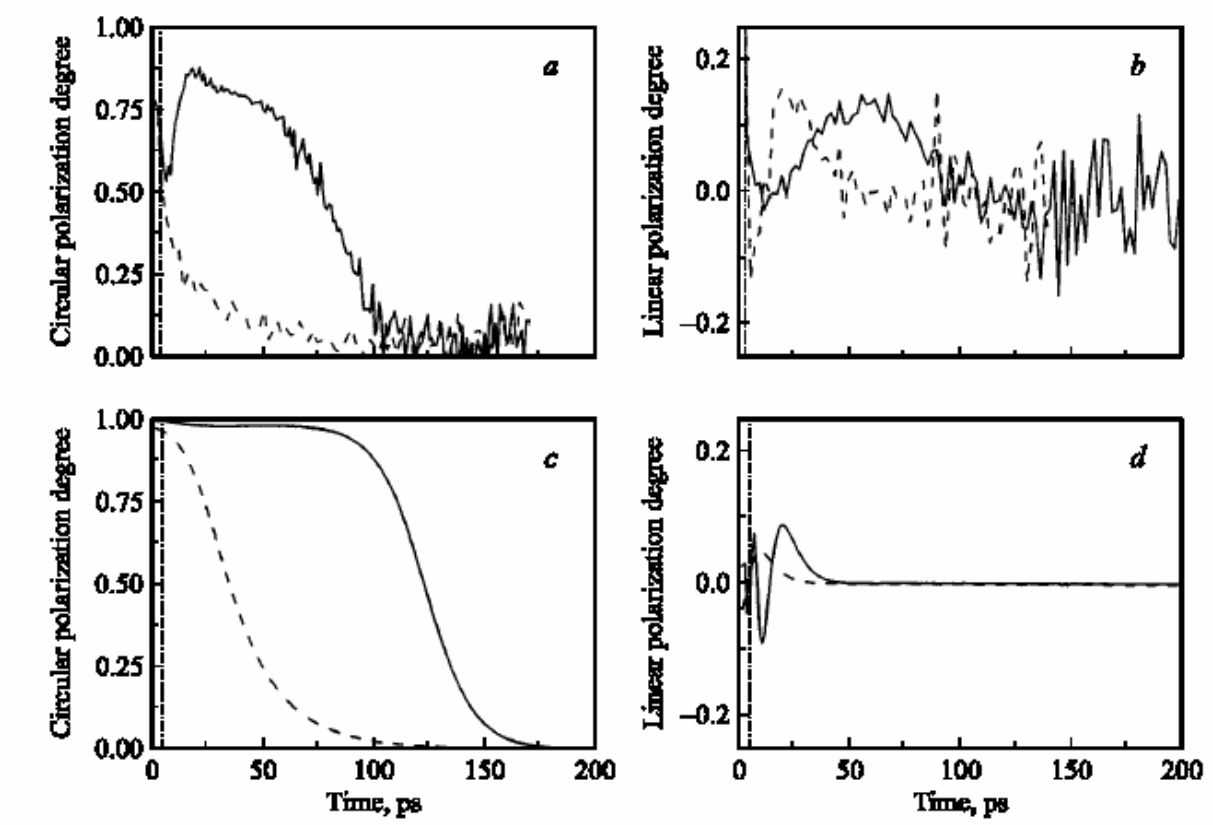

Figure 3.8. Circular and linear polarization degree of the signal emission for elliptically polarized pumping: experiment (a, b) and theory (c, d). Dashed line corresponds to 0.5 W/cm^2 (below threshold) and solid line corresponds to 3 W/cm^2 (above threshold). Note that the initial polarization peak in (a,b) is due to diffusion of the excitation pulse on the sample surface.

3.4. Spin dynamics in diluted magnetic microcavities

In this section we consider a microcavity not in the OPO configuration, but rather in a special experiment with a diluted magnetic quantum well in magnetic fields, which is however well described by the pseudospin formalism for polaritons. The experiment and the theory describing it are published in A. Brunetti *et al* (2006). To describe properly the spin relaxation we had to solve the equation for the density matrix instead of using Markovian approximation described in chapter 1 and earlier in chapter 3.

3.4.1. Time-resolved Kerr rotation

The Kerr rotation is very similar to Faraday rotation – rotation of the plane of polarization of light propagating in magnetic media or in a media with induced magnetization, the difference being that the Kerr rotation is measured in the reflection geometry. Time-resolved Kerr rotation (TRKR) is a pump-probe technique appropriate for probing the spin

dynamics of carriers and excitons in semiconductors. The angle of Kerr rotation, like the angle of Faraday rotation, is directly proportional to the projection of the spin polarization vector on the probe beam propagation direction (see e.g. J.J. Baumberg *et al*, 1994). By changing the delay between pump and probe pulses one monitors the spin dynamics of excitons with a subpicosecond resolution. The method has been proven to be extremely successful in measuring both coherent spin evolution and spin dephasing time for electrons, holes and excitons in semiconductors. In diluted magnetic semiconductors (DMS), TRKR not only provides the information on spin dynamics but also gives direct access to the precession of magnetic ion spins mediated by their interaction with free carriers (see e.g. D.Scalbert *et al*, 2004).

In the experiment described, the spin polarization is introduced into a system of cavity polaritons by the circularly polarized pump pulse and it is probed measuring rotation of the polarization plane of the linearly polarized probe pulse reflected from the microcavity. In contrast with conventional QWs, the magnetic field induced splittings in DMS QWs are very large. In Voigt configuration, when the magnetic field is in the QW plane they are mainly given by the exchange interaction between electrons and magnetic ions. For example for $Cd_{0.95}Mn_{0.05}Te$ QW the spin splitting at saturation is about 15 meV. This is more than enough to mix so-called dark and bright exciton states having the absolute value of total angular momentum projection to the structure axis $J_z = \pm 2$ and $J_z = \pm 1$, respectively.

That is why, the spectrum of exciton-polaritons can no more be described in the framework of two coupled oscillator model (see section 2.1), but requires taking into account three coupled oscillators, namely two exciton states separated by Zeeman splitting and the cavity mode. In the TRKR the splittings of these three states determine the frequencies of the oscillations due to precession of the spin polarization coherently excited by the pump pulse around the in-plane magnetic field. Obviously, the giant Zeeman splitting provides a powerful tool to control the coupling between excitons and photons, since excitonic resonances can be tuned in a broad energy band by applying a magnetic field.

Only two of three frequencies given by the simple three-oscillator model could be observed experimentally in the TRKR spectra of the sample. This is partly due to the strong broadening of the polariton modes, which rapidly destroys correlations between some eigenstates making difficult detection of the corresponding eigenfrequencies in the time domain. Since the finite lifetime of the polariton modes and processes of inelastic electron and hole spin relaxation cannot be self-consistently accounted for within the analytical three state

model we apply the polariton spin density matrix formalism (described below) to fit the experimental data.

The sample under study consists of a $Cd_{0.95}Mn_{0.05}Te$ QW of 8 nm width embedded in the middle of a $\lambda/2$ $Cd_{0.4}Mg_{0.6}Te$ cavity. The asymmetric Bragg mirrors were grown to maximize the magneto-optical Kerr rotation in the presence of small magnetic fields, while the high energy gap of the compounds ensures the absence of Kerr effect in the mirrors at the QW exciton resonance (D. Pereda Cubian *et al*, 2003). The reflectivity of the mirrors was estimated to be 76% for the top and 98% for the back mirror. The cavity is grown on a wedge (12 meV/mm), which allows to tune the cavity mode by simple shift of the laser spot. Here we only discuss the data obtained at the point corresponding to negative detuning between photon and exciton modes of -8 meV at zero field (i.e. the bare photon mode is 8 meV lower than the bare exciton mode).

3.4.2. The model

We are going to describe a pump-probe experiment. We will assume that the probe is affected by the pump, but not vice versa. The pump influences the probe via the energy shift of exciton levels due to interactions. The Hamiltonian expressions for the pump and the probe pulses are essentially similar, with the exception of the interaction term (see below).

The Hamiltonian for the pump pulse writes:

$$H = H_0 + H_R \tag{3.23}$$

The first term describes the coupling of excitons and photons inside the cavity and the second term describes coupling of the cavity photons with the continuum of external photonic modes and coupling of the excitons with the bath of acoustic phonons.

For the probe pulse the Hamiltonian includes an extra term which describes interaction with the pump:

$$H = H_0 + H_R + H_{\text{int}} \tag{3.24}$$

The exciton-photon interaction term reads

$$\begin{aligned} H_0 = \Big[& \varepsilon_{ex}\left(a^+_{ex\uparrow}a_{ex\uparrow} + a^+_{ex\downarrow}a_{ex\downarrow}\right) + \\ & + \varepsilon_{ph}\left(a^+_{ph\uparrow}a_{ph\uparrow} + a^+_{ph\downarrow}a_{ph\downarrow}\right) + \varepsilon_D\left(a^+_{d\uparrow}a_{d\uparrow} + a^+_{d\downarrow}a_{d\downarrow}\right) + \\ & + \Delta_R/2\left(a^+_{ex\uparrow}a_{ph\uparrow} + a^+_{ex\downarrow}a_{ph\downarrow}\right) + \\ & + \alpha_e\left(a^+_{ex\uparrow}a_{d\uparrow} + a_{ex\downarrow}a^+_{d\downarrow}\right) + \alpha_h\left(a^+_{ex\uparrow}a_{d\downarrow} + a_{ex\downarrow}a^+_{d\uparrow}\right)\Big] \\ & + h.c. \end{aligned} \tag{3.25}$$

where the indices *ph*, *ex* and *d* correspond to photons, bright excitons and dark excitons correspondingly. The first two lines in Eq. (3.25) describe the free particles, the third line contains the exciton-photon coupling term, the 4th corresponds to the magnetic field induced mixing of the bright and dark states. The mixing constants are given by

$$\alpha_{e,h} = g_{e,h}\mu_B \left(B_{eff,x} + iB_{eff,y} \right) \tag{3.26}$$

where $g_{e,h}$ is an electron/hole g-factor, the B_{eff} is a sum of the external magnetic field and the exchange magnetic field B_{exch} created by the Mn ions. We shall neglect the field-induced hh-lh mixing and thus we shall suppose $g_h = 0$. The exchange field is given by the following expression:

$$B_{exch} = \frac{N_0 \alpha_e x_{eff} \left\langle S_x \right\rangle}{g_e \mu_B} \tag{3.27}$$

The term H_R describes interactions of the cavity mode with the external continuum of photons and coupling of excitons with the acoustic phonon bath. It reads:

$$\begin{aligned} H_R = & \sum\nolimits_\omega C_\omega \left(a^+_{ph\uparrow} c_{\omega\uparrow} + a^+_{ph\downarrow} c_{\omega\downarrow} \right) + \\ & + \sum\nolimits_\omega B_\omega b_\omega \left(a^+_{ex\downarrow} + a^+_{ex\uparrow} \right) + \\ & + \sum\nolimits_\omega \left[Q_{\omega,e} \left(b_\omega + b^+_\omega \right) \left(a_{ex\uparrow} a^+_{d\uparrow} + a_{ex\downarrow} a^+_{d\downarrow} \right) \right] + \\ & + \sum\nolimits_\omega \left[Q_{\omega,h} \left(b_\omega + b^+_\omega \right) \left(a_{ex\uparrow} a^+_{d\downarrow} + a_{ex\downarrow} a^+_{d\uparrow} \right) \right] + h.c. \end{aligned} \tag{3.28}$$

where $c_{\omega\uparrow,\downarrow}$ are annihilation operators of the right and left circular polarized external photons, b_ω is annihilation operator of the phonon. The first two terms stand for the transitions between cavity mode and external photons and between excitons and acoustic phonons. They are characterized by the coupling constants C_ω and B_ω. The last two terms describe the phonon-assisted spin flips of electrons and holes, leading to their spin relaxation.

Generally, H_R corresponds to the coupling of the quantum system with classical reservoir and can be treated within the framework of the Born-Markov approximation, familiar in the quantum optics. It results in the semiclassical terms describing the finite lifetimes of the cavity mode and the excitons, the external pumping and the processes of inelastic spin relaxation.

The exciton-exciton interactions are essential for the photoinduced Kerr rotation and the corresponding term of the Hamiltonian reads:

$$
\begin{aligned}
H_{\text{int}} &= \frac{V_{ex}^{(1)}}{2}\left(a_{ex\uparrow}^{+}a_{ex\uparrow}a_{ex\uparrow}^{+}a_{ex\uparrow} + a_{ex\downarrow}^{+}a_{ex\downarrow}a_{ex\downarrow}^{+}a_{ex\downarrow}\right) + \\
&+ V_{ex}^{(2)}\left(a_{ex\uparrow}^{+}a_{ex\uparrow}a_{ex\downarrow}^{+}a_{ex\downarrow}\right) + \\
&+ \frac{V_{d}^{(1)}}{2}\left(a_{d\uparrow}^{+}a_{d\uparrow}a_{d\uparrow}^{+}a_{d\uparrow} + a_{d\downarrow}^{+}a_{d\downarrow}a_{d\downarrow}^{+}a_{d\downarrow}\right) + \\
&+ V_{d}^{(2)}\left(a_{d\uparrow}^{+}a_{d\uparrow}a_{d\downarrow}^{+}a_{d\downarrow}\right) + \\
&+ V_{ex-d}^{(1)}\left(a_{ex\uparrow}^{+}a_{ex\uparrow}a_{d\uparrow}^{+}a_{d\uparrow} + a_{ex\downarrow}^{+}a_{ex\downarrow}a_{d\downarrow}^{+}a_{d\downarrow}\right) + \\
&+ V_{ex-d}^{(2)}\left(a_{ex\uparrow}^{+}a_{ex\uparrow}a_{d\downarrow}^{+}a_{d\downarrow} + a_{d\uparrow}^{+}a_{d\uparrow}a_{ex\downarrow}^{+}a_{ex\downarrow}\right)
\end{aligned}
\tag{3.29}
$$

where the matrix elements V_{ex}, V_{d}, V_{ex-d} correspond to the interactions between bright excitons, dark excitons and mutual bright exciton – dark exciton interactions, respectively. The indices (1) and (2) mark triplet and singlet spin configurations, respectively. For the description of Kerr rotation it is sufficient to retain only the term corresponding to the interactions of bright excitons treated in the mean-field approximation. Neglecting all other terms the exciton-exciton interaction Hamiltonian reads:

$$
H_{\text{int}} = \left(V^{(1)}N_{ex\uparrow} + V^{(2)}N_{ex\downarrow}\right)a_{ex\uparrow}^{+}a_{ex\uparrow} + \left(V^{(1)}N_{ex\downarrow} + V^{(2)}N_{ex\uparrow}\right)a_{ex\downarrow}^{+}a_{ex\downarrow} \tag{3.30}
$$

where $N_{ex\uparrow}$ and $N_{ex\downarrow}$ are the occupation numbers of spin-up and spin-down exciton states. In microcavities, interactions between excitons with parallel spin projections on the structure growth axis is much stronger than for the excitons with antiparallel spin projections, $V^{(1)} \gg V^{(2)}$. In the case when the excitonic system has nonzero circular polarization this results in the appearance of the concentration dependent magnetic field directed along *z* axis which induces the Kerr rotation of the linear components of the polarization (self-induced Larmor precession, discussed in section 3.1.2). The matrix element $V^{(1)}$ is given by the usual expression $V^{(1)} = 6E_b a_B^2 / S$, where $E_b = 25\,\text{meV}$, $a_B = 34\,\text{Å}$, $S = \left(150\,\mu\text{m}\right)^2$.

Polariton dynamics in DMS microcavities can be modelled by the Liouville-von Neumann equation for the density matrix ρ with additional Lindblad terms describing the finite lifetime of the polariton modes and inelastic processes of the spin relaxation of electrons and holes forming the exciton. This equation should be written and solved separately for the pump and the probe pulses. The equation for the probe pulse includes the interaction with the pump pulse, and so depends on the pump density matrix. In the Born approximation the Liouville-von Neumann equations read:

$$
\frac{d\rho_{pump}}{dt} = \frac{i}{\hbar}\left[\rho_{pump}, H_0\right] + \Gamma\rho_{pump} + P_{pump} \tag{3.31}
$$

$$\frac{d\rho_{probe}}{dt}=\frac{i}{\hbar}\left[\rho_{probe},H_0+H_{\text{int}}\left(\rho_{pump}\right)\right]+\Gamma\rho_{probe}+P_{probe} \tag{3.32}$$

where the first term describes the evolution of the system in the external in-plane magnetic field, the second term describes the damping processes such as the radiative decay and spin relaxation of electrons and holes, the last terms describe pump and probe action. In the basis of the four exciton and two photon states the diagonal components of the density matrix give the occupation numbers of these states.

The Hamiltonian H_0+H_{int} in this basis is given by a matrix:

$$\begin{pmatrix}
\varepsilon_{ex}+ & 0 & \frac{\Delta_R}{2} & 0 & \alpha_e & 0 \\
+V^{(1)}\rho_{11}+V^{(2)}\rho_{22} & & & & & \\
0 & \varepsilon_{ex}+ & 0 & \frac{\Delta_R}{2} & 0 & \alpha_e \\
 & +V^{(1)}\rho_{22}+V^{(2)}\rho_{11} & & & & \\
\frac{\Delta_R}{2} & 0 & \varepsilon_{ph} & 0 & 0 & 0 \\
0 & \frac{\Delta_R}{2} & 0 & \varepsilon_{ph} & 0 & 0 \\
\alpha_e^* & 0 & 0 & 0 & \varepsilon_d & 0 \\
0 & \alpha_e^* & 0 & 0 & 0 & \varepsilon_d
\end{pmatrix} \tag{3.33}$$

The action of the superoperator Γ can be represented in the Linblad form. It is defined in such a way that, once applied to the density matrix, it yields the following matrix elements:

$$\begin{aligned}
\left(\Gamma\rho\right)_{11}&=\left(\rho_{55}-\rho_{11}\right)/\tau_{e\perp}+\left(\rho_{66}-\rho_{11}\right)/\tau_{h\perp}\\
\left(\Gamma\rho\right)_{22}&=\left(\rho_{66}-\rho_{22}\right)/\tau_{e\perp}+\left(\rho_{55}-\rho_{22}\right)/\tau_{h\perp}\\
\left(\Gamma\rho\right)_{33}&=-\rho_{33}/\tau_{ph}\\
\left(\Gamma\rho\right)_{44}&=-\rho_{44}/\tau_{ph}\\
\left(\Gamma\rho\right)_{55}&=\left(\rho_{11}-\rho_{55}\right)/\tau_{e\perp}+\left(\rho_{22}-\rho_{55}\right)/\tau_{h\perp}\\
\left(\Gamma\rho\right)_{66}&=\left(\rho_{22}-\rho_{66}\right)/\tau_{e\perp}+\left(\rho_{11}-\rho_{66}\right)/\tau_{h\perp}
\end{aligned} \tag{3.34}$$

$$\begin{aligned}
&\left(\Gamma\rho\right)_{13,31}=-\frac{1}{2\tau_{ph}}\rho_{13,31},\quad \left(\Gamma\rho\right)_{14,41}=-\frac{1}{2\tau_{ph}}\rho_{14,41},\quad \left(\Gamma\rho\right)_{23,32}=-\frac{1}{2\tau_{ph}}\rho_{23,32},\\
&\left(\Gamma\rho\right)_{24,42}=-\frac{1}{2\tau_{ph}}\rho_{24,42},\quad \left(\Gamma\rho\right)_{34,43}=-\frac{1}{\tau_{ph}}\rho_{34,43},\quad \left(\Gamma\rho\right)_{35,53}=-\frac{1}{2\tau_{ph}}\rho_{35,53},\\
&\left(\Gamma\rho\right)_{36,63}=-\frac{1}{2\tau_{ph}}\rho_{36,63},\quad \left(\Gamma\rho\right)_{45,54}=-\frac{1}{2\tau_{ph}}\rho_{45,54},\quad \left(\Gamma\rho\right)_{46,64}=-\frac{1}{2\tau_{ph}}\rho_{46,64},\\
&\left(\Gamma\rho\right)_{12,21}=\left(\Gamma\rho\right)_{15,51}=\left(\Gamma\rho\right)_{16,61}=\left(\Gamma\rho\right)_{25,52}=\left(\Gamma\rho\right)_{26,62}=\left(\Gamma\rho\right)_{56,65}=0
\end{aligned} \tag{3.35}$$

where $\tau_{e\perp}, \tau_{h\perp}$ are characteristic relaxation times of the z-projection of the spins of the electrons and holes, the in-plane spin relaxation of the electrons and holes being neglected as it has a negligible impact on the magnetization in z-direction and TRKR signal in our system. We assumed the infinite non-radiative lifetime of the excitonic states, as in reality it is much longer than both the lifetime of the photon mode and spin relaxation times.

Creation of polaritons by the pump and probe pulses is described by the terms P_{pump} and P_{probe} in Eqs. (3.31) and (3.32). For the circularly polarized pump pulse all the matrix elements of P_{pump} are zero, except one:

$$P_{pump,33}(t) = A_{pp}^2 \cos^2(\omega t) \exp\left(-t^2/\tau^2\right) \tag{3.36}$$

These terms are introduced phenomenologically in order to obtain the usual rate equations for the occupation numbers. For the linearly polarized probe pulse term four matrix elements are non-zero:

$$\begin{aligned} &P_{probe,33}(t) = P_{44}(t) = P_{34}(t) = P_{43}(t) = \\ &= A_{pr}^2/2 \cos^2\left(\omega(t-\Delta t)\right) \exp\left(-(t-\Delta t)^2/\tau^2\right) \end{aligned} \tag{3.37}$$

Here τ is the duration of the light pulse, ω is the central frequency, and A_{pp}, A_{pr} are the amplitudes of the pump and probe electric fields. The linear polarization of the emitted signal as a function of time is governed by the following correlator:

$$S_{ph}(t,\Delta t) = \left\langle a_{ph\downarrow}^{+} a_{ph\uparrow} \right\rangle = \rho_{34}^{*}(t,\Delta t) \tag{3.38}$$

The time- integrated linear polarization of the signal is:

$$S_{ph}(\Delta t) = \int_0^\infty \rho_{34}^{*}(t,\Delta t)dt = S_x(\Delta t) + iS_y(\Delta t) \tag{3.39}$$

The angle of the Kerr rotation is then calculated as

$$\phi(\Delta t) = \frac{1}{2}\arctan\left(\frac{S_y(\Delta t)}{S_x(\Delta t)}\right) \tag{3.40}$$

where the factor 1/2 is connected with the fact that 90° rotation of the polarization of the light corresponds to the 180° rotation of the pseudospin.

3.4.3. Experimental results and their simulation

Figure 3.9a shows the TRKR scans measured under in-plane magnetic field from 0 to 5T. One can see that at zero field the signal decays exponentially, while in the presence of the field the oscillations show up. Moreover, above 3T we observe the beats, that is an additional

lower frequency arising in the signal. This can be seen in Fourier spectra of the TRKR signal, Figure 3.9b. The summary of the frequencies observed in the TRKR is reported in Figure 3.10 (circles), together with the polariton splittings calculated using a simple three-oscillator model. We identify the higher frequency beats as the beats between two exciton-like polariton branches (BD) while the lower frequency beats are between P and D states (PD). One can notice, that the peak associated with the exciton spin precession (BD) splits at 3T and has an asymmetric form at higher fields, suggesting exciton spin beats at two different frequencies. We believe that this is a manifestation of the inhomogeneous Mn^{2+} spin heating, an out of equilibrium phenomenon described in F.Teppe *et al* (2003), M. Vladimirova *et al* (2005).

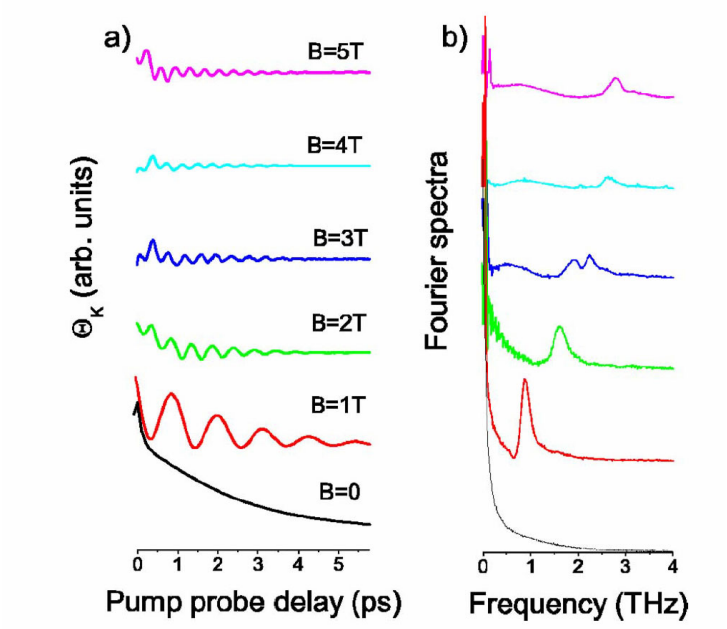

Figure 3.9. (a) Kerr rotation scans under magnetic field in Voigt configuration. (b) Corresponding Fourier spectra (from A. Brunetti *et al*, 2006).

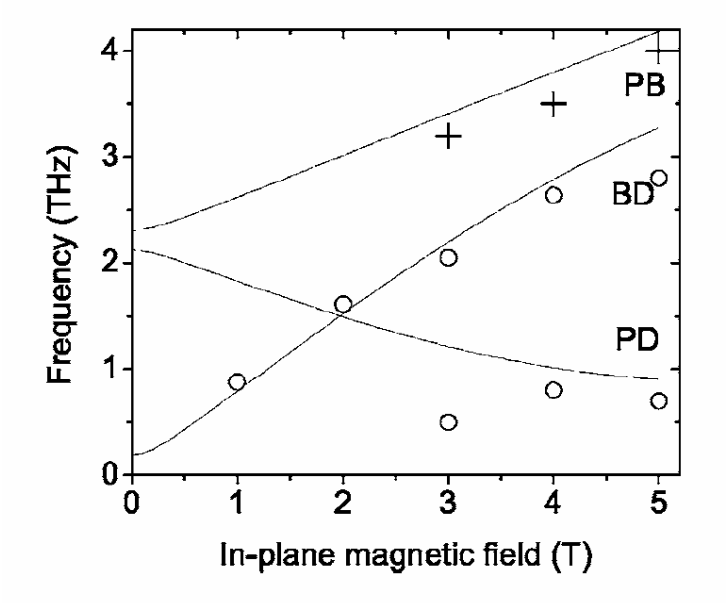

Figure 3.10. Polariton beats frequencies from the Fourier spectra shown in Fig. 3.9b as a function of applied magnetic field (circles, crosses). Solid lines show theoretical prediction (from A. Brunetti *et al*, 2006).

At zero and low fields the absence of the PD beats is not surprising. Since the excitonic states are only weakly mixed, the polariton component D resulting from the exciton dark state is almost not excited by the incident light. As soon as the magnetic field mixes the exciton states the PD beats arise in the signal. However, neither at high nor at low fields the polariton beats between P and B branches are clearly observed. At zero field, the absence of the PB beats is particularly evident since we observe pure exponential decay of the TRKR signal, and neither at high fields the polariton beats between P and B branches are clearly observed. We explain it by a very short photon lifetime τ_{ph} in our sample. Indeed, from the CW reflectivity measurements it can be estimated as $\tau_{ph} = \hbar/\Gamma = 0.25\,\text{ps}$, where Γ = 3 meV is the polariton broadening. The results of the calculation of the TRKR signal for the experimentally explored range of fields in the framework of the polariton spin density matrix formalism assuming $\Delta_R = 5.2$ meV, $\delta = -8.0\,\text{meV}$, T=7 K, and $\tau_{ph} = 0.25\,\text{ps}$ are shown in Figure 3.11. At zero field, the resonance corresponding to the BD beats is visible but is extremely weak. Its amplitude increases when one either increases the photon life time or reduces the detuning between the photon and the exciton mode. To illustrate the effect of the photon lifetime on the amplitude of Rabi oscillations, we show in Figure 3.12a the results of calculation using τ_{ph} = 0.5ps and 0.2 ps at B=0. One can see that the oscillations which are smeared out in the case of τ_{ph} = 0.2 ps and can be clearly distinguished when τ_{ph} = 0.5 ps. Figure 3.12b shows in more details the Fourier spectra of TRKR at 3, 4 and 5T, together with calculated curves. At high fields, the weak and wide spectral features not well separated from BD oscillations peak may be interpreted as rapidly decaying PB beats. The corresponding frequencies are shown by crosses in Figure 3.10. Thus, under magnetic field three resonances appear in our numerical simulations. However, one or two of them remain extremely weak, so that the calculated signal fits rather well the experimental results.

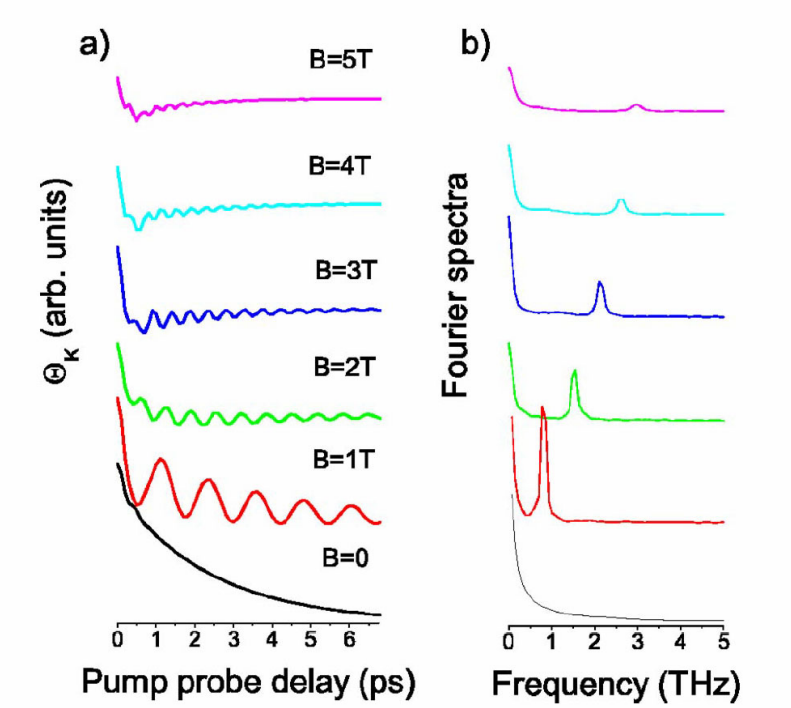

Figure 3.11. (a) Calculated Kerr rotation scans under magnetic field in Voigt configuration. (b) Corresponding Fourier spectra (from A. Brunetti *et al*, 2006).

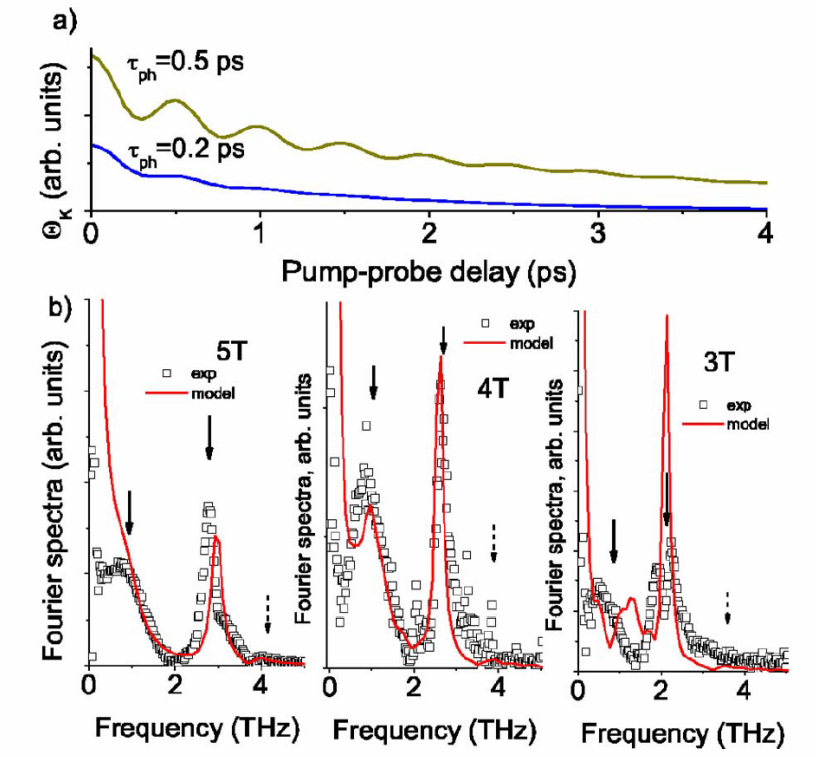

Figure 3.12. (a) Calculated Kerr rotation scans at B=0 and two different values of photon lifetime. One can observe the smearing of Rabi oscillations when the photon lifetime is short. (b) Fourier spectra obtained from calculated and measured Kerr rotation scans from 3 to 5 T. Arrows indicate the resonance frequencies (from A. Brunetti *et al*, 2006).

3.5. Conclusions

The pseudospin formalism and the spin-dependent Boltzmann equations allow to describe quantitatively many interesting polarization effects in polaritonic systems, including TE-TM splitting, self-induced Larmor precession, polarization inversion, and Kerr rotation. The model that we have developed is applicable for a broad range of experiments. In some cases, however, the renormalization of dispersion can lead to other effects that need special treatment (see chapter 4). Another limitation of the present model is that any correlations between the states are neglected, which corresponds to rapid dephasing. If the correlations are to be taken into account, one has to keep high-order correlators and write the quantum equations, like it is done in I.A. Shelykh *et al* (2005). This approach has an advantage over the Gross-Pitaevskii equation in that it allows taking into account such effects as spontaneous scattering and decoherence. They allow to study the transition between quantum and classical limits with increasing decoherence (see I.A. Shelykh *et al*, 2007). Another advantage is that these equations are numerically much less heavy. This direction is a subject of ongoing research.

Chapter 4. Polarization and propagation of a polariton condensate

In this chapter we consider a polariton state with macroscopic occupation, whether it is formed by Bose condensation, or by quasi-resonant pumping. In the first case we call this state a Bose condensate, and in the second – a macrooccupied driven mode. In both cases we will be interested in the polarization of the mode and in the dispersion of the excitations. In a case of pulse pumping one can also study real space propagation together with polarization effects. All these different cases are well described by the spinor Gross-Pitaevskii equation, which takes into account the polarization of the state.

Contents:

4.1. Ballistic propagation of polaritons in real space

We start with a description of propagation of polaritons in real space in the simplest case. We consider a case with low polariton density, when the interaction of polaritons and corresponding renormalization of dispersion can be neglected. We will be interested mostly in the polarization issues. Experimental study of polariton propagation in real space has been first performed by T. Freixanet *et al* (2000) for a GaAs microcavity. The authors have studied polariton group velocity as a function of detuning and excitation wavevector.

Let us consider a microcavity with GaAs QWs which is excited by a relatively long and very narrow (in real space) pulse. Such a pulse could excite polaritons with all wave-vectors, but since it has relatively narrow energy spectrum, it excites only the polaritons with particular wave-vector length. These polaritons then propagate in real-space, and their polarization changes with time as

controlled by the LT splitting. We neglect any disorder-scattering, dephasing or non-linear effects thus assuming that the polaritons propagate ballistically and keep coherence during their lifetime. We calculate the dispersion relations of T- and L-polarized polariton modes using the transfer matrix technique. LT-splitting of the exciton-polaritons mostly comes from the LT-splitting of the photonic eigenmodes of the microcavities $\Omega_{LT} \equiv \omega_L - \omega_T$, where ω_L and ω_T, correspond to the longitudinal and transverse polariton eigenmodes, respectively. We recall the approximate equation from chapter 1 for the optical TE-TM splitting **(1.48)**:

$$\Omega_{LT} \approx \frac{L_c L_{DBR}}{\left(L_c + L_{DBR}\right)^2} \frac{2\cos\varphi_{eff} \sin^2 \varphi_{eff}}{1 - 2\sin^2 \varphi_{eff}} \Delta \tag{4.1}$$

where $\varphi_{eff} \approx \arcsin \frac{\sin\varphi_0}{n_c}$, $L_{DBR} \equiv \frac{n_a n_b \pi c}{\left(n_b - n_a\right)\omega_B}$, φ_0 is the incidence angle in vacuum, L_c is the cavity width, $n_{a,b}$ are the refractive indices of the layers composing the DBRs, n_c is the refractive index of the cavity, ω_B is the central frequency of the optical stop-band of the DBRs, and $\Delta = \omega_B - \omega_c$ is the difference between the cavity-mode eigenfrequency at normal incidence ω_c and ω_B. Eq. **(1.48)** predicts a quadratic dependence of the splitting of the eigen-energies of bare photon modes of the cavity on the incidence angle. For the exciton-polariton modes, this quadratic dependence is altered by the photon fraction of the polariton state, which depends on the angle as well. At very negative detuning and for small in-plane wave vector $k \approx \frac{\omega_B}{c}\sin\varphi_0$, with the light velocity *c*, the photon fraction is close to 1, and the splitting of polariton modes is close to the value given by Eq. **(1.48)**. At larger in-plane wave vectors, the photon fraction of the polariton state rapidly decreases. As a result, the splitting with increasing *k* first shows an inflection, then a maximum and subsequent decrease when the dominantly excitonic region of the low polariton branch is reached. In what follows we shall only consider the lower polariton dispersion branch for simplicity.

The polarization dynamics of exciton-polaritons in microcavities in the linear regime is governed by the beats between coherently excited T- and L- polarized polariton dispersion branches (see e.g. K.V. Kavokin *et al*, 2004, I.A. Shelykh *et al*, 2004). As it was done in previous chapters, we use the pseudospin formalism to describe the polarization dynamics. The components of the pseudospin vector can be found from the elements of the pseudospin density matrix $\rho_{\mathbf{k}}$:

$$\rho_{\mathbf{k}} = \frac{N_{\mathbf{k}}}{2}\hat{I} + \boldsymbol{\sigma}\cdot\mathbf{S}_{\mathbf{k}} \tag{4.2}$$

where $N_{\vec{k}}$ is the sum of populations of T- and L-polarized quantum states having the same wave-vector $\mathbf{k}$, $\boldsymbol{\sigma}$ is the Pauli matrix-vector, and $\hat{I}$ is the identity matrix. The dynamics of $\rho_{\mathbf{k}}$ is given by a Liouville-von Neumann equation

$$i\hbar\frac{\partial\rho_{\mathbf{k}}}{\partial t}=\left[\hat{H}_{\mathbf{k}},\rho_{\mathbf{k}}\right]-i\hat{\Gamma}\rho_{\mathbf{k}} \tag{4.3}$$

where the Hamiltonian $\hat{H}_{\mathbf{k}}$ describes the dispersion of the lower polariton branch $E(k)$ and the LT-splitting:

$$\hat{H}_{\mathbf{k}}=\hbar\bar{\omega}_k\hat{I}+\mu_B g\left(\boldsymbol{\sigma}\cdot\mathbf{B}_{eff}\right) \tag{4.4}$$

with the average polariton dispersion $\bar{\omega}_k=\frac{\omega_T+\omega_L}{2}$, the effective magnetic field $\mathbf{B}_{eff}=\frac{\hbar}{\mu_B g}\boldsymbol{\Omega}$, where $\boldsymbol{\Omega}$ has the components

$$\Omega_x=\frac{\Omega_{LT}}{k^2}\left(k_x^2-k_y^2\right),\ \Omega_y=2\frac{\Omega_{LT}}{k^2}k_xk_y, \tag{4.5}$$

the Bohr magneton μ_B, and the effective exciton Zeeman-factor *g*. The superoperator $\hat{\Gamma}_{\mathbf{k}}\rho_{\mathbf{k}}$ describes the radiative decay of the polariton population due to their tunneling across the DBRs. The similarity of the Hamiltonian (4.4) with the well-known Rashba Hamiltonian for the electrons has inspired a recent proposal by A. Kavokin, G. Malpuech and M. Glazov (2005) of the optical spin Hall effect for exciton-polaritons which consists in the build-up of the circular polarization in the Rayleigh scattering spectra of a linearly polarized light incident on a microcavity. This effect has recently been observed by the group of LKB and has been published in Nature Physics (C. Leyder *et al*, 2007).

Though in general Eq. (4.3) can be solved numerically to obtain the time-dependent polarizations of different polariton states, in the configuration of the experiment we describe the result can be found analytically. Diagonalization of the Hamiltonian (4.4) readily yields a couple of eigen-frequencies $\omega_T(k)$ and $\omega_L(k)$. Accounting for the finite life time of polaritons τ, the electric field amplitudes corresponding to T- and L-polarized modes behave as

$$\begin{aligned}E_T(k,t)&=E_{0T}(k)\exp\left(-i\omega_T(k)t-t/\tau\right)\\E_L(k,t)&=E_{0L}(k)\exp\left(-i\omega_L(k)t-t/\tau\right)\end{aligned} \tag{4.6}$$

where E_{0T} and E_{0L} are initial values of the amplitudes of the T- and L-modes, respectively. The Bragg mirror reflectivity is less for the L than for the T mode, resulting in a smaller lifetime for the L mode as noted in Panzarini *et al* (1999). However, the relative difference of the reflectivity

coefficients for the range of the wavevectors considered is of the order of 10^{-4}. So we assume that the life-time is equal for both modes.

In the case of excitation by *x*-polarized light, the field amplitudes read

$$\begin{aligned} E_{0T}(k) &= -E_{0X}(k)\sin\phi \\ E_{0L}(k) &= E_{0X}(k)\cos\phi \end{aligned} \tag{4.7}$$

where ϕ is the angle between the wave vector $\mathbf{k}$ and *x*-axis.

We use the rotation matrix to rewrite the time-dependent amplitudes (4.6) in the *xy* basis:

$$\begin{bmatrix} E_X(k,t) \\ E_Y(k,t) \end{bmatrix} = E_{0X}(k)e^{-t/\tau}\begin{bmatrix} \cos\phi & -\sin\phi \\ \sin\phi & \cos\phi \end{bmatrix}\begin{bmatrix} e^{-i\omega_L t}\cos\phi \\ -e^{-i\omega_T t}\sin\phi \end{bmatrix} = E_{0X}(k)e^{-i\bar{\omega}_k t - t/\tau_k}\begin{bmatrix} \cos\frac{\Omega_{LT}t}{2} + i\cos 2\phi\sin\frac{\Omega_{LT}t}{2} \\ -i\sin 2\phi\sin\frac{\Omega_{LT}t}{2} \end{bmatrix} \tag{4.8}$$

Eq. (4.8) shows that for a given direction of the wave-vector the amplitudes of *x*- and *y*-polarized components oscillate in time with the frequency $\Omega_{LT}/2$, and it yields the angular dependence of the intensity of the cross-polarized light $|E_y|^2 \propto \sin^2 2\phi$. Note that Eq. (4.8) also allows extracting the dynamics of circular-polarized components of the emission and is therefore suitable to describe the optical spin-Hall effect.

In order to reproduce theoretically the real space propagation of a ring excited by a light pulse we Fourier-transform the amplitude vector (4.8) taking into account the spectral and directional shape $f(\omega)h(k)$ of the excitation pulse field, which is assumed to factorize and have a cylindrical symmetry in the wave-vector distribution *h(k)*. We assume that the frequency width of the pulse is much larger than the LT splitting. Therefore the electric field amplitude created by the excitation light pulse is $E_{0X}(k) = f(\bar{\omega}_k)h(k)$. We notice that the origin of the time axis in this model corresponds to the maximal density of polaritons in the cavity, which is about 1 ps (half width of the pulse) later than the maximum of the excitation pulse because the pulse duration is shorter than the polariton lifetime, and therefore the polariton density continues to increase even after the maximum of the exciting pulse. This time shift had been accounted for in our calculations.

The spatially resolved components of the electric field read:

$$\begin{bmatrix} E_x(\mathbf{r},t) \\ E_y(\mathbf{r},t) \end{bmatrix} = \sqrt{2\pi}\begin{bmatrix} \int_0^\infty e^{-i\bar{\omega}_k t - t/\tau_k}\left(\cos\frac{\Omega_{LT}t}{2}J_0(kr) - i\cos 2\theta\sin\frac{\Omega_{LT}t}{2}J_2(kr)\right)E_{0X}(k)kdk \\ i\sin 2\theta\int_0^\infty e^{-i\bar{\omega}_k t - t/\tau_k}\sin\frac{\Omega_{LT}t}{2}J_2(kr)E_{0X}(k)kdk \end{bmatrix}, \tag{4.9}$$

where θ is the angle between the radius-vector $\mathbf{r}$ and the polarization axis (*x*-axis), and we use the Bessel functions

$$J_n(x) = \frac{i^{-n}}{2\pi} \int_0^{2\pi} e^{i(n\theta + x\cos\theta)} d\theta \,.$$

The intensities of co- and cross-polarized components of the emission are given by

$$I_{co}(\mathbf{r},t) \propto \left|E_x(\mathbf{r},t)\right|^2 \;,\; I_{cross}(\mathbf{r},t) \propto \left|E_y(\mathbf{r},t)\right|^2 . \qquad (4.10)$$

A summary of experimental data of Langbein *et al* (2007) obtained in the experimental conditions described in this chapter (taken for the specific excitation energy $\hbar\omega_e$=1.51682eV) is given in Fig. 4.1. In the upper frames the spatially resolved emission intensities, proportional to the polariton densities, at times 5 ps, 10 ps, and 15 ps after the polariton injection at $t = 0$ ps at the origin by a pulse with τ_e=1.8 ps are shown. The excited polaritons are centered at $\bar{k}$=2.8/μm. The non-resonant reflection close to the excitation position is blocked by a sphere suspended on a wire in the image plane. Due to the short cavity lifetime (2.3 ps), the polariton density reduces rapidly with time. The data scale has been adjusted to compensate for this decay. Ballistic polariton propagation over macroscopic distances is found with a velocity of 6.8μm/ps. A ring-shaped distribution is found, as expected from the excitation geometry. The polaritons were excited with linear polarization along the *x*-axis. Detecting co-linearly polarized (left panels of Fig. 4.1), the intensity is showing a minimum in the diagonal directions. Detecting cross-linearly polarized instead (right panels), the intensity is maximal in the diagonal directions, and zero for propagation along the excitation and detection polarization directions *x* and *y*. This observation is due to the LT-splitting. The excitation polarization along *x* ($\phi = 0$) is not an eigenstate of polaritons with propagation directions other than *x* or *y*, and a polarization beating occurs in these directions.

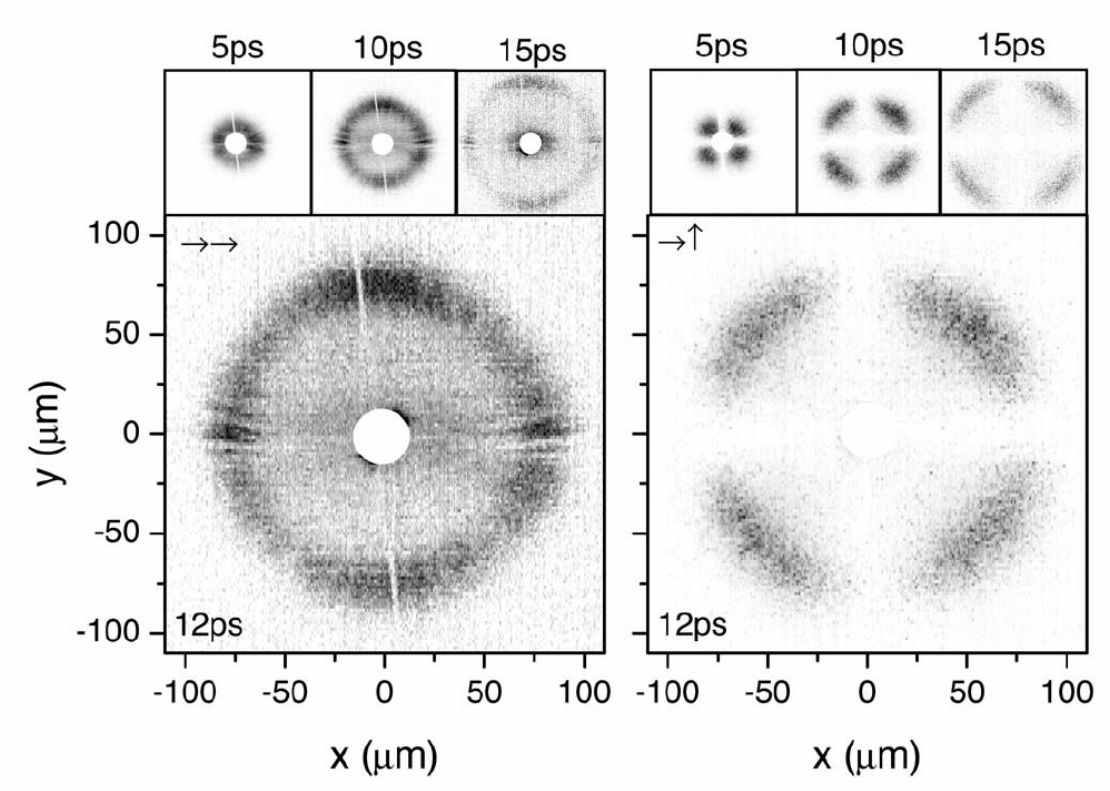

Figure 4.1. Experimental results showing polariton propagation and polarization dynamics in real space ($\bar{k} = 2.8\,\mu\text{m}^{-1}$) (From W. Langbein *et al,* 2007)

We have calculated the intensities of co- and cross-linearly polarized components of the emission from the cavity using Eqs. (4.9) and (4.10), taking into account the calculated polariton dispersion, radiative broadening and LT splitting. For the excited polariton pulse we took $f\left(\bar{\omega}_k\right) = \exp\left(-\left(\bar{\omega}_k - \bar{\omega}_{0k}\right)^2 / \Delta\omega^2\right)$, $h\left(k\right) = \Theta(4/\mu m - k)$, where Θ is the Heaviside function. The spectral width $\Delta\omega$ was 0.6 meV (FWHM 1 meV), and Δk = 1/μm. The excitation frequency $\bar{\omega}_{0k}$ was varied to get the right excitation wavevector.

The resulting spatially resolved images of the intensities of emission of propagating polaritons in co- and cross-polarizations corresponding to the experimental data of Fig. 4.1 are shown in Fig. 4.2. One can see that the propagation speed matches the experimental velocity, which, in its turn, corresponds to the group velocity obtained from the dispersion. The diagonal cross-like shape of cross-polarization and the small anisotropy of the co-polarization, which are due to the pseudospin rotation, are well reproduced.

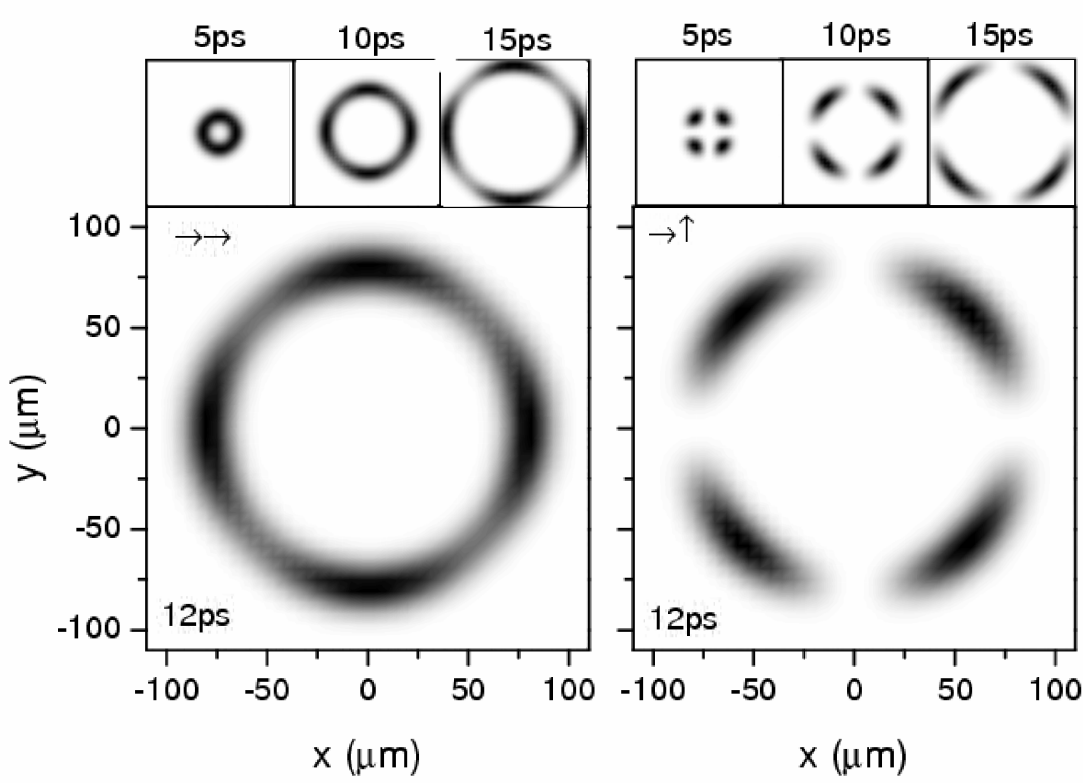

Figure 4.2. Simulated real-space dynamics of polariton propagation and polarization after a point-like excitation ($\bar{k} = 2.8\,\mu\text{m}^{-1}$)

Another comparison of the analytical model with experiment is done on Fig. 4.3. Here we show for the same experiment the experimental and theoretical radial intensity of emission $I(r,\phi,t)\cdot r$ corrected for the cylindrical propagation geometry by multiplying with the radius for co- and cross-polarizations at various times. One can see that initially (after 6 ps) the intensity in co-polarization is much higher than the one in cross-polarization, while after 14 ps they become comparable, due to the pseudospin rotation. The experimental data are quantitatively reproduced by the theory.

We can therefore conclude that the theoretical tool developed in this section works well to describe the experiments performed in linear regime, when the density of polaritons is small enough in order for the renormalization to be negligible. This simplest case has the advantage of having an analytical solution. In more complicated cases one has to solve numerically the spinor Gross-Pitaevskii equations to obtain the spatial and polarization dynamics, as it is done in the following sections.

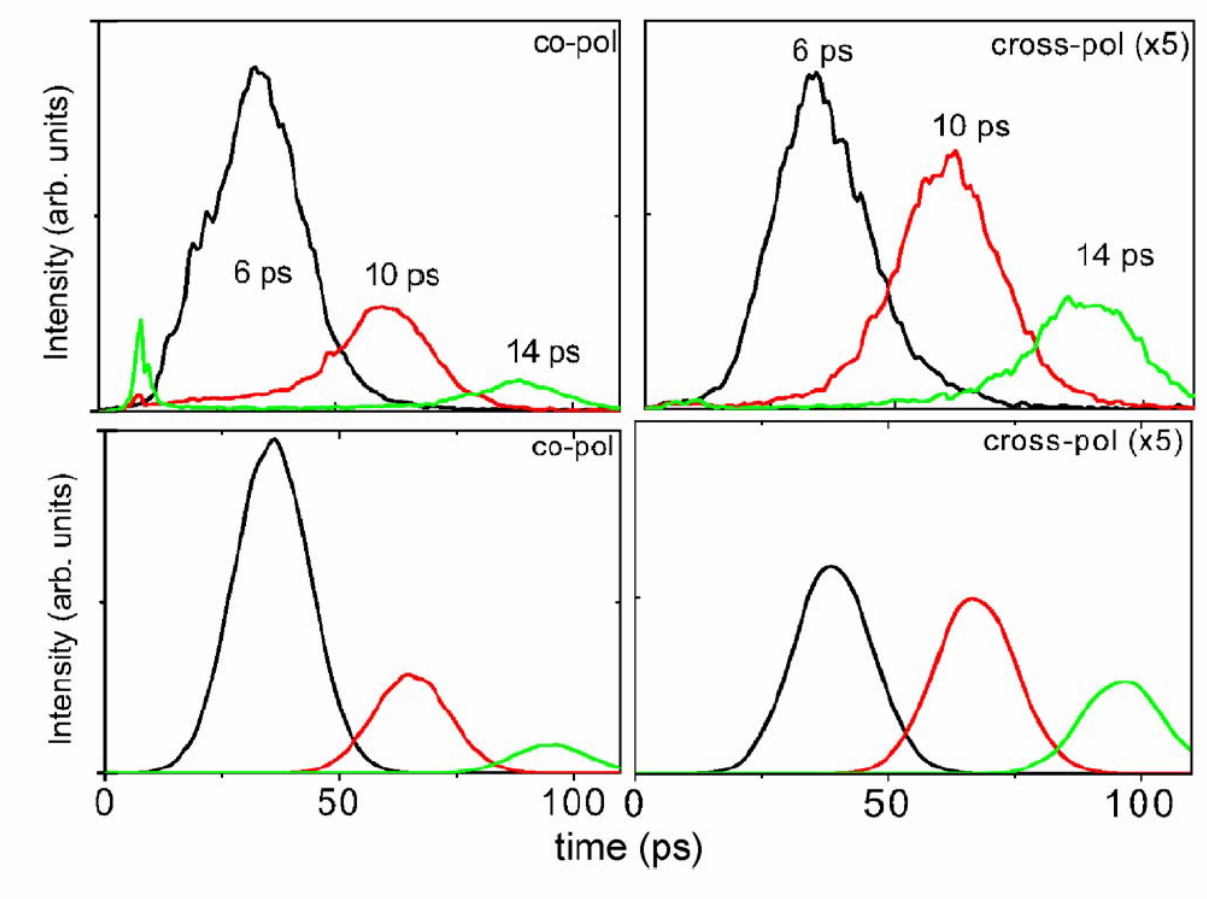

Figure 4.3. Measured and simulated radial intensity distribution $r_c I(r_c,\phi,t)$ corrected for cylindrical propagation, for various times after excitation of polaritons centered at $\bar{k} = 2.8\,\mu\text{m}^{-1}$. Top: measured (from W. Langbein *et al*, 2007). Bottom: simulated. Left: Colinearly polarized for $\phi = \pi/2$. Right: cross-linearly polarized for $\phi = \pi/4$.

4.2. Polarization and evolution of a polariton condensate

In this section we first consider a polariton condensate in thermodynamic limit. We try to determine the polarization of a spontaneously formed condensate, which can be done analytically. Then we consider the time evolution of real-space distribution and polarization of a macroscopic population of polaritons created by a short pulse, and we find ring-like excitations propagating at the speed of sound waves with Bogoliubov dispersion, thus manifesting superfluidity.

4.2.1. Spin effects in atomic condensates

First atomic condensate observed by K.B. Davis *et al* (2005) was observed for a single species of alkali atoms (^{23}Na). Such a condensate could be described by a single scalar wavefunction. Immediately after, a more complex situation has attracted theoretical attention. T.-L. Ho and V.B. Shenoy (1996) have considered a possibility of condensation of a mixture of different

atoms, like ^{23}Na-^{87}Rb or ^{87}Rb-^{85}Rb, or different hyperfine states of the same alkali, like the (F=2, MF=2) and (F=1, MF=1) states of ^{87}Rb. The theoretical approach was to write a wavefunction not as a scalar, but as a vector, and then write the Gross-Pitaevskii equation for this vector. Different configurations can produce various effects like interpenetration or phase separation of the species.

Utilization of optical traps instead of magnetic ones has allowed to study the spin degree of freedom of atomic condensates. The first experimental observation of spin-1 condensate was reported by J. Stenger *et al* (1998), and the various effects like metastability and quantum tunneling across spin domains have been readily explained by D.M. Stamper-Kurn *et al* (1999) and in other papers with the use of spinor Gross-Pitaevskii equations. After that a number of papers have been published, studying the dynamics of spin-2 condensates (e.g. H. Smaljohann *et al*, 2004) and comparing them to the spin-1 condensates (e.g. Nille N. Klausen, John L. Bohn and Chris H. Greene, 2001). One can see that the spinor (or, in general, vector) Gross-Pitaevskii equation is a well-established tool for the description of multi-component condensates in various conditions.

The important differences of exciton-polariton condensates from the atomic ones are 1) TE-TM splitting, which affects the dispersion of excitations; 2) different effective masses for excitons and photons; 3) presence of interaction terms only for excitons. Our final spinor Gross-Pitaevskii equation will have to take into account all these peculiarities. Another non-negligible peculiarity is the finite lifetime of polaritons.

4.2.2. Polarization of the polariton condensate

Let us start with the Hamiltonian density of a polariton system

$$H = \boldsymbol{\psi}^* \cdot \mathbf{T}\left(-i\nabla\right) \cdot \boldsymbol{\psi} + \frac{1}{2}\left[U_0 \left(\boldsymbol{\psi}^* \cdot \boldsymbol{\psi} \right)^2 - U_1 \boldsymbol{\psi}^{*2} \boldsymbol{\psi}^2 \right] \qquad (4.11)$$

Here we assume the cylindrical symmetry of the cavity, which allows only two isotropic quartic invariants. $\boldsymbol{\psi}$ is a two-component vector with components corresponding to TE and TM polarizations. The U_0 term describes polarization independent properties of the condensate, while the U_1 term defines so-called linear-circular dichroism (experimental observation of an effect of this type has been first reported by P.D. Maker, R.W. Terhune, and C.M. Savage, 1964).

We consider the heavy-hole exciton polaritons having only TM and TE modes, and we neglect the mixing with the light-hole polaritons having a split-up mode polarized normally to the quantum-well plane. With respect to the configuration of the in-plane component of the electric field (defined by the 2D vector) and the in-plane 2D wave vector **k**, the TM and TE modes are longitudinal and transverse, respectively. Their dispersions can be found by the transfer matrix technique (chapter 1). The modes are degenerate at $k = 0$ and the energy will be calculated from the bottom of the band. Then, the kinetic energy tensor $\mathbf{T}\left(\mathbf{k}\right)$ is ($\hbar = 1$):

$$T_{ij}(\mathbf{k}) = \omega_t(k)\delta_{ij} + \left[\omega_l(k) - \omega_t(k)\right]\frac{k_i k_j}{k^2} \tag{4.12}$$

When the $\boldsymbol{\psi}$ vector is directed parallel (perpendicular) to $\mathbf{k}$ this expression reduces to the expected $\mathbf{T}(\mathbf{k})\cdot\boldsymbol{\psi} = \omega_{l(t)}\psi$.

The equilibrium properties of polariton condensate at $k = 0$ depend crucially on the presence and the sign of the dichroic U_1 term. For $U_1 > 0$ the free energy density $F = H - \mu\left(\boldsymbol{\psi}^*\cdot\boldsymbol{\psi}\right)$ is minimized at a linear polarization of the condensate (i.e., when $\left[\boldsymbol{\psi}\times\boldsymbol{\psi}^*\right] = 0$). In this case the last term in (4.11) has its maximal possible absolute value and $F_{\min} = -\mu n/2$, where $n = \left(\boldsymbol{\psi}^*\cdot\boldsymbol{\psi}\right)$ is the 2D concentration of condensed polaritons and the chemical potential is $\mu = (U_0 - U_1)n$. Note that μ defines the experimentally measurable blueshift of the polariton emission line due to formation of the condensate. In contrast, in the case $U_1 < 0$ the polariton condensate is formed with a circular polarization ($\boldsymbol{\psi}\cdot\boldsymbol{\psi} = 0$), that assures disappearance of the U_1 term. In the absence of the dichroic term ($U_1 = 0$) there is no superfluid transition at any finite temperature, as it follows from the Landau criterion because one of the dispersion branches is parabolic.

Clearly, the above analysis of the condensate polarization is valid for the very dilute limit and $|U_1| \ll \left(na_s^2\right)U_0$ (a_s is the effective scattering length).

The coupling coefficients U_0 and U_1 can be estimated through the matrix elements of the polariton-polariton scattering in the singlet (α_2) and triplet (α_1) configurations as $U_0 = \alpha_1$ and $U_1 = (\alpha_1 - \alpha_2)/2$. According to Ciuti *et al* (1998) one usually has $\alpha_1 \gg |\alpha_2|$, so that $0 < U_1 < U_0$. Therefore, the polariton condensate is formed with a linear polarization. The condensate ground state can be written as $\boldsymbol{\psi}_{grnd} = \sqrt{n}\mathbf{e}$, where $\mathbf{e} = 1$ is a real unit vector.

4.2.3. Spectrum of excitations

The spectrum of excitations of the polariton condensate at equilibrium can be studied on the basis of Gross-Pitaevskii equation, which will be written here for two polarizations:

$$\begin{aligned} i\frac{\partial\psi_i}{\partial t} &= \frac{\delta F}{\delta\psi_i^*} = \\ &= \left[T_{ij}(-i\nabla) - \mu\delta_{ij}\right]\psi_j + U_0\psi_j^*\psi_j\psi_i - U_1\psi_j\psi_j\psi_i^* \end{aligned} \tag{4.13}$$

Following the linearization method demonstrated in chapter 1, we look for the solutions of Eq. (4.13) in the form

$$\psi(\mathbf{r},t) = \sqrt{n}\mathbf{e} + \mathbf{A}e^{i(\mathbf{kr}-\omega t)} + \mathbf{B}^* e^{-i(\mathbf{kr}-\omega t)} \tag{4.14}$$

Linearizing (4.13) with respect to the small amplitudes A_i and B_i one obtains two equations for these complex amplitudes:

$$\begin{aligned}\left[T_{ij}(\mathbf{k})+(u_0-2u_1)e_ie_j+(u_1-\omega)\delta_{ij}\right]A_j+\left[u_0e_ie_j-u_1\delta_{ij}\right]B_j=0\\ \left[T_{ij}(-\mathbf{k})+(u_0-2u_1)e_ie_j+(u_1+\omega)\delta_{ij}\right]B_j+\left[u_0e_ie_j-u_1\delta_{ij}\right]A_j=0\end{aligned} \qquad (4.15)$$

where $u_0=nU_0$ and $u_1=nU_1$. This system of equations has non-trivial solutions provided the frequency ω satisfies the dispersion equation:

$$\begin{aligned}\omega^4-\left[\omega_l^2+\omega_t^2+2(u_0-u_1)\omega_++2u_1\omega_-\right]\omega^2+\\ +\left[\omega_l\omega_t+2(u_0-u_1)\omega_-\right]\left[\omega_l\omega_t+2u_1\omega_+\right]=0\end{aligned} \qquad (4.16)$$

where $\omega_\pm=\left[\omega_l+\omega_t\pm(\omega_l-\omega_t)\cos(2\varphi)\right]/2$ and φ is the angle between the condensate polarization $\mathbf{e}$ and the wave vector $\mathbf{k}$. In the region of small wave vectors the solutions of the dispersion equation (4.16) give two sound branches of excitation spectrum (i.e. the spectrum is linear). However, the particularity of the polariton condensate is that these branches are anisotropic:

$$\omega^2 \square 2(u_0-u_1)\omega_+,\ \omega^2 \square 2u_1\omega_- \qquad (4.17)$$

The anisotropy of the quasiparticle spectrum is a result of both the cylindrical-symmetry breaking due to the presence of condensate and the existence of LT splitting. The dispersion becomes isotropic and simplifies significantly if one neglects the LT splitting of noninteracting polariton bands by putting $\omega_l=\omega_t=\omega_0$. In this case the result becomes Bogolyubov-like: $\omega^2=\omega_0^2+2(u_0-u_1)\omega_0=\omega_0^2+2\mu\omega_0$ for quasiparticles copolarized with the condensate ($\mathbf{A}\square\mathbf{B}\square\mathbf{e}$), and $\omega^2=\omega_0^2+2u_1\omega_0$ for the cross-polarized quasiparticles ($\mathbf{A}\square\mathbf{B}\perp\mathbf{e}$).

The renormalization and the strong anisotropy of the splitting between the two branches of the polariton spectrum is shown in Figure 4.4 (a,b). The interaction constants are chosen as $U_0=2.4\times10^{-18}\,\mathrm{eV\,m^2}$ and $U_1=0.55U_0$ (which corresponds to $\alpha_2=-0.1\alpha_1$) in accordance with the estimation of P.Renucci *et al* (2005) and the parameters used in the next subsection; the condensate density is $n=10^{15}\,\mathrm{m^{-2}}$. The bare polariton spectrum corresponds to a CdTe microcavity showing a Rabi splitting of 10 meV at zero detuning between exciton and photon modes at $k=0$. The dispersion of polaritons is clearly strongly modified and becomes linear close to k = 0. Note that while the splitting is enhanced in one direction of the wave vector ($\mathbf{k}\perp\mathbf{e}$ in our case), it is suppressed for its perpendicular direction. Moreover, one can observe the crossing of renormalized longitudinal and transverse branches. The strong anisotropy of the splitting is better seen in Fig. 4.4(c).

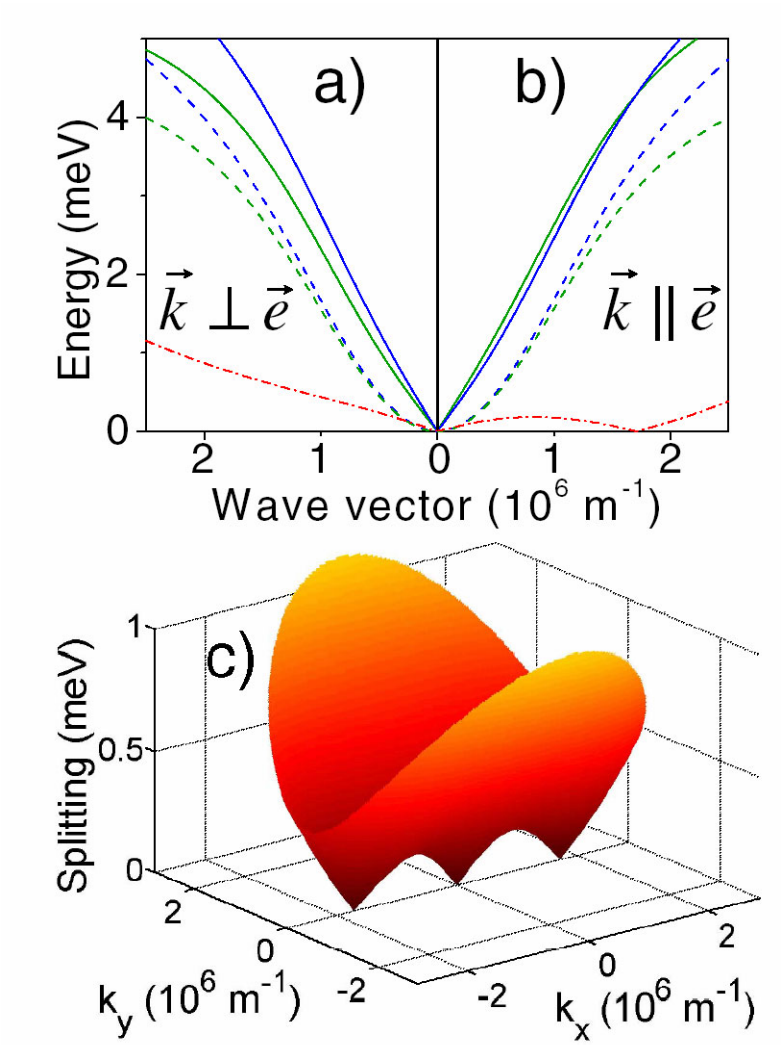

Figure 4.4. The dispersions of bare (dashed lines) and renormalized (solid lines) lower polariton branches in the region of strong coupling. The splitting is shown in a dashed-dotted line. The wave vector is perpendicular to the condensate polarization in panel (a) and collinear with it in panel (b). Panel (c) shows the overall behavior of the splitting.

The Gross-Pitaevskii equation (4.13) describes adequately the excitation spectrum only for the case of a weakly depleted condensate. The non-superfluid fraction n_{out} can be calculated using the Landau quasiparticle formula, which gives a reliable result for the 2D case as shown by D.S. Fisher and P.C. Hohenberg (1988). At low temperatures T, when the phononlike parts of the two branches are mostly occupied, the depletion is

$$n_{out} = \frac{3\zeta(3)}{2\pi}\frac{(k_B T)^3}{\hbar^2 m^*}\left(v_0^{-4} + v_1^{-4}\right) \tag{4.18}$$

where $m^* \sim 10^{-4}$ is the polariton effective mass, $v_0 = \left[\left(U_0 - U_1\right)n/m^*\right]^{1/2}$ and $v_1 = \left[U_1 n/m^*\right]^{1/2}$ are the sound speeds in co- and cross-polarizations, and we neglect LT splitting for simplicity. It is seen from (4.18) that $n_{out} \propto n^{-2}$. For T < 20 K the depletion becomes negligible at $n = 10^{15}\,\mathrm{m}^{-2}$. This particle density corresponds well to the experimentally observed (by M.Richard *et al,* 2005) blueshift $\sim$ 1 meV. Note also that the correction to the blueshift $\left(U_0 - U_1\right)n_{out}$ is of the order of a few μeV, and it is much smaller than the anisotropic splitting seen in Fig. 4.4. The above estimation is confirmed by the numerical calculations allowing for the nonparabolicity of the spectrum (G. Malpuech *et al* 2003).

4.2.4. Real-space dynamics

In this subsection we study numerically the impact of the anisotropic splitting on the real-space coherent dynamics of polariton condensates in nonequilibrium conditions. We take into account the pumping and finite lifetime of polaritons following the approach of I. Carusotto and C. Ciuti (2004). The model of the mentioned paper is, however, generalized by us to take into account the polarization degree of freedom. In this approach, instead of one polariton wave function $\boldsymbol{\psi}(\mathbf{r},t)$, we use its two components, photonic $\boldsymbol{\varphi}(\mathbf{r},t)$ and excitonic $\boldsymbol{\chi}(\mathbf{r},t)$ parts, which satisfy two coupled vector equations (Gross-Pitaevskii for excitons and Schroedinger for photons):

$$\begin{aligned} i\dot{\varphi}_i &= \left[T_{ij}^{(ph)}\left(-i\nabla\right) - i\tau_{ph}^{-1}\delta_{ij}\right]\varphi_j + \Omega_R\chi_i + f_i(\mathbf{r},t) \\ i\dot{\chi}_i &= \left[T_{ij}^{(ex)}\left(-i\nabla\right) - i\tau_{ex}^{-1}\delta_{ij}\right]\chi_j + \Omega_R\varphi_i + V_0\chi_j^*\chi_j\chi_i - V_1\chi_j\chi_j\chi_i^* \end{aligned} \tag{4.19}$$

Here $\mathbf{f}(\mathbf{r},t)$ describes the exciting pump within a limited spot and Ω_R is the Rabi frequency. We consider the case of zero detuning, where the exciton-exciton interaction parameters, V_0 and V_1, are related to the polariton-polariton ones as $V_0 = 4U_0$ and $V_1 = 0.55V_0$. The kinetic **T** tensors have a form of Eq. (4.12) with parabolic free-particle dispersions. Note also that unlike the equilibrium case considered before, the Gross-Pitaevskii equations (4.19) contain the lifetimes $\tau_{ex(ph)}$ in place of chemical potentials.

We consider a 1.8 ps exciting pulse of light having a lateral size of 15 μm. It resonantly excites the ground state of the lower-polariton branch, as well as some of the excited states, because of its finite broadening. It is polarized horizontally (along the x axis). We assume zero temperature, the cavity photon lifetime $\tau_{ph} = 7\,\text{ps}$, and infinite exciton nonradiative lifetime τ_{ex}. Figure 4.6 shows the 2D plot of the absolute value of the photon part of the wave function at different times for both horizontal and vertical polarizations, whereas figure 4.5 shows the corresponding cross-sections. The contrast on the 2d plots has been adjusted to get the best visibility.

The upper panels in Figs. 4.5 and 4.6 show the wave function before the arrival of the maximum of the excitation pulse, when the polariton density is very small and nonlinear effects are negligible. Without the exciton-exciton interaction, the wavefunction would have kept its shape, slowly expanding with time. The *x*-polarized component at small times keeps the Gaussian spatial shape of the exciting pulse. At the same time the *y*-polarized or cross component appears in the diagonal directions, which are the directions where the horizontal and vertical polarizations are no more the quasiparticle eigenstates and the presence of the LT splitting results in the precession of polarization. The mechanism here is the same as in section 4.1 (figures 4.1 and 4.2).

At a time 2.4 ps after the maximum of the pulse, the x-polarized component forms a ring which quickly expands with time (Figs. 4.5 and 4.6, middle panels). This way of motion is characteristic for a linear dispersion[1], and not for a parabolic one. We believe that the observation of such a ring under the described excitation conditions would be a clear experimental evidence of polariton superfluidity, because if the dispersion had stayed parabolic, the ring would not have appeared. The inhomogenity of spatial distribution introduced by the shape of the pulse excites the excitations of the condensate. The condensate itself is formed by the homogeneous fraction of the particle density. This fraction does not move anywhere because it has zero momentum and the dispersion for the motion of the condensate as a whole is parabolic.

After 16.4 ps, the pattern again strongly changes. The *x*-polarized component consists of a central peak, which is not moving or spreading and shows radiative decay only. This static peak can be associated with the ground state polariton condensate. The ring that was formed on the previous stage does not disappear, but new rings of smaller intensity are formed on its surface. At the same time, in *y* polarization the rings propagate without deformations, new rings forming from the center while the external ones are expanding. The velocity of expansion is given by the velocities of sound in different directions $v_0 = \sqrt{(U_0 - U_1)n/m^*}$, $v_1 = \sqrt{U_1 n/m^*}$, as described in chapter 1 and defined

[1] This is most easily understood for a 1D case: with parabolic dispersion a Gaussian excitation with zero group velocity keeps its shape while getting more and more broad, whereas with linear dispersion the same excitation gets separated into two traveling waves moving in opposite directions.

above. These velocities depend on the density *n* of the polariton condensate and they change in time because of the radiative decay of population. Note also that the black cross seen in the bottom right panel in Fig. 4.6 is slightly asymmetric: the horizontal band is wider than the vertical one. It happens because of the anisotropy of the splitting between polariton branches, which appears due to the renormalization of dispersion caused by the condensate formation.

We should note that the experimental and theoretical results presented in section 4.1 cannot be associated with the superfluidity since (i) the interference rings are the result of excitation of polariton excited states and not the ground state, like in this section, and (ii) the observed cross is symmetric. Observation of the superfluid propagation of exciton polaritons remains an important challenge for experimentalists. The problem is mainly related to the presence of imperfections in microcavities able to attract or scatter the condensate wave function, and this problem will be addressed in details in chapter 5.

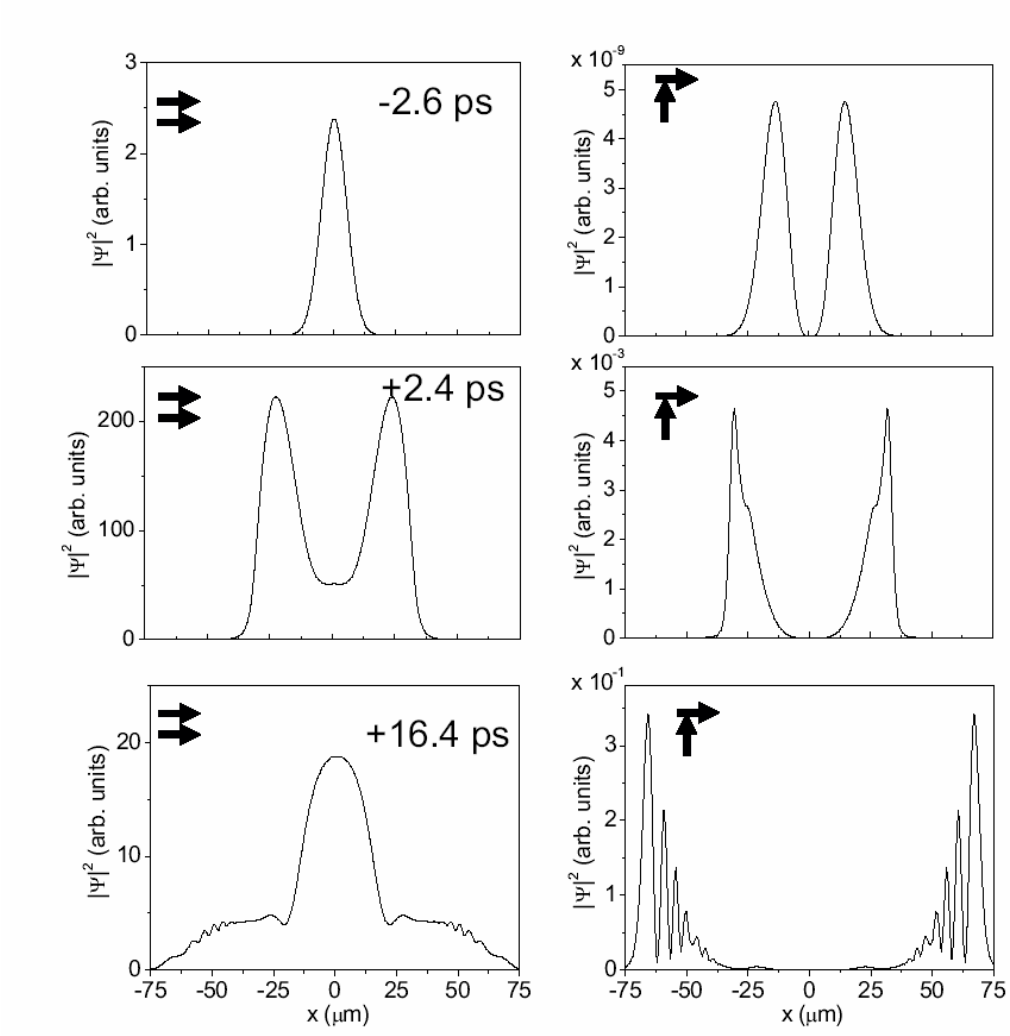

Figure 4.5. Cross-sections of the photon part of the wavefunctions for co- and cross-polarized components.

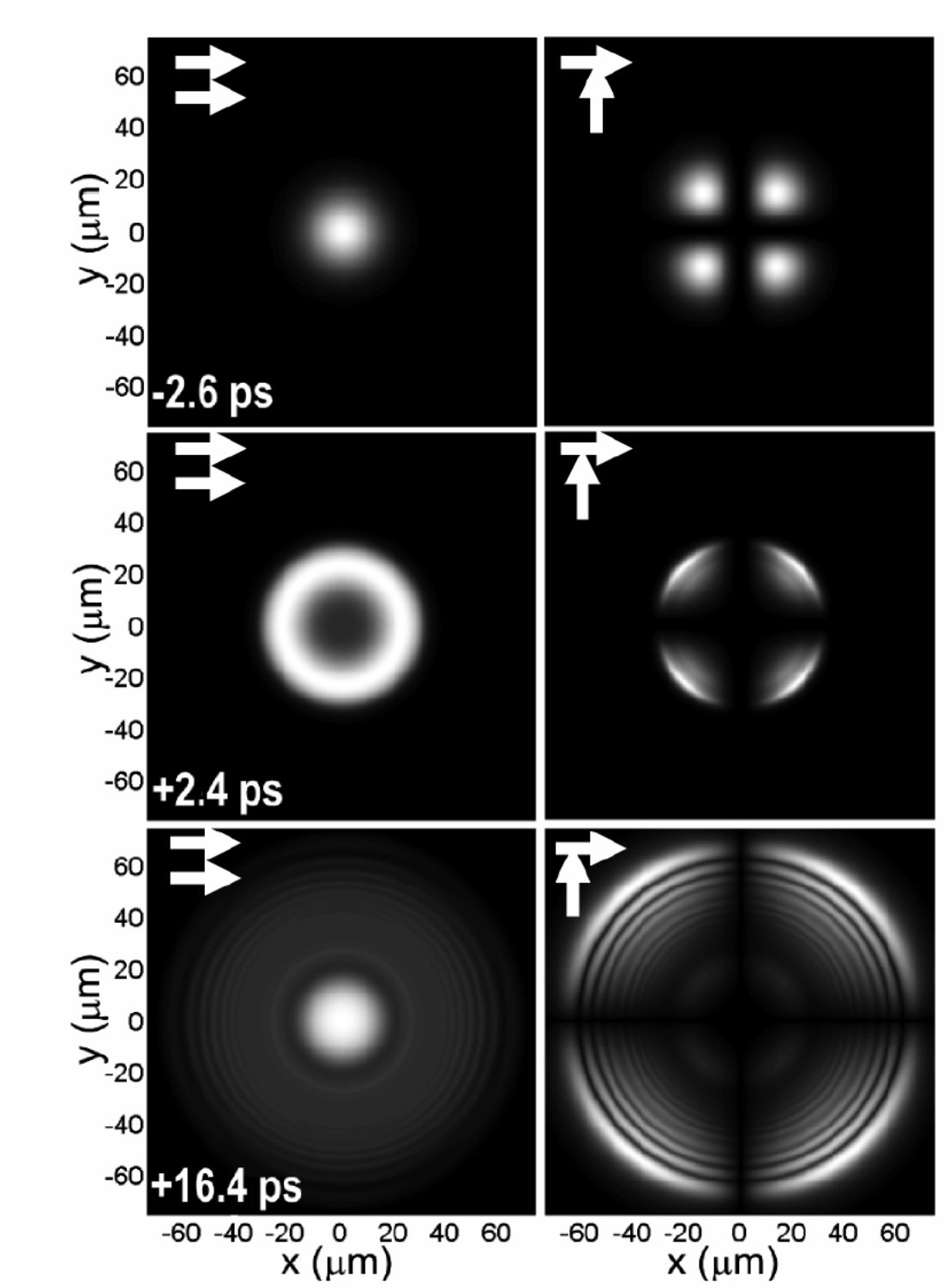

Figure 4.6. Real-space image of the photon part of the wave function, showing evolution of a Gaussian shape pulse in non-linear regime in x and y polarizations. Zero time corresponds to the peak intensity of the pulse.

4.3. Polarization of a driven mode

In this section we consider the polarization of a pumped polariton mode with macroscopic occupation. It will be shown that the polarization of polaritons can be completely different from the polarization of the pumping laser. Therefore, it is very important to investigate this dependence, because it determines the initial conditions for the pseudospin formalism developed in the previous chapter and in the first section of this chapter, and it may affect strongly the results of experiments in the OPO configuration, where as much as three modes can be considered as macroscopically occupied.

To find the polarization of a single macroscopically occupied mode with pumping and decay, we linearize the Gross-Pitaevskii equation for polaritons using the approach demonstrated in section 1.4. Here we neglect the LT splitting for simplicity and work with the ground state of the polariton dispersion.

The Gross-Pitaevskii equation for the polaritons taking into account the pumping of the state $k = 0$ and radiative decay reads ($\hbar = 1$):

$$\begin{aligned} i\frac{\partial \psi_+}{\partial t} &= -i\frac{\psi_+}{\tau} + H_0\psi_+ + \left(\alpha_1|\psi_+|^2 + \alpha_2|\psi_-|^2\right)\psi_+ + P_+e^{-i\omega_0 t} \\ i\frac{\partial \psi_-}{\partial t} &= -i\frac{\psi_-}{\tau} + H_0\psi_- + \left(\alpha_1|\psi_-|^2 + \alpha_2|\psi_+|^2\right)\psi_- + P_-e^{-i\omega_0 t} \end{aligned} \qquad (4.20)$$

It is a simplification of equation (4.13) written in circular basis in order to have simpler terms describing polariton-polariton interaction. The chemical potential μ is replaced by the pumping and decay terms.

Introducing the new variable $\boldsymbol{\psi} = \boldsymbol{\phi}e^{-i\omega_0 t}$ to set the energy of the pump to zero one has

$$\begin{aligned} i\frac{\partial \phi_+}{\partial t} &= -i\frac{\phi_+}{\tau} + (H_0 - \omega_0)\phi_+ + \left(\alpha_1|\phi_+|^2 + \alpha_2|\phi_-|^2\right)\phi_+ + P_+ \\ i\frac{\partial \phi_-}{\partial t} &= -i\frac{\phi_-}{\tau} + (H_0 - \omega_0)\phi_- + \left(\alpha_1|\phi_-|^2 + \alpha_2|\phi_+|^2\right)\phi_- + P_- \end{aligned} \qquad (4.21)$$

Once again we use the linearization method by representing the solution in the following form:

$$\begin{pmatrix}\phi_+\\ \phi_-\end{pmatrix} = \begin{pmatrix}\phi_{0+}\\ \phi_{0-}\end{pmatrix} + \begin{pmatrix}A_+\\ A_-\end{pmatrix}e^{i(kx-\omega' t)} + \begin{pmatrix}B_+^*\\ B_-^*\end{pmatrix}e^{-i\left(kx-\omega^{*\prime} t\right)} \qquad (4.22)$$

Here the frequency ω' can be complex, which is why we need to write ω'^* instead of ω' in the term with $\mathbf{B}^*$ to avoid having a diverging wavefunction. Linearizing (4.21) with respect to small amplitudes and separating the terms with different time dependence one obtains the following large system of equations:

$$\begin{aligned}\left[\left(H_0-\omega_0-\frac{i}{\tau}\right)+\left(\alpha_1\left|\phi_{0+}\right|^2+\alpha_2\left|\phi_{0-}\right|^2\right)\right]\phi_{0+}+P_+=0\\ \left[\left(H_0-\omega_0-\frac{i}{\tau}\right)+\left(\alpha_1\left|\phi_{0+}\right|^2+\alpha_2\left|\phi_{0-}\right|^2\right)\right]\phi_{0-}+P_-=0\end{aligned} \tag{4.23}$$

$$\begin{aligned}&\left(H_0(k)-\omega_0-\omega'-\frac{i}{\tau}+2\alpha_1\left|\phi_{0+}\right|^2+\alpha_2\left|\phi_{0-}\right|^2\right)A_+ +\alpha_1\phi_{0+}^2B_+ +\alpha_2\phi_{0+}\phi_{0-}^*A_- +\alpha_2\phi_{0+}\phi_{0-}B_- =0\\ &\alpha_1\phi_{0+}^{*2}A_+ +\left(H_0(k)-\omega_0+\omega'+\frac{i}{\tau}+2\alpha_1\left|\phi_{0+}\right|^2+\alpha_2\left|\phi_{0-}\right|^2\right)B_+ +\alpha_2\phi_{0+}^*\phi_{0-}^*A_- +\alpha_2\phi_{0+}^*\phi_{0-}B_+ =0\\ &\alpha_2\phi_{0+}^*\phi_{0-}A_+ +\alpha_2\phi_{0+}\phi_{0-}B_+ +\left(H_0(k)-\omega_0-\omega'-\frac{i}{\tau}+2\alpha_1\left|\phi_{0-}\right|^2+\alpha_2\left|\phi_{0+}\right|^2\right)A_- +\alpha_1\phi_{0-}^2B_- =0\\ &\alpha_2\phi_{0+}^*\phi_{0-}^*A_+ +\alpha_2\phi_{0+}\phi_{0-}^*B_+ +\alpha_1\phi_{0-}^{*2}A_- +\left(H_0(k)-\omega_0+\omega'+\frac{i}{\tau}+2\alpha_1\left|\phi_{0-}\right|^2+\alpha_2\left|\phi_{0+}\right|^2\right)B_- =0\end{aligned} \tag{4.24}$$

The equations (4.23) give us the occupation and polarization of the condensate as a function of the pump. It is interesting to note, that in general the polarization of the condensate *does not* coincide with the polarization of the pump. The equations (4.24) allow to find the dispersions of excitations of the macrooccupied mode (see section 4.3.2).

4.3.1. Polarization multistability

From the system (4.23) one can show that the polarization of the polariton system inside the cavity is multistable: for a given external pump (e.g. linear), the polarization inside the cavity can be linear or elliptic (either mostly right- or left-circular polarized). Qualitatively, the multistability can be understood as follows. Assume that the cavity is illuminated by laser light at normal incidence at the frequency above the bottom of the lowest polariton branch (LPB). At low pumping, the pump is not in resonance with the polariton eigenstate, so that the population of the driven mode remains low. At higher pumping, polariton-polariton interactions lead to the blue-shift of the LPB, so that it approaches the pump laser frequency. At resonance, the population jumps up abruptly. If the pumping power is then decreased, the population of the polariton mode jumps down back, but at a lower threshold. As a result the typical S-shape dependence of the polariton density on the pumping intensity, first observed by A. Baas *et al* (2004), appears as Figure 4.7 shows, which means the formation of a hysteresis cycle. The additional polarization degree of freedom makes this picture much more complex and rich.

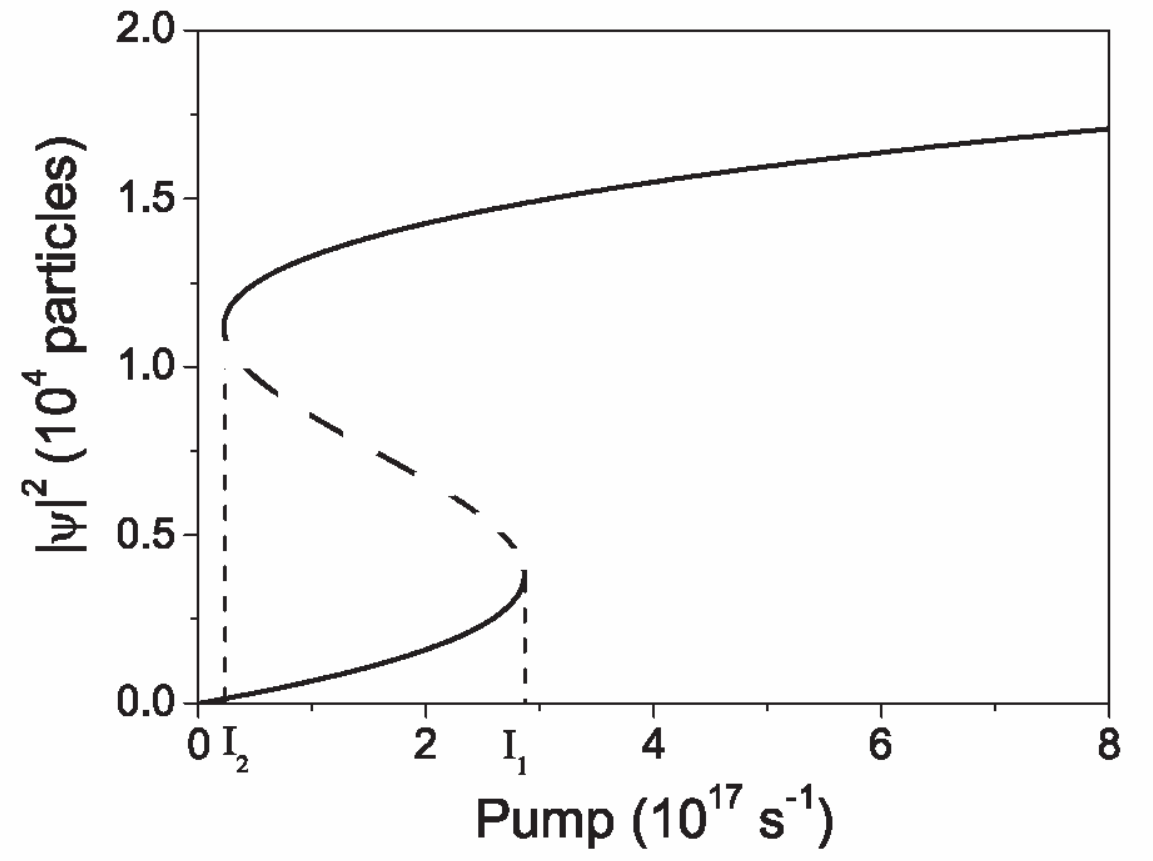

Figure 4.7. Typical S-shape dependence of the polariton population versus pumping intensity for circularly polarized pump. Dashed line shows the unstable region. I1 and I2 mark two jumps in population caused by the increase and decrease of the pumping intensity, respectively.

The energy of the laser ω is chosen above the energy of the bare polariton state, $\omega - \omega_0 = 3\,\text{meV}$, so that the curve shows the classical S-shape. We use $\alpha_1 = 6xE_b a_B^2 / S$, where $a_B = 100\,\dot{A}$ is the two dimensional exciton Bohr radius, $E_b = 8\,\text{meV}$ is the exciton binding energy, $x = 1/2$ is the exciton fraction, and $S = 100\,\mu\text{m}^2$ is the laser spot area. The polariton life-time is $\tau = 2\,\text{ps}$. These parameters are typical for an AlGaAs microcavity, as in section 4.1. We have denoted by I_1 and I_2 the laser intensities corresponding to the bending points of the S-shaped curve taking place with the increase and decrease of pumping intensity, respectively.

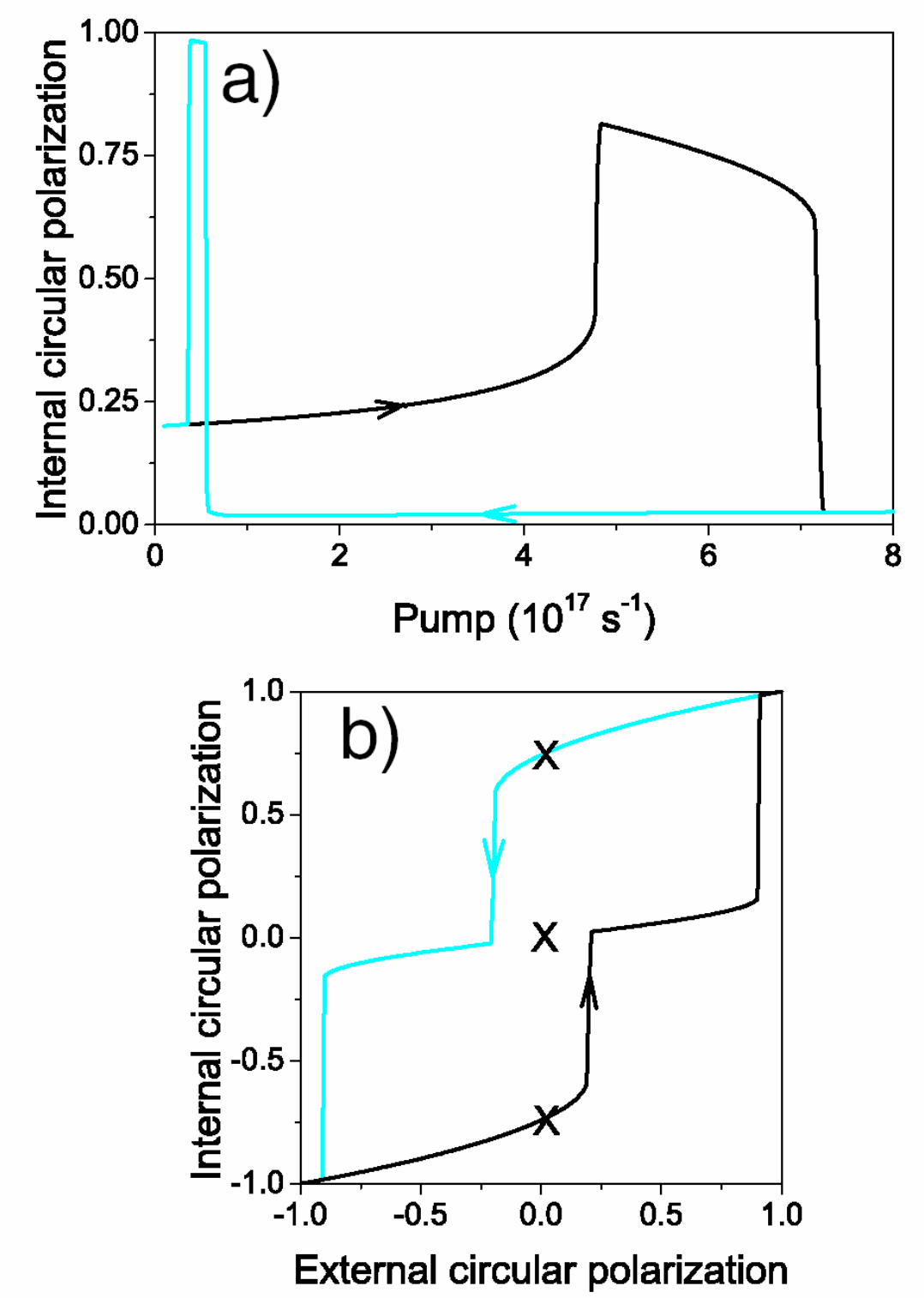

Figure 4.8. (a) Circular polarization degree of the driven mode versus external pumping intensity for slightly elliptical pump $\rho_p = 0.2$. Arrows show the direction in which the pump intensity is changed. (b) Circular polarization degree of the driven mode ρ_c versus circular polarization degree of the pump ρ_p. Arrows show the direction in which the pump polarization degree is changed. The pump intensity is just above I_1. Crosses mark the stable points at $\rho_p = 0$.

The evolution of the internal polarization can be conveniently illustrated and understood considering the case $\alpha_2 = 0$, when Eqs. (4.23) for two polarizations are simply decoupled and the two circular components evolve independently. The change of ρ_c with the total pump intensity is shown in Fig. 4.8(a) for the elliptically polarized pump with $\rho_p = 0.2$, so that σ^+ component slightly exceeds σ^- one. As the intensity of the pump increases, the solution moves along the lower branch of the S-curve for both σ^+ and σ^- components. However, the σ^+ component, since it dominates, reaches the threshold intensity I_1 first. The corresponding intensity of the polariton field jumps abruptly to the upper branch. At the same time, the intensity of the σ^- pump has not yet reached the I_1 bending point. So, the jump of the total polariton density is accompanied by a jump of the circular polarization degree. If the intensity of pump increases further, the intensity of the σ^- mode also reaches I_1. The polariton population increases again, but this now results in an abrupt decrease of the circular polarization degree of the driven mode. If we now reduce the intensity, the reversed process takes place at the pumping intensity I_2 so that hysteresises in both the occupation and polarization power dependencies appear.

Fig. 4.8(b) shows another interesting configuration, where the laser intensity I is kept constant in the domain $I > I_1$ and $I_1 > I/2 > I_2$. The cyan line shows the change of the circular polarization degree of the driven mode ρ_c induced by the laser initially polarized σ^+ and whose polarization is progressively rotated towards the σ^- polarization. One can observe a weak decrease of ρ_c, which however remains quite high even when the pumping is linearly polarized. This is due to the fact that the σ^+ component remains on the upper branch of the S-curve whereas the σ^- drops on the lower branch. Then there are two jumps of polarization corresponding to the jumps of σ^+ and σ^- components of the polariton population, and finally the polarization becomes fully σ^-. The black line shows the evolution of ρ_c with the inverse change of the pump polarization. The stable points corresponding to full linear polarization of the laser are marked with crosses. One can see that the internal polarization can be either nearly σ^+, either nearly σ^-, or fully linear. The latter case is in fact degenerate. There can be two stable driven mode occupations *N* for the same value of the external laser intensity *I*.

Fig. 4.9 shows the functional dependence between σ^+ and σ^- components of the polariton population and the intensity and polarization of pump calculated accounting for the coupling between polaritons with opposite spins described by $\alpha_2 = -0.1\alpha_1$. This value of α_2 corresponds to recent estimations of Renucci *et al* (2005). The circular polarization degree of the pump laser is

represented by the color of the surface of solution and the intensity of the pump is on the vertical *z*-axis. The linear part of the polarization of the laser is kept aligned along *x*-direction.

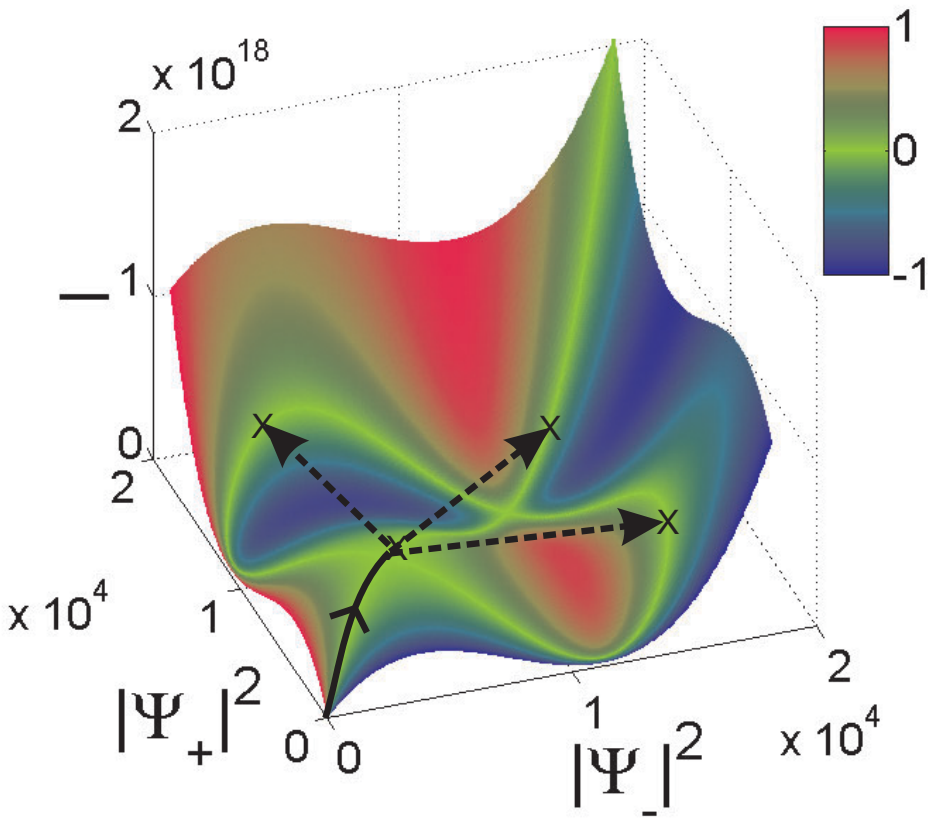

Figure 4.9. The pump intensity I and polarization (color) versus the circular polarized components of the driven mode (bright green corresponds to linear polarization). The crosses mark the four stable points for the driven mode corresponding to the same linearly polarized pump intensity. Arrows show the three possible jumps in case if the pump intensity is slightly increased above the stability point.

The green areas correspond to nearly linearly polarized pumping. If the intensity of the pump increases, while its polarization is kept linear, the system follows the black solid line and black arrows shown in the Fig. 4.9. One can see that from the critical point at the end of the solid black line the system can jump into three possible stable points (shown by crosses). One of them corresponds to linearly polarized state and two others to nearly right- and left-circularly polarized states. The stability of the states was verified using the standard linearization procedure as it is done by N.A. Gippius and S.G. Tikhodeev (2004). The choice of the final state by the system is random and is triggered by fluctuations.

Note also that the jump of the system to the circularly polarized final state induces a red shift of the cross-circular component because of the negative sign of α_2. The red shift drives this component out of resonance with the pump, which leads to stronger polarization of the final state. The positive feedback in polarization of the polariton system would not take place for the case $\alpha_2 = 0$ where only a linearly polarized driven mode would be formed. Experimentally, we expect this effect to have a key impact on the polarization measurements performed with resonantly excited microcavities. It will result in a random sign of the observed polariton polarization changing from one experiment to another.

4.3.2. Chaotic behavior of a multistable system

Dynamical chaos is a developing field of research since its discovery by Jacques Hadamard in 1898. When a system described by deterministic laws exhibits quasi-periodic and unpredictable behavior, this is usually called dynamical chaos. This chaos is generated not by the random properties of the system itself, but from the nonlinearities in the equations governing its behavior.

The theory of chaos has advanced quite far. One of the most important theoretical results in this field is the Poincare-Bendixson theorem, which states that in a continuous dynamic system a strange attractor can arise only if the system has three or more dimensions. This theorem has important consequences for polariton system: without polarization, a polariton system cannot exhibit chaotic behavior although it can be bistable. Apart from arising problems like unpredictability of weather, the chaotic behavior can have positive effects for practical purposes. After the seminal paper about controlling the chaos by E. Ott, C. Grebogi, and J.A. Yorke (1990), the scientists are starting to think “stability good, chaos better” instead of “stability good, chaos bad”. This is true for certain systems, where the chaos can be limited, controlled and used. An interesting idea is the chaotic communications method (L.M. Pecora and T.L. Carroll, 1990; K.M. Cuomo, A.V. Oppenheim, 1993), which has been experimentally realized on the base of semiconductor laser operating in chaotic regime (I. Fischer, Yun Liu, and Peter Davis, 2000).

A multistable system can have chaotic dynamics (this is true even for a bistable system with external control, as shown e.g. by M. Taki, 1997), and it can therefore be used for data encryption and transmission using the chaotic communication method mentioned above. The basic idea of the method is based on the fact that the chaotic oscillations of one system may be driven by the chaotic oscillations of another similar system. If the chaotic output of the driving system is slightly modulated by some useful signal, the oscillations of the driven system will remain non-modulated, because they are determined by the internal properties of this system, and the useful signal can then be extracted from the difference between the modulated signal received from the driving system and

the output of the driven system. Between two systems the signal remains completely chaotic, even if it is modulated, and the data is therefore protected from eavesdropping.

4.3.3. Dispersion of excitations of the driven mode

From the condition that the system of equations (4.24) should have non-trivial solutions for A and B one can find the dispersions of the excitations of the driven macrooccupied mode, like it has been done in chapter 1. The expressions for the general case of elliptic polarization of the pump are cumbersome, and it is more instructive to consider two particular cases: that of a circular pump and that of a linear pump.

In the case of circular pumping the elementary excitations are also circularly polarized. The four dispersion branches are described by the following equations:

$$\begin{aligned}
\omega_{1,2}^{\uparrow} &= \omega_0 - \frac{i}{\tau} \pm \sqrt{\left(E_{LP}(k) - \omega_0 + 2\alpha_1 n\right)^2 - \left(\alpha_1 n\right)^2} \\
\omega_1^{\downarrow} &= -\frac{i}{\tau} + E_{LP}(k) + \alpha_2 n \\
\omega_2^{\downarrow} &= 2\omega_0 - \frac{i}{\tau} - E_{LP}(k) - \alpha_2 n
\end{aligned} \qquad (4.25)$$

where $n = |\Psi_0|^2$. Here we wrote the equations for a σ^+ polarized pump.

The dependencies of real and imaginary parts of $\omega_{1,2}^{\uparrow,\downarrow}(k)$ are shown in Figures 4.10(a,b) and 4.11(a,b) respectively. Figure 4.10 shows the flat dispersion at $k = 0$, whereas figure 4.11 shows the flat dispersion at $k \neq 0$. The bare polariton dispersion $E_{LP}(k)$ is taken parabolic with a polariton mass given by $m_{pol} = 3\times10^{-5} m_0$ where m_0 is the free electron mass. We take $n = 1.1\times10^4, 2.5\times10^3$ for a surface of S=(10 μm)^2. It is seen from (4.25) that renormalization of the dispersion of cross-polarized excitations consists only in the concentration-dependent shift with respect to the bare dispersion. It remains parabolic with a constant imaginary part given by $1/\tau$. This is because polariton-polariton interactions do not mix the circularly polarized components.

The renormalization of the co-polarized dispersion is much more interesting. It follows from (4.25) that it is completely imaginary in the vicinity of the point where $E_{LP} = \omega_0$. Physically it means that the renormalized mode is fully dissipative. The edges of the dissipative zone are given by the following expression $E_{LP}(k) - \omega_0 = \alpha_1 n$, which means that the difference between the energies of the bare polariton state and the pump energy is equal to the mean interaction energy in the driven mode. The increase of *n* resulting from the increase of the pump intensity leads to the spreading of the flat region of dispersion which incorporates the point $k = 0$ when $E_{LP}(0) - \omega_0 = \alpha_1 n$.

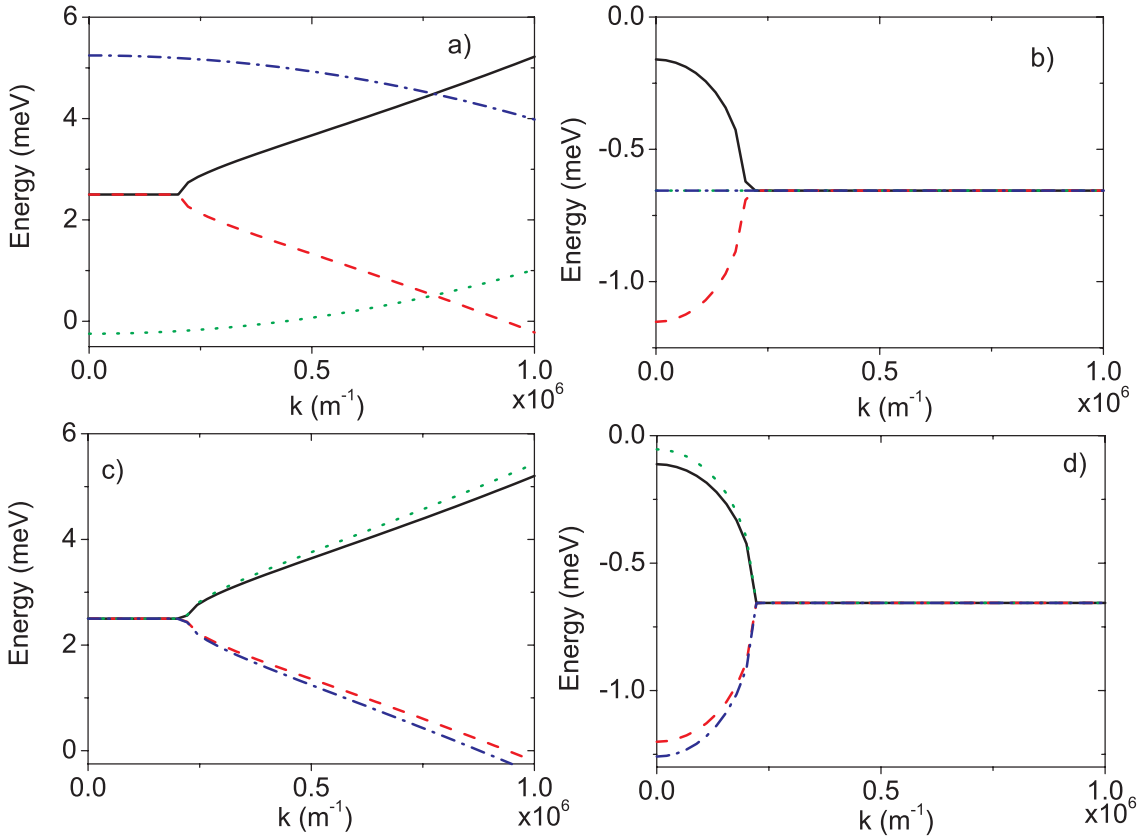

Figure 4.10. Real (a,c) and imaginary (b,d) parts of dispersions of the excitations in the case of circular (a,b) and linear (c,d) polarization of the macroscopically occupied mode with a flat part at k=0.

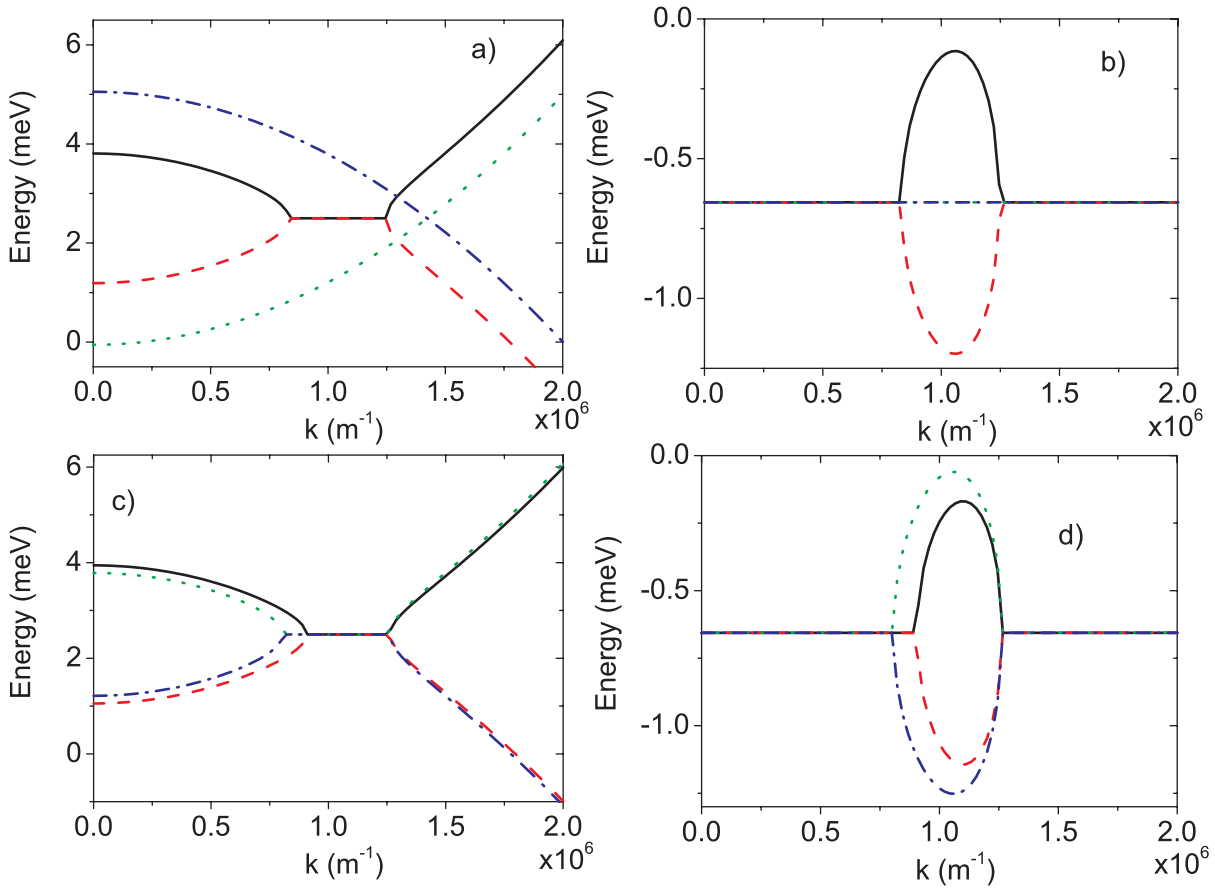

Figure 4.11. Real (a,c) and imaginary (b,d) parts of dispersions of the excitations in the case of circular (a,b) and linear (c,d) polarization of the macroscopically occupied mode with a flat part at |k|>0. Flat region of a real part of dispersion corresponds to an extreme of the imaginary part.

In the case of a linearly polarized driven mode the elementary excitations are also linearly polarized with dispersions given by the following expressions

$$\omega_{1,2}^{co} = \omega_0 - \frac{i}{\tau} \pm \sqrt{\left(E_{LP}(k) - \omega_0 + \alpha_1 n + \alpha_2 n\right)^2 - \frac{1}{4}\left(\alpha_1 n + \alpha_2 n\right)^2}$$
$$\omega_{1,2}^{cross} = \omega_0 - \frac{i}{\tau} \pm \sqrt{\left(E_{LP}(k) - \omega_0 + \alpha_1 n\right)^2 - \frac{1}{4}\left(\alpha_1 n - \alpha_2 n\right)^2} \qquad (4.26)$$

As linear polarizations are mixed by anisotropic polariton-polariton interactions, the dispersions of both co- and cross-polarized modes contain flat parts (purely dissipative regions). Real and imaginary parts of the dispersions in case of linear polarized mode are shown on Figures 4.10(c,d) (flat at $k = 0$) and 4.11(c,d) (flat at $k \neq 0$) respectively. Here we took $n = 2.5\times10^4, 5\times10^3$ for a surface S=(10 μm)^2. The difference in behaviour of co- and cross-polarized components is governed by the value and the sign of α_2. We have considered a realistic case with $\alpha_2 = -0.1\alpha_1$.

4.3.4. Stability analysis

The approach presented above is only valid for a single macroscopically occupied polariton quantum state. This is indeed the case if the imaginary parts of the eigen-frequencies of all excited states are negative. On the other hand, if the imaginary part is positive for one of the upper states, the scattering towards this state becomes stimulated, and the state itself becomes macroscopically occupied. In this section we analyse the stability of the polariton dispersions obtained in the previous section. As before, we shall concentrate on two cases, namely, the circularly polarized mode and the linearly polarized mode. In the further analysis the most important parameter will be the detuning $\Delta = \omega_0 - E_{LP}$.

For a strictly circular pump, only the coefficient α_1 is important, because the amplitude of the cross-polarized component of the polariton state is strictly zero. The driven mode is circularly polarized. The stability condition in this case reads:

$$3\left(a_1 n\right)^2 - 4\Delta\alpha_1 n + \Delta^2 + \frac{1}{\tau^2} > 0 \tag{4.27}$$

Therefore, for a given value of detuning the system is unstable against parametric scattering in the (+k,-k) states if

$$\alpha_1 n \in \left[\frac{2}{\sqrt{3}\tau}, \frac{2\Delta - \sqrt{\Delta^2 - 3/\tau^2}}{3}\right] \tag{4.28}$$

The ground state itself is unstable if

$$\alpha_1 n \in \left[\frac{2\Delta - \sqrt{\Delta^2 - 3/\tau^2}}{3}, \frac{2\Delta + \sqrt{\Delta^2 - 3/\tau^2}}{3}\right] \tag{4.29}$$

The dispersion shows flat parts if the stability condition is verified and if

$$3\left(\alpha_1 n\right)^2 - 4\Delta\alpha_1 n + \Delta^2 < 0 \tag{4.30}$$

which occurs when $\alpha_1 n \in \left[\frac{\Delta}{3}, \Delta\right]$. Therefore if $\alpha_1 n$ is between 0 and $\frac{\Delta}{3}$, the flat parts are present at non zero wave vectors, if $\alpha_1 n$ is between $\Delta/3$ and Δ this flat part is around $k = 0$. The condition $\alpha_1 n = \Delta$ yields a linear spectrum. One should note that this line belongs to the stable region. All these results are summarized in figure 4.12. We took $\hbar/\tau = 1\text{meV}$. The figure shows 6 different regions, 2 of which are unstable and 4 correspond to different types of dispersions. In the region 1 the dispersion shows flat part at some nonzero wavevector *k* (and -*k*); in the region 2 the flat part is centered at $k = 0$; the region 3 has a Bogoliubov-like dispersion (linear at small wavevectors); the region 4 has the original parabolic dispersion; the regions 5 and 6 are unstable.

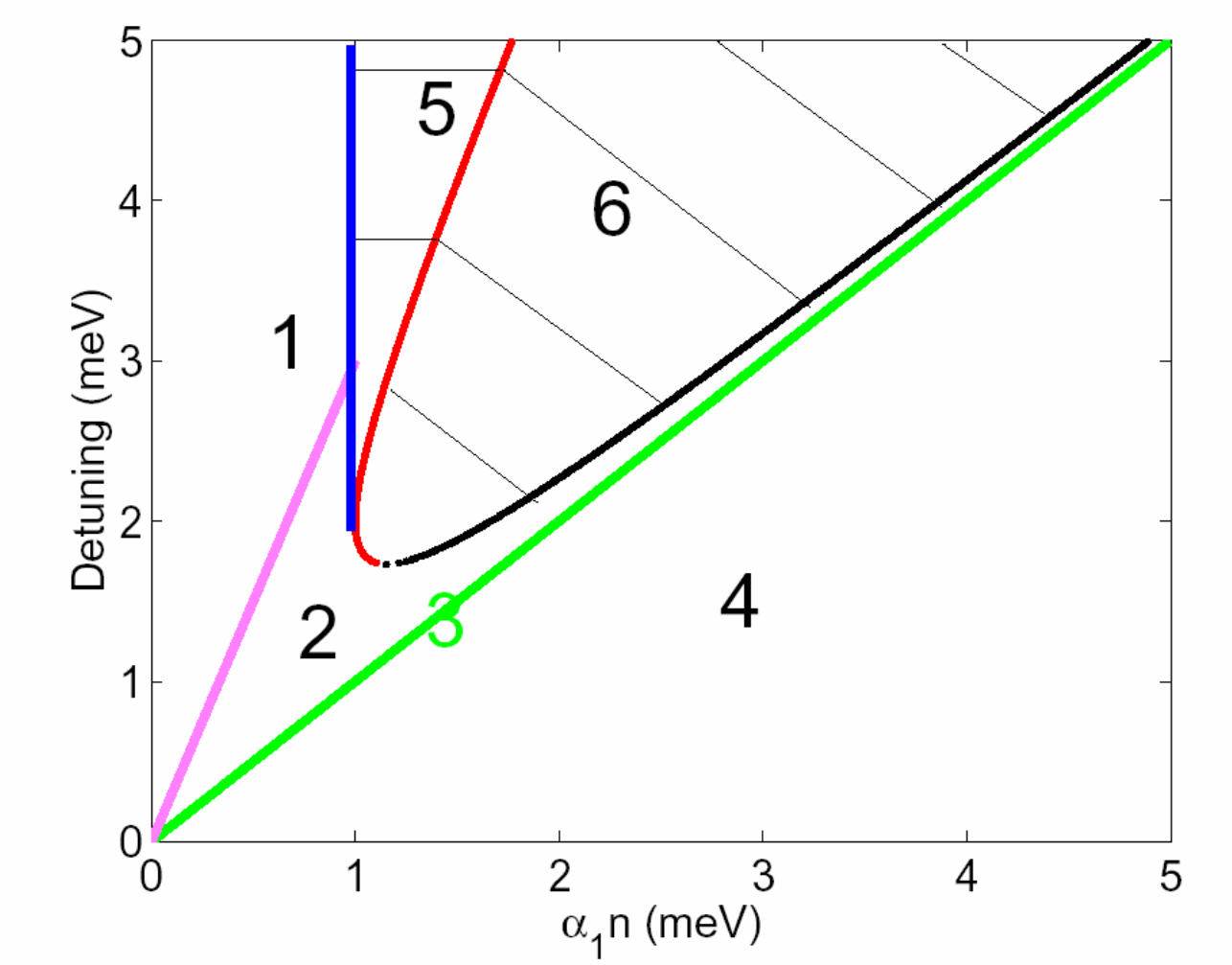

Figure 4.12. Regions of stability for the circularly polarized mode:

1 - Flat part of the spectrum for (+k,-k) states;

2 - Flat part of the spectrum for k=0;

3 - Linear spectrum in k=0;

4 - Parabolic spectrum;

5 - Instability of the (+k,-k) states;

6 - Instability of the ground state.

Let us now consider a linearly polarized macrooccupied mode. This situation can correspond to different pumping polarisations, including, but not limited to, the linear polarization. The stability of the system requires the following conditions to be fulfilled:

$$\begin{aligned}\frac{1}{\tau^2}+\Delta^2-2\Delta\alpha_1 n+n^2\left(\alpha_1^2-\frac{\left(\alpha_1-\alpha_2\right)^2}{4}\right)>0\\ \frac{1}{\tau^2}+\Delta^2-2\left(\alpha_1+\alpha_2\right)\Delta n+n^2\left(\alpha_1^2+\alpha_2^2-\frac{\left(\alpha_1+\alpha_2\right)^2}{4}\right)>0\end{aligned} \tag{4.31}$$

These two conditions are equivalent if $\alpha_2=0$. If α_2 is positive, the condition of stability of the component co-polarised with the macrooccupied mode is the strictest, and therefore it is sufficient to check only this condition. If α_2 is negative, which is the realistic case, the condition on the cross-polarised component becomes stronger. This conclusion agrees well with the current understanding of the spin dependent polariton-polariton scattering. Indeed, it agrees with the fact that two polaritons of a given linear polarisation will scatter preferentially toward cross polarized polariton states if α_2 is negative and co-polarised if α_2 is positive (see chapter 3). Therefore, in the case of negative α_2, elementary excitations of the macrooccupied mode are mainly cross polarised and their stability governs the stability of the whole system. In what follows, we study only the realistic case and check the stability of the cross-polarised component. The system is always stable if:

$$\Delta<\Delta_{\min}=\frac{1}{\tau}\sqrt{4\frac{\alpha_1^2}{\left(\alpha_1-\alpha_2\right)^2}-1} \tag{4.32}$$

Above this value the stability region is limited by the values

$$n_{\pm}=\frac{\alpha_1\Delta\pm 1/2\left(\alpha_1-\alpha_2\right)\sqrt{\Delta^2-\Delta_{\min}^2}}{\alpha_1^2-1/4\left(\alpha_1-\alpha_2\right)^2} \tag{4.33}$$

States with finite wave vectors show flat dispersions on the range

$$n\in\left[0,\frac{\Delta\left(\alpha_1+\alpha_2\right)}{2\alpha_1^2-1/2\left(\alpha_1-\alpha_2\right)^2}\right] \tag{4.34}$$

and the $k=0$ state has flat dispersion on the range

$$n\in\left[\frac{\Delta\left(\alpha_1+\alpha_2\right)}{2\alpha_1^2-1/2\left(\alpha_1-\alpha_2\right)^2},\frac{\Delta\left(3\alpha_1-\alpha_2\right)}{2\alpha_1^2-1/2\left(\alpha_1-\alpha_2\right)^2}\right] \tag{4.35}$$

The result is plotted in figure 4.13. This figure is more complicated than the figure 4.12, because both co- and cross-polarized components can show different types of dispersions. In region 1 the dispersion shows flat part at some nonzero wavevector $\pm k$ (this applies to both polarizations,

as demonstrated by figure 4.11c); in regions 2 and 2' the flat part is centered at $k = 0$ (the prime corresponds to the cross-polarized component); regions 3 and 3' have the Bogoliubov-like dispersion, which takes place at different conditions for the co- and cross-polarized components; the region 4 has an ordinary parabolic dispersion; the regions 5 and 6 are unstable. It is important to note that the results shown here have been obtained for the linearly polarized macrooccupied polariton mode.

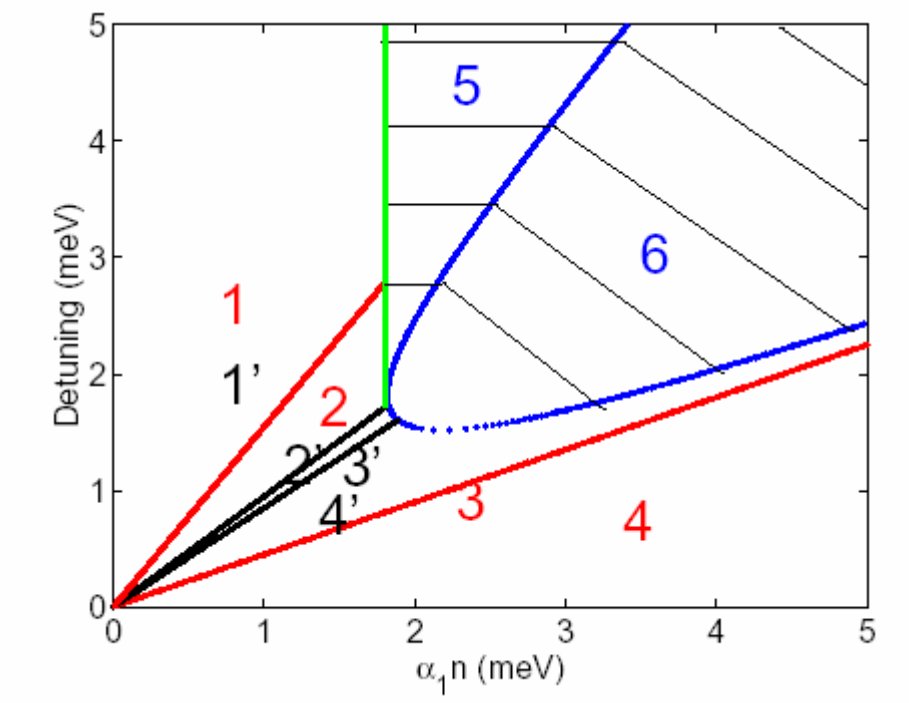

Figure 4.13. Regions of stability for linear polarized mode:

1 - Flat part of the spectrum for (+k,-k) states;

2, 2' - Flat part of the spectrum for k=0;

3, 3' - Linear spectrum in k=0;

4, 4' - Parabolic spectrum;

5 - Instability of the (+k,-k) states;

6 - Instability of the ground state.

4.3.5. Probing renormalization of dispersion by analysing the microcavity emission

The renormalization of the dispersion of elementary excitations of microcavity under resonant pumping affects the emission spectra in the pump-probe geometry. We perform numerical simulation of such an experiment using the coupled Gross-Pitaevskii equation for excitons and Schroedinger equation for photons taking into account their polarization, like discussed in section 4.2. The polariton lifetime is taken equal 1 ps. The circularly polarized pump is spatially homogeneous and detuned by -2.5 meV from the bottom of the low polariton branch. A weak probe of 0.1 ps duration and 1 μm spatial size is sent 15 ps after the pump is turned on. This probe excites the excitations in a broad energy and wave vector range. The photon component of the wavefunction is Fourier-transformed over 100 ps.

Figure 4.14 shows resulting dispersions obtained at increasing pump intensities. Fig. 4.14a shows dispersion with flat regions at $\pm 1 \mu m^{-1}$ (region 1 of Fig. 4.12). One can see the bright emission spots due to the renormalization of the imaginary part of the dispersion. Fig. 4.14b shows flat dispersion centered at $k = 0$ (region 2 of Fig. 4.12). Fig. 4.14c shows the Bogoliubov-like dispersion linear at small wavevectors (region 3 of Fig. 4.12). Fig 4.14d shows the parabolic dispersion corresponding to the region 4 of Fig. 4.12. From the experimental point of view, it may be interesting to work with the linear polarized probe orthogonal to the linear polarized pump. In this configuration it should be easier to detect a system response to the weak probe.

The direct prove for superfluidity of a liquid can be obtained in propagation experiments which would show zero viscosity (no dissipation). In order to reveal the superfluid regime for the ensemble of exciton polaritons, we have modelled the propagation of a Gaussian-shape repulsive potential fluctuation (defect) of 7 μm diameter and 10 meV amplitude propagating at a speed of 5 μm/ps through the polariton condensate in two regimes: 1) when the pumping is such as to make the polariton dispersion parabolic at k=0 (as in Fig.4.12 d); 2) when the pumping is chosen so that to provide a linear dispersion of excitations in the vicinity of k=0 as in (Fig. 4.12c). Similar demonstration of superfluidity but with a polariton liquid flowing around a stationary defect has been performed for the first time in the papers of I. Carusotto and C. Ciuti (2004, 2005). The results are shown in Figure 4.15. If the dispersion is parabolic (Fig. 4.14d), the propagation of the defect induces the supplementary excitations leading to the polariton density waves. They are visible in log scale image about 50 μm away from the defect, even though the lifetime in the system is quite short (1 ps). However, if the pumping intensity is chosen to yield the linear dispersion (Fig. 4.14c), no density waves are seen even in the vicinity of the defect. This is a clear indication that the polaritons are not perturbed by the motion of a defect, and therefore the moving body does not lose its energy by interaction with polaritons. This is characteristic for the dissipationless propagation of

a body through a superfluid. We have checked also that the total density of polaritons does not depend on the fact whether the defect is moving or not, in the case the linear dispersion. As the energy lost by the system per a unit of time is directly proportional to the density of polaritons in the system, this confirms that there is no additional dissipation linked with the motion of the object.

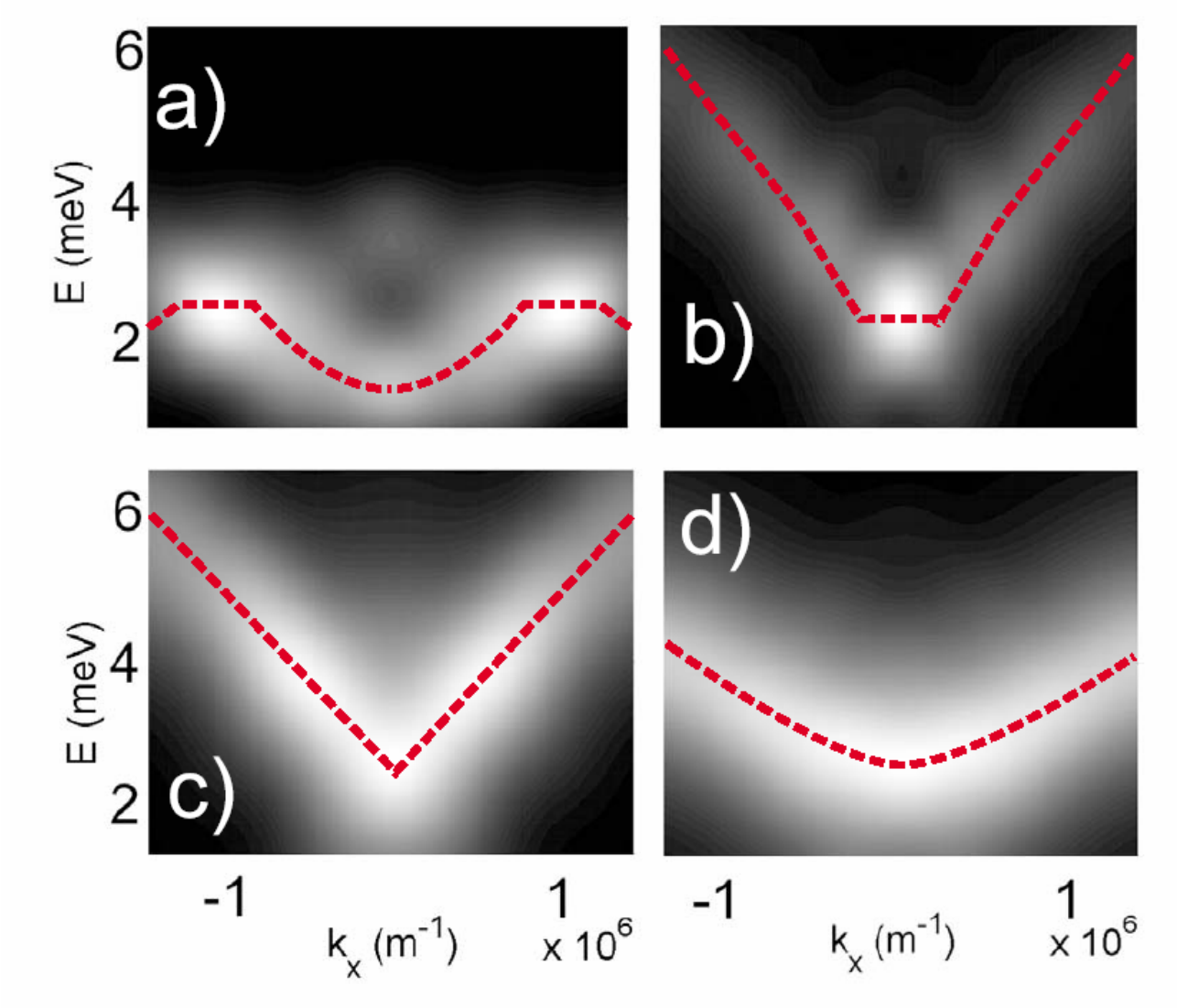

Figure 4.14. Emission spectra showing renormalized dispersions in the order of increasing pumping power: a) flat at $k \neq 0$, b) flat at $k = 0$, c) linear, d) parabolic. The red lines show the real parts of the theoretical dispersions calculated using Eq.(4.25).

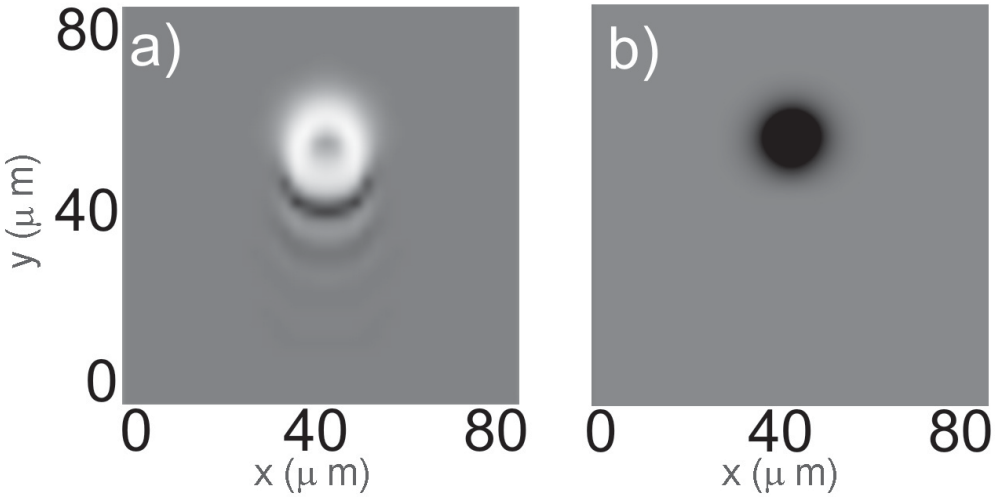

Fig. 4.15. Subsonic motion of a defect through a) normal, b) superfluid polaritons.

4.4. Conclusions

In this chapter we have described propagation and polarization of polaritons both in linear and non-linear regimes. We have demonstrated that the presence of polariton "condensate" should manifest itself in superfluid propagation of ring-like excitations. We have also considered polarization of a driven macrooccupied mode and demonstrated its multistability, which may be a very important property from the point of view of applications. Finally, we have analyzed the excitations of the driven mode and their stability, and we have shown that even in this case polariton system can demonstrate superfluidity, in a particular case when the pump detuning is exactly equal to the blue shift induced by the interactions. An important step further can be to incorporate finite temperature effects e.g. using the Bogoliubov-de Gennes description of thermal clouds, like it has been done in the study of atomic condensates by M. Moreno-Cardoner *et al* (2007).

The exciton-polariton condensates are being very actively studied now, and new papers get published each week. An interesting paper relevant to the present chapter has just been published by A. Amo *et al* (2007). This paper reports observation of polariton superfluidity in the OPO configuration (in the signal state), as predicted by I. Carusotto and C. Ciuti (2004).

Chapter 5. Polariton Bose condensate in a disordered system

Obtaining polariton Bose condensation was a great challenge of physics of microcavities for a long time. Surprisingly, when the condensate had been observed, it did not manifest linear dispersion expected for a weakly interacting Bose condensate. Rather, a flat dispersion with blue shift has been observed (J. Kasprzak *et al*, 2007), corresponding to bright emission from localized spots in real space (M. Richard *et al*, 2005). In this chapter we will explain the theory describing this effect, and find the conditions for the observation of polariton superfluidity. We will study the transitions between the non-condensed polaritons, Bose glass and superfluid phases in CdTe and GaN at T=0 and at non-zero temperatures.

Contents

5.1. Bose glass and superfluidity

In this section we will describe the phases of a polariton condensate in a disordered system: Bose glass and superfluid. We will first describe the behavior of polaritons in disordered systems and introduce the Bose glass phase which is even younger than the Bose-Einstein condensate. We will study the transition between the two on the basis of the Gross-Pitaevskii equation.

5.1.1. Polaritons in a disordered system

This is not the first study of the problems of disorder and Bose condensation of exciton-polaritons. One should give credit to the activity of the Cambridge group of P.B. Littlewood. A paper of J. Keeling *et al* (2004) and a recent paper of F.M. Marchetti *et al* (2006) study the effect of excitonic disorder on the thermodynamics and excitations of

exciton-polariton condensates. These works are based on the idea that exciton-polaritons are formed with localized excitons having the highest oscillator strength, and that the exciton disorder is much more important than the polariton disorder. However, the typical scale of localization observed in recent experiments of M. Richard *et al* (2005) is much larger than that of excitonic disorder, which means that the photonic disorder must be affecting the exciton-polariton condensate in significant way. Moreover, the conclusion that the exciton-polaritons are formed by localized excitons is based on a numerical calculation showing maximum of exciton oscillator strength at negative energies. This numerical calculation can be criticized for several problems, which will not be detailed here. These reasons make further investigation of disorder influence on polariton condensates necessary.

We assume that the polaritons are moving in a random potential $V(\mathbf{r})$ whose mean amplitude and root mean square fluctuation are give by $\langle V(\mathbf{r})\rangle = 0$ and $\sqrt{\langle V^2(\mathbf{r})\rangle} = V_0$ respectively. The correlation length of this potential is $R_0 = \sqrt{\int \langle V(\mathbf{r})V(0)\rangle \mathrm{d}\mathbf{r} / V_0^2}$. As in any disordered system, there are two types of states: the free propagating states and the localized states, separated by the threshold energy E_c. The localization radius scales like $a(E) \propto a_0 V_0^s / (E_c - E)^s$, s being a critical index and $a_0 = \sqrt{\hbar^2 / MV_0}$. In two dimensions E_c is of the order of mean potential energy (i.e. 0 in our case), and $s \approx 0.75$. The quasi-classical density of states is $D(E) \cong M/4\pi\hbar^2 \left(1 + \mathrm{erf}\left(E/V_0\right)\right)$ (see Fig. 5.1). These analytical results are the direct generalization of the results presented in a classical review on disordered semiconductors: A.L. Efros and B.I.Shklovskii (1989).

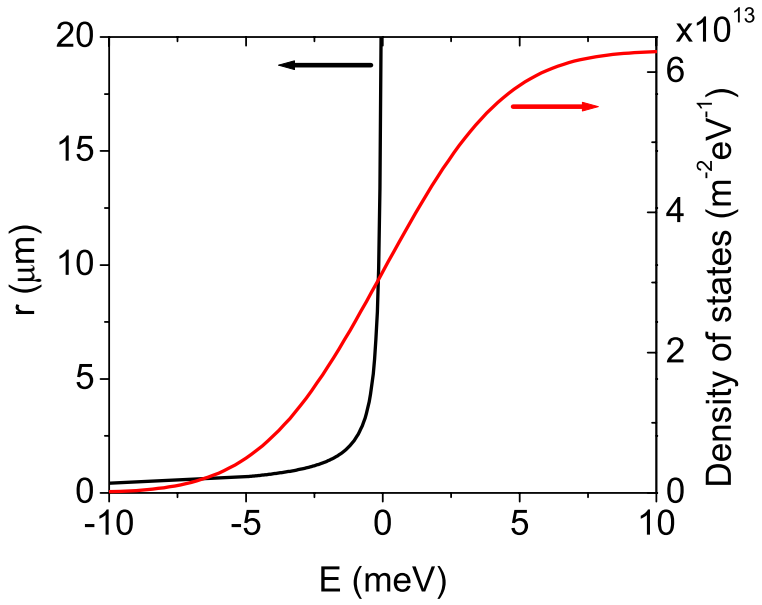

Figure 5.1. Density of states and localization radius for a GaN cavity with 5 meV disorder

If one simplifies the problem that has been posed in the introduction to this chapter, it reduces to a problem of percolation for a classical liquid on a disordered surface. Let us demonstrate that a liquid can flow through an infinite disordered surface with its given height $V(\mathbf{r})$, when the level of the liquid reaches the average value of the height $\langle V(\mathbf{r})\rangle$ (provided that $V(\mathbf{r})$ is symmetric relative to its average value).

The idea is that one should think not only about liquid flowing from one side of the surface to the other, but also about crossing this surface by passing over islands linked with each other without wetting the feet. Let us set the average value $\langle V(\mathbf{r})\rangle = 0$ and call V_c the level of liquid required for the flow, and V_c' the level of liquid required to have the possibility to pass over islands. Now, if for a large enough square the liquid cannot flow from the left side to the right side, it means that one can cross this square over islands from the top side to the bottom side. On the other hand, if a liquid can flow from the left side to the right side, one cannot cross this surface over islands without wetting the feet. For big enough surfaces, there is no need to speak about particular directions, and the above statement is generalized to the

following: the level of liquid required for the flow is the same as the level required for a passage over islands to exist, or

$$V_c = V_c' \tag{5.1}$$

For a function $V(\mathbf{r})$ symmetric relative to its average value it is obvious that

$$V_c = -V_c' \tag{5.2}$$

and, therefore,

$$V_c = V_c' = 0 \tag{5.3}$$

This classical result has been first obtained by Zallen R., Schen H. (1971), Dykhne A.M. (1970). For the system under study it means that the chemical potential of polaritons should be equal to the average value of the disorder potential, for the superfluidity to appear. In the quantum limit, this result is modified, and its modification is considered in section 5.2.

5.1.2. Bose condensation in 2D

We consider formation of a polariton condensate in a disordered 2D system in the thermodynamic limit. Without interactions, the condensate would form in the lowest energy minimum accessible for polaritons. In a finite size system, the lowest energy state always exists. The interactions increase the energy of the lowest state as soon as it starts to get filled by particles, and above some limit it raises to a level of some other state. These states, equivalent from the thermodynamic point of view, now start to be both populated, and so on. Thus a Bose glass phase is formed, consisting of several spatially separated condensates having the same energy. The energy level of these condensates is the chemical potential of the system μ. In order to find it, one should minimize the free energy of the system given the number of particles. The Bose glass phase is characterized by an unusual dispersion of excitations which contains flat part corresponding to localized states.

When the chemical potential reaches a certain threshold that we are going to find, a percolation takes place, which leads to the transition from the Bose glass to the superfluid phase. The particle density is still not completely spatially homogeneous, but does not go to zero anywhere. The dispersion in this phase becomes linear close to $k = 0$, as expected from the Bogoliubov theory (see chapter 1).

Strictly speaking, non-interacting bosons in 2D cannot undergo Bose-Einstein condensation as the number of particles which can be fitted to all the excited states of the system is divergent for any $\mu > -\infty$. Also, the deep localized states of polaritons have a different localization dimensions for excitonic and photonic parts and the quasi-classical

expression for the density of states $D(E)$ given above becomes inapplicable (see V.M. Agranovich and Yu. N. Gartstein, 2007). The situation is thus different from the case of cold atoms trapped in a 2D power-law potential, for which the renormalization of the density of states makes "true" BEC possible (V. Bagnato, D. Kleppner, 1991). Therefore, even in the presence of disorder, BEC cannot take place strictly speaking for cavity polaritons. However, it is possible to define a quasi-phase transition which takes place in finite systems (G. Malpuech *et al,* 2003). Indeed, for a system with a finite size L there is a finite number N_{trap} of potential traps for polaritons, thus, there is an energy spacing between the single particle states. The typical energy distance between the ground and excited states of the finite-size system levels δ under the assumption of long-range potential is approximately given by V_0 / N_{trap} or $\hbar^2 / 2MR_0^2$, whichever is smaller. In this framework the critical density is given by the total number of polaritons which can be accommodated in all the energy levels of the disorder potential except the ground one:

$$n_c(T,L) = \frac{1}{L^2}\sum_{i\neq 0} f_B(E_i, E_0, T) \tag{5.4}$$

where $f_B(E,\mu,T)$ is the Bose-Einstein distribution function, E_0 is the energy of the lowest localized state.

To evaluate the critical density $n_c(T,L)$ the discrete sum is replaced by an integral in (5.4), and we find $n_c(T) \approx D(E_0) k_B T \ln\left(1/\left(1-e^{\delta/k_B T}\right)\right)$ assuming $D(E)$ is a smooth function. Above this density all additional particles are accumulating in the ground state and the concentration of condensed particles n_0 satisfies $n_0 \geq (n - n_c)$ where *n* is the total density of polaritons. It is not a real phase transition since the system has a discrete energy spectrum and the value of the chemical potential never becomes strictly equal to E_0.

5.1.3. Bose glass phase

Although the Bose glass was introduced for the first time as a new phase replacing the Bose condensate in a disordered system in a paper of J.A. Hertz, L. Fleishman, and P.W. Anderson (1979), only 20 years later this concept became a center of great research activity after a seminal paper of M.P.A. Fischer *et al* (1989), which is not even citing the first one.

M.P.A. Fisher *et al* were studying the transition between the Mott insulator and superfluid phases for bosons on a lattice with a presence of a random disorder potential. In

such a system strong particle interaction leads to localization of bosons for commensurate densities, thus a Mott insulator phase appears. This phase is characterized by a presence of a gap for particle-hole excitations, and by zero compressibility. Disorder modifies the properties of the insulating state, leading to appearance of a new phase called Bose glass, which differs from the Mott Insulator in that it has gapless (and flat) dispersion for excitations and its compressibility has finite value. The authors argued that the transition from the Mott insulator to the superfluid phase with increasing hopping strength can take place only through the Bose glass phase, and that for some parameters the Mott insulator does not even exist as a phase.

A few years later in 1991 R.T. Scalettar, G.G. Batrouni, and G.T. Zimanyi have proposed another localized phase for bosons on a lattice, which they called Anderson glass, because it appears from the Anderson localized state (non-interacting particles with any statistics become localized in a disorder potential). This phase has the same properties as the Bose glass phase of M.P.A. Fischer *et al*, the difference being that in the case of Anderson glass the interactions between particles lead to their delocalization, and in the case of Bose glass the interactions lead to the localization of particles. This is demonstrated by figure 5.2, where the superfluid density grows and then drops to zero again with increasing interactions strength, as the system passes from the Anderson glass to the superfluid and then to the Bose glass phases.

This difference between the Bose glass and the Anderson glass of bosons has been introduced for bosons in a lattice, described by the Bose-Hubbard or similar models. The polariton system we are considering is very different from this picture, because the polaritons are not restricted to the lattice sites and there is no localization without disorder. The polariton density is, in the regime of Bose condensation, relatively high and the interactions are relatively small. Moreover, localization can not appear with increasing interaction strength, so the Bose glass in the sense of Bose-Hubbard model can not exist for polaritons. It appears therefore useless to distinguish different types of bosonic glasses, which is why we call the localized phase that we study the Bose glass, even if it is closer to the Anderson glass of bosons in the Bose-Hubbard model.

It is interesting to note here that a proposition to simulate the Bose-Hubbard model within a system of polariton condensates has been recently published by C.W. Lai *et al* (2007). In this paper the authors proposed to make vary the coupling between several condensates localised in the minima of a specially created regular potential, in order to observe superfluid and Mott Insulator phases.

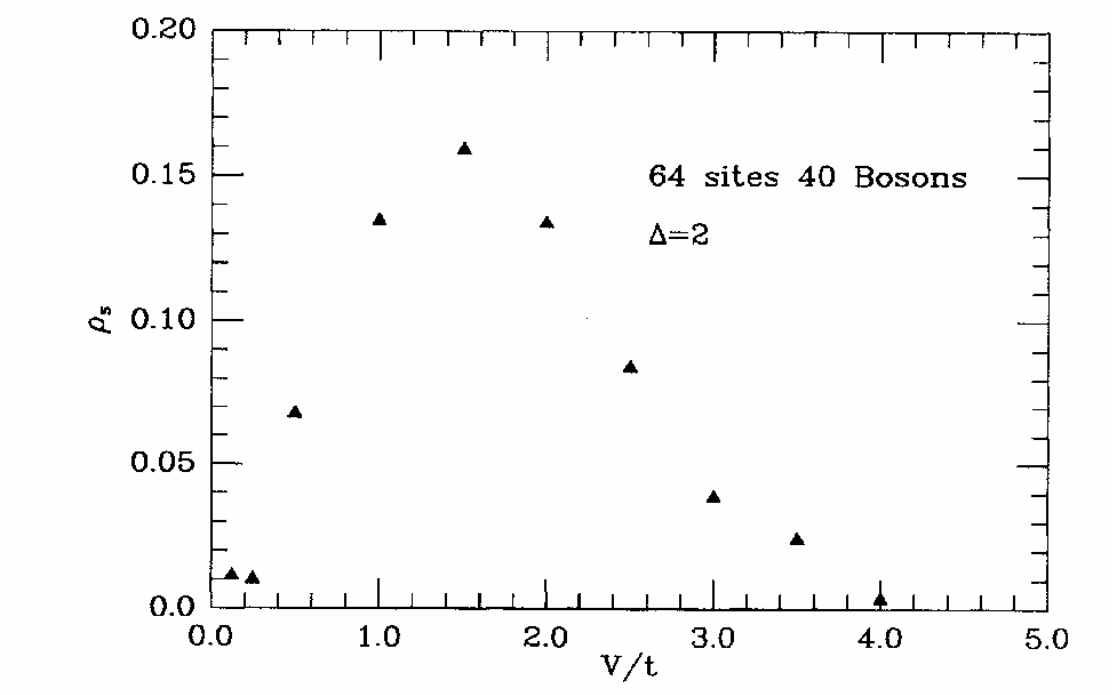

Fig. 5.2. The superfluid density at fixed density $\rho = 0.625$ and varying coupling. ρ_s is zero in the Bose-glass phase at strong coupling, but goes to zero again in the Anderson phase (from R.T. Scalettar, G.G. Batrouni, and G.T. Zimanyi, 1991).

5.1.4. The analogies of atomic condensates

The behaviour of the condensates of cold atoms in disordered systems is a subject of active ongoing research. Many papers are being published each year. However, as it has been mentioned above, the models and the results for atoms do not immediately apply for polaritons, which is why we will not go into a detailed discussion of all the results obtained for the atomic condensates here, restraining to only few examples.

One of the first cases of experimental evidence of superfluidity of atomic BEC after the observation of the BEC itself in 1995 by K.B. Davis *et al* is presented in a paper of C. Raman *et al* (1999) which studied dissipation in an atomic BEC at different velocities. One should also give credit to the paper of R. Onofrio *et al* (2000) reporting observation of superfluid flow of atomic BEC. The transition between superfluid and dissipative behaviour of BEC depending on the potential has been studied experimentally by S. Burger *et al* (2001).

Theoretical research on the condensate localization in various conditions is very extensive in the atomic community, since it allows physical realization of the well-developed Bose-Hubbard model. An implementation proposal for the Bose and Anderson glasses has

been published by B. Damski *et al* (2003). Experimental observation of transition from Mott Insulator to the Bose Glass phase has been recently reported by L. Fallani *et al* (2007).

5.1.5. Interacting polaritons at T=0

Interactions between particles become dominant once the polaritons start to accumulate in the ground state. The quantitative analysis can be carried out in the framework of the Gross-Pitaevskii equation for the condensate wavefunction $\Psi(\mathbf{r},t)$ which reads

$$i\hbar\frac{\partial}{\partial t}\Psi(\mathbf{r},t)=\left(-\frac{\hbar^2}{2M}\Delta+V(\mathbf{r})+\alpha\left|\Psi(\mathbf{r},t)\right|^2\right)\Psi(\mathbf{r},t) \tag{5.5}$$

We write the scalar Gross-Pitaevskii equation for polaritons here without taking into account the non-parabolicity of their dispersion and the LT splitting, in order to avoid overcomplication of the problem. The interaction constant here describes interaction of excitons having the same spin: $\alpha = 3E_b a_B^2 / N_{QW}$. The wave function is normalized for surface. The solution of the equation (5.5) takes the form $\Psi(\mathbf{r},t)=\Psi_0(\mathbf{r})\exp(-i\mu t/\hbar)$. The wavefunction $\Psi_0(\mathbf{r})$ is obtained by numerical minimization of the free energy of the system:

$$F=\int \mathrm{d}\mathbf{r}\frac{\hbar^2}{2M}\left(\nabla\Psi_0(\mathbf{r})\right)^2+\int \mathrm{d}\mathbf{r}\,V(\mathbf{r})\left|\Psi_0(\mathbf{r})\right|^2+\frac{\alpha}{2}\int \mathrm{d}\mathbf{r}\left|\Psi_0(\mathbf{r})\right|^4, \tag{5.6}$$

which is performed under the constraint

$$\int d\mathbf{r}\left|\Psi_0(\mathbf{r})\right|^2 = N \tag{5.7}$$

where N is the number of polaritons in the system.

We have performed the calculations in two different cases: for a CdTe and for a GaN cavity, both at zero detuning. In the first case (CdTe cavity) we have taken the polariton mass $m = 5\times10^{-5} m_0$ where m_0 is the free electron mass, $E_b = 25\,\mathrm{meV}$, $a_B = 34\,\dot{A}$, $N_{QW} = 16$. We have included a random Gaussian disorder potential with $V_0 = 0.5\,\mathrm{meV}$ and $R_0 = 3\,\mu\mathrm{m}$. In the second case (GaN cavity) we have taken the polariton mass $m = 3\times10^{-5} m_0$ where m_0 is the free electron mass, $E_b = 50\,\mathrm{meV}$, $a_B = 20\,\dot{A}$, $N_{QW} = 18$. We have included a random Gaussian disorder potential with $V_0 = 5\,\mathrm{meV}$ and $R_0 = 4\,\mu\mathrm{m}$. As one can immediately see, the main difference is that in GaN the disorder is at least 10 times stronger than in CdTe.

The results of calculations of the spatial distribution of polaritons are shown in Fig. 5.3 (for CdTe) and Fig. 5.4 (for GaN). Panel (a) corresponds to the non-condensed situation. The

spatial profile is given by statistical averaging over all occupied states $n(\mathbf{r}) = \sum_i f_B\left(E_i, \mu(T), T\right)\left|\Psi_i(\mathbf{r})\right|^2$. The temperature in this expression is set to the typical experiment temperature (20 K for CdTe and 300 K for GaN). At this temperature the disorder does not affect the spatial distribution of particles, which stays almost uniform.

Once the condensate is formed one can neglect the thermal occupation of the excited states and the spatial image of the polariton distribution is given by the ground state wavefunction (solution of (5.6)). This case is plotted on panels (b) of figures 5.3 and 5.4. As expected, the condensate is well localized in the minima of the random potential.

When the particle density exceeds the threshold, condensate becomes delocalized, although its wavefunction can still exhibit spatial modulation. The superfluid case is plotted on panels (c) of figures 5.3 and 5.4.

To calculate the quasiparticle spectra shown in lower panels of figures 5.3 and 5.4 we introduce a single-particle Green's function which takes the form

$$G_\omega(\mathbf{r}, \mathbf{r}_0) = \sum_i \frac{\Psi_i(\mathbf{r})\Psi_i^\dagger(\mathbf{r}_0)}{\hbar\omega - E_i} \tag{5.8}$$

where E_i and $\Psi_i(\mathbf{r})$ are the eigenenergies and eigenfunctions of the elementary excitations, found numerically from Eq. (5.5). The spectrum of elementary excitations is given by the poles of the Green's function in the $(\mathbf{k}, \omega)$ representation. This spectrum should not be thought of as a simulation of a real experimental spectrum, because it does not take into account the spectral weight of different states.

For the non-condensed case the panels (d) show typical parabolic dispersion broadened by the disorder potential. For the Bose glass phase we find a parabolic dispersion with a flat part (panels (e) of figures 5.3 and 5.4). For the superfluid case the dispersion becomes linear (panels (f)). The figure 5.4(f) shows the onset of superfluidity, and one can see the transition from linear to parabolic dispersion at high wavevectors, described by the Bogoliubov formula. Panels (b) and (e) reproduce qualitatively the experimental observations of M. Richard *et al* (2005), shown on figure 5.5, and J. Kasprzak *et al* (2007), shown on figure 5.6, which are characteristics of the formation of a Bose glass. Linear dispersions on panels (f) are still to be observed experimentally.

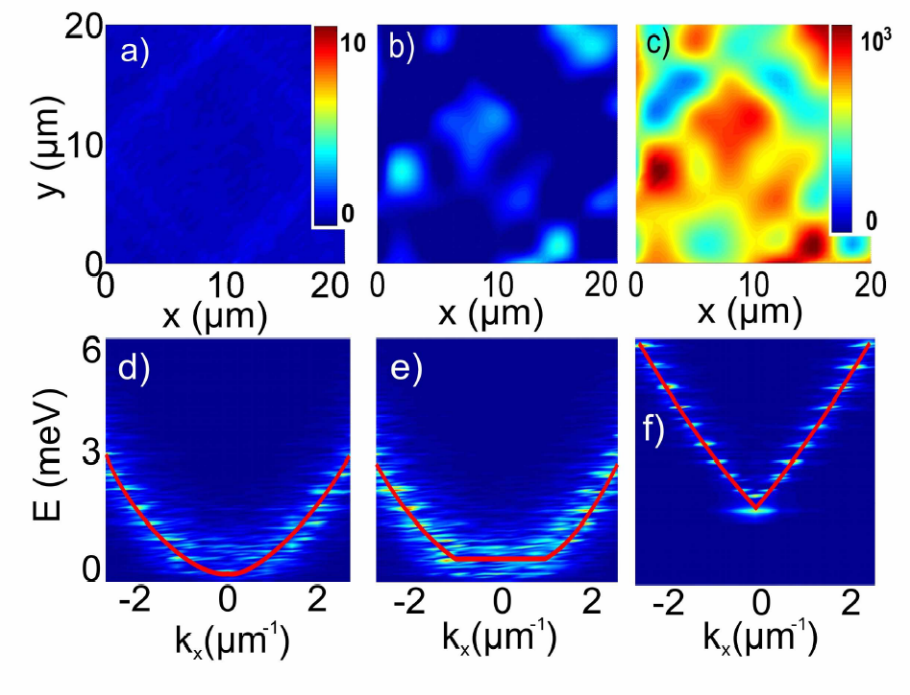

Figure 5.3. Bose glass and superfluid real-space images and dispersions for a CdTe cavity. Red lines are the guides for the eyes. The figures shown correspond to densities 0, $6x10^{10}$, and $2x10^{12}$ cm^{-2}.

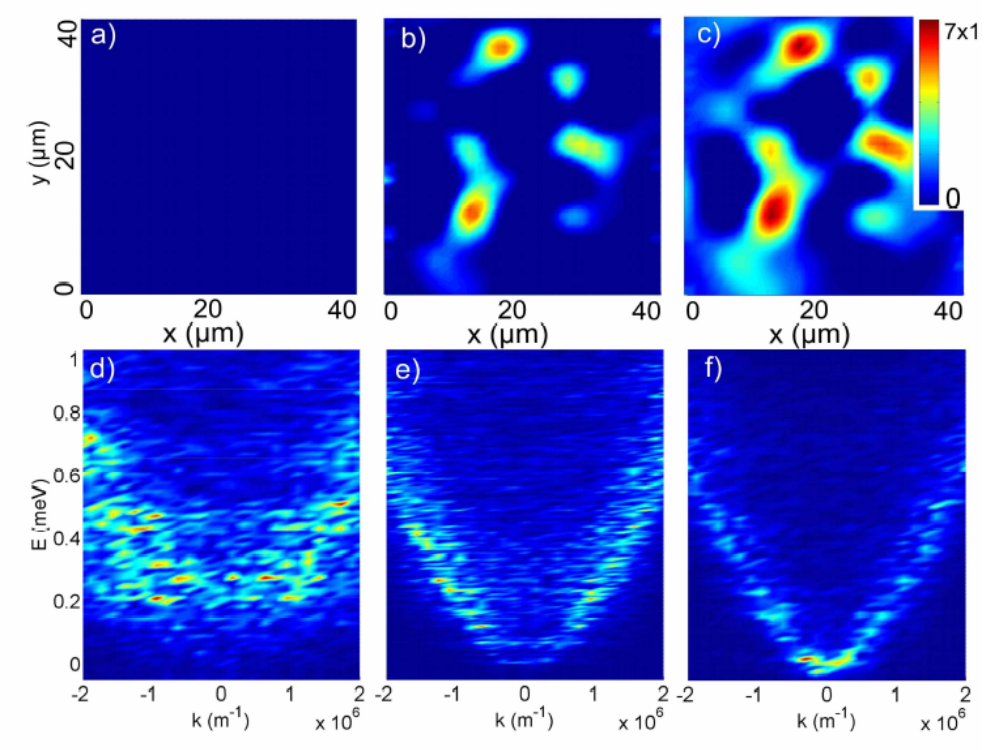

Figure 5.4. Bose glass and superfluid real-space images and dispersions for a GaN cavity. The figures shown correspond to the densities 0, $3x10^{12}$, and $9x10^{12}$ cm^{-2}.

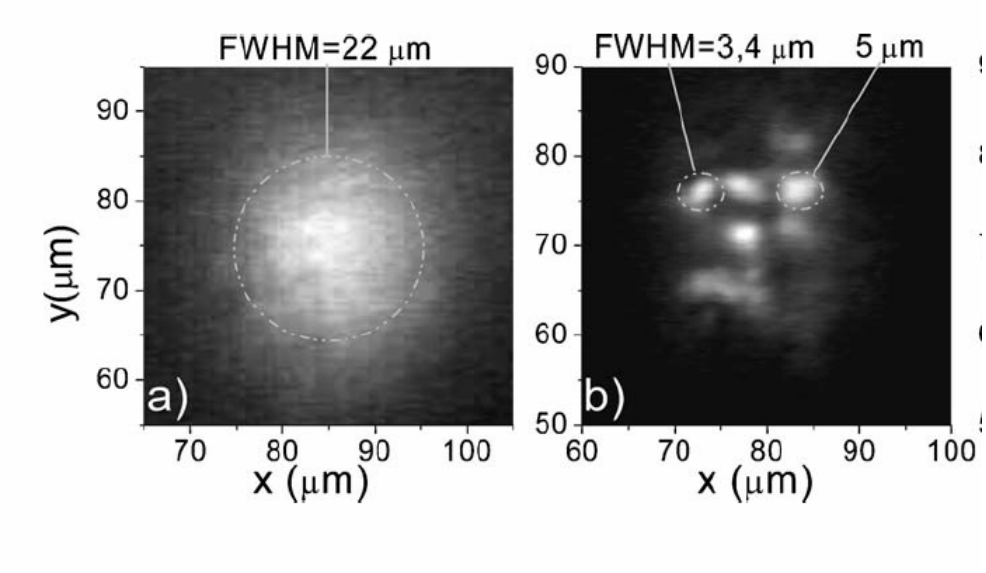

Figure 5.5. Gray-scale two-dimensional images of the near-field polarized PL for different pumping powers. Vertical and horizontal axes are in-plane coordinates in the real space. Image (a) is taken below threshold and image (b) above (from M. Richard *et al*, 2005).

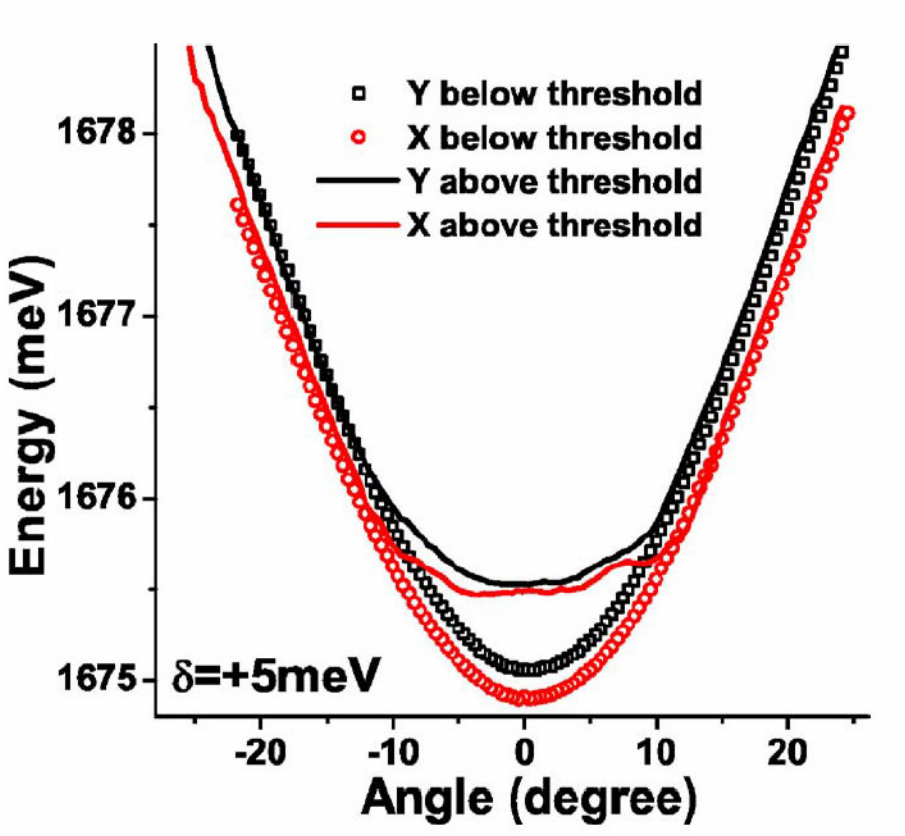

Figure 5.6. Dispersion of x- and y-polarized polariton branches below (open symbols) and above (solid lines) the condensation threshold (from J. Kasprzak *et al*, 2007).

5.2. The twisted boundary conditions method

It is instructive to analyze both the variation of the emission pattern and the quasi-particle spectrum in comparison with the behavior of the superfluid fraction of the polariton system. The latter quantity can be calculated using the twisted boundary conditions method (A.J. Leggett, 1970). Another possible option is to move the disorder potential and estimate the fraction of particles which are dragged with the disorder. This would give the normal fraction, and the part which is not dragged, is superfluid. This approach is equivalent to the twisted boundary conditions, as shown by A. Astrakharchik (2004). However, the twisted boundary condition method is simpler to implement, because the modification of the minimization procedure described in the previous paragraph is evident. Imposing such boundary conditions implies that the condensate wavefunction acquires a phase between the boundaries, namely:

$$\Psi_\theta\left(\mathbf{r}+\mathbf{L}_i\right)=e^{i\theta}\Psi_\theta\left(\mathbf{r}\right) \tag{5.9}$$

where L_i (i=x,y) are the vectors which form the rectangle confining the polaritons and θ is the twisting parameter. The superfluid fraction of the condensate is given by

$$f_s=\frac{n_s}{n}=\lim_{\theta\to 0}\frac{2ML^2\left(\mu_\theta-\mu_0\right)}{\hbar^2 n\theta^2} \tag{5.10}$$

where μ_θ is the chemical potential corresponding to the boundary conditions Eq. (5.9) and μ_0 is the chemical potential corresponding to the periodic boundary conditions ($\theta=0$). In the case of a clean system, $V\left(\mathbf{r}\right)=0$, the plane wave is the solution of (5.5) and $\mu_\theta-\mu_0=n\hbar^2\theta^2/2ML^2$: the superfluid fraction is $f_s=1$. On the contrary, for the strongly localized condensate the wavefunction is exponentially small at the system boundaries and the change of the boundary condition (i.e. variation of θ) does not change the energy of the system, thus $f_s \sim \exp\left(-L/a\left(\mu_0\right)\right)$ and goes to 0 for an infinite system. Due to the exponential tails of the localized wavefunctions a small degree of superfluidity remains in the finite size system. Equations (5.5) and (5.9) allow to study the depletion of the superfluid fraction for arbitrary disorder. The contribution of the disorder to the normal density of polaritons can be represented as

$$n_n^d=\left(1-f_s\right)n \tag{5.11}$$

Figure 5.7 shows the superfluid fraction for the CdTe cavity calculated as a function of the polariton density in the system for $T=0\,\mathrm{K}$. Due to the finiteness of the system considered

the superfluid fraction remains non-zero for any finite density, but a very clear threshold behavior for densities corresponding to the percolation threshold as observed on Fig. 5.2 , is also shown.

For high values of the chemical potential, where $V_0^2 / \mu g \gg 1$, perturbation theory applies and we obtain $n_n^d = V_0^2 / 4\mu g$ for the normal density (O.R. Berman *et al*, 2004), which coincides with the twisted boundary conditions approach for high polariton densities, as shown on Fig. 5.7.

Because the disorder potential and the polariton density vary very strongly in GaN cavity, the twisted boundary conditions method is much more numerically difficult to apply in this case. This is why we show results only for the CdTe cavity.

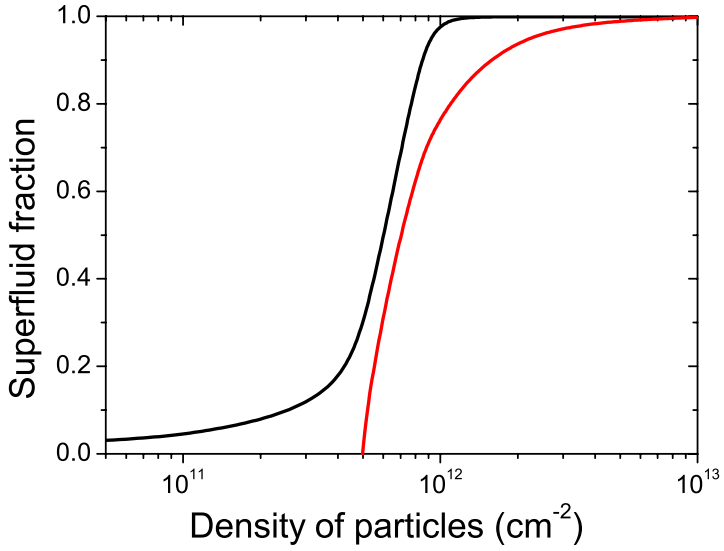

Figure 5.7. Superfluid fraction as a function of density for CdTe cavity, obtained by twisted boundary conditions method (black line) and by using the perturbation theory (red line)

5.3. Phases of a polariton condensate in disordered cavities

We turn now to the calculation of the cavity polariton phase diagrams for disordered CdTe and GaN cavities. Similarly to previous works (e.g. Malpuech *et al,* 2003) we start by roughly defining temperature and density domains where the strong coupling is supposed to hold in both cavities. The limits are shown on Fig. 5.8 and 5.9 as thick dotted lines: the edge temperature is assumed to be equal to the exciton binding energy and the maximum polariton

density is taken $2N_{QW}$ times larger than the bleaching exciton density in a single quantum well. The transition from normal to Bose glass phase can be calculated from Eq. (5.4) and a realistic realization of disorder. The lower solid lines on Figs. 5.8 and 5.9 show $n_c(T)$ for the same realizations of disorder as for Figs. 5.3 and 5.4. The free polariton dispersion is calculated using the geometry of Kasprzak *et al* (2006) for CdTe cavity and the geometry of G. Christmann *et al* (2006) for GaN cavity.

We now calculate the density for the transition between the Bose glass and the superfluid phase. In the low temperature domain, this density is approximately given by the percolation threshold $\mu = E_c$ and does not depend significantly on temperature. This condition corresponds with good accuracy to the abrupt change of the superfluid fraction f_s shown in Fig. 5.7. However, at higher temperature the thermal depletion of the condensate becomes the dominant effect. In that case the chemical potential of the condensate is much higher than the percolation energy E_c and the depletion induced by disorder can be neglected compared to the thermal depletion of the superfluid. The normal density then reads

$$n_n^0(T) = -\frac{2}{(2\pi)^2}\int E(\mathbf{k})\frac{\partial f_B(\varepsilon(\mathbf{k}),\mu=0,T)}{\partial\varepsilon}\mathrm{d}\mathbf{k} \tag{5.12}$$

and the superfluid density of the system given by $n_s(T) = n - n_n^0(T)$ can be substituted into the Kosterlitz-Nelson formula to obtain a self-consistent equation for the transition temperature:

$$T_{KT} = \frac{\hbar^2\pi n_s(T_{KT})}{2M} \tag{5.13}$$

The superfluid phase transition temperature $T_{KT}(n)$ as shown on Figs. 5.8 and 5.9, is determined from the solution of Eq. (5.13).

For CdTe, below 120 K the critical density is given by the percolation threshold and there is no temperature dependence. Above 200 K the superfluid depletion is determined solely by the thermal effects. In the intermediate regime the crossover between the thermal and disorder contributions takes place and our approximations are no longer justified.

For GaN, below 350 K the critical density is given by the percolation threshold and there is no temperature dependence. Above 600 K the superfluid depletion is determined solely by the thermal effects.

We also find that the superfluid transition takes place very close to the weak to strong coupling threshold and for densities 3 orders of magnitude larger than the one of the Bose glass transition at 19 K for CdTe.

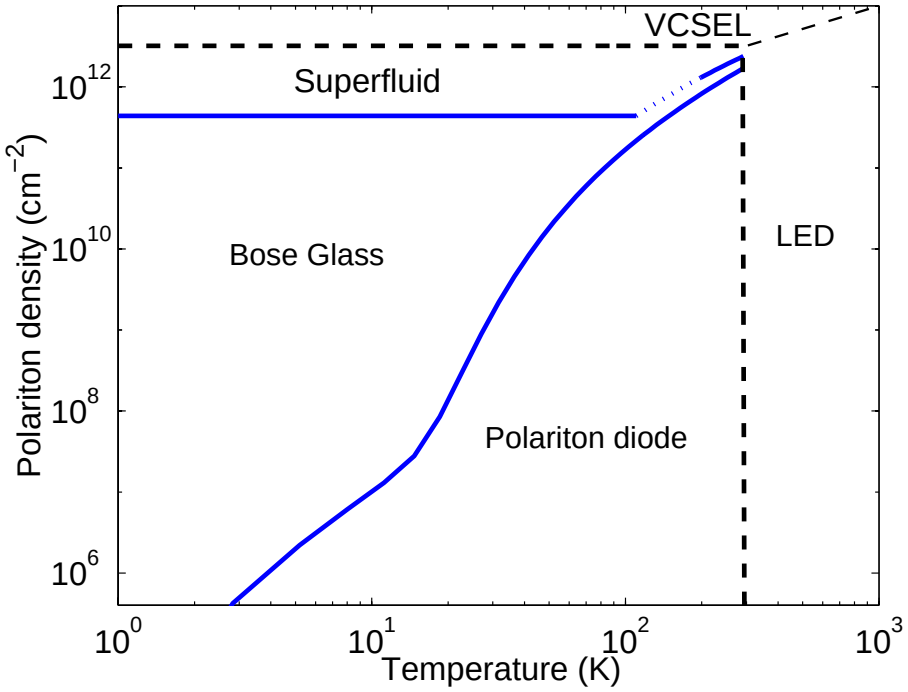

Figure 5.8. Phase diagram for a CdTe cavity

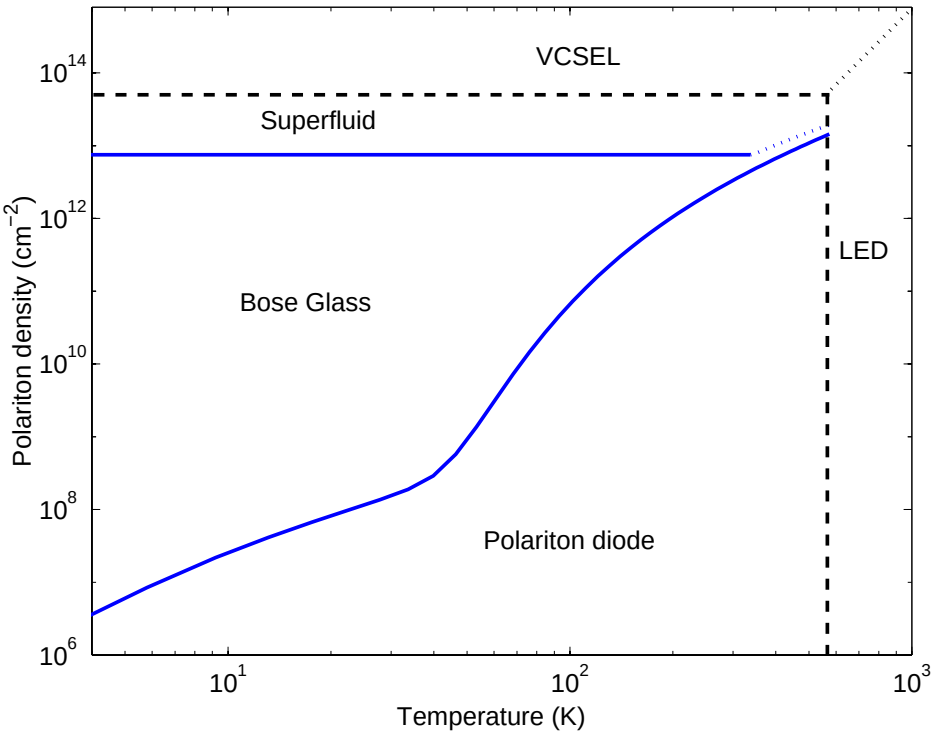

Figure 5.9. Phase diagram for a GaN cavity

5.4. Conclusions

In this last chapter we have analyzed the new phase of polaritons – the Bose glass phase. We have demonstrated that with increasing polariton density the system first exhibits transition to the Bose glass phase, and then to the superfluid one, the latter transition being rather close to the loss of strong coupling threshold. We have analyzed the behaviour of polaritons in two types of disordered cavities: CdTe and GaN, showing that observation of polariton superfluidity should be possible in both.

Appendix I. Derivation of the Boltzmann equation

In this section we will demonstrate the derivation of the spinless Boltzmann equation for bosons interacting with phonons starting from their microscopic Hamiltonian. This procedure is described in A. Kavokin and G. Malpuech (2003). We consider only scattering by the phonons for simplicity, because the derivation for bosonic interactions is lengthier. The final shape of the equations will be different, however, from **(1.57)**, because the nature of interactions is different.

We begin with writing the Liouville-von Neumann equation (analogue of **(1.51)** for a quantum system):

$$i\hbar\frac{d\rho}{dt}=\left[\hat{H}(t),\rho\right] \tag{1.1}$$

where ρ is the density operator of the system in the interaction representation (in which the density matrix is defined as $\rho_I = e^{\frac{iH_0t}{\hbar}}\rho e^{-\frac{iH_0t}{\hbar}}$), and $\hat{H}(t)$ is the time-dependent Hamiltonian describing the interaction of bosons and phonons:

$$\hat{H}(t)=\sum_{\mathbf{k},\mathbf{k}'}V_{\mathbf{k}\mathbf{k}'}e^{i(\Omega_{\mathbf{k}'}-\Omega_{\mathbf{k}}-\omega_{\mathbf{k}'-\mathbf{k}})t}b_{\mathbf{k}'-\mathbf{k}}a_{\mathbf{k}}a^{+}_{\mathbf{k}'}+h.c. \tag{1.2}$$

here $a_{\mathbf{k}}\left(a^{+}_{\mathbf{k}}\right)$ are the annihilation (creation) operators for bosons and $b_{\mathbf{k}}\left(b^{+}_{\mathbf{k}}\right)$ are the annihilation (creation) operators for phonons; $\Omega_{\mathbf{k}}$ is the energy of non-interacting bosons and $\omega_{\mathbf{k}}$ is the energy of phonons, both given by dispersion relations. $V_{\mathbf{k}\mathbf{k}'}$ is the matrix element of the transition.

The Liouville equation can be rewritten in a different form by time-integrating (1.1) and substituting it back into (1.1):

$$\frac{d\rho}{dt}=-\frac{1}{\hbar^2}\int_{-\infty}^{t}\left[\hat{H}(t),\left[\hat{H}(\tau),\rho(\tau)\right]\right]d\tau \tag{1.3}$$

We apply the Markov approximation, which means physically that the system is assumed to have no phase memory. This allows to integrate in (1.3) and obtain:

$$\begin{aligned}\frac{d\rho}{dt}=&\frac{1}{2}\sum_{\mathbf{k}'}\sum_{\mathbf{k}\neq\mathbf{k}'}W^{phon}_{\mathbf{k}'\to\mathbf{k}}\left(2a^{+}_{\mathbf{k}}a_{\mathbf{k}'}\rho a^{+}_{\mathbf{k}'}a_{\mathbf{k}}-a_{\mathbf{k}}a^{+}_{\mathbf{k}}a^{+}_{\mathbf{k}'}a_{\mathbf{k}'}\rho-\rho a_{\mathbf{k}}a^{+}_{\mathbf{k}}a^{+}_{\mathbf{k}'}a_{\mathbf{k}'}\right)\\&+\frac{1}{2}\sum_{\mathbf{k}'}\sum_{\mathbf{k}\neq\mathbf{k}'}W^{phon}_{\mathbf{k}\to\mathbf{k}'}\left(2a^{+}_{\mathbf{k}'}a_{\mathbf{k}}\rho a_{\mathbf{k}'}a^{+}_{\mathbf{k}}-a_{\mathbf{k}'}a^{+}_{\mathbf{k}'}a^{+}_{\mathbf{k}}a_{\mathbf{k}}\rho-\rho a_{\mathbf{k}'}a^{+}_{\mathbf{k}'}a^{+}_{\mathbf{k}}a_{\mathbf{k}}\right)\end{aligned} \tag{1.4}$$

where

$$W_{\mathbf{k}\to\mathbf{k}'}^{phon} = \frac{2\pi}{\hbar}\sum_{\mathbf{k}-\mathbf{k}'}\left|V_{\mathbf{k}\mathbf{k}'}\right|^2 (0,1+n_{\mathbf{k}-\mathbf{k}'})\delta\left(E(k')-E(k)\mp\hbar\omega_{\mathbf{k}-\mathbf{k}'}\right) \tag{1.5}$$

The density matrix can be factorized into the product of phonon density matrix and boson density matrices corresponding to the different states in the reciprocal space by using the Born approximation:

$$\rho = \rho_{ph}\otimes\prod_{\mathbf{k}}\rho_{\mathbf{k}} \tag{1.6}$$

The diagonal elements of the density matrix $\rho_{\mathbf{k}}$ give the populations of the bosonic states with wave vector **k**: $n_{\mathbf{k}} = Tr\left(a_{\mathbf{k}}^{+}a_{\mathbf{k}}\rho_{\mathbf{k}}\right)$, and the same for phonons, whose populations are assumed to be given by an equilibrium distribution. Finally we obtain:

$$\frac{dn_{\mathbf{k}}}{dt} = -n_{\mathbf{k}}\sum_{\mathbf{k}'}W_{\mathbf{k}\to\mathbf{k}'}\left(1+n_{\mathbf{k}'}\right)+\left(1+n_{\mathbf{k}}\right)\sum_{\mathbf{k}'}W_{\mathbf{k}'\to\mathbf{k}}n_{\mathbf{k}'} \tag{1.7}$$

One can extend this equation to incorporate the pump and decay, and the bosonic interactions, and write the general Boltzmann equation for particles in a system with pump and decay in reciprocal space:

$$\frac{dn_{\mathbf{k}}}{dt} = P_{\mathbf{k}}-\Gamma_{\mathbf{k}}n_{\mathbf{k}}-n_{\mathbf{k}}\sum_{\mathbf{k}'}W_{\mathbf{k}\to\mathbf{k}'}+\sum_{\mathbf{k}'}W_{\mathbf{k}'\to\mathbf{k}}n_{\mathbf{k}'} \tag{1.8}$$

where $P_{\mathbf{k}}$ is the generation term (number of particles appearing at **k** due to pumping per unit of time), $\Gamma_{\mathbf{k}}$ is the particle decay rate (defined similar to generation) and $W_{\mathbf{k}\to\mathbf{k}'}$ is the total scattering rate between the states **k** and **k**' due to any kind of physical process (an example for interaction of bosons and phonons is given by equation (1.5)).

The Bibliography

V. M. Agranovich and Yu. N. Gartstein, *Nature and dynamics of low-energy exciton polaritons in semiconductor microcavities*, Phys. Rev. B **75**, 075302 (2007).

A. Alemu, B. Gil, M. Julier, S. Nakamura, *Optical properties of wurtzite GaN epilayers grown on A-plane sapphire*, Phys. Rev. B **57**, 3761 (1998).

A. Amo, D. Sanvitto, D. Ballarini, F.P. Laussy, E. del Valle, M.D. Martin, A. Lemaitre, J. Bloch, D.N. Krizhanovskii, M.S. Skolnick, C. Tejedor, and L. Viña, *Observation of driven superfluidity of polaritons in a semiconductor microcavity*, arXiv:0711.1539 (2007).

L.C. Andreani, F. Tassone, F. Bassani, *Radiative lifetime of free excitons in quantum wells*, Solid State Commun. **77**, 641 (1991).

A. Astrakharchik, *Quantum Monte-Carlo Study of Ultracold Gases*, Tesi di Dottorato di Ricerca in Fisica, Universita degli Studi di Trento (2004).

A. Baas, J.-Ph. Karr, M. Romanelli, A. Bramati, and E. Giacobino, *Optical bistability in semiconductor microcavities in the nondegenerate parametric oscillation regime: Analogy with the optical parametric oscillator*, Phys. Rev. B **70**, 161307R (2004).

V. Bagnato, D. Kleppner, *Bose-Einstein condensation in two-dimensional traps*, Phys. Rev. A **44**, 7439 (1991).

G. Baldassarri Höger von Högersthal, S. Christopoulos, A. Grundy, P.G. Lagoudakis, and J.J. Baumberg, G. Christmann, R. Butté, E. Feltin, J.-F. Carlin, and N. Grandjean, *Nonlinear Coherent Emission from Strong-Coupled GaN Microcavities at Room Temperature*, Abstracts of the 3rd International Conference on Spontaneous Coherence in Excitonic systems (ICSCE3, 2007).

R. Balili, V. Hartwell, D. Snoke, L. Pfeiffer, K. West, *Bose-Einstein Condensation of Microcavity Polaritons in a Trap*, Science **316**, 1007 (2007).

D.G. Barci, E.S. Fraga, and R.O. Ramos, *Nonequilibrium Field Theory Description of the Bose-Einstein Condensate*, Phys. Rev. Lett. **85**, 479 (2000).

J.J. Baumberg, L. Viña, and S. Quin (editors), *Special Issue on Microcavities*, Semicond. Sci. Technol. **18**, S279 (2003).

J.J. Baumberg, D.D. Awschalom, N. Samarth, H. Luo, and J.K. Furdyna, *Spin Beats and Dynamical Magnetization in Quantum Structures*, Phys. Rev. Lett. **72**, 717 (1994).

Oleg L. Berman, Yurii E. Lozovik, David W. Snoke, and Rob D. Coalson, *Collective properties of indirect excitons in coupled quantum wells in a random field*, Phys. Rev. B **70**, 235310 (2004).

A.I. Bobrysheva, S.A. Moskalenko, and Yu.M. Shvera, *On the Bi-Exciton Formation in Crystals*, phys. stat. solidi (b) **53**, 71 (1972).

A. Brunetti, M. Vladimirova, and D. Scalbert, R. André, D. Solnyshkov and G. Malpuech, I. A. Shelykh and A. V. Kavokin, *Coherent spin dynamics of exciton-polaritons in diluted magnetic microcavities*, Phys. Rev. B **73**, 205337 (2006).

S. Burger, F. S. Cataliotti, C. Fort, F. Minardi, and M. Inguscio, M. L. Chiofalo and M. P. Tosi, *Superfluid and Dissipative Dynamics of a Bose-Einstein Condensate in a Periodic Optical Potential*, Phys. Rev. Lett. **86**, 4447 (2001).

R. Butté, E. Feltin, J. Dorsaz, G. Christmann, J.-F. Carlin, N. Grandjean, and M. Ilegems, *Nitride microcavities*, Jpn. J. Appl. Phys. **44**, 7207 (2005).

R. Butté, G. Christmann, E. Feltin, J.-F. Carlin, M. Mosca, M. Ilegems, and N. Grandjean, *Room-temperature polariton luminescence from a bulk GaN microcavity*, Phys. Rev. B **73**, 033315 (2006).

Iacopo Carusotto and Cristiano Ciuti, *Probing Microcavity Polariton Superfluidity through Resonant Rayleigh Scattering*, Phys. Rev. Lett. **93**, 166401 (2004).

G. Christmann, D. Simeonov, R. Butté, E. Feltin, J.-F. Carlin, and N. Grandjean, *Impact of disorder on high quality factor III-V nitride microcavities*, Appl. Phys. Lett. **89**, 261101 (2006).

G. Christmann, R. Butté, E. Feltin, J.-F. Carlin, and N. Grandjean, *Impact of inhomogeneous excitonic broadening on the strong exciton-photon coupling in quantum well nitride microcavities*, Phys. Rev. B **73**, 153305 (2006).

S. Christopoulos, G. Baldassarri Hoger von Hogersthal, A. J. D. Grundy, P. G. Lagoudakis, A.V. Kavokin, and J. J. Baumberg, *Room-Temperature Polariton Lasing in Semiconductor Microcavities*, Phys. Rev. Lett. **98**, 126405 (2007).

Cristiano Ciuti and Iacopo Carusotto, *Quantum fluid effects and parametric instabilities in microcavities*, phys. stat. sol. (b) **242**, 2224 (2005).

C. Ciuti, P. Schwendimann, B. Deveaud, and A. Quattropani, *Theory of the angle-resonant polariton amplifier*, Phys. Rev. B **62**, R4825 (2000).

C. Cuiti, P. Schwendimann, and A. Quattropani, *Parametric luminescence of microcavity polaritons*, Phys. Rev. B **63**, 041303 (2001).

C. Ciuti, V. Savona, C. Piermarocchi, A. Quattropani, P. Schwendimann, *Role of the exchange of carriers in elastic exciton-exciton scattering in quantum wells*, Phys. Rev. B **58**, 7926 (1998).

E. Cohen and M.D. Sturge, *Fluorescence line narrowing, localized exciton states, and spectral diffusion in the mixed semiconductor* CdS_xSe_{1-x}, Phys. Rev. B **25**, 3828 (1982).

K.M. Cuomo and A.V. Oppenheim, *Circuit Implementation of Synchronized Chaos with Applications to Communications*, Phys. Rev. Lett. **71**, 65 (1993).

G. Dasbach, C. Diederichs, J. Tignon, C. Ciuti, Ph. Roussignol, C. Delalande, M. Bayer, and A. Forchel, *Polarization inversion via parametric scattering in quasi-one-dimensional microcavities*, Phys. Rev. B **71**, 161308R (2005).

K. B. Davis, M.-O. Mewes, M. R. Andrews, N. J. van Druten, D. S. Durfee, D. M. Kurn, and W. Ketterle, *Bose-Einstein Condensation in a Gas of Sodium Atoms*, Phys. Rev. Lett. **75**, 3969 (1995).

B. Damski, J. Zakrzewski, L. Santos, P. Zoller, and M. Lewenstein, *Atomic Bose and Anderson Glasses in Optical Lattices*, Phys. Rev. Lett. **91**, 8 (2003).

R. Dingle, D.D. Sell, S.E. Sokowski, and M. Ilegems, *Absorption, Reflectance, and Luminescence of GaN Epitaxial Layers*, Phys. Rev. B **4**, 1211 (1971).

A.M. Dykhne, *The conductivity of a two-dimensional two-phase system*, JETP **59**, 110 (1970).

A. L. Efros and B. I. Shklovskii, *Electronic Properties of Doped Semiconductors* (Springer, Heidelberg, 1989).

A. Einstein, Sitz. Ber. Preuss. Akad. Wiss. (Berlin) **1**, 3 (1925).

L. Fallani, J.E. Lye, V. Guarrera, C. Fort, and M. Inguscio, *Ultracold Atoms in a Disordered Crystal of Light: Towards a Bose Glass*, Phys. Rev. Lett. **98**, 130404 (2007).

D.S. Fischer and P.C. Hohenberg, *Dilute Bose gas in two dimensions*, Phys. Rev. B **37**, 4936 (1988).

Ingo Fischer, Yun Liu, and Peter Davis, *Synchronization of chaotic semiconductor laser dynamics on subnanosecond timescales and its potential for chaos communication*, Phys. Rev. A **62**, 011801R (2000).

T. Freixanet, B. Sermage, A. Tiberj, and R. Panel, I*n-plane propagation of excitonic cavity polaritons*, Phys. Rev. B **61**, 7233 (2000).

H. Froehlich, Proc. Roy. Soc. A **160**, 230 (1937).

B. Gil (edited by), *Low-dimensional nitride semiconductors* (Oxford University Press, 2002).

N. A. Gippius, S. G. Tikhodeev, V. D. Kulakovskii, D. N. Krizhanovskii, and A. I. Tartakovskii, *Nonlinear dynamics of polariton scattering in semiconductor microcavity: Bistability vs. stimulated scattering*, Europhys. Lett. **67**, 997 (2004).

N.A. Gippius and S.G. Tikhodeev, *Multiple-polariton scattering in a semiconductor microcavity*, J. Phys.: Condens. Matter **16**, S3653 (2004).

M.M. Glazov, I.A. Shelykh, G. Malpuech, K.V. Kavokin, A.V. Kavokin and D.D. Solnyshkov, *Anisotropic polariton scattering and spin dynamics of cavity polaritons*, Solid State Commun. **134**, 117 (2005).

S. V. Gupalov, E. L. Ivchenko, and A. V. Kavokin, *Fine structure of localized exciton levels in quantum wells*, JETP **86**, 388 (1998).

H. Haug, S. Koch, *On the Theory of Laser Action in Dense Exciton Systems*, phys. stat. sol. (b) **82**, 531 (1977).

K. Helmerson *et al*, Physics World **12**, 31 (1999).

J.A. Hertz, L. Fleishman, and P.W. Anderson, *Marginal Fluctuations in a Bose Glass*, Phys. Rev. Lett. **43**, 942 (1979).

T.-L. Ho and V.B. Shenoy, *Binary Mixtures of Bose Condensates of Alkali Atoms*, Phys. Rev. Lett. **77**, 3276 (1996).

J.J. Hopfield, Theory of the Contribution of Excitons to the Complex Dielectric Constants of Crystals, Phys. Rev. 112, 1555 (1958).

A. Imamoglu, R.J. Ram, S. Pau, Y. Yamamoto, *Nonequilibrium condensates and lasers without inversion: Exciton-polariton lasers*, Phys. Rev. A **53**, 4250 (1996).

S. Inouye, M. R. Andrews, J. Stenger, H.-J. Miesner, D. M. Stamper-Kurn, W. Ketterle, *Observation of Feshbach resonances in a Bose–Einstein condensate*, Nature **396**, 345 (1998).

E.L. Ivchenko, *Excitonic polaritons in periodic quantum well structures*, Sov. Phys. Solid State **33**, 1344 (1991).

J. Kasprzak, M. Richard, S. Kundermann, A. Baas, P. Jeambrun, J. M. J. Keeling, F. M. Marchetti, M. H. Szymanska, R. Andre, J. L. Staehli, V. Savona, P. B. Littlewood, B. Deveaud & Le Si Dang, *Bose–Einstein condensation of exciton polaritons*, Nature **443**, 409 (2006).

J. Kasprzak, R. André, Le Si Dang, I.A. Shelykh, A.V. Kavokin, Yu. G. Rubo, K.V. Kavokin, G. Malpuech, *Build up and pinning of linear polarization in the Bose condensates of exciton polaritons*, Phys. Rev. B **75**, 045326 (2007).

A. Kavokin and B. Gil, *GaN microcavities: Giant Rabi splitting and optical anisotropy*, Appl. Phys. Lett. **72**, 2880 (1998).

A. Kavokin and G. Malpuech, *Cavity polaritons* (Elsevier, 2003).

Alexey Kavokin, Guillaume Malpuech, and Mikhail Glazov, *Optical Spin Hall Effect*, Phys. Rev. Lett. **95**, 136601 (2005).

K.V. Kavokin, I. A. Shelykh, A.V. Kavokin, G. Malpuech, and P. Bigenwald, *Quantum Theory of Spin Dynamics of Exciton-Polaritons in Microcavities*, Phys. Rev. Lett. **92**, 017401 (2004).

K.V. Kavokin, P. Renucci ,T. Amand, X. Marie, P. Senellart, J. Bloch, and B. Sermage, *Linear polarisation inversion: A signature of Coulomb scattering of cavity polaritons with opposite spins*, phys. stat. sol. (c) 2, 763 (2005).

Jonathan Keeling, P. R. Eastham, M. H. Szymanska, and P. B. Littlewood, *Polariton Condensation with Localized Excitons and Propagating Photons*, Phys. Rev. Lett. **93**, 226403 (2004).

Nille N. Klausen, John L. Bohn and Chris H. Greene, *Nature of spinor Bose-Einstein condensates in rubidium*, Phys. Rev. A **64**, 053602 (2001).

D. N. Krizhanovskii, D. Sanvitto, I. A. Shelykh, M. M. Glazov, G. Malpuech, D. D. Solnyshkov, A. Kavokin, S. Ceccarelli, M. S. Skolnick, and J. S. Roberts, *Rotation of the plane of polarization of light in a semiconductor microcavity*, Phys. Rev. B **73**, 073303 (2006).

J. Lagois, *Dielectric theory of interacting excitonic resonances*, Phys. Rev. B **16**, 1699 (1977).

C. W. Lai, N. Y. Kim, S. Utsunomiya, G. Roumpos, H. Deng, M. D. Fraser, T. Byrnes, P. Recher, N. Kumada, T. Fujisawa, and Y. Yamamoto, *Coherent zero-state and p-state in an exciton–polariton condensate array*, Nature **450**, 529 (2007).

T. Lahaye, J.M. Vogels, K. J. Gu¨nter, Z.Wang, J. Dalibard, and D. Guery-Odelin, *Realization of a Magnetically Guided Atomic Beam in the Collisional Regime*, Phys. Rev. Lett. **93**, 093003 (1999).

W. Langbein, I. Shelykh, D. Solnyshkov, G. Malpuech, Yu. Rubo, and A. Kavokin, *Polarization beats in ballistic propagation of exciton-polaritons in microcavities*, Phys. Rev. B **75**, 075323 (2007).

A.J. Leggett, *Can a Solid be "Superfluid"?*, Phys. Rev. Lett. **25**, 1543 (1970).

E. Levich and V. Yakhot, *Time evolution of a Bose system passing through the critical point*, Phys. Rev. B **15**, 243 (1977).

C. Leyder, M. Romanelli, J. Ph. Karr, E. Giacobino, T. C. H. Liew, M. M. Glazov, A. V. Kavokin, G. Malpuech, and A. Bramati, *Observation of the optical spin Hall effect*, Nature Physics **3**, 628 (2007).

E. M. Lifshitz and L. P. Pitaevskii, *Statistical Physics* (Pergamon Press, New York, 1980).

P.D. Maker, R.W. Terhune, and C.M. Savage, *Intensity-dependent changes in the refractive index of liquids*, Phys. Rev. Lett. **12**, 507 (1964).

G. Malpuech, A. Di Carlo, A. Kavokin, J. J. Baumberg, M. Zamfirescu, P. Lugli, *Room-temperature polariton lasers based on GaN microcavities*, Appl. Phys. Lett. **81**, 412 (2002).

G. Malpuech, A. Kavokin, A. Di Carlo, and J. J. Baumberg, *Polariton lasing by exciton-electron scattering in semiconductor microcavities*, Phys. Rev. B **65**, 153310 (2002).

G. Malpuech, M.M. Glazov, I.A. Shelykh, P. Bigenwald, K.V. Kavokin, *Electronic control of the polarization of light emitted by polariton lasers*, Appl. Phys. Lett. **88**, 111118 (2006).

G. Malpuech, Y. G. Rubo, F. P. Laussy, P. Bigenwald, and A. V. Kavokin, *Polariton laser: thermodynamics and quantum kinetic theory*, Semiconductor Science and Technology **18**, S395 (2003).

F. M. Marchetti, J. Keeling, M. H. Szymanska, and P. B. Littlewood, *Thermodynamics and Excitations of Condensed Polaritons in Disordered Microcavities*, Phys. Rev. Lett. **96**, 066405 (2006).

M. Moreno-Cardoner, J. Mur-Petit, M. Guilleumas, A. Polls, A. Sanpera, and M. Lewenstein, *Predicting Spinor Condensate Dynamics from Simple Principles*, Phys. Rev. Lett. **99**, 020404 (2007).

F. Natali, D. Byrne, M. Leroux, B. Damilano, F. Semond, A. Le Louarn, S. Vezian, N. Grandjean, and J. Massies, *Inhomogeneous broadening of $Al_xGa_{1-x}N/GaN$ quantum wells*, Phys. Rev. B 71, 075311 (2005).

R. Onforio, C. Raman, J. M. Vogels, J. R. Abo-Shaeer, A. P. Chikkatur, and W. Ketterle, *Observation of Superfluid Flow in a Bose-Einstein Condensed Gas*, Phys. Rev. Lett. 85, 2228 (2000).

E. Ott, C. Grebogi, and J.A. Yorke, *Controlling Chaos*, Phys. Rev. Lett. 64, 1196 (1990).

A.N. Oraevskii, *Coherent Bosonic States*, Soviet Quantum Electronics 24, 1127 (1997).

G. Panzarini, L.C. Andreani, A. Armitage, D. Baxter, M.S. Skolnick, V.N. Astratov, J.S. Roberts, A.V. Kavokin, M.R. Vladimirova, M.A. Kaliteevski, *Exciton-light coupling in single and coupled semiconductor microcavities: Polariton dispersion and polarization splitting*, Phys. Rev. B 59, 5082 (1999).

P. P. Paskov, T. Paskova, P. O. Holtz, and B. Monemar, *Polarized photoluminescence of exciton–polaritons in free-standing GaN*, phys. stat. sol. (a) 201, 678 (2004).

P. P. Paskov, T. Paskova, P. O. Holtz, and B. Monemar, *Spin-exchange splitting of excitons in GaN*, Phys. Rev. B 64, 115201 (2001).

Louis M. Pecora and Thomas L. Carroll, *Synchronization in chaotic systems*, Phys. Rev. Lett. 64, 821 (1990).

D. Pereda Cubian, M. Haddad, R. Andre´, R. Frey, G. Roosen, J. L. Arce Diego, and C. Flytzanis, *Photoinduced magneto-optic Kerr effects in asymmetric semiconductor microcavities*, Phys. Rev. B 67, 045308 (2003).

L. Pitaevskii and S. Stringari, *Bose-Einstein Condensation* (Clarendon Press, 2003).

D. Porras, C. Ciuti, J.J. Baumberg, and C. Tejedor, *Polariton dynamics and Bose-Einstein condensation in semiconductor microcavities*, Phys. Rev. B **66**, 085304 (2002).

C. Raman, M. Köhl, R. Onofrio, D. S. Durfee, C. E. Kuklewicz, Z. Hadzibabic, and W. Ketterle, *Evidence for a Critical Velocity in a Bose-Einstein Condensed Gas*, Phys. Rev. Lett. **83**, 2502 (1999).

P. Renucci, T. Amand, X. Marie, P. Senellart, J. Bloch, B. Sermage, K. V. Kavokin, *Microcavity polariton spin quantum beats without a magnetic field: A manifestation of Coulomb exchange in dense and polarized polariton systems*, Phys. Rev. B 72, 075317 (2005).

M. Richard, J. Kasprzak, R. André, R. Romestain, Le Si Dang, G. Malpuech, and A. Kavokin, *Experimental evidence for nonequilibrium Bose condensation of exciton polaritons*, Phys. Rev. B 72, 201301R (2005).

P. G. Savvidis, J. J. Baumberg, R. M. Stevenson, M. S. Skolnick, D. M. Whittaker, and J. S. Roberts, *Angle-Resonant Stimulated Polariton Amplifier*, Phys. Rev. Lett. 84, 1547 (2000).

D. Scalbert, F. Teppe, and M. Vladimirova, S. Tatarenko, J. Cibert, M. Nawrocki, *Softening of spin resonance at low temperature in p-doped $Cd_{1-x}Mn_xTe$ quantum wells*, Phys. Rev. B 70, 245304 (2004).

R.T. Scalettar, G.G. Batrouni, G.T. Zimanyi, *Localization in Interacting, Disordered, Bose systems*, Phys. Rev. Lett. **66**, 3144 (1991).

I. R. Sellers, F. Semond, M. Leroux, J. Massies, P. Disseix, A-L. Henneghien, J. Leymarie, and A. Vasson, *Strong coupling of light with A and B excitons in GaN microcavities grown on silicon*, Phys. Rev. B 73, 033304 (2006).

F. Semond, I. R. Sellers, F. Natali, D. Byrne, M. Leroux, J. Massies, N. Ollier, J. Leymarie, P. Disseix, and A. Vasson, *Strong light-matter coupling at room temperature in simple geometry GaN microcavities grown on silicon*, Appl. Phys. Lett. 87, 021102 (2005).

I. A. Shelykh, M. M. Glazov, D. D. Solnyshkov, N. G. Galkin, A. V. Kavokin, and G. Malpuech, *Spin dynamics of polariton parametric amplifiers*, phys. stat. sol. (c) 2, 768 (2005).

I.A. Shelykh, R. Johne, D.D. Solnyshkov, A.V. Kavokin, N.A. Gippius, and G. Malpuech, *Quantum kinetic equations for interacting bosons and their application for polariton parametric oscillators*, Phys. Rev. B **76**, 155308 (2007).

I. Shelykh, G. Malpuech, K. V. Kavokin, A. V. Kavokin, and P. Bigenwald, *Spin dynamics of interacting exciton polaritons in microcavities*, Phys. Rev. B 70, 115301 (2004).

T. V. Shubina, V. N. Jmerik, S. V. Ivanov, D. D. Solnyshkov, N. A. Cherkashin, K. F. Karlsson, P. O. Holtz, A. Waag, P. S. Kop'ev, and B. Monemar, *Polarized micro-photoluminescence spectroscopy of GaN nanocolumns*, phys. stat. sol. (c) **0**, 7 (2003).

D.D. Solnyshkov, I.A. Shelykh, M.M. Glazov, G. Malpuech, T. Amand, P. Renucci, X. Marie, A.V. Kavokin, *Nonlinear effects in spin relaxation of cavity polaritons*, Semiconductors **41**, 1099 (2007).

Takao Someya, Ralph Werner, Alfred Forchel, Massimo Catalano, Roberto Cingolani, Yasuhiko Arakawa, *Room Temperature Lasing at Blue Wavelengths in Gallium Nitride Microcavities*, Science **285**, 1905 (1999).

D.M. Stamper-Kurn, H.-J. Miesner, A. P. Chikkatur, S. Inouye, J. Stenger, and W. Ketterle, *Quantum Tunneling across Spin Domains in a Bose-Einstein Condensate*, Phys. Rev. Letters **83**, 661 (1999).

H.T.C. Stoof, Formation of the Condensate in a Dilute Bose Gas, Phys. Rev. Lett. **66**, 3148 (1991).

H.T.C. Stoof, Initial Stages of Bose-Einstein Condensation, Phys. Rev. Lett. **78**, 768 (1997).

M. Taki, *Horseshoe chaos in a bistable optical system under a modulated incident field*, Phys. Rev. E **56**, 6033 (1997).

F. Tassone and Y. Yamamoto, *Exciton-exciton scattering dynamics in a semiconductor microcavity and stimulated scattering into polaritons*, Phys. Rev. B **59**, 10830 (1999).

F. Tassone, C. Piermarocchi, V. Savona, A. Quattropani, P. Schwendimann, *Bottleneck effects in the relaxation and photoluminescence of microcavity polaritons*, Phys. Rev. B **56**, 7554 (1997).

F. Teppe, M. Vladimirova, D. Scalbert, T. Wojtowicz, J. Kossut, *Optically induced instability of spin precession in magnetic quantum wells*, Phys. Rev. B **67**, 033304 (2003).

M. Vladimirova, D. Scalbert, C. Misbah, *Pattern formation in paramagnetic diluted magnetic semiconductors*, Phys. Rev. B **71**, 233203 (2005).

C. Weisbuch, M. Nishioka, A. Ishikawa, and Y. Arakawa, *Observation of a Coupled Exciton-Photon Mode Splitting in a Semiconductor Quantum Microcavity*, Phys. Rev. Lett. **69**, 3314 (1992).

M. Wouters and I. Carusotto, Excitations in a Nonequilibrium Bose-Einstein Condensate of Exciton Polaritons, Phys. Rev. Lett. **99**, 140402 (2007).

R. Zallen, H. Scher, *Percolation on a continuum and the localization-delocalization transition in amorphous semiconductors*, Phys. Rev. B **4**, 4471 (1971).

Marian Zamfirescu, Alexey Kavokin, Bernard Gil, Guillaume Malpuech, and Mikhail Kaliteevski, *ZnO as a material mostly adapted for the realization of room-temperature polariton lasers*, Phys. Rev. B **65**, 161205R (2002).

List of published papers

Regular papers

1) A.A.Toropov, A.V.Lebedev, S.V.Sorokin, **D.D.Solnyshkov**, S.V.Ivanov, P.S.Kop'ev, I.A.Buyanova, W.M.Chen, and B.Monemar, *ZnMnSe/ZnSSe Type-II Semimagnetic Superlattices: Growth and Magnetoluminescence Properties*, Semiconductors **36**, 1288 (2002)

2) T.V. Shubina, S.V. Ivanov, A.A. Toropov, S.V. Sorokin, A.V. Lebedev, R.N. Kyutt, **D.D. Solnyshkov**, G.R. Pozina, B. Monemar, M. Willander, A. Waag, and G. Landwehr, *Interface Effects in Type II CdSe/BeTe Quantum Dots*, Phys. Stat. Sol. (b) **229** (1), 489 (2002)

3) A. A. Toropov, A. V. Lebedev, S. V. Sorokin, **D. D. Solnyshkov**, S. V. Ivanov, P. S. Kop'ev, I. A. Buyanova, W. M. Chen and B. Monemar, *Magneto-photoluminescence studies of diluted magnetic semiconductor type-II quantum wells ZnMnSe/ZnSSe*, Physica E: Low-dimensional Systems and Nanostructures, **17**, 352 (2003)

4) A. A. Toropov, O. V. Nekrutkina, M. O. Nestoklon, S. V. Sorokin, **D. D. Solnyshkov**, S. V. Ivanov, A. Waag, and G. Landwehr, *Gamma-X electron level crossover in ZnSe/BeTe multiple quantum wells*, Phys. Rev. B **67**, 113307 (2003)

5) A. A. Toropov, S. V. Sorokin, T. V. Shubina, O. V. Nekrutkina, **D. D. Solnyshkov**, S. V. Ivanov, A. Waag, and G. Landwehr, *Optical anisotropy of non-common-atom quantum wells and dots: effects of interface symmetry reduction*, Phys. stat. sol. (a) **195** (3), 551 (2003)

6) R. N. Kyutt, T. V. Shubina, S. V. Sorokin, **D. D. Solnyshkov**, S. V. Ivanov, M. Willander, *X-ray diffraction determination of the interface structure of CdSe/BeTe superlattices,* J. Phys. D: Appl. Phys. **36**, A166 (2003)

7) Ivanov S.V., Shubina T.V., Sedova I.V., Sorokin S.V., Kyutt R.N., Sitnikova A.A., **Solnyshkov D.D.**, Nekrutkina O.V., Toropov A.A., Kop'ev P.S., Semiconductor

nanostructures with CdSe quantum dots: MBE growth, properties and applications, Surface **10**, 4 (2003).

8) T.V. Shubina, S. V. Ivanov, V. N. Jmerik, **D.D. Solnyshkov**, V. A. Vekshin, P.S. Kop'ev, A. Vasson, J. Leymarie, A. Kavokin, H. Amano, K. Shimono, A. Kasik, B. Monemar, *Mie Resonances, Infrared Emission, and the Band Gap of InN*, Phys. Rev. Lett **92**, 117407 (2004)

9) S. Ivanov, A.A. Toropov, T.V. Shubina, S.V. Sorokin, R.N. Kyutt, A.A. Sitnikova, **D.D. Solnyshkov**, and O.V. Nekrutkina, *CdSe-based nanostructures: growth, properties, lasers*, Phys. Stat. Sol. (b), **241** (3), 531-537 (2004)

10) Pierre Bigenwald, Valentin V. Nikolaev, **Dmitry Solnyshkov**, Alexey Kavokin, Guillaume Malpuech, Bernard Gil, *Polariton lasers based on semiconductor quantum microspheres*, Phys. Rev. B **70**, 205343 (2004)

11) V. A. Solov'ev, O. G. Lyublinskaya, A. N. Semenov, B. Ya. Meltser, **D. D. Solnyshkov**, Ya. V. Terent'ev, L. A. Prokopova, A. A. Toropov, S. V. Ivanov and P. S. Kop'ev, *Room-temperature 3.9 - 4.3 mkm photoluminescence from InSb submonolayers grown by molecular beam epitaxy in an InAs matrix*, Appl. Phys. Lett. **86**, 011109 (2005)

12) M.M. Glazov, I.A. Shelykh, G. Malpuech, K.V. Kavokin, A.V. Kavokin and **D.D. Solnyshkov**, *Anisotropic polariton scattering and spin dynamics of cavity polaritons*, Solid State Communications **134**, 117 (2005)

13) D.N. Krizhanovskii, D. Sanvitto, I.A. Shelykh, M.M. Glazov, G.Malpuech, **D.D. Solnyshkov**, A. Kavokin, S.Ceccarelli, M.S. Skolnick and J.S. Roberts, *Rotation of the plane of polarization of light in a semiconductor microcavity*, Phys. Rev. B **73**, 073303 (2005)

14) A. Brunetti, M. Vladimirova, D. Scalbert, R. André, **D. Solnyshkov**, G. Malpuech, I. A. Shelykh, and A. V. Kavokin, *Coherent spin dynamics of exciton-polaritons in diluted magnetic microcavities*, Phys. Rev. B **73**, 205337 (2006)

15) I. A. Shelykh, Yu. G. Rubo, G. Malpuech, **D. D. Solnyshkov**, and A. Kavokin, *Polarization and Propagation of Polariton Condensates*, Phys. Rev. Lett. **97**, 066402 (2006)

16) W. Langbein, I. Shelykh, **D. Solnyshkov**, G. Malpuech, Yu. Rubo, and A. Kavokin, Polarization beats in ballistic propagation of exciton-polaritons in microcavities, Phys. Rev. B **75**, 075323 (2007)

17) G. Malpuech, **D. D. Solnyshkov**, H. Ouerdane, M. M. Glazov, and I. Shelykh, *Bose Glass and Superfluid Phases of Cavity Polaritons*, Phys. Rev. Lett. **98**, 206402 (2007)

18) N. A. Gippius, I. A. Shelykh, **D. D. Solnyshkov**, S. S. Gavrilov, Yuri G. Rubo, A. V. Kavokin, S. G. Tikhodeev, and G. Malpuech, *Polarization Multistability of Cavity Polaritons*, Phys. Rev. Lett. **98**, 236401 (2007)

19) **D.D.Solnyshkov**, I.A.Shelykh, M.M.Glazov , G.Malpuech, T.Amand, P.Renucci, X.Marie, A.V.Kavokin, *Nonlinear effects in spin relaxation of cavity polaritons*, Semiconductors **41**, 1099 (2007).

20) A. Kavokin, **D. Solnyshkov**, G. Malpuech, *Quatron-polaritons : charged quasi-particles having the bosonic statistics*, J. Phys.: Condens. Matter **19**, 295212 (2007).

28) **D.D. Solnyshkov**, H. Ouerdane, M.M. Glazov, I.A. Shelykh, G.Malpuech, *Bose glass and superfluid phase transitions of exciton–polaritons in GaN microcavities*, Solid State Comm. **144**, 390 (2007).

21) I. A. Shelykh, R. Johne, **D.D. Solnyshkov**, A.V. Kavokin, N. A. Gippius and G. Malpuech, *Quantum kinetic equations for interacting bosons and their application for polariton parametric oscillators*, Phys. Rev. B 76, 155308 (2007).

22) **D. Solnyshkov**, H. Ouerdane, G. Malpuech, Kinetic phase diagrams of GaN-based polariton lasers, accepted to Journal of Appl. Physics (2007).

23) **D.D. Solnyshkov**, I.A. Shelykh, N.A. Gippius, A.V. Kavokin, and G. Malpuech, Dispersion of interacting spinor cavity polaritons out of thermal equilibrium, accepted to Phys. Rev. B (2007).

Conference abstracts and proceedings

1) **Solnyshkov D.D.**, Ivanov S.V., Growth of CdSe/BeTe quantum dots, Abstracts of International Winter School on Semiconductor Physics, (2003)

2) V.A. Solov'ev, O.G. Lyublinskaya, B.Ya. Meltser, A.N. Semenov, L.A. Prokopova, **D.D. Solnyshkov**, A.A. Toropov, S.V. Ivanov, and P.S. Kop'ev, InSb/InAs nanostructures with InSb sub-monolayers emitting in the 3.4-4.2 mkm spectral range, Proceedings of 12th Int. Symposium "Nanostructures: Physics and Technology", St. Peterburg, Russia, 60-61 (2004)

3) P. S. Kop'ev, T.V. Shubina, S.V. Ivanov, V. N. Jmerik, **D. D. Solnyshkov**, V. A. Vekshin, Effects of Stoichoimetry Violation and Indium Nano-Clusters Formation on Band Gap of InN, Proceedings of 12th Int. Symposium "Nanostructures: Physics and Technology", St. Peterburg, Russia, 374-375 (2004)

4) A.N. Semenov, V.A. Solov'ev, O.G. Lyublinskaya, B.Ya. Meltser, **D.D. Solnyshkov**, L.A. Prokopova, A.A. Sitnikova, A.A. Toropov, S.V. Ivanov, and P.S. Kop'ev, Molecular beam epitaxy of InSb sub-monolayers emitting at room-temperature near 4.0mkm, Abstracts of 6th Int. Conf. on "Mid-infrared Optoelectronic Materials and Devices", St. Peterburg, Russia, 147-148 (2004)

5) S.V. Ivanov, A.N. Semenov, V.A. Solov'ev, O.G. Lyublinskaya, B.Ya. Meltser, **D.D. Solnyshkov**, L.A. Prokopova, A.A. Sitnikova, A.A. Toropov, and P.S. Kop'ev, Molecular beam epitaxy of type II InSb/InAs nanostructures with InAs sub-monolayers, Abstracts of 13th Int. Conf. on Molecular Beam Epitaxy, Edinburgh, 21 (2004).

6) O.G. Lyublinskaya, Ya.V. Terent'ev, L.A. Prokopova, V.A. Solov'ev, B.Ya. Meltser, A.N. Semenov, D.D. Solnyshkov, A.A. Sitnikova, A.A. Toropov, S.V. Ivanov, K.

Thonke, R. Sauer, Photoluminescence of InSb quantum dots in InAs matrix grown by molecular beam epitaxy, Abstracts of ICPS-27, Flagstaff, USA, P5.008 (2004)

7) A.A. Toropov, A.V. Lebedev, S.V. Sorokin, **D.D. Solnyshkov**, S.V. Ivanov, P.S. Kop'ev, I.A. Buyanova, W.M. Chen, and B. Monemar, *Growth and magneto-optical studies of diluted magnetic semiconductor type II quantum wells ZnMnSe/ZnSSe*, Physica E, 17, 352-354 (2003)

8) T. V. Shubina, V. N. Jmerik, S. V. Ivanov, **D. D. Solnyshkov**, N. A. Cherkashin, K. F. Karlsson, P. O. Holtz, A. Waag, P. S. Kop'ev, B. Monemar, *Polarized micro-photoluminescence spectroscopy of GaN nanocolumns*, phys. stat. sol. (c) **0**, 2602 (2003)

9) I. A. Shelykh, M. M. Glazov, **D. D. Solnyshkov**, N. G. Galkin, A. V. Kavokin, G. Malpuech, *Spin dynamics of polariton parametric amplifiers*, phys. stat. sol. (c) **2**, 768 (2005)

10) **D.D. Solnyshkov**, I.V. Sedova, A.A. Toropov and S.V. Ivanov, *Combined (ZnSe/MgS)/ZnCdSe Bragg Reflectors Grown Using ZnS as a Sulphur Source*, Acta Physica Polonica A 108 (5) 873 (2005).

11) I. V. Sedova, O. G. Lyublinskaya, S. V. Sorokin, A. A. Sitnikova, **D. D. Solnyshkov**, O. V. Rykhova, A. A. Toropov, S. V. Ivanov, *Influence of CdTe sub-monolayer stressor on CdSe quantum dot self-assembling in ZnSe*, physica status solidi (c) **3,** 916 (2006).

12) S. V. Sorokin*, **D. D. Solnyshkov**, I. V. Sedova, A. A. Toropov, S. V. Ivanov, and P. S. Kop'ev; (*ZnSe/MgS)/ZnCdSe DBRs grown by molecular beam epitaxy using ZnS as a sulphur source*, phys. stat. sol. (c) 3, No. 4, 763–766 (2006) / DOI 10.1002/pssc.200564675

13) **D. Solnyshkov**, G. Malpuech, *A polariton laser based on a bulk GaN microcavity*, Superlattices and Microstructures (2007), doi:10.1016/j.spmi.2007.03.013

14) D. Scalbert, M. Vladimirova, A. Brunetti, S. Cronenberger, M. Nawrocki, J. Bloch, A.V. Kavokin, I.A. Shelykh, R. Andre, **D. Solnyshkov**, G. Malpuech, *Polariton spin*

beats in semiconductor quantum well microcavities, Superlattices and Microstructures, doi:10.1016/j.spmi.2007.06.017 (2007).